Chapter 5. Microscopic Structure of Breaking and Persistency of "Phonon-plus-Odd-Quasi-Particle Picture"

Atsushi KURIYAMA, Toshio MARUMORI,* Kenichi MATSUYANAGI,**
Ryoji OKAMOTO and Tōru SUZUKI**

Department of Physics, Kyushu University, Fukuoka 812
**Institute for Nuclear Study, University of Tokyo, Tanashi, Tokyo 188*
***Department of Physics, Kyoto University, Kyoto 606*

(Received June 13, 1975)

§1. Introduction

In the preceding chapter, we have obtained a conclusion that, in almost all spherical odd-mass nuclei, the dressed three-quasi-particle (3QP) states with spin $I=(j-1)$ are expected to appear in the neighbourhood of the 1QP states with spin $j\geqq 5/2$. Furthermore, we have emphasized that the roles of the 3QP correlations should be regarded not only as to bring about the general presence of the $(j-1)$ states but also as to play an essential role in characterizing the low-energy excitation structure in almost all spherical odd-mass nuclei.

This conclusion leads us inevitably to change the customarily used "phonon-plus-odd-quasi-particle picture" in which elementary modes of excitation (characterizing low-lying states in spherical odd-mass nuclei) are assumed to be odd-quasi-particle modes and phonon modes.[1),2)] In the conventional quasi-particle-phonon-coupling (QPC) theory,[1),2)] as is well known, the phonons are described by random-phase approximation (RPA) assuming them to be ideal bosons (and hence are commutable with the odd quasi-particles). Boson expansion methods for odd-mass nuclei[3)~5)] can also be regarded as perturbational approaches to describe the system starting from these (independent) elementary excitation modes.

In contrast to these approaches, the theory developed in Chap. 2 (which may be called the "method of new-Tamm-Dancoff (NTD) space") is free from introducing the concept of phonon to odd-mass nuclei and, furthermore, includes the QPC theory as a specially approximated version (in which the kinematical effects due to the Pauli principle among quasi-particles more than two are all neglected). The proposed theory enables us to classify both the complicated "anharmonicity effects" and the roles of residual interactions in a systematic way. Furthermore, by using the theory, we are able to investigate the mutual relationships between various aspects of "anharmonicity effects." Thus it now becomes possible to investigate the microscopic structure of break-

ing and persistency of the conventional "phonon-plus-odd-quasi-particle picture," from the new point of view obtained in the previous chapters. In this chapter, special emphasis will be put on extracting (from the complicated "anharmonicity effects") the essential correlations which necessarily lead us to adopt a new picture for the low-lying collective excited states in spherical odd-mass nuclei.

In §2, starting from the basic picture of the QPC theory, some criteria for investigating the breaking and persistency of the conventional phonon picture in spherical odd-mass nuclei are set up. In §3, characteristics of the collective 3QP correlations in many j-shell model are discussed exemplifying the results calculated for odd-proton ^{133}Cs and ^{135}La nuclei. Here, with the aid of the criteria set up in §2, various aspects of the 3QP correlations are investigated by paying attention to their relation with shell structure. It will be shown that, although simple phonon picture is drastically changed due to the action of collective 3QP correlations, one element of the phonon picture which is characterized by the concept of "phonon-band" can persist under a certain condition of shell structure. In §4, we briefly discuss the roles of correlations between proton- and neutron-quasi-particles (in characterizing the dressed 3QP modes) by showing the results calculated for ^{97}Mo and ^{105}Pd nuclei. The results calculated for ^{117}Sn and ^{115}Cd nuclei are also presented in §5 in order to supplement the statement given in §4 and to show the possibility of complete breakdown of the phonon-band character under another situation in shell structure.

In §6, after the investigations on the microscopic structure of the eigenmodes themselves, we turn to estimate the effect of the *interactive force* H_Y. In the conventional QPC theory, as is well known, the coupling between the odd quasi-particle and the phonon comes entirely from the interactive force H_Y and plays a role changing the number of phonons by one. However, in this section, an important difference between the evaluation of the H_Y effect in the "ideal-boson-fermion space" (implicitly assumed in the QPC theory) and that in the "quasi-particle NTD space" (characterizing the proposed theory) will be shown.

In order to keep a close contact with the conventional QPC theory, all discussions in this chapter will be made by adopting the pairing-plus-quadrupole ($P+QQ$) force model.[6]

§2. Criteria for breaking and persistency of phonon-bands

In this section, in order to investigate the microscopic structure of breaking and persistency of "phonon-plus-odd-quasi-particle picture," we first recapitulate the characteristics of the excitation spectrum and of $E2$-transition properties given by the unperturbed Hamiltonian $\mathcal{H}^{(0)}$ of the QPC theory.[1),2)]

The $P+QQ$ Hamiltonian can be divided into the following parts in the quasi-particle representation:

$$\left.\begin{aligned} &H=H_0+:H_{QQ}:, \\ &:H_{QQ}:=H_X+H_V+H_Y, \end{aligned}\right\} \tag{2·1}$$

where H_0 denotes the free quasi-particle Hamiltonian and each part of $:H_{QQ}:$ is schematically represented in Fig. 1. In the conventional QPC theory, two-quasi-particle (2QP) correlation diagrams originated from the H_X- and H_V-type interactions are summed up to all orders in the sense of NTD approximation. Then the part, $H_0+H_X+H_V$, is transformed into the free Hamiltonian $\mathcal{H}^{(0)}$ which describes a system composed of (non-interacting) odd quasi-particle plus phonons. On the other hand, the part H_Y is considered to give rise to the coupling between the odd quasi-particle and phonon in the "ideal-boson-fermion space." Thus the model Hamiltonian of the conventional QPC theory takes the following form:

$$\left.\begin{aligned} &\mathcal{H}=\mathcal{H}^{(0)}+\mathcal{H}^{(\mathrm{int})}, \\ &\mathcal{H}^{(0)}=\sum_{a} E_a \dot{a}_a^{\dagger}\dot{a}_a+\sum_{JM(J\neq 2)}(E_a+E_b)\dot{A}_{JM}^{\dagger}(ab)\dot{A}_{JM}(ab) \\ &\qquad\qquad +\sum_{\nu}\sum_{M}\omega_\nu \Gamma_{2M}^{\dagger}(\nu)\Gamma_{2M}(\nu), \\ &\mathcal{H}^{(\mathrm{int})}=\sum_{\nu}\sum_{M a\beta}\bar{\chi}_{a\beta}(\nu)\{\Gamma_{2\widetilde{M}}^{\dagger}(\nu)+\Gamma_{2M}(\nu)\}\dot{a}_a^{\dagger}\dot{a}_{\tilde{\beta}}, \end{aligned}\right\} \tag{2·2}$$

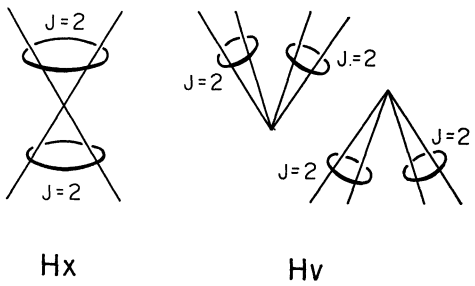

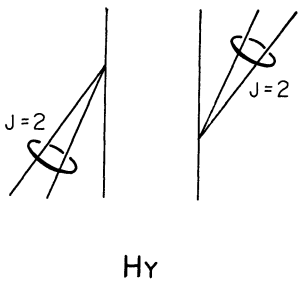

Fig. 1. Graphic representation of the matrix elements of the quadrupole force. Part H_X represents a scattering of the pair of quasi-particles coupled to $J^{\pi}=2^{+}$, while part H_Y represents a pair-creation and a pair-annihilation of quasi-particles coupled to $J^{\pi}=2^{+}$. Parts H_X and H_V are called the *constructive force*. Part H_Y represents a creation and an annihilation of the quasi-particles coupled to $J^{\pi}=2^{+}$, accompanying a scattering of a quasi-particle. Part H_Y is called the *interactive force*.

where $\dot{a}^{\dagger}_{\alpha}$, $\dot{A}^{\dagger}_{JM}(ab)$ and $\Gamma^{\dagger}_{2M}(\nu)=\sum_{ab}\{\psi_{\nu}(ab)\dot{A}^{\dagger}_{2M}(ab)-\varphi_{\nu}(ab)\dot{A}\widetilde{}_{2M}(ab)\}$ represent the creation operators of ideal-odd-quasi-particle, ideal boson corresponding to quasi-particle pair and ideal-phonon, respectively. In Eq. (2·2), the Greek letter ν distinguishes various eigensolutions of phonon modes and, as an additional approximation,[1),2)] non-collective phonons have often been neglected together with the second term of $\mathcal{H}^{(0)}$. In the same way the mass-quadrupole operator is expressed as

$$\hat{Q}_{2M}=\sum_{\nu}Q_{M}(\nu)\{\Gamma^{\dagger}_{2M}(\nu)+\Gamma\widetilde{}_{2M}(\nu)\}+\sum_{\alpha\beta}q_{M}(\alpha\beta)\dot{a}^{\dagger}_{\alpha}\dot{a}_{\tilde{\beta}}, \tag{2·3}$$

where $Q_{M}(\nu)$ and $q_{M}(\alpha\beta)$ represent the collective and single-quasi-particle matrix elements, respectively. A theoretical foundation for deriving the model operators in the QPC theory has been known as boson expansion methods in odd-mass nuclei,[3)~5)] in which the unperturbed Hamiltonian $\mathcal{H}^{(0)}$ and the expression (2·3) are considered as a zeroth-order approximation for boson expansion.

Now, one of the characteristics of the basis states given by $\mathcal{H}^{(0)}$ is that they are classified into definite sets of states each of which can be called *a phonon-band*. The phonon-bands are distinguished with one another by the quantum numbers of the single-particle orbit $a=(nlj)$, to which the odd quasi-particle belongs. As illustrated in Fig. 2, each phonon-band consists of a series of degenerate multiplets in which the odd quasi-particle is coupled with some number of phonons. The excitation spectrum and the $E2$-transition properties obey the well known pattern of the harmonic oscillators. It should be emphasized here that the $E2$ transitions between different phonon-bands (inter-band transitions) are forbidden if we neglect the second term in (2·3).

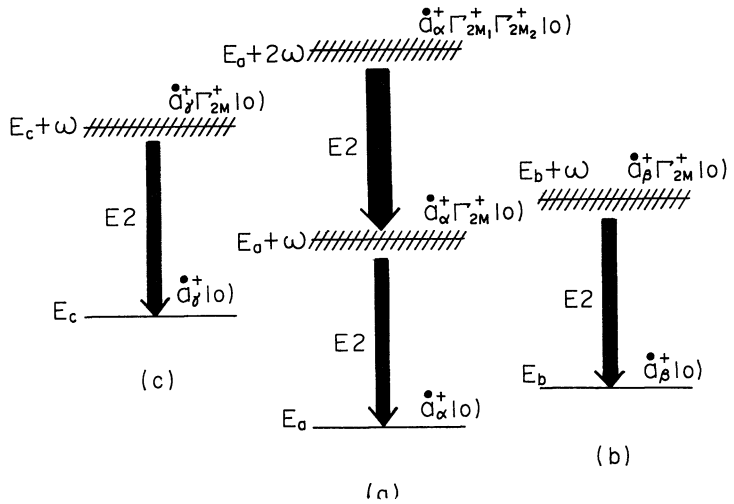

Fig. 2. Schematic representation of the concept of phonon-bands.

In particular, the inter $E2$ transitions from the multiplet (composed of the odd quasi-particle *in the orbit a* coupled with one phonon) to the band-head (the odd quasi-particle state in *the orbit b*) which belongs to the other phonon-bands are strictly forbidden.

Starting from this zeroth-order picture of the QPC theory, let us switch on the 3QP correlations and follow up the process of breaking of the picture. Then we can consider two cases for the way of the breaking;

A) the case where the 3QP correlation among quasi-particles in the same single-particle orbit plays a predominant role (Fig. 3-A),

B) the case where the 3QP correlation among quasi-particles in different single-particle orbits plays a predominant role (Fig. 3-B).

A typical example of case A is the AC states. As was shown in Chap. 3, in the case of the AC states the triggering effect of the 3QP correlations (which strongly violate the concept of phonon in odd-mass nuclei) is restricted among quasi-particles in a specific high-spin and unique-parity orbit, because of the parity-selection property of the quadrupole force. Hence, in this case, we can look into the breaking of the *simple phonon picture* within a "(isolated) single phonon-band." (See Fig. 16(a) in Chap. 3, which shows the splitting of the "quintet" composed of the $g_{9/2}$ odd quasi-particle coupled with the 2^+ phonon.)

As was discussed in Chap. 4, we can also expect the other situation which belongs to case A, that is, in spite of the fact that many orbits with the same parity lie close and equally active for the 3QP correlations, effect B is highly reduced compared to effect A. An important characteristic in this case is that, although the energy splittings of the multiplets are very large (due to effect A), the $E2$ transitions between different phonon-bands (the inter-band transitions) are hindered compared to the intra-band transitions. (See Fig. 4.) In this sense, we can say that the concept of phonon-band is preserved in case A.

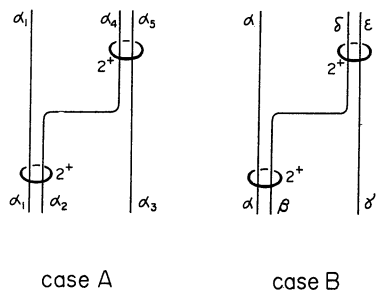

Fig. 3. Illustrations for two types of the 3QP correlations.
case A: 3QP correlation among quasi-particles in the same orbit.
case B: 3QP correlation among quasi-particles in different orbits ($a \neq b \neq c$, $a \neq b = c$, $a = b \neq c$ *or* $b \neq c = a$).
The subscript i ($=1, 2, \ldots, 5$) of α is used to specify the single-particle states with different magnetic quantum numbers in the same orbit a.

The situation belonging to case A seems to resemble to that given by the phenomenological core-excitation model,[7] in the point that the inter-band transitions are forbidden approximately. However, there exist important differences, which are; 1) the center of gravity theorem is violated, 2) the $B(E2)$ values for the transitions from the multiplet to their band-head (one-quasi-particle) state are different from one another and 3) they are also not equal to the phonon transition $B(E2; 2^+ \to 0^+)$ in the even-even core. This is because of the fact that, from our viewpoint, the microscopic structure of the core excitation (phonon) itself is changed in a way which depends on the spin I of the multiplet, due to the 3QP correlation at a specific orbit.

On the other hand, in case B, the members with the same spin which belong to different phonon-bands couple with one another strongly (due to the 3QP correlation among different orbits), as is evident from Fig. 3-B. Then the (approximate) selection rule for the $E2$ transitions mentioned above is violated and, therefore, in this case we cannot identify the phonon-bands. It should be emphasized that such an effect of "band-mixing" never occur in the conventional QPC theory. Namely the "band-mixing" due to the 3QP correlation is a "direct mixing" originated from the H_X and H_V interactions, whereas in the QPC theory the "band-mixing" can occur only through "indirect mixing" mediated by the coupling to the 1QP states (originated from the H_V interaction).

The way and the extent of the breaking of the "phonon-plus-odd-quasi-particle picture" will depend on various conditions. For instance, depending on shell structure and on the spins of collective states, there may exist a phonon-band which couples easily (or hardly) to the other bands. Therefore, we will investigate, in the following sections, the microscopic structure of breaking and persistency of the "phonon-plus-odd-quasi-particle picture" with the aid of the criteria given here.

§3. Persistency of phonon-band character and breaking of simple phonon picture

In the theory of the intrinsic excitations in spherical odd-mass nuclei, which is formulated in Chap. 2, the original $P+QQ$ Hamiltonian is transcribed into the "quasi-particle NTD space" as follows:

$$\left.\begin{aligned} &\boldsymbol{H}=\boldsymbol{H}^{(0)}+\boldsymbol{H}^{(\mathrm{int})}, \\ &\boldsymbol{H}^{(0)}=\mathbf{1}\cdot(H_0+H_X+H_V)\cdot\mathbf{1}=\sum_{\delta} E_\delta \boldsymbol{a}_\delta^\dagger \boldsymbol{a}_\delta+\sum_{nIK}\omega_{nI}\boldsymbol{Y}_{nIK}^\dagger \boldsymbol{Y}_{nIK}, \\ &\boldsymbol{H}^{(\mathrm{int})}=\mathbf{1}\cdot H_V\cdot\mathbf{1}=\sum_{\delta,nIK} V_{\mathrm{int}}(\delta, nI)\{\boldsymbol{Y}_{nIK}^\dagger \boldsymbol{a}_\delta+\boldsymbol{a}_\delta^\dagger \boldsymbol{Y}_{nIK}\}, \end{aligned}\right\} \quad (3\cdot1)$$

where $\boldsymbol{a}_\delta^\dagger$ and $\boldsymbol{Y}_{nIK}^\dagger$ denote the creation operators of the 1QP and dressed 3QP modes in the space, respectively. Here we have adopted the projection operator onto the "quasi-particle NTD subspace," $\mathbf{1}$, by which the modes with trans-

ferred seniority higher than three are neglected.

In the same way as in the conventional QPC theory, we have a free Hamiltonian $\boldsymbol{H}^{(0)}$ for the new type of elementary excitation modes if the (original) interactive force H_Y is neglected. However, since the collective 3QP correlations have already been taken into account in constructing the dressed 3QP modes, the spectra given by $\boldsymbol{H}^{(0)}$ now acquire abundant structures. The dressed 3QP mode can of course be decomposed into a phonon coupled with an odd quasi-particle in the limit where various 3QP correlation diagrams are all neglected. Hence, by comparing the characteristics of the low-energy excitation structures given by $\boldsymbol{H}^{(0)}$ with those of $\mathcal{H}^{(0)}$, we can see the breaking and persistency of the phonon-band in the QPC picture due to the collective 3QP correlations.

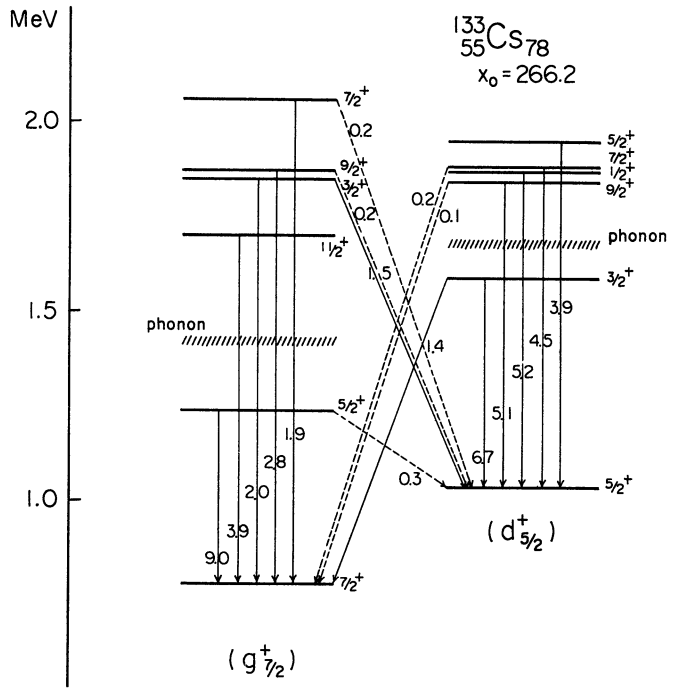

Fig. 4(a). Result of the calculations for the dressed 3QP states in ^{133}Cs. They are presented to show the breaking and persistency of the quintet structures based on the 1QP states with orbits $1g_{7/2}$ and $2d_{5/2}$. The presented level energies are those measured from the correlated ground state. The numbers appearing on the transition arrows give the $B(E2)$ values in unit of $e^2 10^{-50}$ cm^4, which are calculated with polarization charge $\delta e = 0.5e$ and with harmonic-oscillator-range parameter $b^2 = 1.0A^{1/3}$. The adopted value of χ_0 is related with the quadrupole-force strength χ through $\chi_0 = \chi b^4 A^{5/3}$ (MeV). For simplicity, the $E2$ transitions smaller than 0.1 and the other higher-lying states are both omitted from the figure. The parameters of the shell-model space used in this calculation are the same as those adopted by Kisslinger and Sorensen.[1]

With this aim, the calculated excitation spectra for odd-proton ^{133}Cs and ^{135}La are presented in Fig. 4. In this figure, the calculated $B(E2)$ values are also written on the transition arrows. Method of calculations and the adopted parameters are the same as are described in §2-Chap. 4. The quadrupole-force strengths are fixed so as to reproduce, by means of the RPA, the average energies of the 2^+ phonon states in the adjacent even-even nuclei. It should be noted here that the numerical examples are presented for ^{133}Cs and ^{135}La whose even-even neighbours are considered as exhibiting vibrational spectra.

The format of Fig. 4 is made so that the relationship to the spectrum characterized by the concept of phonon-band is visible. In odd-proton ^{133}Cs and ^{135}La, the $1g_{7/2}$ and $2d_{5/2}$ orbits lie near the chemical potential of protons. In this figure we are able to identify two families of states which belong to the phonon-band based on the $1g_{7/2}$- and the $2d_{5/2}$-1QP states, respectively. Needless to say, the two "quintets" (composed of the 2^+ phonon coupled with the $g_{7/2}$- and $d_{5/2}$-odd-quasi-particle, respectively) should be degenerated in energy in the hatched regions, *if we neglect the collective* $3QP$ *correlations completely*.

From Fig. 4, we can see the following characteristics:

(1) The energy-splittings of the quintets are very large, i.e., the level structure

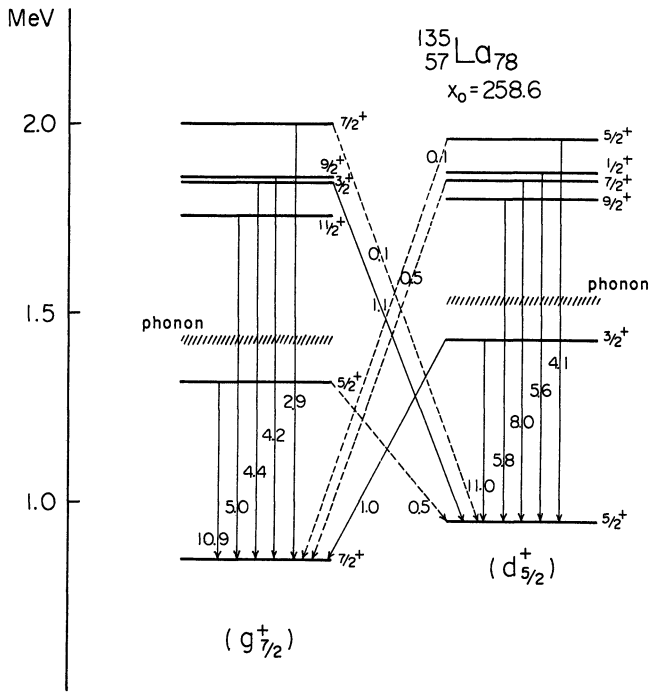

Fig. 4(b). Result of calculation for the dressed 3QP states in ^{135}La. Notations and parameters used are the same as in Fig. 4(a).

shows a drastic change from that of the simple phonon picture. The magnitudes of the splittings are comparable to (or even larger than) the excitation energies of phonons themselves. Clearly we are in a situation far from the zeroth-order picture of the QPC theory. Of course, from the viewpoint of the boson expansion methods, this fact implies that the couplings between the ideal-odd-quasi-particles and the ideal-phonons are too strong to be treated within a perturbational method.

(2) The splitting of the quintet which belongs to the ground band is larger than that of the excited band. The magnitude of the splitting decreases as the excitation energy of the band-head 1QP state becomes higher.

(3) Corresponding to the changes in level structure, the $E2$-transition probabilities (from the quintet to their band-head) also become different among the members of the quintet. As a gross property, the lower the excitation energy of the level, the larger the $B(E2)$ value.

(4) In each quintet with band-head spin j, the sum of $B(E2)$, $\sum_I B(E2; I\to j)$, becomes smaller than $5\times B(E2; 2^+\to 0^+)$ of the phonon transition calculated by means of the RPA. (In the phenomenological core-excitation model, we have $\sum_I B(E2; I\to j)=5\times B(E2; 2^+\to 0^+)$.)

In spite of these drastic changes of the excitation structure which evidently show the breaking of the simple phonon picture, we can still find the following characteristic:

(5) The property (characterizing the concept of phonon-band) that the inter $E2$ transitions are hindered compared to the intra $E2$ transitions is seen to persist rather well (aside from the $3/2^+$ states of ^{133}Cs in which the inter-transitions compete with the intra-transitions).

In the region of Cs and La isotopes, the low-energy-excitation structure is determined mainly by the competitions among the three effects; effect A (shown in Fig. 3-A) in the orbit $g_{7/2}$, effect A in the orbit $d_{5/2}$ and effect B (shown in Fig. 3-B) involving the orbits $g_{7/2}$ and $d_{5/2}$. Therefore, characteristic (5) suggests that, according to the criterion given in §2, effects A are dominant to effect B.

We can find the origin of this trend as follows: In the 3QP correlations among quasi-particles in different orbits (the effects B), the one which couples the $g_{7/2}$-band to the $d_{5/2}$-band contains, as a major part, the spin-flip matrix element $(d_{5/2}\|r^2Y_2\|g_{7/2})$ which is considerably smaller than the diagonal matrix elements, $(g_{7/2}\|r^2Y_2\|g_{7/2})$ and $(d_{5/2}\|r^2Y_2\|d_{5/2})$, contributing to effects A. Therefore, in spite of the drastic breaking of the simple phonon picture mentioned as characteristics (1)~(4), the concept of phonon-band is expected to persist in such a situation for shell structure. It is also interesting to recall that this condition of shell structure is common to that for the appearance of the dressed 3QP modes having ACS-like structure, e.g., the $5/2_2^+$ states in Cs and La isotopes.

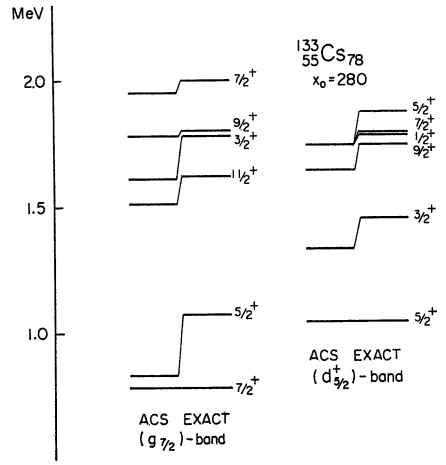

Fig. 5. Comparison between the result of exact calculation ("EXACT") and that of approximated one ("ACS") for the dressed 3QP states in ^{133}Cs. See the text for interpretation.

Figure 5 has been made to show the dominant role of effect A. Here the result of the exact calculation for the dressed 3QP modes is compared with that of the approximated one in which effects B are completely neglected. When effects B are neglected, the eigenvalue equation for the dressed 3QP modes is reduced to Eq. (3·23) of Chap. 3 with the orbit p now denoting the orbit of each band-head 1QP mode. We call such an approximation as "single-band approximation" or "ACS approximation." From Fig. 5, we can see that the excitation structure is determined in a major way by effects A, that is, the characteristics coming from effects A persist clearly even when effects B are included.

Then, as shown in §3-Chap. 3, the splitting of the multiplet depends on three factors; (i) the enhancement factor u_jv_j in the orbit j of the band-head 1QP mode, (ii) the enhancement factors $(u_bv_c+v_bu_c)$ in the core and (iii) the value of spin j of the band-head 1QP mode which is involved in the 3QP-correlation factor defined by Eq. (3·22) of Chap. 3.

Among these, an important consequence of the effect (i) is seen as the characteristic property (2) mentioned above. Remembering the fact that the more the orbit j of the odd quasi-particle becomes close to the chemical potential λ the larger the u_jv_j factor becomes, we can easily understand the origin of this property. Thus the role of the 3QP correlations, especially the one among quasi-particles in the same orbit lying near the chemical potential, is essential to determine the low-energy-excitation structure and becomes less important for high-energy excitations.

In concluding this section, however, it should also be stressed that the competition between effects A and B depends rather sensitively on the spin of the dressed 3QP mode*) and the quasi-particle-energy difference between

*) For instance, notice that effect A in the orbit $d_{5/2}$ is forbidden for the modes with spins 1/2, 5/2 and 7/2.

the shell-model orbits of interest. For instance, the breaking of the band structure for the specific states with spin $3/2^+$ in Cs isotopes can be understood to be a result of the balance of these effects. In fact, by comparing Fig. 4(a) with Fig. 4(b), we can see that the band character for the $3/2^+$ states is enhanced in La isotopes where effect A in the orbit $d_{5/2}$ becomes dominant for the first $3/2^+$ state (i.e., the ACS-like structure of the $3/2^+_1$ state is realized).

§4. Roles of correlation between proton- and neutron-quasi-particles

In this section, we investigate the microscopic structure of the dressed 3QP modes from the viewpoint of correlation between proton- and neutron-quasi-particles. At first, it should be mentioned that a strong correlation between proton- and neutron-quasi-particles is implicitly assumed in setting up the criterion given in §2. When we consider the difference in the effective charges of protons and neutrons, it is easy to understand that, without this strong correlation, the criterion given in conjunction with $E2$-transition property cannot be applied irrespective of odd-proton or odd-neutron nuclei. The reason is based on the fact that the motions of proton-quasi-particle-pairs and of neutron-quasi-particle-pairs are coupled strongly with each other due

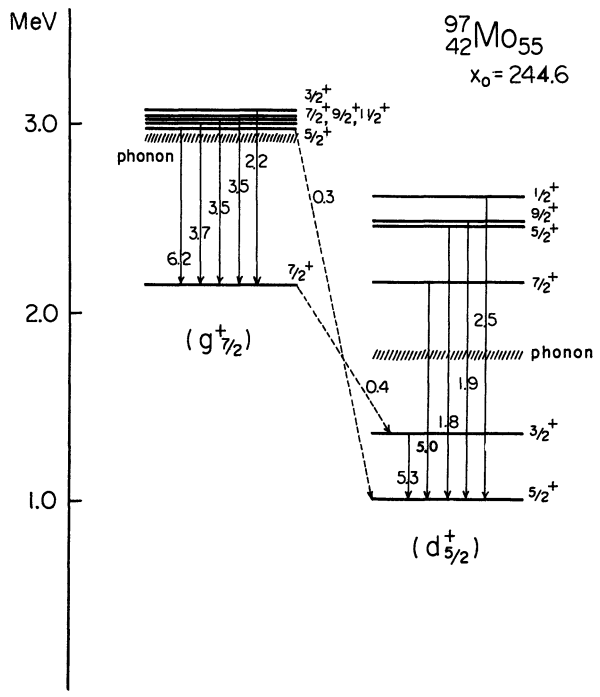

Fig. 6(a). Result of calculation for the dressed 3QP states in ^{97}Mo. Notations and parameters used are the same as in Fig. 4(a).

to the QQ force and the ground-state correlations play a role to enhance the cooperative effect between the motions of proton- and neutron-quasi-particle-pairs. This situation is just the same as in the case of the 2^+ phonon modes (in the doubly open even-even nuclei) described by means of the RPA with the $P+QQ$ force. Hence, as long as the shell structures in the vicinity of the chemical potential (for odd-number nucleons) are the same, we expect similar $E2$-transition property irrespective of odd-proton or odd-neutron nuclei.

Figure 6 shows the calculated results for odd-neutron ^{97}Mo and ^{105}Pd nuclei. The orbits participating most actively in the 3QP correlations in ^{97}Mo and ^{105}Pd are the $2d_{5/2}$ and $1g_{7/2}$ orbits which are the same as in ^{133}Cs and ^{135}La nuclei discussed in §3. By comparing the excitation structure shown in Fig. 6 with that of the odd-proton ^{133}Cs and ^{135}La nuclei shown in Fig. 4, we can see that the characteristics similar to those described as (1)~(5) in §3 hold also in the case of odd-neutron ^{97}Mo and ^{105}Pd nuclei. For ^{105}Pd nucleus, the picture of core-excitation model[7] has sometimes been used in interpreting

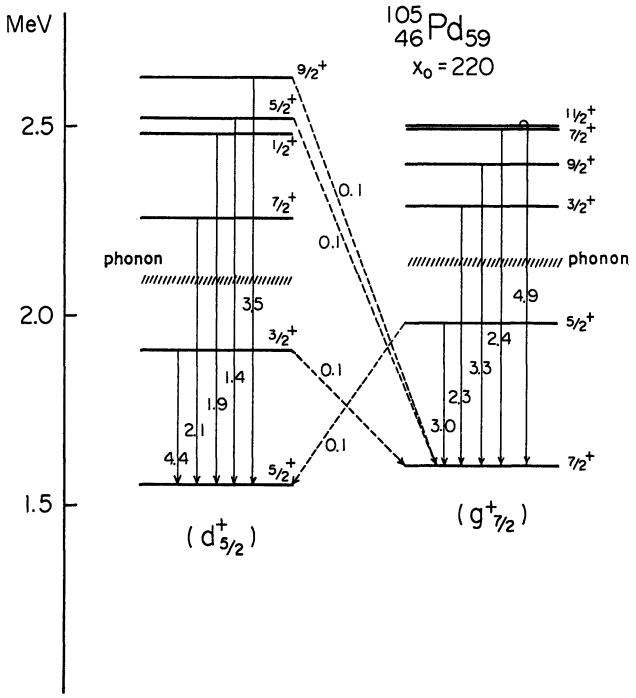

Fig. 6(b). Result of calculation for the dressed 3QP states in ^{105}Pd. Notations and parameters used are the same as in Fig. 4(a) except the following:
neutron single-particle energies;
$\epsilon(d_{5/2})=0.0$, $\epsilon(g_{7/2})=1.6$, $\epsilon(s_{1/2})=1.9$,
$\epsilon(h_{11/2})=2.0$ and $\epsilon(d_{3/2})=2.5$.
pairing-force strengths;
$G_p=29/A$ and $G_n=21/A$. (all in MeV)

the experimental data.[8),9)] From the present point of view, however, it is clear that such experimental facts can be considered to reflect the persistency of phonon-band character in ^{105}Pd and never to imply a realization of the weak coupling picture underlying the core-excitation model.

Now let us consider in more detail the role of proton-quasi-particles in the dressed 3QP modes in odd-neutron nuclei. (The same consideration can also be made for the role of neutron-quasi-particles in odd-proton nuclei.) As was already emphasized, the 3QP correlations can be regarded, in the language of quasi-particle-phonon-coupling picture, as arising from Pauli principle between the neutron-odd-quasi-particle and the quasi-particles constructing the phonon. Consequently, because of the absence of Pauli principle between proton- and neutron-quasi-particles, the triggering effects of the 3QP correlations (which violate the concept of phonon in odd-mass nuclei) are restricted within the neutron-quasi-particles. The following fact should be noted however. In the dressed 3QP mode, the component $\psi_{nI}(\rho\sigma;\alpha)$ and $\varphi_{nI}(\rho\sigma;\alpha)$,*) composed of proton-quasi-particle-pair $(\rho\sigma)$ plus a neutron-quasi-particle α *in the orbit a, can couple* with the component of the same type, $\psi_{nI}(\rho\sigma;\beta)$ and $\varphi_{nI}(\rho\sigma;\beta)$, having the neutron-quasi-particle β *in the orbit b* different from the orbit $a(b\neq a)$.**) This kind of "coupling" is mediated by the 3QP correlations among neutron-quasi-particles. (See Fig. 7.) Since the motion of proton-quasi-particles couples strongly with that of neutron-quasi-particles (through the QQ force), the magnitude of the mixing among the components, $\psi_{nI}(\rho\sigma;\alpha)$ and $\varphi_{nI}(\rho\sigma;\alpha)$ with various a, depends quite obediently on the magnitude of effects B in the 3QP correlations among neutrons. In this way, the fact that there exists a strong correlation between proton- and neutron-quasi-particles makes it possible to say as follows: "If effects B in the 3QP correlations are sufficiently strong among neutron-quasi-particles, then we can observe the breaking of the phonon-band structure in terms of the $E2$-transition properties." We can confirm this point from the comparison between Fig. 6(b) and Fig. 8(b). As will be discussed in §5, effect B in odd-neutron ^{115}Cd nucleus is considerably stronger than that in odd-neutron ^{105}Pd nucleus. As a con-

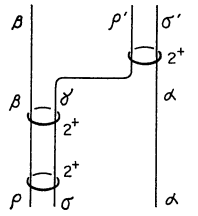

Fig. 7. Illustration of the 3QP correlation discussed in the text. Here, α, β, γ, ... denote the quantum numbers of the single-particle states for neutrons and ρ, σ, ... those for protons.

*) For definition of the amplitudes of the dressed 3QP mode, see Eq. (2.1) in Chap. 4.

**) Within the limit of neglecting the 3QP correlations, these two sets of components belong to different multiplets in the QPC theory, $(\dot{a}^{\dagger}_{a}\Gamma^{\dagger}_{2M})_{IK}|0)$ and $(\dot{a}^{\dagger}_{\beta}\Gamma^{\dagger}_{2M})_{IK}|0)$, characterized by the quantum numbers a and b, respectively.

sequence, we can see that the inter-band transitions in ^{115}Cd are larger than those in ^{105}Pd.

Now, recalling the enhancement factor (ii) mentioned in §3 (which is applicable for both cases A and B, of the 3QP correlations), we can say as follows: The major role of the proton-quasi-particles in the odd-neutron dressed 3QP mode is to enhance the collectivity of the mode, accompanying a rapid growth of the ground-state correlation. The growth of the collectivity due to such an effect is clearly seen by comparing the spectrum of single-closed-shell nucleus ^{117}Sn (Fig. 8(a)) with that of ^{115}Cd (Fig. 8(b)) in which two proton-holes are added to ^{117}Sn. Thus, although the proton-quasi-particles do not produce any 3QP correlations by themselves, they play an indispensable role to form the concept of dressed 3QP mode (in odd-neutron nuclei) as a collective mode of excitation.

§5. Case of low-spin orbits

Let us consider the calculated result for ^{115}Cd shown in Fig. 8(b). In this nucleus, the chemical potential for neutrons lies in the vicinity of the orbits $3s_{1/2}$ and $2d_{3/2}$. Since effects A are strictly forbidden in the orbit with spin

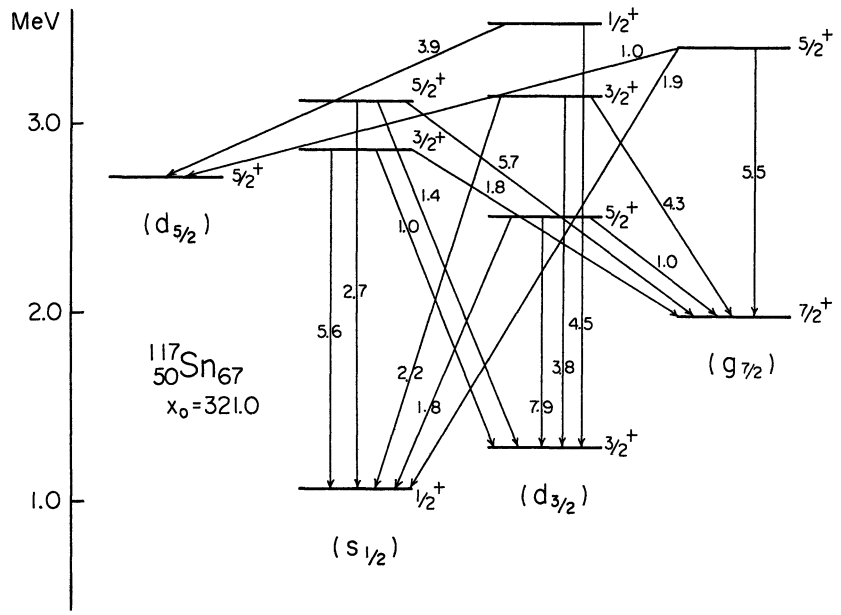

Fig. 8(a). Result of calculation for the dressed 3QP states in ^{117}Sn. Notations and parameters used are the same as in Fig. 4(a) except the following:
neutron single-particle energies;
$\epsilon(d_{5/2})=0.0$, $\epsilon(g_{7/2})=1.27$, $\epsilon(s_{1/2})=2.55$,
$\epsilon(h_{11/2})=3.25$, $\epsilon(d_{3/2})=3.24$. (all in MeV)
These values are taken from Ref. 10). The unit of $B(E2)$ values is $e^2\cdot10^{-51}$ cm^4.

$j<5/2$, effects B are expected to manifest themselves, in a relatively pure form, in the dressed 3QP modes which largely involve the low-spin orbits such as $3s_{1/2}$ and $2d_{3/2}$. In fact, Fig. 8(b) shows that we cannot definitely classify these dressed 3QP modes in terms of the criterion given in §2, since the many inter-band transitions are of the same order in magnitude with the intra-band transitions.*) This implies that, for the collective excitations standing on the 1QP states with low-spin ($j<5/2$) and with normal parity, the concept of phonon-band is broken down completely due to effect B.

It is noticeable in Fig. 8(b) that the "doublet" with spins $3/2^+$ and $5/2^+$, belonging to the $s_{1/2}$ phonon-band, is considerably shifted up in energy. The reason is understood as follows: In nuclei in which the $s_{1/2}$ orbit lies close to the chemical potential, the 2^+ phonon is largely composed of the quasi-particle-pair involving the $s_{1/2}$ quasi-particle. When the odd quasi-particle is lying just at the $s_{1/2}$ orbit, however, the excitations of such quasi-particle-pairs are strictly forbidden. This is easily understood when we recall the fact that the 3QP configurations with seniority $v=3$ are forbidden due to the Pauli principle if there exist *two* quasi-particles at the $s_{1/2}$ orbit. Thus, the excitation of the

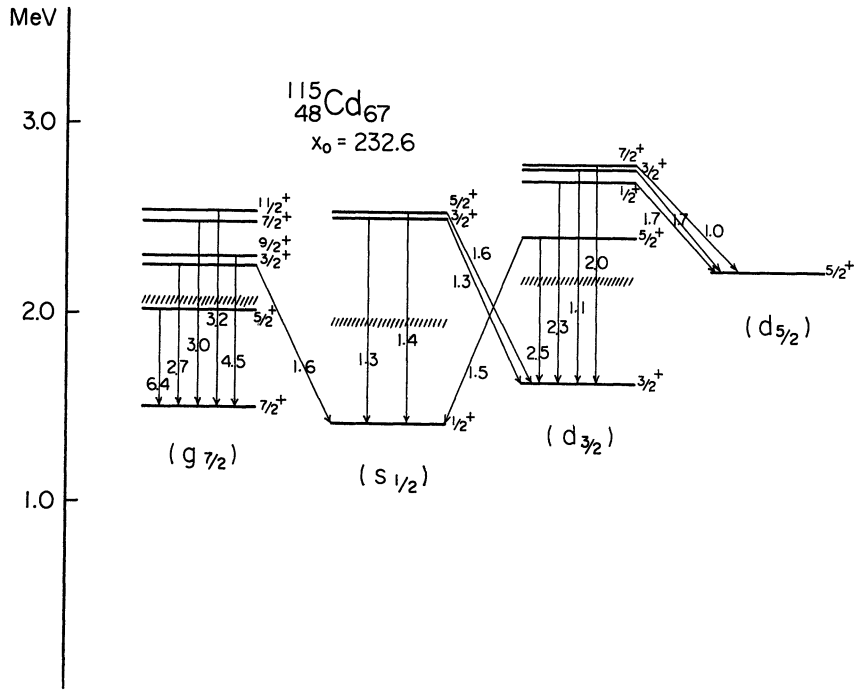

Fig. 8(b). Result of calculation for the dressed 3QP states in ^{115}Cd. Notations and parameters are the same as in Fig. 4(a).

*) Since the phonon-bands are difficult to identify in this case, the dressed 3QP states are classified in a rather arbitrary way in Fig. 8.

2^+ phonon of the core is highly hindered when there already exists the $s_{1/2}$ odd quasi-particle. Furthermore, in this case, we can expect the following trend: The microscopic structure of the 2^+ phonon itself should be changed drastically, since the main components of the 2^+ phonon are forbidden. As a consequence, the 3QP correlation among quasi-particles in different orbits tends to play an increasingly important role.

We have seen two typical examples in which either effect A or effect B is playing an essential role to govern the low-energy-excitation spectrum: In nuclei in which the orbits with spin $j \geqq 5/2$, such as $d_{5/2}$ and $g_{7/2}$, lie in the vicinity of the chemical potential, the 3QP correlation in the same orbit plays a dominant role (case A). On the other hand, in nuclei in which the orbits with spin $j<5/2$, such as $s_{1/2}$ and $d_{3/2}$, lie in the vicinity of the chemical potential, the 3QP correlation among different orbits plays a dominant role (case B). The degree of the breaking of the phonon-band character is determined by the competition between effects A and B. Although present accumulation of the experimental

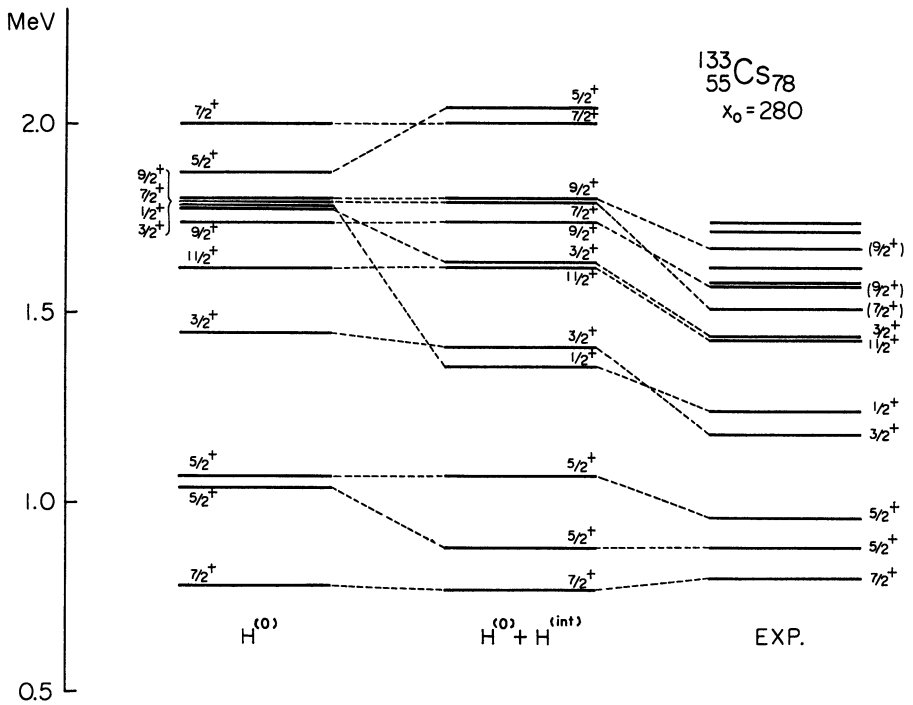

Fig. 9(a). Energy shifts due to the coupling effects between the dressed 3QP- and 1QP-modes in ^{133}Cs. The energy levels denoted by $\boldsymbol{H}^{(0)}$ show the result calculated by neglecting the coupling effects, while those denoted by $\boldsymbol{H}^{(0)}+\boldsymbol{H}^{(\mathrm{int})}$ show the result calculated by taking the coupling effects into account. The experimental energy levels denoted by EXP are taken from Ref. 11). The parameters of the calculations are the same as in Fig. 4(a) except that the adopted quadrupole-force parameter χ_0 is a little stronger.

data on the $E2$ transitions between excited states is not sufficient to allow us a systematic comparison with the theoretical calculations, the current rapid progress in the measurement of these transitions is expected to elucidate further many interesting structures of the 3QP correlations.

§6. Couplings between dressed 3QP- and 1QP-modes

So far, we have neglected the effects originating from the interactive force H_Y. The essential role of this type of interactions is to produce couplings between different kinds of elementary excitation modes. In the QPC theory, the effects are represented by $\mathcal{H}^{(\mathrm{int})}$ in Eq. (2·2), which change the number of phonons by one accompanying a scattering of odd quasi-particle. On the other hand, in the theory developed in Chap. 2, the effects manifest themselves as couplings between the dressed 3QP modes and the 1QP modes, $\boldsymbol{H}^{(\mathrm{int})}$ in Eq. (3·1), in the quasi-particle NTD subspace. Since in the QPC theory, the change of excitation spectrum from that given by $\mathcal{H}^{(0)}$ is attributed entirely to this special type of couplings $\mathcal{H}^{(\mathrm{int})}$, and also since the low-lying spectrum given

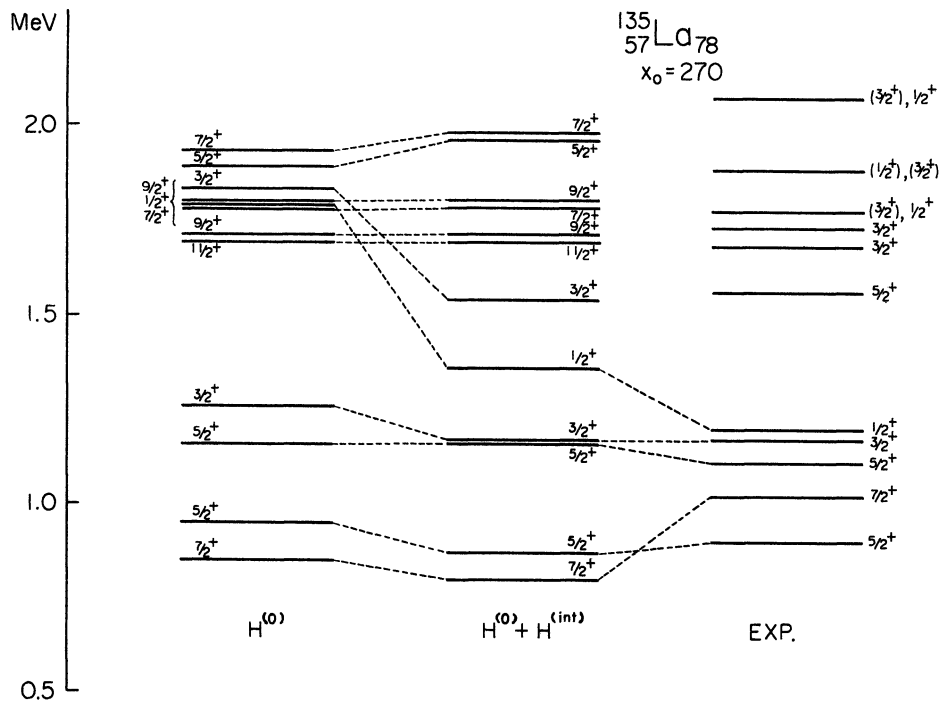

Fig. 9(b). Energy shifts due to the coupling effects between the dressed 3QP- and 1QP-modes in ^{135}La. Notations are the same as in Fig. 9(a). The experimental energy levels are taken from Ref. 12). The parameters of the calculation are the same as in Fig. 4(b) except that the adopted quadrupole-force parameter χ_0 is a little stronger.

by $\boldsymbol{H}^{(0)}+\boldsymbol{H}^{(\mathrm{int})}$ corresponds to that given by $\mathcal{H}^{(0)}+\mathcal{H}^{(\mathrm{int})}$ *if we neglect the 3QP correlations completely,* the problem of how the effects of H_Y are changed (from those evaluated in the QPC theory) by the inclusion of the 3QP correlations will be of great significance.

Figure 9 and Tables I and II show the calculated results for ^{133}Cs and ^{135}La. From the comparison between the spectrum of $\boldsymbol{H}^{(0)}$ and that of $\boldsymbol{H}^{(0)}+\boldsymbol{H}^{(\mathrm{int})}$, we can see that $\boldsymbol{H}^{(\mathrm{int})}$ does not change the low-energy-excitation spectrum given by $\boldsymbol{H}^{(0)}$ so drastically, except for some states with low-spins $1/2^+$ and $3/2^+$. This is because of the newly arised reduction effect which is absent in the QPC theory and makes the effects of H_Y interaction to be less important for low-lying states.

The mechanism of this reduction effect can be understood as follows: Let us consider two sets of diagrams (with $a \neq b$) shown in Fig. 10. In the QPC theory, each sum of the diagrams, Figs. 10(a) and 10(b), contributes *separately* to the effective coupling strength, $\bar{\chi}_{\delta a}(\nu)$ or $\bar{\chi}_{\delta\beta}(\nu)$, in $\mathcal{H}^{(\mathrm{int})}$. However, when we take the 3QP correlations into account, these two sets of diagrams *both* contribute to the *single* effective coupling strength $V_{\mathrm{int}}(d; nI)$ in $\boldsymbol{H}^{(\mathrm{int})}$. As is seen from the expression of $V_{\mathrm{int}}(d; nI)$ given by (4·3) in

Table I. Calculated $B(E2)$ values for ^{133}Cs. The states in the first column are labeled according to the level ordering given in Fig. 9(a). The parameters used are the same as in Fig. 9(a). The $B(E2)$ values calculated by neglecting the coupling effects are listed in the second column, while those calculated by taking account of the coupling effects are listed in the third column. They are compared to the experimental values listed in the fourth column. The unit is $e^2\cdot 10^{-50}\,\mathrm{cm}^4$. The polarization charge $\delta e=0.5e$ and the harmonic-oscillater-range parameter $b^2=1.0A^{1/3}$ are used in the calculation. Experimental data are taken from Ref. 11).

transitions	$B(E2)^{1)}$	$B(E2)^{2)}$	$B(E2)^{\mathrm{exp}}$
$5/2_2^+ \to 7/2_1^+$	11.69	11.62	10.4±1.2
$11/2_1^+ \to 7/2_1^+$	4.25	4.21	10.0±1.1
$3/2_2^+ \to 7/2_1^+$	2.41	3.83	1.4±0.2
$9/2_2^+ \to 7/2_1^+$	3.09	3.06	7.4±0.8
$7/2_3^+ \to 7/2_1^+$	1.94	1.90	1.42±0.17
$3/2_1^+ \to 5/2_1^+$	9.48	9.52	
$9/2_1^+ \to 5/2_1^+$	5.94	5.10	
$1/2_1^+ \to 5/2_1^+$	5.89	7.27	
$7/2_2^+ \to 5/2_1^+$	5.24	4.46	
$5/2_3^+ \to 5/2_1^+$	4.28	1.42	
$3/2_2^+ \to 5/2_1^+$	1.27	0.11	
$3/2_1^+ \to 7/2_1^+$	1.33	0.31	7.2±0.8
$5/2_2^+ \to 5/2_1^+$	0.46	0.35	
$5/2_1^+ \to 7/2_1^+$	0.02	0.27	

Table II. Calculated $B(E2)$ values for ^{135}La. Notations and the parameters used are the same as in Table I and Fig. 9(b), respectively. Experimental data are taken from Ref. 12).

transitions	$B(E2)^{1)}$	$B(E2)^{2)}$	$B(E2)^{exp}$
$5/2_2^+ \to 7/2_1^+$	18.86	18.13	22.6
$11/2_1^+ \to 7/2_1^+$	5.45	5.21	
$3/2_2^+ \to 7/2_1^+$	5.47	7.47	
$9/2_2^+ \to 7/2_1^+$	4.55	4.35	
$7/2_3^+ \to 7/2_1^+$	4.16	1.37	
$3/2_1^+ \to 5/2_1^+$	15.41	14.09	$\geqq$4.9
$9/2_1^+ \to 5/2_1^+$	6.46	5.79	
$7/2_2^+ \to 5/2_1^+$	5.78	5.18	
$1/2_1^+ \to 5/2_1^+$	6.07	7.68	$\geqq$20.2
$5/2_3^+ \to 5/2_1^+$	4.71	2.85	
$3/2_2^+ \to 5/2_1^+$	0.62	0.32	
$3/2_1^+ \to 7/2_1^+$	1.15	0.002	$\geqq$0.1
$5/2_2^+ \to 5/2_1^+$	0.92	0.25	1.7
$5/2_1^+ \to 7/2_1^+$	0.003	0.31	1.8

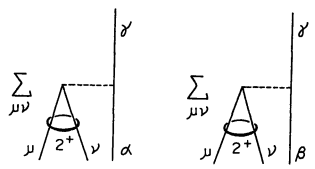

(a) (b)

Fig. 10. Two sets of the matrix elements of interactive force H_Y. The sets (a) and (b) are distinguished with each other by the difference in one of the shell-model orbits, i.e., $a \neq b$. The quantum numbers written in this figure, $\alpha \equiv (a, m_a) \equiv (n_a l_a j_a, m_a)$, $\beta, \gamma, \ldots$ can be interpreted as; for instance, α, β and γ denote the quantum numbers of the single-particle states for neutrons and μ and ν those for protons. The diagrams in the sets (a) and (b) contribute separately to the effective coupling strength $\bar{\chi}_{\gamma\alpha}$ and $\bar{\chi}_{\gamma\beta}$, respectively, in the QPC theory. On the other hand, they both contribute simultaneously to the effective coupling strength $V_{\text{int}}(c; nI)$ in the proposed theory.

Chap. 4, the phase relations between the matrix elements belonging to different sets of diagrams (each of which is represented in Fig. 10(a) or Fig. 10(b)) are governed by the relative phases of the amplitudes, e.g., $\psi_{nI}[rs(2)a]$ and $\psi_{nI}[rs(2)b]$, and also by the quadrupole matrix elements, $R(ad) \equiv 5^{-1/2} (a \| r^2 Y_2 \| d) \cdot (u_a u_d - v_a v_d)$ and $R(bd)$. Consequently, even when all the diagrams belonging to a single set (with definite a) contribute in phase, we have no guarantee of the coherent property among different sets of diagrams (with various a). In fact, the calculated results show that they contribute generally

in random phase, namely, they cancell one another. This is the case especially for the lowest-lying mode with a given spin $I>1/2$.

Additional reasons to weaken the effective coupling strength $V_{\text{int}}(d; nI)$ were already stated in §4-Chap. 4.

Now let us recall the characteristic dependence of the H_Y interaction on the reduction factor, $(u_a u_{\bar{a}}-v_a v_{\bar{a}})$. This factor is *small* for the quasi-particles lying near the chemical potential. In the special cases where a pair of orbits a and d are occupied just so as to make the factor nearly zero, e.g., each just half full, the effect of H_Y vanishes. Within the framework of the QPC theory, a consequence of such a property has indeed been confirmed experimentarily in the $E2$-transition properties between the low-lying states which are both mainly composed of the 1QP states.[6] Since this property of H_Y is endowed to the effective coupling strengths, both in the QPC theory and in the present theory, it is evident that the latter conserves the major success of the former. Furthermore, in the proposed theory, we have the (afore-mentioned) new reduction effect originated from the 3QP correlations which depend on the enhancement factor $(u_a v_{\bar{a}}+v_a u_{\bar{a}})$ becoming large in the neighbourhood of the chemical potential. Obviously, this fact magnifies the above-mentioned property of reducing the H_Y effect.

Thus we can say that the couplings of the dressed 3QP modes to the 1QP modes are significantly hindered *if they are both in low-lying states near the ground state.* This fact is in accord with the general principle: "If eigenmodes were properly chosen, couplings to different eigenmodes should be weak."

On the other hand, for the higher excitations, the (above-mentioned) mechanism becomes less effective. Thereby, if the 1QP modes lie in higher excited states, their couplings to the dressed 3QP modes (lying below them) become relatively significant. This is the case for the $1/2^+$ and $3/2^+$ states in ^{133}Cs and ^{135}La nuclei shown in Fig. 9.

A tentative comparison between the calculated results and the experimental data (Fig. 9) shows that the proposed theory can reproduce qualitative characteristics of the low-energy excitations quite well. Here it should be stressed that we have adopted no systematical fitting-procedures by adjusting parameters. Therefore, in view of the rapid accumulation of experimental data, more detailed analysis based on the proposed theory should be very promising.

We conclude this section by observing the following point which is exceptional to this promising results of calculations: Although level structures are nicely reproduced, the calculated excitation energies of the dressed 3QP states are, in average, higher than the corresponding experimental ones, if we choose the strength of the QQ force so as to fit the average energy of 2^+ phonons in the adjacent even-even nuclei, $\bar{\omega}_{2^+}(N,Z)=1/2\{\omega_{2^+}(N,Z-1)+\omega_{2^+}(N,Z+1)\}$.

This rather general tendency may be due to the present limited truncation of the quasi-particle NTD space, that is, the neglect of modes with transferred seniority higher than three. In addition to this, the following fact should also be emphasized: What we have discussed up to now is the intrinsic excitation modes in the quasi-spin space, and the couplings between intrinsic- and (pairing-) collective-modes have been completely neglected.

§7. Concluding remarks

Microscopic structure of breaking and persistency of the conventional "phonon-plus-odd-quasi-particle picture" has been investigated by putting special emphasis on the deviations of $E2$-transition properties from those expected by the concept of phonon-band. It has been demonstrated that the simple phonon picture for spherical odd-mass nuclei is seriously broken due to the collective 3QP correlations among quasi-particles lying near the chemical potential. In particular, the breaking and persistency of the phonon-band character have been shown to be essentially dependent on the characteristics of the 3QP correlation. The effect of H_V interaction has also been shown to be significantly affected by the inclusion of this correlation. The microscopic structure of the 3QP correlation depends, in turn, on details of the shell structure in the vicinity of the chemical potential. Accordingly, results of the calculation have been exemplified for two classes of nuclei in which either high-spin or low-spin orbits lie near the chemical potential. From these investigations, it is now clear that the 3QP correlation should be regarded as an elementary correlation in low-energy excitations. In fact, a large body of experimental data illuminating rich aspects of the many-quasi-particle correlations is now accumulating. (See, for instance, the progress report by Meyer.[13])

The effects of the 3QP correlation (based on the Pauli principle between the odd quasi-particle and the quasi-particles composing the phonon) have so far been neglected by the argument that a phonon contains only a small amplitude for the presence of any particular quasi-particle.[6] However, this argument is not correct. The 3QP correlation is essentially different from the "static" effects such as the blocking effect. Rather, it is a "dynamical" correlation induced by the presence of the odd quasi-particle: In such low-energy-excitation mode as the 2^+ phonon, as is well known, the quasi-particles lying near the chemical potential play an essential role in constructing the mode. When the "odd quasi-particle" is also added near the chemical potential, the quadrupole force (H_X and H_V) acts upon both the quasi-particles constructing the 2^+ phonon and the "odd quasi-particle" without discrimination. Therefore, the collective 3QP correlation also tends to grow significantly, as the collective 2QP correlation becomes stronger (,i.e., as the excitation energy of the 2^+ phonon becomes smaller). What we have investigated from Chap. 3

to this chapter can be regarded as clarifying the actual physical situation for this process. The conclusions obtained here are, therefore, closely connected with the dynamics of the $P+QQ$ force model.[6] Accordingly, the problem whether they are specific to the $P+QQ$ force model or more general will be examined in the succeeding chapter.

Of course, these conclusions do not exclude a possibility of a decomposition among many-quasi-particles if, e.g., some of them lie far from the chemical potential: In some cases of physical situations in shell structure, there may be frequent occurrence of a possibility that the dressed n-quasi-particle mode with $n>3$ can be approximately decomposed into the correlated cluster in the valence shell and the phonons of the "core." Recall here that such a possibility was already pointed out in Chaps. 3 and 4 in relating the picture of the dressed 3QP mode to that of the Alaga model.[14),15)]

References

1) L. S. Kisslinger and R. A. Sorensen, Rev. Mod. Phys. **35** (1963), 853.
2) S. Yoshida, Nucl. Phys. **38** (1962), 380.
3) M. Yamamura, Prog. Theor. Phys. **33** (1965), 199.
4) F. Dönau and D. Janssen, Nucl. Phys. **A209** (1973), 109.
5) E. Marshalek, Nucl. Phys. **A224** (1974), 221, 245.
6) D. R. Bes and R. A. Sorensen, *The pairing-plus-quadrupole model, Advances in Nuclear Physics* (Plenum Press), Vol. 2 (1969), p. 129.
7) A. de Shalit, Phys. Rev. **122** (1961), 1530.
8) H. Kawakami and K. Hisatake, Nucl. Phys. **A149** (1970), 523.
9) K. Krien, E. H. Spejewski, R. A. Nauman and H. Hubel, Phys. Rev. **C6** (1972), 1847.
10) E. J. Schneid, A. Prakash and B. L. Cohen, Phys. Rev. **156** (1967), 1316.
11) B. W. Renwick et al., Nucl. Phys. **A208** (1973), 574.
12) Y. Nagai and K. Hisatake, J. Phys. Soc. Japan **36** (1974), 1501.
13) R. A. Meyer, "*Recent Developments in the Description of Odd-Mass Nuclei.*", in *International Conference on γ-Ray Transition Probabilities, Delhi, India, 1974.*
14) G. Alaga, Bull. Am. Phys. Soc. **4** (1959), 359; *Rendiconti Scuola Internazionale,* Varenna, 40 corso (1967), 28.
15) V. Paar, Nucl. Phys. **A211** (1973), 29.

Chapter 6. Comparison between Results with the $P+QQ$ Force and with More Complex Residual Force

Masahiko FUYUKI, Atsushi KURIYAMA,*
Kenichi MATSUYANAGI** and Tōru SUZUKI**

Department of Physics, Osaka University, Toyonaka, Osaka 560
**Department of Physics, Kyushu University, Fukuoka 812*
***Department of Physics, Kyoto University, Kyoto 606*

(Received June 30, 1975)

§ 1. Introduction

From Chap. 3 to Chap. 5, microscopic structure of collective excitations in spherical odd-mass nuclei has been discussed with the use of the pairing-plus-quadrupole ($P+QQ$) force. Since we have widely employed characteristic properties of the quadrupole force, it is indispensable to examine whether or not the conclusions obtained from Chap. 3 to Chap. 5 are specific to the $P+QQ$ force. The aim of this chapter is to examine the effects of the other components of residual interaction which are neglected in the $P+QQ$ force model. With this aim, we make a comparison between the results calculated by using the quadrupole force and those calculated by using the central force with Gaussian radial dependence. In §§ 2 and 3, comparisons between the results of the $P+QQ$ force and those of the Gaussian force are made for the case of collective excited states with positive parity in Se isotopes. These states provide a good example in which we can see the effects of the other components of residual interaction in a relatively simple way. In § 4, as an alternative example, we present the results for single closed shell Sn isotopes in which quadrupole collectivity of the excited states is not so strong as in the case of Se isotopes. Hence, we can learn from these examples the relative importance of the neglected components of residual interaction in relation to the quadrupole collectivity of the states of interest. Needless to say, the theory developed in Chap. 2 is applicable for any residual interaction. However, we do not extend our present purpose to looking into the details of residual interactions themselves. In § 5, we add a few remarks concerning further refinements of the analysis.

§ 2. Dressed three-quasi-particle $7/2^+$ states in Se isotopes

We solve the eigenvalue equation for the dressed three-quasi-particle (3QP) mode given by Eq. (3·3) of Chap. 2 with the use of conventional Gaussian

force. The full expression of the matrix elements entering into the eigenvalue equation is given in Appendix 6A. The Gaussian force adopted here is the one without any exchange mixture, i.e.,

$$V(r) = -V_0 \exp(-r^2/r_0^2) \tag{2·1}$$

with $r=|\boldsymbol{r}_1-\boldsymbol{r}_2|$. As usual, the matrix elements of the Gaussian force are calculated by using harmonic oscillator wave functions with $\hbar\omega=41A^{-1/3}$ MeV. Then the matrix elements depend only on the ratio of the force-range r_0 to the range-parameter of the harmonic oscillator potential $b=(\hbar/M\omega)^{1/2}$. We adopt the method of Horie and Sasaki[1] in calculating these matrix elements.

Figure 1 shows the result of calculations for the "anomalous coupling" $7/2^+$ states in Se isotopes as the dressed 3QP states. The shell-model space adopted here is composed of the orbits $\{1f_{5/2}, 2p_{3/2}, 2p_{1/2}, 1g_{9/2}\}$ for both protons and neutrons. The single-particle energies used are the same as those of Kisslinger and Sorensen.[2] In the conventional treatment, where we use the Gaussian force as an effective interaction, the BCS equation determining the quasi-particle energies E_a and the coefficients of the Bogoliubov transformation (u_a, v_a) is also solved by using the Gaussian force. However, in this calculation, we have used the constant pairing force in the BCS equation, since our aim is to compare the results of the Gaussian-force case with those of the $P+QQ$ force case. This implies that the Gaussian force is regarded

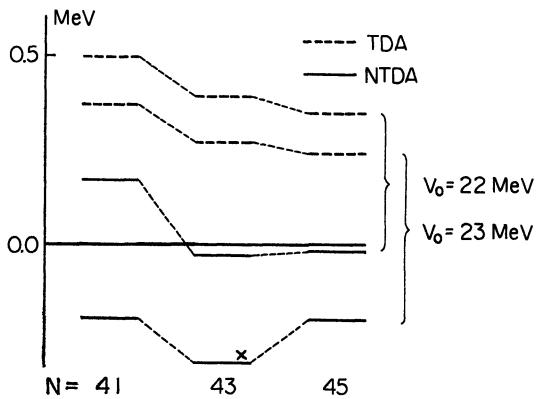

Fig. 1. Excitation energies of the dressed 3QP $7/2^+$ states in Se isotopes calculated with the use of the Gaussian force. The energies are measured from the 1QP $9/2^+$ states. The range parameter of the Gaussian force defined by (2·1) is fixed at 2.0 fm, while the calculated results for two choices of the force-strength V_0, i.e., V_0=22MeV and 23MeV, are shown. The solid lines represent the results in the new-Tamm-Dancoff approximation, while the broken lines in the Tamm-Dancoff approximation. The symbol × denotes the occurrence of complex eigenenergy.

here as a residual interaction among quasi-particles. This is in accord with our present aim of looking into the difference between the Gaussian and quadrupole forces in characterizing the microscopic structure of the dressed 3QP mode.

From Fig. 1, we can see that the $7/2^+$ states become the lowest-lying dressed 3QP states for a reasonable choice of the force-range parameter r_0. The reason for this particular favouring of the $7/2^+$ state is very similar to that in the $P+QQ$ force model (discussed in detail in Chap. 3): Since the square cfp of the type $[j^2(2), j;\ I|\}j^3;\ I\ v=3]^2$ takes the maximum value when $I=j-1$, the $7/2^+$ state involves the component $\{g^2_{9/2}(J=2)g_{9/2}\}_{I=7/2}$ as the maximum one among the components of the type $\{g^2_{9/2}(J)g_{9/2}\}_I$.*) Accordingly, the $7/2^+$ state has a large energy gain due to the relatively large matrix elements of the force, $G((\nu g_{9/2})^2\ (\nu g_{9/2})^2;\ 2)$ and $F(rs(\nu g_{9/2})^2;\ 2)$.**) The matrix element $G((\nu g_{9/2})^2\ (\nu g_{9/2})^2;\ 2)$ mainly contributes to increase the diagonal matrix element in the eigenvalue equation (3·3) of Chap. 2, while the matrix elements $F(rs(\nu g_{9/2})^2;\ 2)$ mainly contributes to increase the components of the type $\{rs(2^+)\nu g_{9/2}\}$.

One of the important characteristics of the quadrupole force is the special parity-selection property, i.e.,

$$(a\|r^2 Y_2\|b)=0 \qquad \text{when } (-)^{l_a+l_b}=-1. \tag{2·2}$$

This property of the quadrupole force plays an efficient role in the discussion of the $7/2^+$ state in terms of the $P+QQ$ force, owing to the special situation of shell structure in which the high-spin, unique-parity orbit is being filled with odd-number nucleons. In fact, the parity-selection property greatly simplified the discussions in Chap. 3. In the case of the Gaussian force, we have no such property. Accordingly, the dressed 3QP $7/2^+$ mode under consideration contains various kinds of components, for example, the components corresponding to the $p_{1/2}$ quasi-particle coupled with the 3^- phonon. In spite of the inclusion of such kinds of components into the eigenvalue equation, we can see that the predominant role of the quadrupole correlation in characterizing the microscopic structure of the $7/2^+$ state does not change in any significant way. Namely, these components neglected in the $P+QQ$ force model contribute only as a small perturbation to the low-lying $7/2^+$ state.

Now, in order to see the effect of the backward-going diagrams (originated from the ground-state correlation) on the excitation energy of the $7/2^+$ state, let us consider the quantity

*) The components of the amplitudes of the dressed 3QP modes are defined in Appendix 6A; see also Appendix 4A for the method of providing the orthonormal basis vectors in the coupled-angular-momentum representation.

**) The matrix elements of the force, G and F, are defined in Appendix 1A.

$$\delta B=\frac{\omega_{TD}-\omega_{NTD}}{3E-\omega_{TD}}, \tag{2·3}$$

where E denotes the energy of the $g_{9/2}$ neutron quasi-particle and $\omega_{TD}(\omega_{NTD})$ the energy of the (dressed) 3QP mode in the (new) Tamm-Dancoff approximation. For the parameters $V_0=23$ MeV and $r_0=2$ fm, the ratio of δB (Gaussian) to δB (quadrupole) takes the following value:

$$\frac{\delta B(\text{Gaussian})}{\delta B(\text{quadrupole})}=\frac{0.21}{0.94}=0.22 \tag{2·4}$$

for the $7/2^+$ state in ^{79}Se. Thus, in the case of the Gaussian force, the effect of the backward-going diagrams becomes smaller compared to the case of the quadrupole force. However, it should be emphasized that they sensitively affect both the excitation energy and the amplitudes (of the dressed 3QP mode), since the $7/2^+$ states lie very near to the critical point for the instability of the spherical BCS vacuum.

Figure 2 shows the main amplitudes of the dressed 3QP $7/2^+$ mode under consideration. In this figure, the corresponding amplitudes calculated by using the quadrupole force are also written for the sake of comparison. We can see that the correspondence between the amplitudes given by the Gaussian force and those given by the quadrupole force is remarkable in both their relative phases and magnitudes.*) For instance, the main components are, for both cases, of the types $\{(g_{9/2})^3\}$, $\{ab(2^+)g_{9/2}\}$ and $\{rs(2^+)g_{9/2}\}$. Furthermore, their relative magnitudes show the similar trend for both cases.

As for the difference between the two cases, we can see in Fig. 2 that, in the ^{79}Se nucleus, the backward-going amplitudes in the case of the quadrupole force are larger than those in the case of the Gaussian force. Correspondingly, the forward-going amplitudes in this case are amplified as a whole. In Fig. 2, we can also see that the backward-going amplitude of the type $\{(g_{9/2})^3\}$ becomes notably smaller in the case of the Gaussian force. The reason for this may be found in the fact that, in the Gaussian-force case, the G-type and F-type matrix elements cancel each other[3] in the submatrix $\boldsymbol{A}$ in the eigenvalue equation (3·3) of Chap. 2. Therefore, the phase relation among different components connecting neutron-quasi-particle pairs in the submatrix $\boldsymbol{A}$ becomes quite random in comparison with that among corresponding components in the submatrix $\boldsymbol{D}$ for the forward-going amplitudes. This trend is similar to that in the RPA with the use of the Gaussian force (for the single-closed shell nuclei). However, we should be careful in the fact that the relative magnitude of the G-type and F-type matrix elements depends sensitively on the range parameter r_0. On the other hand, such a destructive

*) In the comparison, we should be careful in treating the phase convention of the single-particle wave-functions.

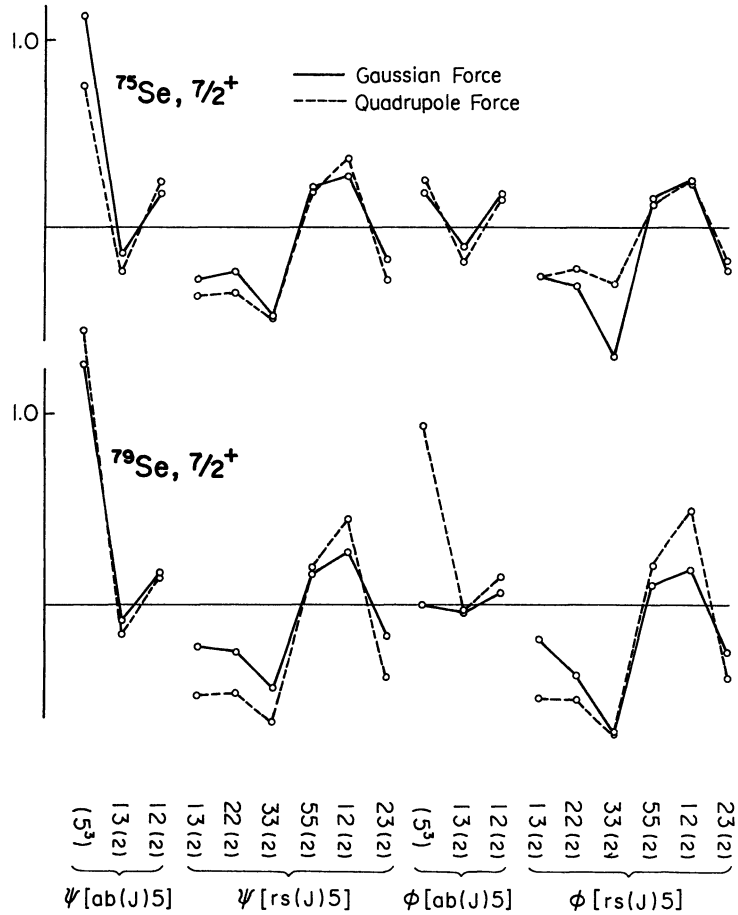

Fig. 2. Main amplitudes of the dressed 3QP $7/2^+$ modes in Se isotopes. The results calculated with the Gaussian force are connected by solid lines, while those with the quadrupole force are connected by broken lines. The range parameter and force strength of the Gaussian force are fixed at $r_0=2.0$ fm and $V_0=23$MeV, respectively. (These values are always adopted in the discussion in §§2 and 3.) The $P+QQ$ force-parameters are; $G=24/A$ MeV for both protons and neutrons, $\chi_0=230$ MeV. The definition of the amplitudes is given in Appendices 6A and 4A. In this figure, the following abbreviation is used to specify the shell-model orbit:

$1\equiv(2p_{1/2})$, $2\equiv(2p_{3/2})$, $3\equiv(1f_{5/2})$, $5\equiv(1g_{9/2})$.

effect between the G-type and F-type matrix elements is absent in the matrix elements connecting proton and neutron quasi-particle pairs.[3] Consequently, the backward-going amplitudes of the type $\{rs(2^+)g_{9/2}\}$ become significantly large in the Gaussian-force case as well as in the quadrupole-force case.

Although we can find such a few differences in fine structure which are dependent on details of the force, the correspondence of the main amplitudes between the two cases is remarkable. Thus, we can conclude that the micro-

scopic structure of the collective $7/2^+$ state in the Gaussian-force case is very similar to that in the quadrupole-force case.

§ 3. Other collective states with positive parity in Se isotopes

Next, let us consider other collective states with positive parity in Se isotopes. These states are the ones corresponding to the quintet composed of one-quasi-particle and one-phonon in the quasi-particle-phonon-coupling theory. Considering these states also as the dressed 3QP states, we have carried out the calculation with the use of the Gaussian force. The parameters used are the same as in the preceding section.

Figure 3 shows the result of the calculation. In this figure, the result obtained by using the quadrupole force is also shown for the sake of comparison. We can clearly see that the calculated level sequence is the same as that in the case of the quadrupole force. This fact indicates that the microscopic structure of these states obtained by using the Gaussian force is very similar to that obtained by using the quadrupole force. The main amplitudes of the dressed 3QP modes are shown in Figs. 4 and 5. In Fig. 4 are shown the main amplitudes of the $5/2^+$ mode. From the comparison between the Gaussian-force case (solid line) and the quadrupole-force case (broken line), we can say that the correspondence between the two cases holds fairly well not

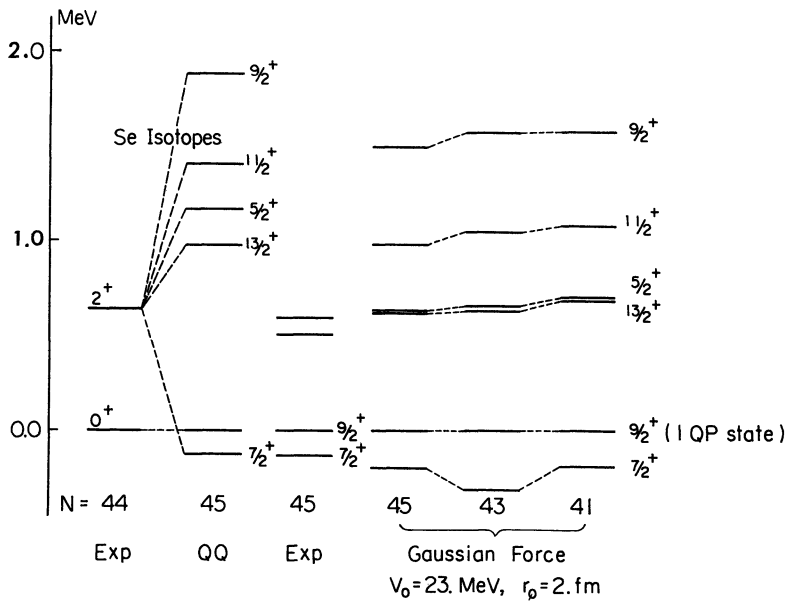

Fig. 3. Excitation energies of the dressed 3QP states with positive parity in Se isotopes. Results calculated by using the Gaussian force are compared with those by the quadrupole force. Parameters used are the same as in Fig. 2.

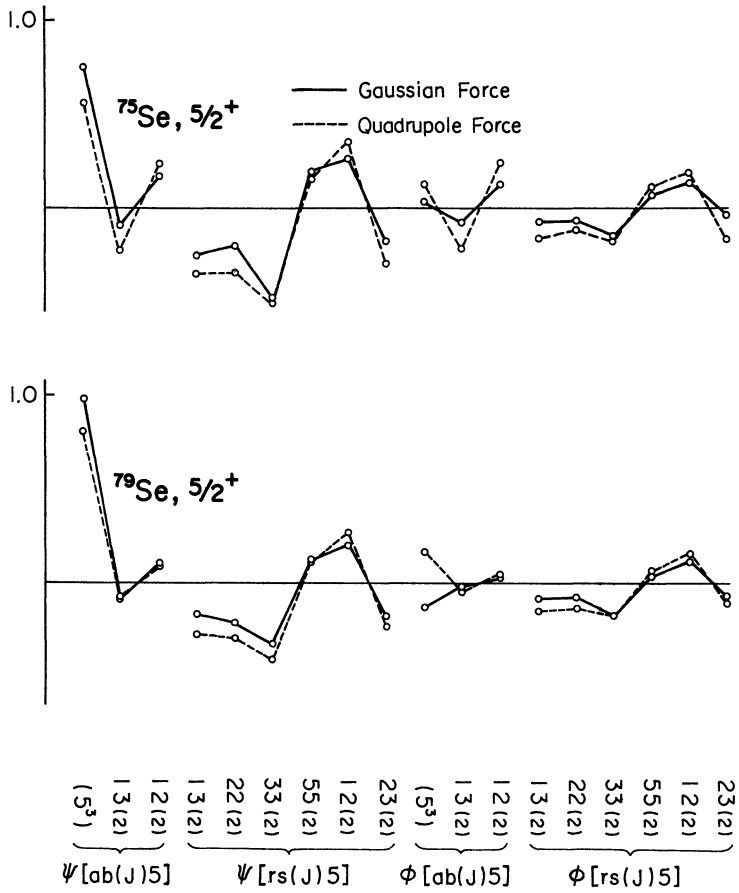

Fig. 4. Main amplitudes of the dressed 3QP 5/2$^+$ modes in Se isotopes. Notations and parameters used are the same as in Fig. 2.

only for the forward-going amplitudes but also for the backward-going amplitudes. The main amplitudes of the modes with spins from 5/2$^+$ to 13/2$^+$ are compared in Figs. 5 (a) and 5 (b). Figure 5 (a) shows the result calculated by using the quadrupole force, while Fig. 5 (b) shows the result calculated by using the Gaussian force. In these figures, the magnitudes of the amplitudes of the modes with spins from 5/2$^+$ to 13/2$^+$ are collectively shown on each position representing a specific component of the amplitudes. From these figures, we can see that, in each component, the relative magnitudes among the amplitudes of the modes with spins from 5/2$^+$ to 13/2$^+$ are similar between the Gaussian-force and quadrupole-force cases. This fact shows the reason why we have obtained the same level sequence irrespective of the forces adopted.

It has been expected that the neutron-proton short-range interaction, which has been neglected in the $P+QQ$ force model (except for its field

producing parts), becomes important in the region $28 \leq Z \leq 50$ and $28 \leq N \leq 50$.[2] The effect of this kind is automatically taken into account in this calculation with the Gaussian force. The result of this calculation shows, however, that the effect does not bring about appreciable differences from the result of the $P+QQ$ force case, at least for low-lying collective states with positive parity in Se isotopes.

As for the difference between the two cases, we can point out that the energy-splitting of the "quintet" in the Gaussian-force case is somewhat smaller than that in the quadrupole-force case. The main reason for this is that the effect of the backward-going diagrams is especially strong for the $7/2^+$ state in the quadrupole-force case. (See the values in (2·4) which show the difference between the two cases in lowering the energy of the $7/2^+$ state.) Another different point is that the mass-number dependence of the excitation energies becomes smooth in the Gaussian-force case, compared to that in the quadrupole-force case. This is the trend similar to that well known in the RPA for even-even nuclei. Therefore, its origin may be attributed to the fact that, in the Gaussian-force case, not only the force-element of the type $F(abcd;\ 2^+)$ but also of the type $G(abcd;J)$ are effective. (The F and G type force-elements are defined in Appendix 1A.) The more detailed differences between the two cases can be seen when we look into the fine structure of the amplitudes. For example, in the Gaussian-force case, the backward-going component $\phi[(g_{9/2})^3]$ in the $5/2^+$ mode becomes very small (in ^{75}Se) and has even the phase opposite to that in the quadrupole-force case (in ^{79}Se). (See Fig. 4.) Besides this, in the $9/2^+_2$ state in ^{79}Se which lies in the relatively higher energy region, the forward-going component $\{(\pi p_{3/2}\pi f_{5/2})_4{}^+\nu g_{9/2}\}$ in the Gaussian-force case becomes non-negligible, i.e., $\psi[23(4)5]=0.109$.

Although we can find some differences between the two cases as mentioned above, it should be emphasized that the correspondence of the main amplitudes between the two cases does hold fairly well. Thus we can say that the nature of the dressed 3QP modes discussed in terms of the $P+QQ$ force model is also maintained in the Gaussian-force model, as long as they are low-lying in energy.

§ 4. Collective excited states in Sn isotopes

In the preceding sections, we have seen that the characteristics of the dressed 3QP mode derived from theoretical calculations are essentially the same between the quadrupole-force case and the Gaussian-force case. This conclusion implies that, for such collective states as the low-lying excited states in Se isotopes, the quadrupole collectivity is so dominant that the other correlations do not play significant roles. Accordingly, the other components of residual interaction which are neglected in the $P+QQ$ force model are expected to play appreciable roles when we consider the nuclei in which the

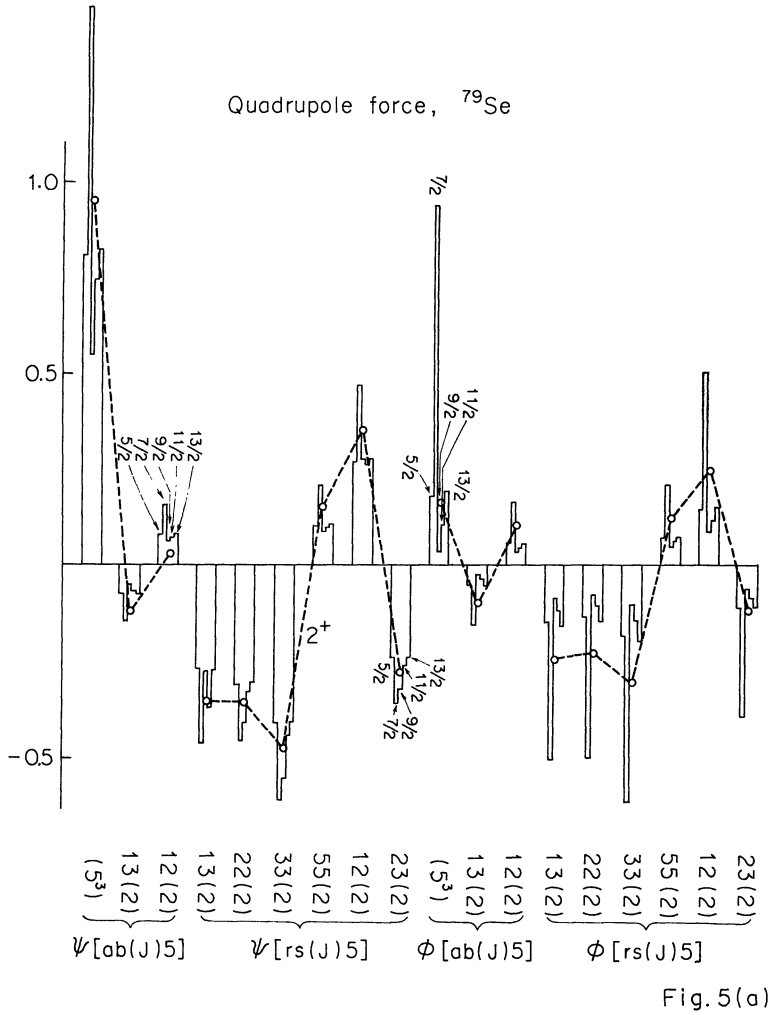

(a) The quadrupole-force case.

Fig. 5. Main amplitudes of the dressed 3QP modes with positive parity in ^{79}Se. The magnitudes of the amplitudes of the modes with spins from $5/2^+$ to $13/2^+$ are collectively shown on each position representing a specific component of the amplitudes. The set of states with spins from $5/2^+$ to $13/2^+$ corresponds to the "quintet" composed of the 1QP $9/2^+$ mode coupled with the 2^+ phonon in the quasi-particle-phonon-coupling theory. For the sake of comparison, the corresponding amplitudes of the 2^+ phonon calculated by the RPA in ^{78}Se are

quadrupole collectivity is not strong. In this section, in order to show this possibility, we present the results for single-closed shell ^{117}Sn and ^{119}Sn calculated by using the Gaussian force. As was pointed out in § 5-Chap. 5, the Sn isotopes belong to the situation where the chemical potential lies near the low-spin orbits so that the phonon-band character is expected to be broken

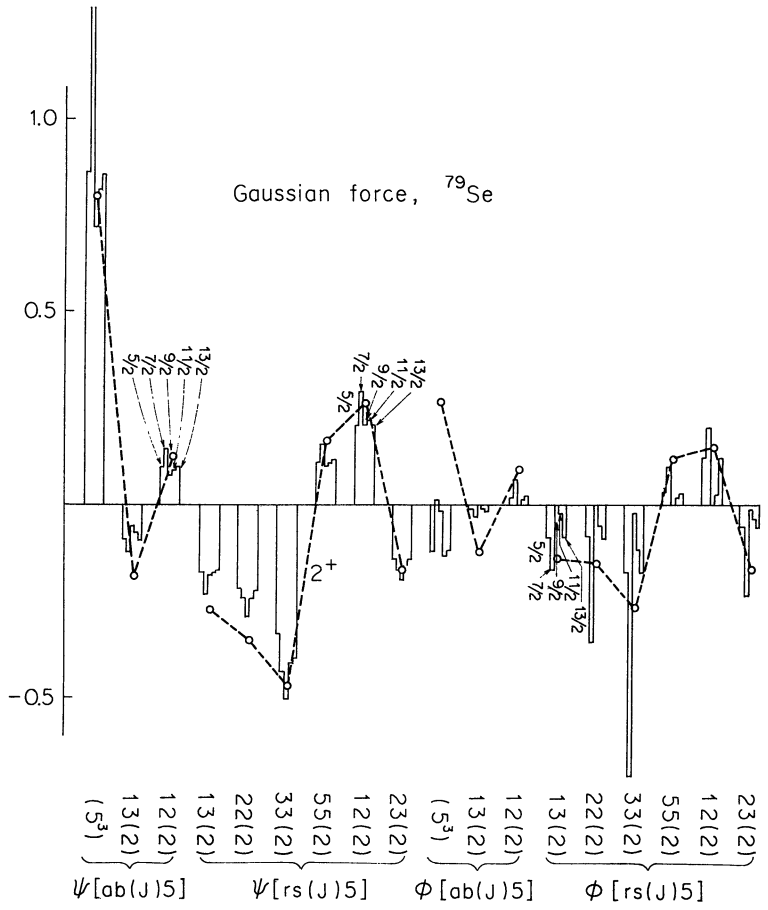

Fig. 5(b)

(b) The Gaussian-force case.

shown by the symbol ∘ connected with broken lines. The strengths of the quadrupole force and of the Gaussian force are chosen to approximately reproduce the experimental excitation energies of the $7/2^+$ and 2^+ states, i.e., the energy difference between the collective $7/2^+$ and 1QP $9/2^+$ states in ^{79}Se and the excitation energy of the 2^+ state in ^{78}Se. They are; $\chi_0=230$ (MeV) for ^{79}Se, $\chi_0=220$ (MeV) for ^{78}Se, $V_0=23$ MeV and $r_0=2.0$ fm for ^{79}Se, $V_0=21$ MeV and $r_0=2.0$ fm for ^{78}Se.

remarkably. If this is the case, then we can also expect that the relative magnitude between the inter and intra phonon-band $E2$ transitions is sensitively dependent on details of many conditions, for example, such as relative occupation probabilities among shell-model orbits. Because of this situation and also because of the relative weakness of the quadrupole collectivity, we can expect that the properties of the collective excited states in Sn isotopes

are very sensitive to details of the wave functions.

Figures 6 and 7 show the calculated results for ^{117}Sn and ^{119}Sn. These figures are made in a form in which the breaking and persistency of the phonon-band character is easy to see. By comparing the results of the Gaussian-force case to those of the quadrupole-force case, we see that the level sequence within a "phonon-band" is almost the same between the two cases. Although the gross structure of the excitation spectra displays some similarity, the energy shift due to the ground-state correlation differs in magnitude between the two cases. For example, the energy shift for the $3/2_2^+$ state in ^{119}Sn is about 300 keV in the quadrupole-force case, while the corresponding energy shift is reduced to about 40 keV in the Gaussian-force case. This reduction of energy shift in the Gaussian-force case is rather special for the single-closed shell nuclei such as Sn isotopes under consideration, since, as we have seen in § 3, the ground-state correlation in the Gaussian-force case is mainly caused by the F-type matrix elements between proton and neutron quasi-particle pairs.

A more interesting difference between the two cases is found when we

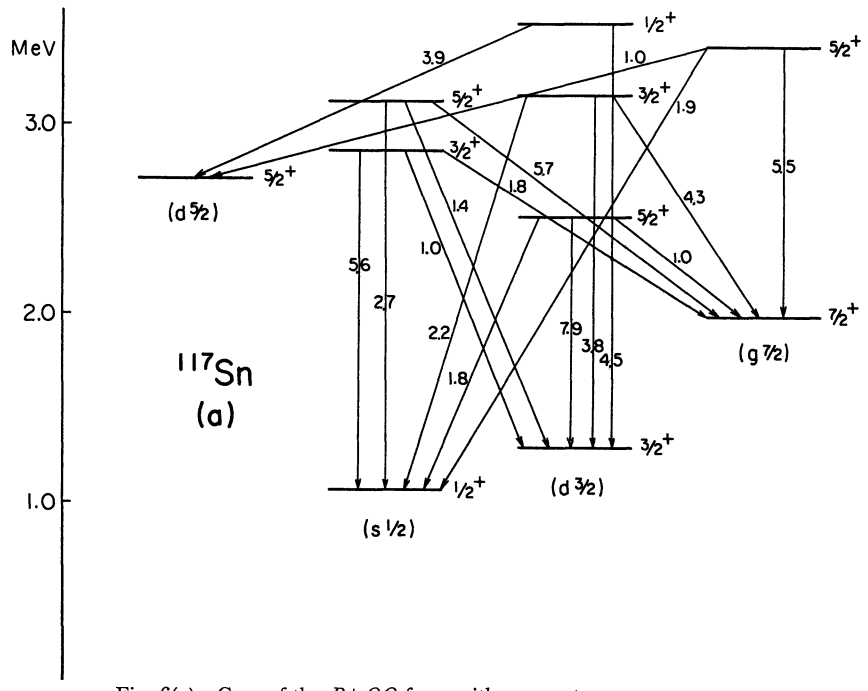

Fig. 6(a) Case of the $P+QQ$ force with parameters;
$G=0.205$, $\chi_0=\chi b^4 A^{5/3}=321.0$ (MeV)

Fig. 6. Results of calculation for the dressed 3QP states with spin $I \leqq 5/2^+$ in ^{117}Sn. They are presented to show the breaking and persistency of the multiplet structures standing over the 1QP states with orbits $3s_{1/2}$, $2d_{3/2}$ and $1g_{7/2}$. The presented level energies are those measured from the correlated ground state. The numbers appearing on the transition arrows give the $B(E2)$ values in unit of $e^2 10^{-51}$ cm^4, which are calculated with polarization charge

compare the magnitudes of the inter-band transitions. These figures show that many inter-band transitions compete with intra-band transitions. This trend is clearly seen for both ^{117}Sn and ^{119}Sn in the quadrupole-force case (Figs. 6(a) and 7(a)). Similar trend is seen for ^{119}Sn also in the Gaussian-force case (Fig. 7(b)). On the other hand, the inter-band transitions are relatively smaller for ^{117}Sn in this case (Fig. 6(b)). In this way, the nucleon-number dependence of the inter-band transitions seems to be very sensitive to the residual interaction adopted. (Similar property is seen in the relative magnitudes among some inter-band transitions.) Such a situation is exactly the expected one: Since the magnitude of the inter-band transition depends sensitively on the relative magnitudes among many components of the amplitudes of the dressed 3QP mode, the magnitude of the inter-band transition tends to change significantly from one isotope to another isotope. The fine structure of the relative magnitude among many components, in turn, depends on the details of the residual interaction. (Note that the (u, v) dependence is more complex in the Gaussian-force case than in the quadrupole-force case, since, in the former case, G-type and F-type matrix elements enter into the

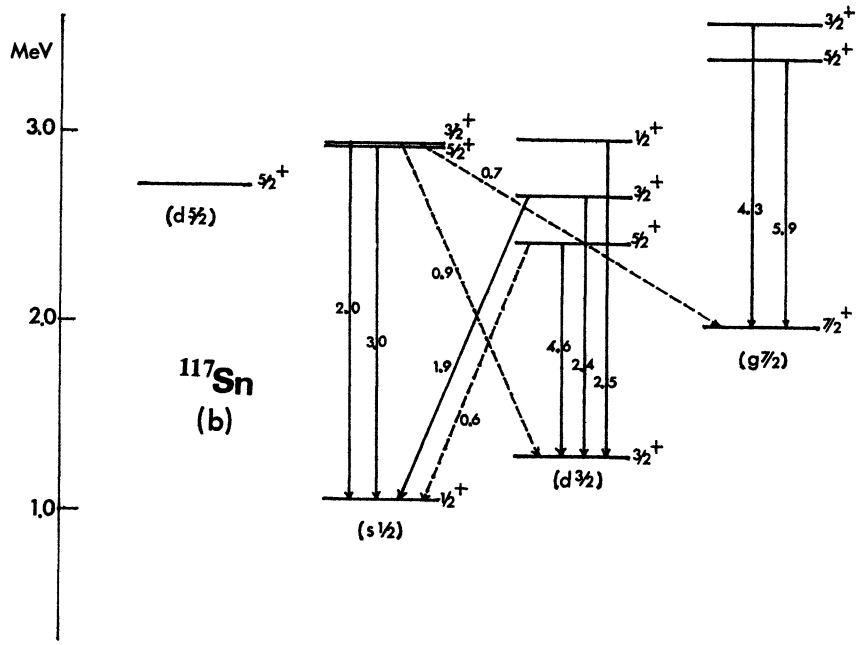

Fig. 6(b) Case of the Gaussian force with parameters;
V_0=35 MeV, r_0=1.720 fm.

δe=1.0 and harmonic-oscillator-range parameter b^2=1.0$A^{1/3}$. For simplicity, the $E2$ transitions smaller than 1.0 (in case (a)) or 0.5 (in case (b)) and other higher-lying states are omitted from the figure. The single-particle energies are taken from Ref. 5):
$\varepsilon(d_{5/2})$=0.0, $\varepsilon(g_{7/2})$=0.83, $\varepsilon(s_{1/2})$=2.29, $\varepsilon(h_{11/2})$=3.53, $\varepsilon(d_{3/2})$=3.26. (all in MeV)

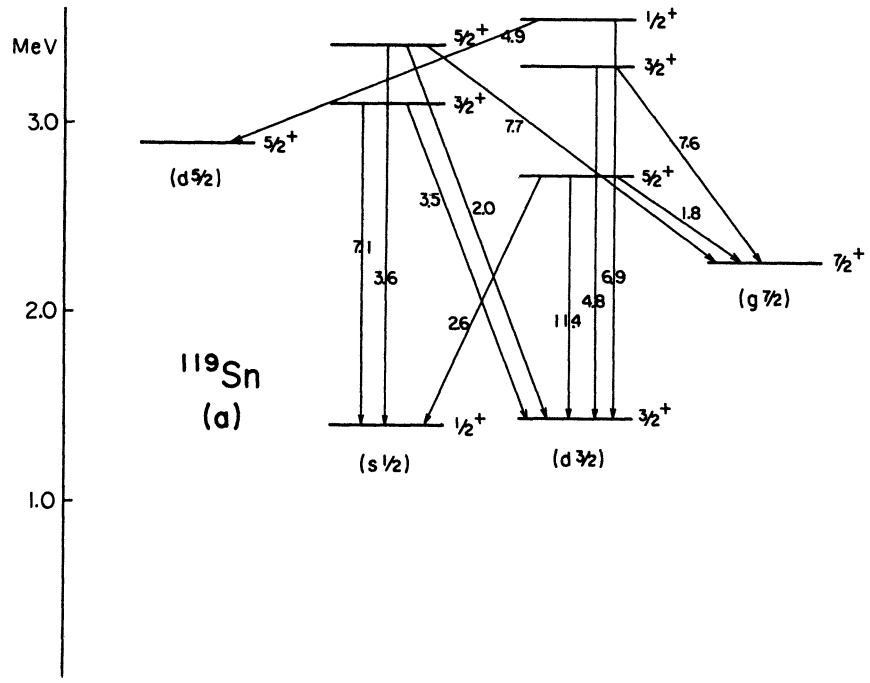

Fig. 7(a) Case of the $P+QQ$ force with parameters;
$G=0.227$, $\chi_0=322.3$. (MeV)

Fig. 7. Result of calculation for the dressed 3QP states with spin $I \leqq 5/2^+$ in ^{119}Sn. Notations are the same as in Fig. 6. The single-particle energies are taken from Ref. 5):
$\varepsilon(d_{5/2})=0.0$, $\varepsilon(g_{7/2})=0.75$, $\varepsilon(s_{1/2})=2.39$, $\varepsilon(h_{11/2})=3.15$, $\varepsilon(d_{3/2})=2.87$.
(all in MeV)

eigenvalue equation with different (u, v) dependence.)

Some inter $E2$ transitions between the $s_{1/2}$ and $d_{3/2}$ phonon-bands have been measured by Stelson et al.[4] For the inter $E2$ transition between the $5/2^+$ state (belonging approximately to the $d_{3/2}$ "phonon-band") and the 1QP $1/2^+$ state, the data indicate that its magnitude drastically changes from ^{117}Sn to ^{119}Sn; i.e., the ratio $B(E2; 5/2^+_{(d_{3/2})} \to 1/2^+_1)/B(E2; 5/2^+_{(d_{3/2})} \to 3/2^+_1)$ is smaller than 0.1 in ^{117}Sn, whereas it is about 0.9 in ^{119}Sn. Concerning this specific transition, the result calculated by the Gaussian force agrees with the data better than the result calculated by the quadrupole force. For the inter $E2$ transitions from the $3/2^+$ and $5/2^+$ states (belonging approximately to the $s_{1/2}$ "phonon-band") to the 1QP $3/2^+$ states, the calculated $B(E2)$ values, especially in the quadrupole-force case, seem to be larger than the corresponding experimental data.[4] We furthermore see that the splitting of the "doublet" ($3/2^+$ and $5/2^+$) is very small in the Gaussian-force case and seems to agree better with the data. However, it does not necessarily imply that the "weak-coupling character" holds, since the inter-band transitions

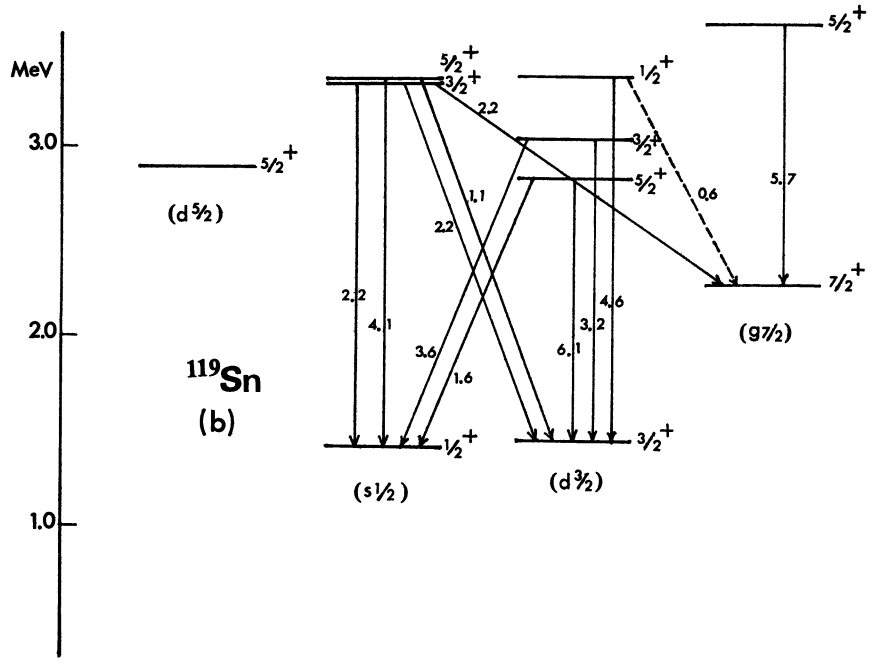

Fig. 7(b) Case of the Gaussian force with parameters;
V_0=35 MeV, r_0=1.725 fm.

to the 1QP $7/2^+$ and $3/2^+$ states can become large even in this case. (See Fig. 7(b).) Even when the inter-band transitions become relatively smaller as in the case of Fig. 6(b), the structure of the excited states under consideration differs from that of the odd-quasi-particle plus 2^+ phonon; this property is merely a consequence of the dominance of the component $\{\nu s_{1/2}(\nu h_{11/2})^2\}$ in this case. Thus, the definite conclusion for the properties of a particular state should be made only after we carefully examine the parameters to be adopted in the calculation. Furthermore, the coupling effect of the pairing-collective excitations and also the coupling effect between the dressed 3QP- and 1QP-modes should be taken into account, since the effects of such kinds are expected to be appreciable for the states under consideration.[6]

§ 5. Further refinements

So far, we have seen that the effects of the other components which are neglected in the $P+QQ$ force model are not appreciable, if the states of interest are of sufficiently (quadrupole-) collective character. However, when we consider a physical quantity which sensitively reflects such small components, we must be careful in treating the fine details of such components and their relations to the dominant components (i.e., here the quadrupole components).

In this section, we briefly discuss such a situation by exemplifying the cases of treating allowed Gamow-Teller (GT) beta decay between odd-mass nuclei and of calculating the $M1$ moments.

The $P+QQ$ force model is by itself not capable of accounting for the retardation of GT transition rates which are regularly observed in medium-mass nuclei. It has been shown that the proton-neutron residual interaction of charge-exchange and spin-flip type, i.e., $(\boldsymbol{\sigma}\cdot\boldsymbol{\sigma})(\boldsymbol{\tau}\cdot\boldsymbol{\tau})$ type, is responsible for the hindrance of non-l-forbidden GT transition rates between one-quasi-particle states.[7] The $(\boldsymbol{\sigma}\cdot\boldsymbol{\sigma})(\boldsymbol{\tau}\cdot\boldsymbol{\tau})$ type residual interaction (which is called the GT force hereafter) brings about the coupling of the "$J^\pi=1^+$" proton-neutron quasi-particle pairs to the one-quasi-particle state. Although the mixing of this kind of quasi-particle pairs in the one-quasi-particle state is small, they contribute so coherently that their effects on the beta-decay rate become significant.[7] Thus, we are forced to simultaneously take account of both the GT type correlation and the quadrupole correlation, since we are interested in the GT transition between (non-deformed) odd-mass nuclei exhibiting the quadrupole collective character.

A simple way of simultaneously treating these two kinds of correlations may be to introduce the GT force in addition to the $P+QQ$ force. In the method of quasi-particle-phonon-coupling theory, the "$J^\pi=1^+$" phonon composed of proton-neutron quasi-particle pairs is introduced by treating the GT force with the unlike-particle RPA (describing the odd-odd nuclei).[8] With this method, the effect of the GT force is treated independently to that of the quadrupole force responsible for the low-lying 2^+ phonon. Consequently, a difficulty of this method arises from the non-commutability between the (higher-lying) 1^+ phonon and the (low-lying) 2^+ phonon. It should be noted here that the excitation of the "$J^\pi=1^+$" quasi-particle pairs takes place mostly in the same shell-model space as that for the "$J^\pi=2^+$" quasi-particle pairs. (When the shell-model space is enlarged so as to include the spin-orbit partners of all single-particle orbits in the filling major shell, the shell-model space becomes exactly the same for these excitations.) The difficulty in evaluating the GT matrix element (, for example, between the one-proton-quasi-particle state and the one-neutron-quasi-particle-plus-one-2^+-phonon state,) is closely connected with the basic approximation of treating the two correlations independently.[8] This is seen when we attempt to unambiguously expand the GT transition operator in terms of the quasi-particle, 2^+ phonon and 1^+ phonon operators which are assumed to be mutually commutable.

The difficulty of this kind can be overcome when we adopt the method developed in Chap. 2. With this method, by introducing the GT force in addition to the $P+QQ$ force, we can simply achieve the aim of treating the GT and quadrupole correlations on an equal footing.[10] When calculation of this kind is performed by this method, the $J^\pi=1^+$ proton-neutron quasi-

particle pairs participate in the dressed 3QP mode as one of the constituents. Then we have a new dressed 3QP state predominantly exhibiting the GT correlated character at a higher energy region. On the other hand, the low-lying dressed 3QP states which predominantly are of quadrupole character remains essentially the same as in the $P+QQ$ force model except for a small perturbative effect due to the GT force. Of course, the one-quasi-particle state couples with both kinds of the dressed 3QP states. After diagonalizing the effective Hamiltonian defined by (5·11) of Chap. 2 in the quasi-particle new-Tamm-Dancoff space, we can evaluate any GT transition matrix element between the obtained eigenstates by making use of the transcription rule developed in § 5-Chap. 2. This procedure is exactly the same as in the case of evaluating the electromagnetic transition matrix elements. As for the difference of nucleon numbers between the initial and final states, we can take it into account by using the method described in Appendix 6B. For details of this kind of application, see Ref. 10).

An analogous situation occurs in the case of evaluating the $M1$ moments. In the calculation of $M1$ moments, we used the effective spin g factor, g_s^{eff}, in Chaps. 3 and 4. The use of g_s^{eff} is regarded as representing the effect of coupling of the $J^\pi=1^+$ quasi-particle pairs to the one-quasi-particle mode (i.e., the effect of $M1$ core polarization). As is well known, one of the important assumptions in using such an "effective quantity" is that the excitation of the $J^\pi=1^+$ quasi-particle pairs is approximately independent of the other kind of excitations. On the other hand, we can explicitly take into account such a kind of excitations by adopting, for example, a delta-function force with suitable spin-dependence in the calculation.[11] In this case, the ($M1$-type) $J^\pi=1^+$ quasi-particle pairs participate in the dressed 3QP mode as one of the constituents. Consequently, we will have a new dressed 3QP state predominantly exhibiting the $M1$-type correlated character at a higher energy region, and the 1QP state couples with this state. (In this calculation, of course, the shell-model space should be chosen so as to include the spin-orbit partners of all single-particle orbits in the filling major shell.) Then there may be no need to use the "effective quantity" such as g_s^{eff}. Hence, the investigation in which this $M1$-type correlation is explicitly taken into account together with the quadrupole correlation will enable us to examine the validity of the use of the effective spin g factor g_s^{eff}. Of course, the introduction of such small components (representing the $J^\pi=1^+$ quasi-particle pairs) will bring about no essential change in the nature of the low-lying dressed 3QP states which have been described in terms of the $P+QQ$ force model. We can expect this trend from the results in §§ 2 and 3, since the calculation with the use of the Gaussian force have already included such small components. The detailed investigation into the direction remarked here remains to be done.

§ 6. Concluding remarks

With the use of a central force with Gaussian radial dependence, we have investigated whether or not the nature of the dressed 3QP modes in the $P+QQ$ force model is essentially dependent on the special properties of the quadrupole force. It has been shown that the microscopic structure of the dressed 3QP modes obtained by the Gaussian force is very similar to that obtained by the $P+QQ$ force, at least for the low-excited states with positive parity in Se isotopes. Thus we expect that the conclusions obtained in Chaps. 3, 4 and 5 do not always rely on the special properties of the quadrupole force but possess more general significance. On the other hand, we also expect that other types of correlation which cannot emerge from the $P+QQ$ force model itself becomes appreciable when we consider, for example, the excited state in which the dominant role of the quadrupole correlation is relatively relaxed.

It should also be noted that the situations, in which the quadrupole collectivity is dominant but the simple phonon-band character tends to be broken, remain to be investigated in more details for both the $P+QQ$ force case and the Gaussian-force case. Needless to say, the framework of the proposed theory is general enough to be used with any residual interaction. Thus, it is very interesting to investigate the relation between the effective interaction and the microscopic structure of the dressed 3QP mode by adopting more complex effective interactions than the $P+QQ$ force or the Gaussian force without any exchange mixture.

Appendix 6A. Matrix elements of the secular equation for the dressed 3QP modes in the coupled-angular-momentum representation

Here, we give the explicit form of the matrix elements of the secular equation for the dressed 3QP modes, Eq. (3·3) in Chap. 2, in the coupled-angular-momentum representation. We can straightforwardly obtain the explicit form by transforming the matrix elements (in the m-scheme) given in Appendix 2B into the coupled-angular-momentum representation.

6A-1 *The case of general interaction*

In this representation, the creation operator of the dressed 3QP mode given by Eq. (3·1) in Chap. 2 is represented as

$$C^{\dagger}_{nIK}=\frac{1}{\sqrt{3!}}\sum_{abcJ}\psi_{nI}[ab(J)c]\sum_{m_\alpha m_\beta m_\gamma M}(j_a j_b m_\alpha m_\beta|JM)$$
$$\times(Jj_c M m_\gamma|IK)a^{\dagger}_\alpha a^{\dagger}_\beta a^{\dagger}_\gamma$$

$$
\begin{aligned}
&+\sum_{(rs)cJ}\frac{\psi_{nI}[rs(J)c]}{\sqrt{1+\delta_{rs}}}\sum_{m_\rho m_\sigma m_\gamma M}(j_r j_s m_\rho m_\sigma|JM)(Jj_c M m_\gamma|IK)a_\rho^\dagger a_\sigma^\dagger a_\gamma^\dagger \\
&+\frac{1}{\sqrt{3!}}\sum_{aJ}\phi_{nI}^{(1)}[aa(J)a]\sum_{m_{a_1}m_{a_2}m_{a_3}M}(j_a j_a m_{a_1}m_{a_2}|JM) \\
&\qquad\times(Jj_a M m_{a_3}|IK)\mathring{T}_{3/2,-1/2}(\alpha_1\alpha_2\alpha_3) \\
&+\frac{1}{\sqrt{2!}}\sum_{\substack{acJ\\(a\neq c)}}\phi_{nI}^{(2)}[aa(J);c]\sum_{m_{a_1}m_{a_2}m_\gamma M}(j_a j_a m_{a_1}m_{a_2}|JM) \\
&\qquad\times(Jj_c M m_\gamma|IK)\mathring{T}_{10}(\alpha_1\alpha_2)a_{\tilde{\gamma}} \\
&+\sum_{\substack{(ab)cJ\\(a,b\neq c)}}\frac{\phi_{nI}^{(3)}[ab(J);c]}{\sqrt{1+\delta_{ab}}}\sum_{m_\alpha m_\beta m_\gamma M}(j_a j_b m_\alpha m_\beta|JM)\,(Jj_c M m_\gamma|IK)a_\gamma^\dagger a_{\tilde{\alpha}}a_{\tilde{\beta}} \\
&+\sum_{(rs)cJ}\frac{\phi_{nI}^{(3)}[rs(J);c]}{\sqrt{1+\delta_{rs}}}\sum_{m_\rho m_\sigma m_\gamma M}(j_r j_s m_\rho m_\sigma|JM)\,(Jj_c M m_\gamma|IK)a_\gamma^\dagger a_{\tilde{\rho}}a_{\tilde{\sigma}} \\
&+\frac{1}{\sqrt{2}}\sum_{rcJ}\phi_{nI}^{(2)}[rr(J);c]\sum_{m_{\rho_1}m_{\rho_2}m_\gamma M}(j_r j_r m_{\rho_1}m_{\rho_2}|JM)\,(Jj_c M m_\gamma|IK) \\
&\qquad\times\mathring{T}_{10}(\rho_1\rho_2)a_{\tilde{\gamma}} \\
&+\sum_{\substack{rscJ\\(r\neq s)}}\phi_{nI}^{(3)}[rc(J);s]\sum_{m_\rho m_\sigma m_\gamma M}(j_r j_c m_\rho m_\gamma|JM)\,(Jj_s M m_\sigma|IK)a_\sigma^\dagger a_{\tilde{\rho}}a_{\tilde{\gamma}},
\end{aligned}
\tag{6A·1}
$$

where the Greek letters $\alpha=(a,\ m_a)$, β, $\gamma,\cdots$ are used to designate the single-particle states for neutrons (protons), and $\rho=(r,\ m_\rho)$, $\sigma=(s,\ m_\sigma),\cdots$ for protons (neutrons). In the text, we have called, for example, the amplitudes $\psi_{nI}[rs(J)c]$ and $\phi_{nI}^{(3)}[rs(J)c]$ the components of the type $\{rs(2)\nu g_{9/2}\}$ when c denotes the $1g_{9/2}$ orbit for neutrons and $J=2$. (In this case, r and s denote the orbits for protons.) The antisymmetric properties of the three-body correlation amplitudes are then expressed as follows:

$$
\begin{aligned}
&\psi_{nI}[ab(J)c]=\sum_{a'b'c'J'}P_I(ab(J)c|a'b'(J')c')\psi_{nI}[a'b'(J')c'], \\
&\phi_{nI}^{(1)}[aa(J)a]=\sum_{J'}P_I(aa(J)a|aa(J')a)\phi_{nI}^{(1)}[aa(J')a], \\
&\phi_{nI}^{(2)}[aa(J);c]=\frac{(1-\delta_{J0})\,(1+(-)^J)}{2}\phi_{nI}^{(2)}[aa(J);c], \\
&\phi_{nI}^{(3)}[ab(J);c]=-(-)^{j_a+j_b-J}(1-\delta_{J0})\phi_{nI}^{(3)}[ba(J);c], \\
&\phi_{nI}^{(3)}[rs(J);c]=-(-)^{j_r+j_s-J}(1-\delta_{J0})\phi_{nI}^{(3)}[sr(J);c],
\end{aligned}
\tag{6A·2}
$$

where the projection operators $P_I(ab(J)c|a'b'(J')c')$ defined in Appendix 2A are used.

The matrix elements in the coupled-angular-momentum representation are explicitly given as follows:

$$3D_I[ab(J)c|a'b'(J')c']=(E_a+E_b+E_c)P_I(ab(J)c|a'b'(J')c')$$
$$+3\sum_{a_1b_1c_1J_1}\sum_{a_1'b_1'c_1'J_1'}P_I(ab(J)c|a_1b_1(J_1)c_1)V^{(f)}(a_1b_1a_1'b_1';J_1)\delta_{J_1J_1'}\delta_{c_1c_1'}$$
$$\times P_I(a_1'b_1'(J_1')c_1'|a'b'(J')c'),$$

$$3D_I[ab(J)c|r's'(J')c']=\frac{\sqrt{6}}{\sqrt{1+\delta_{r's'}}}\sum_{a_1b_1c_1}P_I(ab(J)c|a_1b_1(J')c_1)$$
$$\times V^{(f)}(a_1b_1r's';J')\delta_{c_1c'},$$

$$3D_I[rs(J)c|r's'(J')c']=(E_r+E_s+E_c)\delta_{rr'}\delta_{ss'}\delta_{cc'}\delta_{JJ'}$$
$$+\frac{2}{\sqrt{(1+\delta_{rs})(1+\delta_{r's'})}}\Big[V^{(f)}(rsr's';J)\delta_{JJ'}\delta_{cc'}$$
$$+(-)^{j_s+j_c+j_{s'}+j_{c'}}\hat{J}\hat{J}'\sum_{J''}(2J''+1)\begin{Bmatrix}j_r & j_s & J\\ j_c & I & J''\end{Bmatrix}\begin{Bmatrix}j_{r'} & j_{s'} & J'\\ j_{c'} & I & J''\end{Bmatrix}V^{(f)}(scs'c';J'')\delta_{rr'}$$
$$+(-)^{j_s+j_c+j_{s'}+j_{c'}+J'}\hat{J}\hat{J}'\sum_{J''}(2J''+1)\begin{Bmatrix}j_r & j_s & J\\ j_c & I & J''\end{Bmatrix}\begin{Bmatrix}j_{s'} & j_{r'} & J'\\ j_{c'} & I & J''\end{Bmatrix}V^{(f)}(scr'c';J'')\delta_{rs'}$$
$$+(-)^{j_s+j_c+j_{s'}+j_{c'}+J}\hat{J}\hat{J}'\sum_{J''}(2J''+1)\begin{Bmatrix}j_s & j_r & J\\ j_c & I & J''\end{Bmatrix}\begin{Bmatrix}j_{r'} & j_{s'} & J'\\ j_{c'} & I & J''\end{Bmatrix}V^{(f)}(rcs'c';J'')\delta_{sr'}$$
$$+(-)^{j_s+j_c+j_{s'}+j_{c'}+J+J'}\hat{J}\hat{J}'\sum_{J''}(2J''+1)\begin{Bmatrix}j_s & j_r & J\\ j_c & I & J''\end{Bmatrix}\begin{Bmatrix}j_{s'} & j_{r'} & J'\\ j_{c'} & I & J''\end{Bmatrix}V^{(f)}(rcr'c';J'')\delta_{ss'}\Big],$$
(6A·3a)

$$d_I[aa(J)a|a'a'(J')a']=E_aP_I(aa(J)a|a'a'(J')a')$$
$$+\sum_{a_1J_1}\sum_{a_1'J_1'}P_I(aa(J)a|a_1a_1(J_1)a_1)V^{(f)}(a_1'a_1'a_1a_1;J_1)\delta_{J_1J_1'}\delta_{a_1a_1'}$$
$$\times P_I(a_1'a_1'(J_1')a_1'|a'a'(J')a'),$$

$$d_I[aa(J)a|a'a'(J');c']=-\sqrt{2}\sum_{J_1}P_I(aa(J)a|aa(J_1)a)$$
$$\times(-)^{j_{a'}+j_{c'}}\hat{J}_1\hat{J}'\begin{Bmatrix}j_{a'} & j_{a'} & J'\\ j_{c'} & I & J_1\end{Bmatrix}V^{(f)}(a'c'aa;J_1)\delta_{aa'},$$

$$d_I[aa(J)a|a'b'(J');c']=\frac{\sqrt{2}}{\sqrt{1+\delta_{a'b'}}}P_I(aa(J)a|aa(J')a)V^{(f)}(a'b'aa;J')\delta_{ac'},$$

$$d_I[aa(J)a|rs(J');c']=\frac{\sqrt{2}}{\sqrt{1+\delta_{rs}}}P_I(aa(J)a|aa(J')a)V^{(f)}(rsaa;J')\delta_{ac'},$$

$$d_I[aa(J);c|a'a'(J');c']=E_c\delta_{aa'}\delta_{cc'}\delta_{JJ'}+2(-)^{j_a+j_c+j_{a'}+j_{c'}}\hat{J}\hat{J}'\sum_{J''}(2J''+1)$$
$$\times\begin{Bmatrix}j_a & j_a & J\\ j_c & I & J''\end{Bmatrix}\begin{Bmatrix}j_{a'} & j_{a'} & J'\\ j_{c'} & I & J''\end{Bmatrix}V^{(f)}(a'c'ac;J'')\delta_{aa'},$$

$$d_I[aa(J);c|a'b'(J');c']=-\frac{2}{\sqrt{1+\delta_{a'b'}}}(-)^{j_a+j_c+J'}\hat{J}\hat{J}'\begin{Bmatrix}j_a & j_a & J\\ j_c & I & J'\end{Bmatrix}V^{(f)}(a'b'ac;J')\delta_{ac'},$$

$$d_I[aa(J);\,c|rs(J');\,c']=-\frac{2}{\sqrt{1+\delta_{rs}}}(-)^{j_a+j_c+J'}\hat{J}\hat{J}'\begin{Bmatrix} j_a & j_a & J \\ j_c & I & J' \end{Bmatrix}V^{(f)}(rsac;J')\delta_{ac'},$$

$$d_I[ab(J);\,c|a'b'(J');\,c']=(E_a+E_b-E_c)\delta_{aa'}\delta_{bb'}\delta_{cc'}\delta_{JJ'}$$
$$+\frac{2}{\sqrt{(1+\delta_{ab})(1+\delta_{a'b'})}}V^{(f)}(a'b'ab;J)\delta_{JJ'}\delta_{cc'},$$

$$d_I[ab(J);\,c|rs(J');\,c']=\frac{2}{\sqrt{(1+\delta_{ab})\,(1+\delta_{rs})}}V^{(f)}(rsab;J)\delta_{JJ'}\delta_{cc'},$$

$$d_I[rs(J);\,c|r's'(J');\,c']=(E_r+E_s-E_c)\delta_{rr'}\delta_{ss'}\delta'_{cc'}\delta_{JJ'}$$
$$+\frac{2}{\sqrt{(1+\delta_{rs})(1+\delta_{r's'})}}V^{(f)}(r's'rs;J)\delta_{JJ'}\delta_{cc'},$$

$$d_I[rr(J);c|r'r'(J');\,c']=E_c\delta_{rr'}\delta_{cc'}\delta_{JJ'}+2(-)^{j_r+j_c+j_{r'}+j_{c'}}\hat{J}\hat{J}'\sum_{J''}(2J''+1)$$
$$\times\begin{Bmatrix} j_r & j_r & J \\ j_c & I & J'' \end{Bmatrix}\begin{Bmatrix} j_{r'} & j_{r'} & J' \\ j_{c'} & I & J'' \end{Bmatrix}V^{(f)}(r'c'rc;J'')\delta_{rr'},$$

$$d_I[rr(J);\,c|r'c'(J');\,s']=-2(-)^{j_r+j_c+J'}\hat{J}\hat{J}'\begin{Bmatrix} j_r & j_r & J \\ j_c & I & J' \end{Bmatrix}V^{(f)}(r'c'rc;J')\delta_{rs'},$$

$$d_I[rc(J);\,s|r'c'(J');\,s']=(E_r+E_c-E_s)\delta_{rr'}\delta_{cc'}\delta_{ss'}\delta_{JJ'}+2V^{(f)}(r'c'rc;J)\delta_{JJ'}\delta_{ss'},$$

(6A·3b)

$$A_I[ab(J)c|a'a'(J')a']=\sqrt{3}\sum_{a_1b_1c_1J''}P_I(ab(J)c|a_1b_1(J'')c_1)V^{(b)}(a_1b_1a'a';J'')\delta_{c_1a'}$$
$$\times P_I(a'a'(J'')a'|a'a'(J')a'),$$

$$A_I[ab(J)c|a'a'(J');\,c']=-\sqrt{6}\sum_{a_1b_1c_1J''}P_I(ab(J)c|a_1b_1(J'')c_1)(-)^{j_{a'}+j_{c'}+J''}\hat{J}'\hat{J}''$$
$$\times\begin{Bmatrix} j_{a'} & j_{a'} & J' \\ j_{c'} & I & J'' \end{Bmatrix}V^{(b)}(a_1b_1a'c';J'')\delta_{c_1a'},$$

$$A_I[ab(J)c|a'b'(J');\,c']=\frac{\sqrt{6}}{\sqrt{1+\delta_{a'b'}}}\sum_{a_1b_1c_1}P_I(ab(J)c|a_1b_1(J')c_1)V^{(b)}(a_1b_1a'b';J')\delta_{c_1c'},$$

$$A_I[ab(J)c|rs(J');\,c']=\frac{\sqrt{6}}{\sqrt{1+\delta_{rs}}}\sum_{a_1b_1c_1}P_I(ab(J)c|a_1b_1(J')c_1)V^{(b)}(a_1b_1rs;J')\delta_{c_1c'},$$

$$A_I[rs(J)c|a'a'(J')a']=\frac{\sqrt{2}}{\sqrt{1+\delta_{rs}}}V^{(b)}(rsa'a';J)\delta_{ca'}P_I(a'a'(J)a'|a'a'(J')a'),$$

$$A_I[rs(J)c|a'a'(J');\,c']=-\frac{2}{\sqrt{1+\delta_{rs}}}(-)^{j_{a'}+j_{c'}+J}\hat{J}\hat{J}'\begin{Bmatrix} j_{a'} & j_{a'} & J' \\ j_{c'} & I & J \end{Bmatrix}V^{(b)}(rsa'c';J)\delta_{ca'},$$

$$A_I[rs(J)c|a'b'(J');\,c']=\frac{2}{\sqrt{(1+\delta_{rs})\,(1+\delta_{a'b'})}}V^{(b)}(rsa'b';J)\delta_{JJ'}\delta_{cc'},$$

$$A_I[rs(J)c|r's'(J');\,c']=\frac{2}{\sqrt{(1+\delta_{rs})\,(1+\delta_{r's'})}}V^{(b)}(rsr's';J)\delta_{JJ'}\delta_{cc'},$$

$$A_I[rs(J)c|r'r'(J');\,c']=\frac{2}{\sqrt{1+\delta_{rs}}}(-)^{j_s+j_c+j_{r'}+j_{c'}}\hat{J}\hat{J}'$$
$$\times\Sigma_{J''}(2J''+1)\left[\begin{Bmatrix} j_r & j_s & J \\ I & j_c & J'' \end{Bmatrix}\begin{Bmatrix} j_{r'} & j_{r'} & J' \\ I & j_{c'} & J'' \end{Bmatrix}V^{(b)}(scr'c';J'')\delta_{rr'}\right.$$
$$\left.+(-)^J\begin{Bmatrix} j_r & j_s & J \\ j_c & I & J'' \end{Bmatrix}\begin{Bmatrix} j_{r'} & j_{r'} & J' \\ j_{c'} & I & J'' \end{Bmatrix}V^{(b)}(rcr'c';J'')\delta_{sr'}\right],$$
$$A_I[rs(J)c|r'c'(J');\,s']=-\frac{2}{\sqrt{1+\delta_{rs}}}(-)^{j_s+j_c+J'}\hat{J}'\hat{J}\left[\begin{Bmatrix} j_r & j_s & J \\ j_c & I & J' \end{Bmatrix}V^{(b)}(scr'c';J')\delta_{rs'}\right.$$
$$\left.+(-)^J\begin{Bmatrix} j_r & j_s & J \\ I & j_c & J' \end{Bmatrix}V^{(b)}(rcr'c';J')\delta_{ss'}\right], \tag{6A·3c}$$

where $\hat{J}=\sqrt{2J+1}$. We have used the following notations for the matrix elements of the interaction:

$$\begin{aligned} V^{(f)}(abcd;J)&=-(u_au_bu_cu_d+v_av_bv_cv_d)G(abcd;J)\\ &\quad-(u_au_bu_cv_d+v_au_bv_cu_d)F(abcd;J)\\ &\quad+(-)^{j_a+j_b+J}(v_au_bu_cv_d+u_av_bv_cu_d)F(bacd;J),\\ V^{(b)}(abcd;J)&=-(u_au_bv_cv_d+v_av_bu_cu_d)G(abcd;J)\\ &\quad+(u_av_bv_cu_d+v_au_bu_cv_d)F(abcd;J)\\ &\quad-(-)^{j_a+j_b+J}(v_au_bv_cu_d+u_av_bu_cv_d)F(bacd;J), \end{aligned} \tag{6A·4}$$

where the G and F type matrix elements are defined in Appendix 1A. In the text, we have expressed, for example, $F(rsaa;J)$ as $F(rs(\nu g_{9/2})^2;2)$ when a denotes the $1g^+_{9/2}$ orbit for neutrons and $J=2$.

6A-2 *The case of pairing-plus-quadrupole force*

When we adopt the pairing-plus-quadrupole force, the matrix elements are simply obtained from Eq. (6A·3) by the following replacement:

$$\begin{aligned} &V^{(f)}(abcd;J)=-V^{(b)}(abcd;J)\\ &\quad\Longrightarrow-\frac{1}{2}\chi Q(ab)Q(cd)\delta_{J2}, \end{aligned} \tag{6A·5}$$

where

$$Q(ab)=\frac{1}{\sqrt{5}}(a\|r^2Y_2\|b)\cdot(u_av_b+v_au_b).$$

Appendix 6B. Method of calculating transition matrix elements between nuclei with different nucleon numbers[9)]

In the case of evaluating beta-decay matrix elements or nucleon-transfer matrix elements, we must calculate the matrix elements between nuclei with different nucleon numbers. Since the quasi-particle representation is introduced by solving the BCS equations, i.e., (3·5) in Chap. 1, with given nucleon numbers (proton and neutron numbers) corresponding to a specific nucleus of interest, we must know the method of calculating transition matrix element between the states expressed by different quasi-particle representations. Here, within the intrinsic subspace in the quasi-spin space, we give a method suitable for this purpose.

Since Bogoliubov transformation is nothing but the rotation of the coordinate system around the y-axis in the quasi-spin space (composed of the direct product of quasi-spin subspace defined in each single-particle orbit), any quasi-particle representation is characterized by the set of rotation angles $\boldsymbol{\theta}=(\theta_a, \theta_b, \cdots)$, θ_a being the rotation angle for the subspace in the orbit a. (See Chap. 1.) The initial and final state vectors are therefore represented by $|\Gamma^{(i)}, \boldsymbol{\theta}^{(i)}\rangle$ and $|\Gamma^{(f)}, \boldsymbol{\theta}^{(f)}\rangle$, respectively. Here, $\Gamma^{(i)}$ and $\Gamma^{(f)}$ denote the sets of quantum numbers characterizing the initial and final states, respectively, and $\boldsymbol{\theta}^{(i)}$ and $\boldsymbol{\theta}^{(f)}$ the corresponding sets of rotation angles. In the intrinsic subspace (in the quasi-spin space), these states satisfy the condition

$$\hat{S}_{-}^{(i)}(a)|\Gamma^{(i)}, \boldsymbol{\theta}^{(i)}\rangle=\hat{S}_{-}^{(f)}(a)|\Gamma^{(f)}, \boldsymbol{\theta}^{(f)}\rangle=0, \tag{6B·1}$$

where superscript (i) or (f) of the quasi-spin operator $\hat{S}_{-}(a)$ denotes that it is represented in terms of the quasi-particle representation corresponding to the initial or final states, respectively. (See Chap. 1.)

Let us first notice that the initial state vector can also be expressed in the quasi-particle representation corresponding to the final state as

$$|\Gamma^{(i)}, \boldsymbol{\theta}^{(f)}\rangle=R(\boldsymbol{\theta}^{(f)}-\boldsymbol{\theta}^{(i)})|\Gamma^{(i)}, \boldsymbol{\theta}^{(i)}\rangle, \tag{6B·2}$$

where $R(\boldsymbol{\theta})=\exp\{i\sum_a \theta_a \hat{S}_y(a)\}$. (Since $\hat{S}_y(a)$ is invariant under this transformation, the superscript (i) or (f) is unnecessary for $\hat{S}_y(a)$.) The condition (6B·1) for the initial state is then re-expressed as

$$\hat{S}_{-}^{(f)}(a)|\Gamma^{(i)}, \boldsymbol{\theta}^{(f)}\rangle=0 \tag{6B·3}$$

for all $\hat{S}_{-}^{(f)}(a)$. Let $\hat{O}$ be the transition operator which is generally written as

$$\begin{aligned}\hat{O}&=\hat{O}([c_\alpha^\dagger], [c_\beta^\dagger], \cdots, [c_\gamma], [c_\delta], \cdots)\\ &=\sum\langle\alpha\beta\cdots|O|\gamma\delta\cdots\rangle\, c_\alpha^\dagger c_\beta^\dagger\cdots c_\gamma c_\delta\cdots.\end{aligned}$$

When $\hat{O}$ is expressed in terms of the quasi-particle operators in the representation corresponding to the final state, the transition matrix element under consideration takes the following form:

$$\begin{aligned}&\langle \Gamma^{(f)}, \boldsymbol{\theta}^{(f)}|\hat{O}|\Gamma^{(i)}, \boldsymbol{\theta}^{(i)}\rangle \\ &=\langle \Gamma^{(f)}, \boldsymbol{\theta}^{(f)}|\hat{O}([u_a^{(f)}a_a^{(f)\dagger}+v_a^{(f)}a_{\bar{a}}^{(f)}], \cdots \\ &\qquad [u_c^{(f)}a_\gamma^{(f)}+v_c^{(f)}a_{\bar{\gamma}}^{(f)\dagger}], \cdots)R^{-1}(\boldsymbol{\theta}^{(f)}-\boldsymbol{\theta}^{(i)})|\Gamma^{(i)}, \boldsymbol{\theta}^{(f)}\rangle,\end{aligned} \tag{6B·4}$$

where we have used the inverse transformation of (6B·2). In the above expression, all quasi-particle operators refer to the representation corresponding to the final state. By making full use of the conditions (6B·1) and (6B·3) with the aid of the identity

$$\begin{aligned}&\exp[\Delta\theta_a\{\hat{S}_+(a)-\hat{S}_-(a)\}/2] \\ &\quad=\exp[\hat{S}_+(a)\tan(\Delta\theta_a/2)]\cdot\exp[-2\hat{S}_0(a)\log\cos(\Delta\theta_a/2)] \\ &\qquad\times\exp[-\hat{S}_-(a)\tan(\Delta\theta_a/2)],\end{aligned} \tag{6B·5}$$

we finally obtain the expression suitable for the present purpose:

$$\langle \Gamma^{(f)}, \boldsymbol{\theta}^{(f)}|\hat{O}|\Gamma^{(i)}, \boldsymbol{\theta}^{(i)}\rangle=\langle \Gamma^{(f)}, \boldsymbol{\theta}|\hat{\mathcal{O}}|\Gamma^{(i)}, \boldsymbol{\theta}\rangle, \tag{6B·6}$$

$$\begin{aligned}\hat{\mathcal{O}}&=\hat{O}([u_a^{(i)}D(a)^{-1}a_a^\dagger+v_a^{(f)}a_{\bar{a}}], \cdots, \\ &\qquad [u_c^{(f)}a_\gamma+v_c^{(i)}D(c)^{-1}a_{\bar{\gamma}}^\dagger], \cdots)\cdot\hat{G} \\ &=\hat{G}\cdot\hat{O}([u_a^{(i)}a_a^\dagger+v_a^{(f)}D(a)^{-1}a_{\bar{a}}], \cdots, \\ &\qquad [u_c^{(f)}D(c)^{-1}a_\gamma+v_c^{(i)}a_{\bar{\gamma}}^\dagger], \cdots)\end{aligned} \tag{6B·7}$$

with

$$\hat{G}=\exp[-2\textstyle\sum_a\hat{S}_0(a)\log D(a)],$$

where $D(a)=\cos(\Delta\theta_a/2)=u_a^{(i)}u_a^{(f)}+v_a^{(i)}v_a^{(f)}$, $\Delta\theta_a$ being defined by $\Delta\theta_a=\theta_a^{(i)}-\theta_a^{(f)}$.

In the right-hand side of Eq. (6B·6), we have omitted the superscript (f) for the set of rotation angles $\boldsymbol{\theta}$ and the quasi-particle operators; since, as is easily proved by the same procedure as above, the set of rotation angles to which we refer in evaluating the transition matrix element can be chosen arbitrarily. Thus, by replacing $\hat{O}$ with the "effective transition operator" $\hat{\mathcal{O}}$, we can exactly take account of the difference of nucleon numbers between the initial and final states. In the actual calculations, it may be sufficient to consider only the first order terms in $\Delta\theta_a$. Then, the effective operator $\hat{\mathcal{O}}$ takes much simplified form:

$$\hat{O} \simeq \hat{O}([u_a^{(i)} a_a^\dagger + v_a^{(f)} a_{\bar{a}}], \cdots, [u_c^{(f)} a_\gamma + v_c^{(i)} a_{\bar{\gamma}}^\dagger], \cdots). \tag{6B·8}$$

References

1) H. Horie and K. Sasaki, Prog. Theor. Phys. **25** (1961), 475.
2) L. S. Kisslinger and R. A. Sorensen, Rev. Mod. Phys. **35** (1963), 853.
3) H. Bando, Prog. Theor. Phys. **38** (1967), 1285.
4) P. H. Stelson et al., Nucl. Phys. **A190** (1972), 197.
5) E. J. Schneid, A. Prakash and B. L. Cohen, Phys. Rev. **156** (1967), 1316.
6) T. T. S. Kuo, E. U. Baranger and M. Baranger, Nucl. Phys. **79** (1966), 513.
7) J-I. Fujita and K. Ikeda, Nucl. Phys. **67** (1965), 145; Prog. Theor. Phys. **35** (1966), 622.
8) J. A. Halbleib and R. A. Sorensen, Nucl. Phys. **A98** (1968), 542.
9) M. Fuyuki, Prog. Theor. Phys. **51** (1974), 1633.
10) M. Fuyuki, Prog. Theor. Phys. **53** (1975), 1691.
11) A. Arima and H. Horie, Prog. Theor. Phys. **12** (1954), 623.
H. Noya, A. Arima and H. Horie, Prog. Theor. Phys. Suppl. No. 8 (1958), 33.

Part IV. A Next Subject

Chapter 7. Coupling between Collective and Intrinsic Modes of Excitation

Atsushi KURIYAMA, Toshio MARUMORI,* Kenichi MATSUYANAGI,**
Fumihiko SAKATA* and Tōru SUZUKI**

Department of Physics, Kyushu University, Fukuoka 812
**Institute for Nuclear Study, University of Tokyo*
Tanashi, Tokyo 188
***Department of Physics, Kyoto University, Kyoto 606*

(Received July 15, 1975)

§ 1. Introduction

In the preceding chapters we have shown that the low-lying collective excited states in spherical odd-mass nuclei can be successfully described in terms of the dressed nQP modes prescribed by the concept of transferred seniority. Since the dressed nQP modes are defined in the "intrinsic space," which does not involve any $J=0$-coupled quasi-particle pair, they are independent of the "collective" modes of pairing correlation within the NTD approximation. In this chapter we investigate the coupling between such independent modes of excitation.

Now, according to the canonical transformation method developed in Chap. 1, we can regard the space of states in terms of quasi-particles as a product space consisting of the "intrinsic" space and the "collective" (boson) space. In this representation, the original quasi-particle interaction is classified into three types: The first represents an interaction causing the mixing among the "intrinsic" states, the second among the "collective" states and the last between "collective" and "intrinsic" states. As has been shown in § 2 of Chap. 2, the first-type interaction in the intrinsic space can furthermore be divided into two parts, i.e., the constructive force which is responsible for constructing the dressed nQP modes, and the interactive force which manifests itself as the coupling among the different nQP modes. What we have investigated in Part III as the coupling effect is nothing but the effect originating from this interactive force.

The other new type of coupling effect may arise from the third-type interaction which causes the mixing between the collective and intrinsic states. Since the collective space involves all of the quantum fluctuations of the

pairing field, i.e., the excitation modes of $J=0$-coupled quasi-particle pairs, the third-type interaction manifests itself as a coupling between the pairing vibrational modes and the dressed nQP modes. In treating the mutual interweaving of such composite modes of excitation, there are well-known difficulties such as the overcompleteness in the degrees of freedom and the violation of Pauli principle. However, the independency of the "collective" pairing modes and the dressed nQP modes enables us to overcome these difficulties.

The main purpose of this chapter is to investigate the formal structure and physical implication of this coupling, leaving the detailed analysis of its effect in comparison with experiment as a next subject.

§ 2. The pairing Hamiltonian in collective representation

The original quasi-particle interaction H_{int} given by Eq. (1·3·4)*) may be divided into two parts:

$$H_{\text{int}}=H_{\text{int}}^{(1)}+H_{\text{int}}^{(2)}, \tag{2·1}$$

where the first-kind interaction $H_{\text{int}}^{(1)}$ satisfies

$$[\hat{\boldsymbol{S}}(a)^2, H_{\text{int}}^{(1)}]=0 \text{ for each orbit } a, \tag{2·2}$$

and the second-kind interaction is defined by

$$[\hat{\boldsymbol{S}}(a)^2, H_{\text{int}}^{(2)}]\neq 0. \tag{2·3}$$

Here $\hat{\boldsymbol{S}}(\text{a})^2$ is the quasi-spin operator of orbit a,

$$\hat{\boldsymbol{S}}(a)^2=\hat{S}_+(a)\hat{S}_-(a)+\hat{S}_0(a)^2-\hat{S}_0(a),$$

where $\hat{S}_\pm(a)$ and $\hat{S}_0(a)$ are defined in Eq. (1·2·18). Since the quasi-spin quantum number $S(a)$ is known to be related to the seniority number v_a of orbit a through

$$S(a)=\frac{1}{2}(\Omega_a-v_a), \quad \left(\Omega_a\equiv j_a+\frac{1}{2}\right),$$

Eqs. (2·2) and (2·3) imply that the first-kind interaction $H_{\text{int}}^{(1)}$ does not violate the seniority number v_a of each orbit, while the second-kind interaction $H_{\text{int}}^{(2)}$ changes the seniority number v_a.

In this section, we investigate the coupling between the "collective" and "intrinsic" degrees of freedom which originates from the first-kind interaction $H_{\text{int}}^{(1)}$. A typical example of the first-kind interaction is known to be the pairing interaction. Therefore, we adopt the pairing Hamiltonian given

*) We cite the equations in different chapters by adding the chapter number to the first place of the equation number.

by Eq. (1B·2) in Appendix 1B as an illustrative example. As a matter of convenience, we here leave the parameters (u_a, v_a) of Bogoliubov transformation undetermined, although it is custom to determine the parameters (u_a, v_a) so as to eliminate the "dangerous term" $H_1^{(p)}$ in Eq. (1B·2).

Applying the canonical transformation (1·5·8), we obtain the pairing Hamiltonian in the collective representation:

$$
\begin{aligned}
&\boldsymbol{H}^{(p)} = U^{(p)} + \boldsymbol{H}_0^{(p)} + \boldsymbol{H}_1^{(p)} + \boldsymbol{H}_{\mathrm{int}}^{(p)}, \qquad (2\cdot4)\\
&U^{(p)} = \sum_a 2\Omega_a \left\{ \left(\eta_a + \frac{1}{2} G v_a^2 \right) v_a^2 - \frac{1}{2} u_a v_a \Delta \right\},\\
&\boldsymbol{H}_0^{(p)} = \sum_a \{ \eta_a (u_a^2 - v_a^2) + 2 u_a v_a \Delta \} \{ \hat{n}_a + 2\hat{\boldsymbol{N}}(a) \},\\
&\boldsymbol{H}_1^{(p)} = \sum_a \{ 2\eta_a u_a v_a - (u_a^2 - v_a^2)\Delta \} \{ \boldsymbol{b}_a^\dagger \sqrt{\Omega_a - \hat{n}_a - \hat{\boldsymbol{N}}(a)} + \sqrt{\Omega_a - \hat{n}_a - \hat{\boldsymbol{N}}(a)}\, \boldsymbol{b}_a \},\\
&\boldsymbol{H}_{\mathrm{int}}^{(p)} = \boldsymbol{H}_X^{(p)} + \boldsymbol{H}_{V'}^{(p)} + \boldsymbol{H}_{V}^{(p)} + \boldsymbol{H}_{\mathrm{exch}}^{(p)},
\end{aligned}
$$

where

$$
\begin{aligned}
&\eta_a = \epsilon_a - \lambda - G v_a^2, \qquad \Omega_a = j_a + \frac{1}{2}, \qquad \Delta = G \sum_a \Omega_a u_a v_a,\\
&\hat{n}_a = \sum_{m_a} a_a^\dagger a_a, \qquad \hat{\boldsymbol{N}}(a) = \boldsymbol{b}_a^\dagger \boldsymbol{b}_a,
\end{aligned}
\qquad (2\cdot5)
$$

and

$$
\begin{aligned}
&\boldsymbol{H}_X^{(p)} = -G \sum_{ac} (u_a^2 u_c^2 + v_a^2 v_c^2) \boldsymbol{b}_a^\dagger \sqrt{\Omega_a - \hat{n}_a - \hat{\boldsymbol{N}}(a)} \cdot \sqrt{\Omega_c - \hat{n}_c - \hat{\boldsymbol{N}}(c)}\, \boldsymbol{b}_c \},\\
&\boldsymbol{H}_{V'}^{(p)} = \frac{1}{2} G \sum_{ac} (u_a^2 v_c^2 + v_a^2 u_c^2) \{ \boldsymbol{b}_a^\dagger \sqrt{\Omega_a - \hat{n}_a - \hat{\boldsymbol{N}}(a)} \cdot \boldsymbol{b}_c^\dagger \sqrt{\Omega_c - \hat{n}_c - \hat{\boldsymbol{N}}(c)} + \mathrm{h.c.} \},\\
&\boldsymbol{H}_{V}^{(p)} = G \sum_{ac} (u_a^2 - v_a^2) u_c v_c [\boldsymbol{b}_a^\dagger \sqrt{\Omega_a - \hat{n}_a - \hat{\boldsymbol{N}}(a)} \cdot \{ \hat{n}_c + 2\hat{\boldsymbol{N}}(c) \} + \mathrm{h.c.}],\\
&\boldsymbol{H}_{\mathrm{exch}}^{(p)} = -G \sum_{ac} u_a v_a u_c v_c [\{ \hat{n}_a + 2\hat{\boldsymbol{N}}(a) \} \{ \hat{n}_c + 2\hat{\boldsymbol{N}}(c) \} - \{ \hat{n}_a + 2\hat{\boldsymbol{N}}(a) \} \delta_{ac}].
\end{aligned}
\qquad (2\cdot6)
$$

In this collective representation, the boson operators $(\boldsymbol{b}_a^\dagger, \boldsymbol{b}_a)$ and the quasi-particle operators $(a_a^\dagger, a_a)$ describe the collective and intrinsic degrees of freedom respectively, and therefore their mutual interweaving is clearly visualized. Needless to say, the quasi-particle number n_a of each orbit a in this representation must be the same as the seniority number v_a, because of the supplementary condition (1·6·10) for the "intrinsic" state. In the case of the Hamiltonian with the first-kind interaction satisfying (2·2), therefore, we always have

$$
[\hat{n}_a, \boldsymbol{H}^{(p)}] = 0, \qquad (2\cdot7)
$$

which shows that the "intrinsic" state $|\phi_{\mathrm{intr}}\rangle$ must be an eigenstate of the quasi-particle number $\hat{n}_a$ of each orbit, i.e.,

$$
|\phi_{\mathrm{intr}}\rangle = |S(a), S_0(a) = -S(a); S(b), S_0(b) = -S(b); \cdots; \Gamma\rangle \qquad (2\cdot8)
$$

where Γ denotes a set of additional quantum numbers to specify the intrinsic

eigenstate. This implies that the Tamm-Dancoff basis vectors in the "intrinsic" space discussed in §2-1 of Chap. 2 themselves become the intrinsic eigenstates of the Hamiltonian with the first-kind interaction, and they are never mixed with each other through their interweaving with collective pairing modes.

Now, according to the method developed in § 6 of Chap. 1, let us expand the pairing Hamiltonian (2·4) in terms of the creation and annihilation operators of the pairing vibrations

$$\begin{aligned} \boldsymbol{X}_{\mu}^{\dagger} &= \sum_{a}\{\psi_{\mu}(a)\boldsymbol{b}_{a}^{\dagger}+\phi_{\mu}(a)\boldsymbol{b}_{a}\}, \\ \boldsymbol{X}_{\mu} &= \sum_{a}\{\psi_{\mu}(a)\boldsymbol{b}_{a}+\phi_{\mu}(a)\boldsymbol{b}_{a}^{\dagger}\}, \end{aligned} \tag{2·9}$$

the details of which are given in Appendix 1B. Then, the expanded Hamiltonian takes the form given by Eq. (1·6·7):

$$\begin{aligned} \boldsymbol{H}^{(p)} &= H_{\mathrm{intr}}^{(p)}+\boldsymbol{H}_{\mathrm{I}}^{(p)}+\boldsymbol{H}_{\mathrm{II}}^{(p)}, \\ H_{\mathrm{intr}}^{(p)} &= \hat{h}_{00}^{(p)}, \\ \boldsymbol{H}_{\mathrm{I}}^{(p)} &= \sum_{\mu}\{\boldsymbol{X}_{\mu}^{\dagger}\hat{h}_{10}^{(p)}(\mu)+\boldsymbol{X}_{\mu}\hat{h}_{01}^{(p)}(\mu)\}, \\ \boldsymbol{H}_{\mathrm{II}}^{(p)} &= \frac{1}{2}\sum_{\mu\nu}\{\boldsymbol{X}_{\mu}^{\dagger}\boldsymbol{X}_{\nu}^{\dagger}\hat{h}_{20}^{(p)}(\mu\nu)+\boldsymbol{X}_{\nu}\boldsymbol{X}_{\mu}\hat{h}_{02}^{(p)}(\mu\nu)+2\boldsymbol{X}_{\mu}^{\dagger}\boldsymbol{X}_{\nu}\hat{h}_{11}^{(p)}(\mu\nu)\}, \end{aligned} \tag{2·10}$$

where we have consistently neglected all terms which involve commutators of $\mathring{H}^{(p)}$ with $X_{\mu}^{\dagger}$ (or X_{μ}) higher than double. The operators $\hat{h}_{ij}^{(p)}$ only involve the intrinsic degrees of freedom represented in terms of the quasi-particles and are defined by Eq. (1·6·8). According to the same procedure as used in deriving Eq. (1·6·14b), the pairing Hamiltonian (2·10) can be effectively reduced to the form

$$\begin{aligned} \boldsymbol{H}^{(p)} &= H_{\mathrm{intr}}^{(p)}+\boldsymbol{H}_{\mathrm{I}}^{(p)}+\boldsymbol{H}_{\mathrm{II}}^{(p)}, \\ H_{\mathrm{intr}}^{(p)} &= \mathring{H}^{(p)}-\frac{1}{2}\sum_{\mu\nu a}\phi_{\mu}(a)\phi_{\nu}(a)\{[X_{\mu},[\mathring{H}^{(p)},X_{\nu}^{\dagger}]]+\mathrm{h.c.}\} \\ &\quad -\frac{1}{2}\sum_{\mu\nu a}\phi_{\mu}(a)\psi_{\nu}(a)\{[X_{\mu},[X_{\nu},\mathring{H}^{(p)}]]+[[\mathring{H}^{(p)},X_{\nu}^{\dagger}],X_{\mu}^{\dagger}]\}, \\ \boldsymbol{H}_{\mathrm{I}}^{(p)} &= \sum_{\mu}\{\boldsymbol{X}_{\mu}^{\dagger}[X_{\mu},\mathring{H}^{(p)}]+\boldsymbol{X}_{\mu}[\mathring{H}^{(p)},X_{\mu}^{\dagger}]\}, \\ \boldsymbol{H}_{\mathrm{II}}^{(p)} &= \frac{1}{2}\sum_{\mu\nu}\{\boldsymbol{X}_{\mu}^{\dagger}\boldsymbol{X}_{\nu}^{\dagger}[X_{\mu},[X_{\nu},\mathring{H}^{(p)}]]+\boldsymbol{X}_{\nu}\boldsymbol{X}_{\mu}[[\mathring{H}^{(p)},X_{\nu}^{\dagger}],X_{\mu}^{\dagger}] \\ &\qquad +2\boldsymbol{X}_{\mu}^{\dagger}\boldsymbol{X}_{\nu}[X_{\mu},[\mathring{H}^{(p)},X_{\nu}^{\dagger}]\}. \end{aligned} \tag{2·11}$$

In the case of the pairing Hamiltonian, the commutators of $\mathring{H}^{(p)}$ with $X_{\mu}^{\dagger}$ (or X_{μ}) which appear in Eq. (2·11) are easily calculated: Provided that the supplementary condition (1·6·10) is always kept to be satisfied properly, we obtain

$$[X_\mu, \mathring{H}^{(p)}]=[\mathring{H}^{(p)}, X_\mu^\dagger]$$
$$=\sum_a\{\psi_\mu(a)-\phi_\mu(a)\}\{2\eta_a u_a v_a-(u_a^2-v_a^2)\hat{\Delta}'\}\sqrt{\Omega_a-\hat{n}_a}\,, \quad (2\cdot12a)$$

$$[X_\mu, [\mathring{H}^{(p)}, X_\nu^\dagger]]=(\boldsymbol{\phi}_\mu^T, \boldsymbol{\psi}_\mu^T)\begin{bmatrix}\hat{\boldsymbol{d}}' & \hat{\boldsymbol{a}}'\\ \hat{\boldsymbol{a}}' & \hat{\boldsymbol{d}}'\end{bmatrix}\begin{bmatrix}\boldsymbol{\psi}_\nu\\ \boldsymbol{\phi}_\nu\end{bmatrix}, \quad (2\cdot12b)$$

$$[X_\mu, [X_\nu, \mathring{H}^{(p)}]]=[[\mathring{H}^{(p)}, X_\nu^\dagger], X_\mu^\dagger]=-(\boldsymbol{\phi}_\mu^T, \boldsymbol{\psi}_\mu^T)\begin{bmatrix}\hat{\boldsymbol{d}}' & \hat{\boldsymbol{a}}'\\ \hat{\boldsymbol{a}}' & \hat{\boldsymbol{d}}'\end{bmatrix}\begin{bmatrix}\boldsymbol{\psi}_\nu\\ \boldsymbol{\phi}_\nu\end{bmatrix}, \quad (2\cdot12c)$$

where the matrices $\hat{\boldsymbol{a}}'$ and $\hat{\boldsymbol{d}}'$ are defined by

$$\begin{aligned}\hat{d}'_{ab}&=2(\hat{E}'_a-Gu_a^2v_a^2)\delta_{ab}-G(u_a^2u_b^2+v_a^2v_b^2)\sqrt{(\Omega_a-\hat{n}_a)(\Omega_b-\hat{n}_b)}\,,\\ \hat{a}'_{ab}&=2Gu_a^2v_a^2\delta_{ab}-G(u_a^2v_b^2+v_a^2u_b^2)\sqrt{(\Omega_a-\hat{n}_a)(\Omega_b-\hat{n}_b)}\end{aligned} \quad (2\cdot13)$$

with

$$\begin{aligned}\hat{\Delta}'&\equiv G\sum_a u_a v_a(\Omega_a-\hat{n}_a),\\ \hat{E}'_a&\equiv\eta_a(u_a^2-v_a^2)+2u_a v_a\hat{\Delta}'.\end{aligned} \quad (2\cdot14)$$

At this step, let us self-consistently determine the parameters (u_a, v_a) of Bogoliubov transformation and the amplitudes $(\psi_\mu(a), \phi_\mu(a))$ of the pairing vibrational modes in Eq. (2·7). The parameters (u_a, v_a) are determined, with the aid of the intrinsic eigenstate (2·8), by the condition

$$\langle\phi_{\text{intr}}|\boldsymbol{H}_{\text{I}}^{(p)}|\phi_{\text{intr}}\rangle=0, \quad (2\cdot15)$$

$$2\eta_a u_a v_a-G(u_a^2-v_a^2)\sum_b(\Omega_b-n_b)u_b v_b=0, \quad (2\cdot16)$$

which is just the gap equation with the blocking effects. The amplitudes $(\psi_\mu(a), \phi_\mu(a))$ are then determined in order to diagonalize the matrix $\langle\phi_{\text{intr}}|\boldsymbol{H}_{\text{II}}^{(p)}|\phi_{\text{intr}}\rangle$, i.e.,

$$\begin{bmatrix}\boldsymbol{d}' & \boldsymbol{a}'\\ -\boldsymbol{a}' & -\boldsymbol{d}'\end{bmatrix}\begin{bmatrix}\boldsymbol{\psi}_\mu\\ \boldsymbol{\phi}_\mu\end{bmatrix}=\omega_\mu\begin{bmatrix}\boldsymbol{\psi}_\mu\\ \boldsymbol{\phi}_\mu\end{bmatrix}, \quad \omega_\mu\geq 0, \quad (2\cdot17)$$

where the c-number matrices $\boldsymbol{a}'$ and $\boldsymbol{d}'$ are given by replacing the quasi-particle number operator $\hat{n}_a$ in the matrices $\hat{\boldsymbol{a}}'$ and $\hat{\boldsymbol{d}}'$ with its eigenvalue n_a in the intrinsic eigenstate (2·8). Equation (2·17) is just the eigenvalue equation of the pairing vibrational modes with the blocking effects. Here it is worthy of note that, in spite of the inclusion of the blocking effects, Eq. (2·17) certainly has the zero-energy solution just as the usual eigenvalue equation (without the blocking effects) does.

It is now clear that the main effects of the coupling between the "collective" and "intrinsic" degrees of freedom, which originates from the first-kind

interaction $H_{\mathrm{int}}^{(1)}$, can be renormalized into both the quasi-particle field and the pairing vibrational modes.

§3. Expressions of the Hamiltonian and electromagnetic multipole operators in terms of pairing vibrational modes and dressed nQP modes

In this section we develop a theory in which the mutual interweaving of the "collective" and "intrinsic" degrees of freedom can be treated in terms of the "collective" pairing vibrational modes and the "intrinsic" dressed nQP modes. The independency of the pairing vibrational modes and the dressed nQP modes (within the NTD approximation) enables us to overcome the well-known difficulties in determining the coupling between composite modes, such as the overcompleteness in the degrees of freedom and the violation of Pauli principle.

3-1 *Coupling Hamiltonian*

Contrary to the first-kind interaction $H_{\mathrm{int}}^{(1)}$, the second-kind interaction $H_{\mathrm{int}}^{(2)}$ changes the seniority number of each orbit. Hence the second-kind interaction remarkably affects the structure of the "intrinsic" space, the basis vectors of which are characterized by the seniority number v_a of each orbit. In fact, as shown in Part II, this kind of interaction constitutes the main part of the quasi-particle interaction in the intrinsic Hamiltonian H_{intr} given by Eq. (1·6·14). In Part III we have investigated the various effects on the structure of the "intrinsic" states, that are caused mainly by the second-kind interaction, and shown that many properties of the spherical odd-mass nuclei are characterized by these effects. Also in the coupling between the "collective" and "intrinsic" degrees of freedom, we expect that the second-kind interaction causes more complex effects than those originating from the first-kind interaction.

When the second-kind interaction becomes effective, the eigenvector of the quasi-spin operator (2·8) is no longer the eigenvector of the intrinsic space. In this case, the coupling between the collective and intrinsic degrees of freedom, which originates from the first-kind interaction, becomes difficult to be simply renormalized into the quasi-particle field or the pairing vibrational modes. Therefore, in this section we treat the original quasi-particle interaction as a whole, without insisting on such a separation of the interaction into the first- and second-kind interactions.

We start our discussion with the collective representation of the original Hamiltonian H given by Eq. (1·6·14):

$$H \longrightarrow \text{const}+\boldsymbol{H}_{\mathrm{col}}+H_{\mathrm{intr}}+H_{\mathrm{coupl}},$$
$$\boldsymbol{H}_{\mathrm{col}}=\sum_{\mu}\omega_{\mu}\boldsymbol{X}_{\mu}^{\dagger}\boldsymbol{X}_{\mu},$$

$$H_{\text{intr}}=H-\frac{1}{2}\sum_{\mu\nu a}\phi_{\mu}(a)\phi_{\nu}(a)\{[X_{\mu}, Z_{\nu}]+\text{h.c.}\}$$
$$-\frac{1}{2}\sum_{\mu\nu a}\phi_{\mu}(a)\psi_{\nu}(a)\{[X_{\mu}, Z_{\nu}^{\dagger}]+[Z_{\mu}, X_{\nu}^{\dagger}]\},$$

$$H_{\text{coupl}}=\sum_{\mu}(\boldsymbol{X}_{\mu}^{\dagger}Z_{\mu}^{\dagger}+\boldsymbol{X}_{\mu}Z_{\mu})+\frac{1}{2}\sum_{\mu\nu}\{2\boldsymbol{X}_{\mu}^{\dagger}\boldsymbol{X}_{\nu}[X_{\mu}, Z_{\nu}]$$
$$+\boldsymbol{X}_{\mu}^{\dagger}\boldsymbol{X}_{\nu}^{\dagger}[X_{\mu}, Z_{\nu}^{\dagger}]+\boldsymbol{X}_{\nu}\boldsymbol{X}_{\mu}[Z_{\nu}, X_{\mu}^{\dagger}]\},$$

where Z denotes the interaction which is neglected in constructing the pairing vibrational modes within the RPA, and where all terms which involve the commutators of Z_{ν} (or $Z_{\nu}^{\dagger}$) with $X_{\mu}^{\dagger}$ (or X_{μ}) higher than single are neglected. In § 5-2 of Chap. 2, we have given the transcription rule, by which any physical operator depending only on the intrinsic degrees of freedom can be unambiguously transcribed into the quasi-particle NTD space. With the aid of the transcription rule, the intrinsic Hamiltonian H_{intr} has already been expressed in terms of the dressed nQP modes (see § 5-3 of Chap. 2). Now we express the coupling Hamiltonian H_{coupl} in terms of the pairing vibrational modes and the dressed nQP modes. The parts written by thin letters in the coupling Hamiltonian H_{coupl} only involve the intrinsic degrees of freedom represented in terms of the quasi-particle operators. Thus, with the aid of the transcription rule, these parts can also be transcribed into the quasi-particle NTD space as the intrinsic space: With the creation and annihilation operators of the dressed nQP modes ($Y_{s\lambda}^{\dagger}$, $Y_{s\lambda}$), we have

$$H_{\text{coupl}}\longrightarrow\sum_{s\lambda s'\lambda'\mu}\langle\Phi_0|Y_{s\lambda}Z_{\mu}Y_{s'\lambda'}^{\dagger}|\Phi_0\rangle(\boldsymbol{Y}_{s\lambda}^{\dagger}\boldsymbol{Y}_{s'\lambda'}\boldsymbol{X}_{\mu}+\text{h.c.})$$
$$+\sum_{s\lambda s'\lambda'\mu\mu'}\langle\Phi_0|Y_{s\lambda}[X_{\mu}, Z_{\mu'}]Y_{s'\lambda'}^{\dagger}|\Phi_0\rangle\boldsymbol{X}_{\mu}^{\dagger}\boldsymbol{Y}_{s\lambda}^{\dagger}\boldsymbol{Y}_{s'\lambda'}\boldsymbol{X}_{\mu'}$$
$$+\frac{1}{2}\sum_{s\lambda s'\lambda'\mu\mu'}\langle\Phi_0|Y_{s\lambda}[Z_{\mu'}, X_{\mu}^{\dagger}]Y_{s'\lambda'}^{\dagger}|\Phi_0\rangle(\boldsymbol{Y}_{s\lambda}^{\dagger}\boldsymbol{Y}_{s'\lambda'}\boldsymbol{X}_{\mu'}\boldsymbol{X}_{\mu}+\text{h.c.}). \quad (3\cdot1)$$

The matrix elements in the above expression are then easily evaluated using the transcription rule (2·5·8).

Thus, the original Hamiltonian is expressed in terms of the pairing vibrational modes and the dressed nQP modes as follows:

$$H\longrightarrow\text{const}+\boldsymbol{H}_{\text{col}}+\boldsymbol{H}_{\text{intr}}+\boldsymbol{H}_{\text{coupl}}, \quad (3\cdot2a)$$
$$\boldsymbol{H}_{\text{col}}=\sum_{\mu}\omega_{\mu}\boldsymbol{X}_{\mu}^{\dagger}\boldsymbol{X}_{\mu},$$
$$\boldsymbol{H}_{\text{intr}}=\sum_{\alpha}E_{\alpha}\boldsymbol{a}_{\alpha}^{\dagger}\boldsymbol{a}_{\alpha}+\sum_{\lambda}\omega_{\lambda}\boldsymbol{Y}_{\lambda}^{\dagger}\boldsymbol{Y}_{\lambda}+\sum_{\alpha\lambda}V_{\text{int}}(\alpha, \lambda)(\boldsymbol{Y}_{\lambda}^{\dagger}\boldsymbol{a}_{\alpha}+\boldsymbol{a}_{\alpha}^{\dagger}\boldsymbol{Y}_{\lambda}), \quad (3\cdot2b)$$
$$\boldsymbol{H}_{\text{coupl}}=\sum_{\alpha\mu}E_{\alpha}(\mu)(\boldsymbol{X}_{\mu}^{\dagger}+\boldsymbol{X}_{\mu})\boldsymbol{a}_{\alpha}^{\dagger}\boldsymbol{a}_{\alpha}+\sum_{\lambda\lambda'\mu}V_{\text{int}}(\mu; \lambda, \lambda')(\boldsymbol{Y}_{\lambda}^{\dagger}\boldsymbol{Y}_{\lambda'}\boldsymbol{X}_{\mu}+\text{h.c.})$$
$$+\sum_{\alpha\lambda\mu}V_{\text{int}}(\mu; \lambda, \alpha)(\boldsymbol{Y}_{\lambda}^{\dagger}\boldsymbol{a}_{\alpha}\boldsymbol{X}_{\mu}+\text{h.c.})+\sum_{\alpha\lambda\mu}V_{\text{int}}(\mu; \alpha, \lambda)(\boldsymbol{a}_{\alpha}^{\dagger}\boldsymbol{Y}_{\lambda}\boldsymbol{X}_{\mu}+\text{h.c.}).$$

In the above expression we have adopted the same quasi-particle NTD subspace as employed in § 5 of Chap. 2, which consists of the 1QP and dressed

3QP modes, and furthermore we have given explicitly the effects of lowest order of the coupling between the collective and intrinsic degrees of freedom. The explicit forms of $E_a(\mu)$ and $V_{\rm int}(\mu;\cdots)$ are given in Appendix 7A.

3-2 *Effective electromagnetic multipole operators in collective-intrinsic-coupled system*

For the investigation of the system in which the collective and intrinsic modes are coupled to each other, it is necessary to express physical operators such as electromagnetic multipole operators in terms of the collective and intrinsic modes of excitation. This is easily performed in the same way as was done for the Hamiltonian. Any physical operator $\hat{F}$ is first transformed into the collective representation in terms of the pairing-vibration modes $(\boldsymbol{X}^\dagger_\mu,\ \boldsymbol{X}_\mu)$:

$$\begin{aligned}\hat{\boldsymbol{F}} &\equiv U_{\rm col}\cdot\mathring{F}\cdot U^{-1}_{\rm col}\\ &=\mathring{F}+\sum_\mu\{\boldsymbol{X}^\dagger_\mu[X_\mu,\mathring{F}]+\boldsymbol{X}_\mu[\mathring{F},X^\dagger_\mu]\}+\cdots,\end{aligned}\tag{3·3}$$

where $U_{\rm col}$ is the canonical transformation defined by Eq. (1·5·8) and $\mathring{F}$ denotes the operator extended into the extended quasi-spin space discussed in § 4 of Chap. 1. The first term depends only on the intrinsic degrees of freedom represented in terms of the quasi-particle operators. Therefore, in the same way as was done in § 5-3 of Chap. 2, the first term can be expressed in terms of the dressed nQP modes by the use of the transcription rule. The parts written by thin letters in the second term are composed of the quasi-particle operators representing the intrinsic degrees of freedom. Consequently, these parts can also be easily expressed in terms of the dressed nQP modes, with the aid of the transcription rule (2·5·8). Here, we give the expression for the case where the operator $\hat{F}$ represent the electromagnetic multipole operator $\hat{O}^{(\pm)}_{LM}$: In this case, the term corresponding to the first term of Eq. (3·3) has already been expressed by Eq. (2·5·14). For the corresponding second term, we obtain

$$\begin{aligned}&\sum_\mu\{\boldsymbol{X}^\dagger_\mu[X_\mu,\mathring{O}^{(\pm)}_{LM}]+\boldsymbol{X}_\mu[\mathring{O}^{(\pm)}_{LM},X^\dagger_\mu]\}\\ &\quad\longrightarrow\sum_{\alpha\beta\mu}\{\langle\Phi_0|a_\alpha[X_\mu,\mathring{O}^{(\pm)}_{LM}]a^\dagger_\beta|\Phi_0\rangle\boldsymbol{X}^\dagger_\mu\boldsymbol{a}^\dagger_\alpha\boldsymbol{a}_\beta\\ &\qquad+\langle\Phi_0|a_\alpha[\mathring{O}^{(\pm)}_{LM},X^\dagger_\mu]a^\dagger_\beta|\Phi_0\rangle\boldsymbol{a}^\dagger_\alpha\boldsymbol{a}_\beta\boldsymbol{X}_\mu\}\\ &\qquad+\sum_{\lambda\lambda'\mu}\{\langle\Phi_0|Y_\lambda[X_\mu,\mathring{O}^{(\pm)}_{LM}]Y^\dagger_{\lambda'}|\Phi_0\rangle\boldsymbol{X}^\dagger_\mu\boldsymbol{Y}^\dagger_\lambda\boldsymbol{Y}_{\lambda'}\\ &\qquad+\langle\Phi_0|Y_\lambda[\mathring{O}^{(\pm)}_{LM},X^\dagger_\mu]Y^\dagger_{\lambda'}|\Phi_0\rangle\boldsymbol{Y}^\dagger_\lambda\boldsymbol{Y}_{\lambda'}\boldsymbol{X}_\mu\},\end{aligned}\tag{3·4a}$$

$$\begin{aligned}&\sum_\mu\{\boldsymbol{X}^\dagger_\mu[X_\mu,\bar{O}^{(\pm)}_{LM}]+\boldsymbol{X}_\mu[\bar{O}^{(\pm)}_{LM},X^\dagger_\mu]\}\\ &\quad\longrightarrow\sum_{\alpha\lambda\mu}\{\langle\Phi_0|Y_\lambda[X_\mu,\bar{O}^{(\pm)}_{LM}]a^\dagger_\alpha|\Phi_0\rangle\boldsymbol{X}^\dagger_\mu\boldsymbol{Y}^\dagger_\lambda\boldsymbol{a}_\alpha\\ &\qquad+\langle\Phi_0|a_\alpha[X_\mu,\bar{O}^{(\pm)}_{LM}]Y^\dagger_\lambda|\Phi_0\rangle\boldsymbol{X}^\dagger_\mu\boldsymbol{a}^\dagger_\alpha\boldsymbol{Y}_\lambda\}\\ &\qquad+\sum_{\alpha\lambda\mu}\{\langle\Phi_0|Y_\lambda[\bar{O}^{(\pm)}_{LM},X^\dagger_\mu]a^\dagger_\alpha|\Phi_0\rangle\boldsymbol{Y}^\dagger_\lambda\boldsymbol{a}_\alpha\boldsymbol{X}_\mu\\ &\qquad+\langle\Phi_0|a_\alpha[\bar{O}^{(\pm)}_{LM},X^\dagger_\mu]Y^\dagger_\lambda|\Phi_0\rangle\boldsymbol{a}^\dagger_\alpha\boldsymbol{Y}_\lambda\boldsymbol{X}_\mu\}.\end{aligned}\tag{3·4b}$$

The explicit forms of the matrix elements in the above expressions are given in Appendix 7B.

Thus we have derived all necessary expressions for the Hamiltonian and the electromagnetic multipole operators, in terms of the "collective" pairing vibrational modes and the "intrinsic" dressed nQP modes. In this way, we have obtained a theory, by which we can systematically study the structure of the coupling between the pairing vibrational modes and the dressed nQP modes.

§4. Concluding remarks

We have studied some physical implications of the coupling between the "collective" and "intrinsic" degrees of freedom, according to the method developed in § 6 of Chap. 1. In this method, all physical operators such as the Hamiltonian and the electromagnetic multipole operators are expressed in a form of expansion in terms of the creation and annihilation operators of the pairing vibrational modes. When the interaction of the original Hamiltonian does not violate the seniority number v_a of each orbit, the coupling between the collective and intrinsic degrees of freedom becomes very simple. We have shown by adopting the pairing Hamiltonian that the coupling can be renormalized into both the quasi-particle field and the pairing vibrational modes as the blocking effects. On the other hand, as shown in Part III, the interaction which does change the seniority number v_a of each orbit causes various significant effects on the structure of the intrinsic states. Such a kind of interaction causes also the coupling between the collective and intrinsic degrees of freedom bringing about abundant effects on the structure of the spherical odd-mass nuclei.

Since the dressed nQP modes are defined in the intrinsic space, which does not involve any $J=0$-coupled quasi-particle pair, they are independent of the "collective" modes of pairing correlation within the NTD approximation. This independency of the dressed nQP modes and the pairing vibrational modes enables us to overcome the well-known difficulties in treating the mutual interweaving of the composite modes, such as the overcompleteness in the degrees of freedom and the violation of Pauli principle. Thus, using this independency, we have developed a theory, by which the coupling between the collective and the intrinsic degrees of freedom can be systematically studied in terms of the interplay between the pairing vibrational modes and the dressed nQP modes.

Recent accumulation of various kinds of experimental data is illuminating the structure of the couplings among composite modes of excitation. In the light of experimental development, the method of mode-mode coupling becomes one of hopeful approaches to understand the mechanism of the change in the structure of nuclei. The "collective" pairing vibrational modes represent

just the fluctuation of the "spherical" quasi-particle field. Hence, the coupling between the "collective" pairing vibrational modes and the "intrinsic" dressed nQP modes is expected to provide a wealth of information on the mechanism of the change of the "spherical" quasi-particle field into, for example, a "deformed" field. Thus, it is one of the subjects of growing interest to systematically study the coupling between the pairing vibrational modes and the dressed nQP modes in comparison with experimental data.

Appendix 7A. Coupling between pairing vibrational modes and dressed nQP modes

We give the explicit forms of the matrix elements appearing in the coupling Hamiltonian, $\boldsymbol{H}_{\text{coupl}}$, defined by Eq. (3·2b).

7A-1 *Coupling originating from part H_Y of original interaction*

The coupling originating from the part H_Y of the original interaction H_{int} given by (1·3·4) is obtained by using the commutator of H_Y with the pairing vibrational mode $X_\mu^\dagger$ (or X_μ):

$$[H_Y, X_\mu^\dagger]=\Sigma_\alpha E_\alpha(\mu)\hat{n}_\alpha+H_X(\mu)+H_V(\mu), \tag{7A·1}$$

$$H_X(\mu)\equiv\Sigma_{\alpha\beta\gamma\delta}V_X(\mu;\,\alpha\beta\gamma\delta)a_\alpha^\dagger a_\beta^\dagger a_\delta a_\gamma,$$

$$H_V(\mu)\equiv\Sigma_{\alpha\beta\gamma\delta}\{V_{V1}(\mu;\,\alpha\beta\tilde{\gamma}\tilde{\delta})a_\alpha^\dagger a_\beta^\dagger a_\delta^\dagger a_\gamma^\dagger+V_{V2}(\mu;\,\alpha\beta\tilde{\gamma}\tilde{\delta})a_\gamma a_\delta a_\beta a_\alpha\},$$

where the following notations are used;

$$E_\alpha(\mu)\equiv-\sqrt{2}\,\Sigma_{\varepsilon_1\varepsilon_2}[\{V_Y(\varepsilon_1\varepsilon_2\alpha\tilde{\alpha})+2V_Y(\alpha\varepsilon_1\alpha\tilde{\varepsilon}_2)\}\{\psi_\mu(\varepsilon_1\varepsilon_2)-\phi_\mu(\tilde{\varepsilon}_1\tilde{\varepsilon}_2)\}], \tag{7A·2a}$$

$$V_X(\mu;\,\alpha\beta\gamma\delta)\equiv-\frac{1}{\sqrt{2}}\Sigma_{\varepsilon_1\varepsilon_2}[\{V_Y'(\gamma\delta\alpha\tilde{\varepsilon}_1)\delta_{\beta\varepsilon_2}-V_Y'(\gamma\delta\beta\tilde{\varepsilon}_1)\delta_{\alpha\varepsilon_2}\}\psi_\mu(\varepsilon_1\varepsilon_2)$$
$$-\{V_Y'(\alpha\beta\gamma\tilde{\varepsilon}_1)\delta_{\delta\varepsilon_2}-V_Y'(\alpha\beta\delta\tilde{\varepsilon}_1)\delta_{\gamma\varepsilon_2}\}\phi_\mu(\tilde{\varepsilon}_1\tilde{\varepsilon}_2)], \tag{7A·2b}$$

$$V_Y'(\alpha\beta\gamma\tilde{\delta})\equiv V_Y(\alpha\beta\gamma\tilde{\delta})+V_Y(\delta\alpha\gamma\tilde{\beta})-V_Y(\delta\beta\gamma\tilde{\alpha}),$$

$$V_{V1}(\mu;\,\alpha\beta\tilde{\gamma}\tilde{\delta})\equiv-\frac{1}{\sqrt{2}}\Sigma_{\varepsilon_1\varepsilon_2}\{V_Y(\alpha\beta\varepsilon_1\tilde{\delta})\delta_{\gamma\varepsilon_2}-V_Y(\alpha\beta\varepsilon_1\tilde{\gamma})\delta_{\delta\varepsilon_2}\}\psi_\mu(\varepsilon_1\varepsilon_2), \tag{7A·2c}$$

$$V_{V2}(\mu;\,\alpha\beta\tilde{\gamma}\tilde{\delta})\equiv-\frac{1}{\sqrt{2}}\Sigma_{\varepsilon_1\varepsilon_2}\{V_Y(\alpha\beta\varepsilon_1\tilde{\gamma})\delta_{\delta\varepsilon_2}-V_Y(\alpha\beta\varepsilon_1\tilde{\delta})\delta_{\gamma\varepsilon_2}\}\phi_\mu(\tilde{\varepsilon}_1\tilde{\varepsilon}_2). \tag{7A·2d}$$

Here the amplitudes of the pairing vibrational modes, $\psi_\mu(\varepsilon_1\varepsilon_2)$ and $\phi_\mu(\varepsilon_1\varepsilon_2)$, are related to those defined by Eq. (1B·9) in Appendix 1B through

$$\psi_\mu(\varepsilon_1\varepsilon_2)=(j_e j_e m_{\varepsilon_1} m_{\varepsilon_2}|00)\psi_\mu(e),$$

$$\phi_\mu(\varepsilon_1\varepsilon_2)=(j_e j_e m_{\varepsilon_1} m_{\varepsilon_1}|00)\phi_\mu(e),$$

and the matrix element of the original H_Y-type interaction, $V_Y(\alpha\beta\gamma\delta)$, are

given after Eq. (1·3·4). In Eq. (7A·1), we have adopted the notations similar to those for the original Hamiltonian, such as E_a, H_X and H_V, paying attention to their formal similarity. However, it should be noted that, contrary to the original Hamiltonian, the $H_X(\mu)$ and $H_V(\mu)$ are not hermitian and hence the order of the indices of the matrix element $V_X(\mu;\ \alpha\beta\gamma\delta)$ and the indices i of $V_{Vi}(\mu;\ \alpha\beta\gamma\delta)$ have important meanings.

In the same way as in the case of the intrinsic Hamiltonian, the transcription of the operator (7A·1) into the quasi-particle NTD space can be easily performed by the use of the transcription rule (2·5·8). Using the matrices $\boldsymbol{D}^i$, $\boldsymbol{d}^i$ and $\boldsymbol{A}^i$ defined in Appendix 2B, the matrix element $V_{\rm int}(\mu;\ \lambda,\ \lambda')$ in Eq. (3·2b) is given by

$$\begin{aligned} V_{\rm int}(\mu;\ \lambda,\lambda') &= \langle \Phi_0 |\, Y_\lambda [H_V,\ X_\mu^\dagger]\, Y_{\lambda'}^\dagger |\, \Phi_0 \rangle \\ &= (\boldsymbol{\phi}_\lambda^T,\ \boldsymbol{\phi}_\lambda^T) \begin{bmatrix} 3\boldsymbol{D}^i & -\boldsymbol{A}^1 \\ (-\boldsymbol{A}^2)^T & \boldsymbol{d}^i \end{bmatrix} \begin{bmatrix} \boldsymbol{\phi}_{\lambda'} \\ \boldsymbol{\phi}_{\lambda'} \end{bmatrix}, \end{aligned} \tag{7A·3}$$

with the following replacements in the matrix elements of $\boldsymbol{D}^i$, $\boldsymbol{d}^i$ and $\boldsymbol{A}^i$ $(i=1, 2)$:

$$\begin{aligned} &E_a^i \Rightarrow E_a(\mu), \quad V_{\alpha\beta\gamma\delta}^{(fi)} \Rightarrow 2V_X(\mu;\ \alpha\beta\gamma\delta), \quad V_{V1}(\alpha\beta\gamma\delta) \Rightarrow V_{V1}(\mu;\ \alpha\beta\gamma\delta), \\ &V_{V2}(\alpha\beta\gamma\delta) \Rightarrow V_{V2}(\mu;\ \alpha\beta\gamma\delta). \end{aligned} \tag{7A·4}$$

7A-2 *Coupling originating from parts H_X and H_V of original interaction*

The coupling resulting from the parts H_X and H_V of the original interaction $H_{\rm int}$ is derived from the commutator of H_X+H_V with $X_\mu^\dagger$ (or X_μ):

$$\begin{aligned} [H_X+H_V,\ X_\mu^\dagger] &\Rightarrow \sum_{\alpha\beta\gamma\delta} \{ V_{V1}(\mu;\ \alpha\beta\gamma\delta) a_\alpha^\dagger a_\beta^\dagger a_{\tilde\delta}^\dagger a_\gamma + V_{V2}(\mu;\ \alpha\beta\gamma\delta) a_\gamma^\dagger a_{\tilde\delta} a_\beta a_\alpha \}, \\ &\equiv H_V(\mu), \end{aligned} \tag{7A·5}$$

where

$$\begin{aligned} V_{V1}(\mu;\ \alpha\beta\gamma\tilde\delta) \equiv & -2\sqrt{2} \sum_{\varepsilon_1\varepsilon_2} [V_X(\alpha\beta\gamma\varepsilon_1)\delta_{\delta\varepsilon_2}\psi_\mu(\varepsilon_1\varepsilon_2) \\ & - \{ V_V(\tilde\alpha\tilde\beta\varepsilon_1\delta) + V_V(\varepsilon_1\delta\tilde\alpha\tilde\beta) \} \delta_{\gamma\varepsilon_2}\phi_\mu(\tilde\varepsilon_1\tilde\varepsilon_2)], \end{aligned} \tag{7A·6a}$$

$$\begin{aligned} V_{V2}(\mu;\ \alpha\beta\gamma\tilde\delta) \equiv & 2\sqrt{2} \sum_{\varepsilon_1\varepsilon_2} [V_X(\alpha\beta\gamma\varepsilon_1)\delta_{\delta\varepsilon_2}\phi_\mu(\tilde\varepsilon_1\tilde\varepsilon_2) \\ & - \{ V_V(\tilde\alpha\tilde\beta\varepsilon_1\delta) + V_V(\varepsilon_1\delta\tilde\alpha\tilde\beta) \} \delta_{\gamma\varepsilon_2}\psi_\mu(\varepsilon_1\varepsilon_2)], \end{aligned} \tag{7A·6b}$$

and the matrix elements of the original H_X- and H_V-type interactions, $V_X(\alpha\beta\gamma\delta)$ and $V_V(\alpha\beta\gamma\delta)$, are given after Eq. (1·3·4). Needless to say, the operator $H_V(\mu)$ is not hermitian.

Paying attention to the formal similarity of $H_V(\mu)$ to H_V, we can express the operator (7A·5) in terms of the 1QP and dressed 3QP modes, with the aid of the transcription rule (2·5·8). Using the vector $\boldsymbol{B}(\alpha)$ defined in Appendix 2C, the matrix elements $V_{\rm int}(\mu;\ \lambda,\ \alpha)$ and $V_{\rm int}(\mu;\ \alpha,\ \lambda)$ in Eq. (3·2b) are given by

$$V_{\rm int}(\mu;\,\lambda,\,\alpha)=\langle\Phi_0|\,Y_\lambda[H_X+H_V,\,X_\mu^\dagger]a_\alpha^\dagger|\Phi_0\rangle$$
$$=(\boldsymbol{\psi}_\lambda^T,\,\boldsymbol{\phi}_\lambda^T)\cdot\boldsymbol{B}(\alpha),\qquad(7\text{A}\cdot7\text{a})$$

$$V_{\rm int}(\mu;\,\alpha,\,\lambda)=\langle\Phi_0|a_\alpha[H_X+H_V,\,X_\mu^\dagger]\,Y_\lambda^\dagger|\Phi_0\rangle$$
$$=\boldsymbol{B}^T(\alpha)\cdot\begin{bmatrix}\boldsymbol{\psi}_\lambda\\ \boldsymbol{\phi}_\lambda\end{bmatrix}\qquad(7\text{A}\cdot7\text{b})$$

with the following replacements in the elements of $\boldsymbol{B}(\alpha)$:

$$V_{Y1}(\alpha\beta\gamma\delta)\Rightarrow V_{Y1}(\mu;\,\alpha\beta\gamma\delta),\quad V_{Y2}(\alpha\beta\gamma\delta)\Rightarrow V_{Y2}(\mu;\,\alpha\beta\gamma\delta),\qquad(7\text{A}\cdot8)$$

for the former relation (7A·7a), and

$$V_{Y1}(\alpha\beta\gamma\delta)\Rightarrow V_{Y2}(\mu;\,\alpha\beta\gamma\delta),\quad V_{Y2}(\alpha\beta\gamma\delta)\Rightarrow V_{Y1}(\mu;\,\alpha\beta\gamma\delta),\qquad(7\text{A}\cdot9)$$

for the latter relation (7A·7b).

Appendix 7B. Matrix elements of electromagnetic multipole operators in collective-intrinsic-coupled system

For the study of the system in which the collective and intrinsic modes of excitation are coupled to each other, it is necessary to express the electromagnetic multipole operators in terms of the collective and intrinsic modes of excitation. Here, we give the explicit forms of the matrix elements involved in the expressions (3·4a) and (3·4b).

We first take the commutator of the electromagnetic operator $\hat{O}_{LM}^{(\pm)}$ with the pairing vibrational mode $X_\mu^\dagger$ (or X_μ):

$$[\mathring{O}_{LM}^{(\pm)},\,X_\mu^\dagger]=C_{LM}^{(\pm)}(\mu)+\sum_{\alpha\beta}\bar{O}_{LM}^{(\pm)}(\mu;\,\alpha\beta)a_\alpha^\dagger a_\beta,\qquad(7\text{B}\cdot1\text{a})$$

$$[\bar{O}_{LM}^{(\pm)},\,X_\mu^\dagger]=\sum_{\alpha\beta}\{\mathring{O}_{1LM}^{(\pm)}(\mu;\,\alpha\beta)a_\alpha^\dagger a_{\tilde{\beta}}^\dagger\pm\mathring{O}_{2LM}^{(\pm)}(\mu;\,\alpha\beta)a_{\tilde{\beta}}a_{\tilde{\alpha}}\},\qquad(7\text{B}\cdot1\text{b})$$

where $\mathring{O}_{LM}^{(\pm)}$ and $\bar{O}_{LM}^{(\pm)}$ denote the first and second terms of $\hat{O}_{LM}^{(\pm)}$ defined by Eq. (1·5·12), respectively, and the following notations are used;

$$C_{LM}^{(\pm)}(\mu)\equiv\sqrt{8}\sum_{\varepsilon_1\varepsilon_2}\{\mathring{O}_{LM}^{(\pm)}(\varepsilon_1\varepsilon_2)\{\psi_\mu(\varepsilon_1\varepsilon_2)\mp\phi_\mu(\tilde{\varepsilon}_1\tilde{\varepsilon}_2)\}\frac{1\pm1}{2},\qquad(7\text{B}\cdot2\text{a})$$

$$\bar{O}_{LM}^{(\pm)}(\mu;\,\alpha\beta)\equiv\mp2\sqrt{2}\sum_{\varepsilon_1\varepsilon_2}\{\mathring{O}_{LM}^{(\pm)}(\tilde{\varepsilon}_1\tilde{\beta})\delta_{\alpha\varepsilon_2}\psi_\mu(\varepsilon_1\varepsilon_2)\pm\mathring{O}_{LM}^{(\pm)}(\tilde{\varepsilon}_1\alpha)\delta_{\tilde{\beta}\varepsilon_2}\phi_\mu(\tilde{\varepsilon}_1\tilde{\varepsilon}_2)\},\qquad(7\text{B}\cdot2\text{b})$$

$$\mathring{O}_{1LM}^{(\pm)}(\mu;\,\alpha\beta)\equiv\frac{1}{\sqrt{2}}\sum_{\varepsilon_1\varepsilon_2}\{\bar{O}_{LM}^{(\pm)}(\alpha\varepsilon_1)\delta_{\beta\varepsilon_2}-\bar{O}_{LM}^{(\pm)}(\beta\varepsilon_1)\delta_{\alpha\varepsilon_2}\}\psi_\mu(\varepsilon_1\varepsilon_2),\qquad(7\text{B}\cdot2\text{c})$$

$$\mathring{O}_{2LM}^{(\pm)}(\mu;\,\alpha\beta)\equiv-\frac{1}{\sqrt{2}}\sum_{\varepsilon_1\varepsilon_2}\{\bar{O}_{LM}^{(\pm)}(\alpha\varepsilon_1)\delta_{\beta\varepsilon_2}-\bar{O}_{LM}^{(\pm)}(\beta\varepsilon_1)\delta_{\alpha\varepsilon_2}\}\phi_\mu(\tilde{\varepsilon}_1\tilde{\varepsilon}_2).\qquad(7\text{B}\cdot2\text{d})$$

Here we have used notations similar to the original electromagnetic multipole matrix elements $\mathring{O}^{(\pm)}_{LM}(\alpha\beta)$ and $\bar{O}^{(\pm)}_{LM}(\alpha\beta)$ defined by Eq. (1·5·13). It should be noted, however, that the time-reversal property of the quantities defined by Eq. (7B·2) is different from that of the original matrix elements $\mathring{O}^{(\pm)}_{LM}(\alpha\beta)$ and $\bar{O}^{(\pm)}_{LM}(\alpha\beta)$.

In the same way as was done in § 5-3 of Chap. 2, the operators (7B·1a) and (7B·1b) can be easily expressed in terms of the 1QP and dressed 3QP modes, because they involve only the intrinsic degrees of freedom represented in terms of the quasi-particle operators. Thus, using the matrix elements explicitly defined by Eq. (2D·3) in Appendix 2D, the matrix elements in the expression (3·4) are given by

$$\langle\Phi_0|\, Y_\lambda[\bar{O}^{(\pm)}_{LM}, X^\dagger_\mu]a^\dagger_\alpha|\Phi_0\rangle=\langle\Phi_0|\, Y_\lambda\mathring{F}^{(\pm)}_{LM}a^\dagger_\alpha|\Phi_0\rangle, \tag{7B·3a}$$

$$\langle\Phi_0|a_\alpha[\bar{O}^{(\pm)}_{LM}, X^\dagger_\mu]\, Y^\dagger_\lambda|\Phi_0\rangle=\langle\Phi_0|a_\alpha\mathring{F}^{(\pm)}_{LM}\, Y^\dagger_\lambda|\Phi_0\rangle, \tag{7B·3b}$$

$$\begin{aligned}\langle\Phi_0|a_\alpha[\mathring{O}^{(\pm)}_{LM}, X^\dagger_\mu]a^\dagger_\beta|\Phi_0\rangle&=C^{(\pm)}_{LM}(\mu)\delta_{\alpha\beta}+\langle\Phi_0|a_\alpha\bar{F}^{(\pm)}_{LM}a^\dagger_\beta|\Phi_0\rangle\\&=C^{(\pm)}_{LM}(\mu)\delta_{\alpha\beta}+\bar{O}^{(\pm)}_{LM}(\mu;\alpha\beta),\end{aligned} \tag{7B·3c}$$

$$\langle\Phi_0|\, Y_\lambda[\mathring{O}^{(\pm)}_{LM}, X^\dagger_\mu]\, Y^\dagger_{\lambda'}|\Phi_0\rangle=C^{(\pm)}_{LM}(\mu)\delta_{\lambda\lambda'}+\langle\Phi_0|\, Y_\lambda\bar{F}^{(\pm)}_{LM}\, Y^\dagger_{\lambda'}|\Phi_0\rangle \tag{7B·3d}$$

with the following replacements in the matrix elements of $\mathring{F}^{(\pm)}_{LM}$ and $\bar{F}^{(\pm)}_{LM}$:

$$\mathring{F}^{(\pm)}_{\{\}LM}(\alpha\beta)\Rightarrow\mathring{O}^{(\pm)}_{\{\}LM}(\mu;\alpha\beta),\qquad\bar{F}^{(\pm)}_{LM}(\alpha\beta)\Rightarrow\bar{O}^{(\pm)}_{LM}(\mu;\alpha\beta). \tag{7B·4}$$

The other matrix elements in the expressions (3·4a) and (3·4b) are given in a similar form.

Progress of Theoretical Physics, Vol. 56, No. 4, October 1976

Interplay of Pairing and Intrinsic Modes of Excitation in Nuclei. I

——*Transcription of Nucleon System into Ideal Boson-Quasi-Particle Space**)——

Tōru SUZUKI and Kenichi MATSUYANAGI

Department of Physics, Kyoto University, Kyoto 606

(Received April 12, 1976)

A new method treating the interplay of pairing and intrinsic modes of excitation is proposed. In this method, the pairing mode associated with the $J=0$-coupled nucleon pairs is represented by pairing bosons and the intrinsic mode characterized by the seniority quantum number is explicitly treated by *ideal quasi-particle operators*. We obtain a closed expression of the single-nucleon operator in terms of pairing bosons and ideal quasi-particles. As a simple illustration, the superconducting system is treated by introducing the coherent state of pairing bosons and the relation to the Bogoliubov transformation is discussed. The relation between this method and the canonical transformation method with auxiliary variables is also clarified.

§ 1. Introduction

Recent investigations on the anharmonicity effects in low-excited states in transitional even-even nuclei seem to suggest peculiar properties of the "two-phonon" 0^+ states:[1),2)] A typical example is the anomalous excited 0^+ states in Ge, Se and Mo isotopes which appear in the vicinity of the one-phonon 2^+ states. Very recently, Iwasaki, Marumori, Sakata and Takada[3)] showed that the dressed four-quasi-particle 0^+ states (which approximately correspond to the two-phonon 0^+ states in the conventional phonon model) couple strongly to the pairing vibrational states in nuclei with N or $Z\approx 40$, and that this drastic coupling explains the special lowering of the excited 0^+ states. They have also shown[4)] that the concept of quadrupole phonon is seriously broken down in some excited states if the pairing degree of freedom is *not* excluded from the model space. Thus it becomes one of the important subjects in the current nuclear study to develop the mode-mode coupling theory which systematically deals with the interplay of the pairing and quadrupole modes of excitation.

The microscopic investigation on the interplay of different modes of collective excitation is in a very early stage. One of the reasons is due to the well-known difficulties, i.e., the overcompleteness in the degrees of freedom and the violation of the Pauli principle, which are essentially related to the composite nature of the

*) A preliminary report of this work has been published in this journal, **55** (1976), 1680.

collective modes of excitation. In recent years, however, interest has greatly increased in the investigation to overcome such difficulties.[5] Under such circumstances, the authors with Kuriyama, Marumori and Sakata[6] have proposed a theory which enables us to deal with mutual interweaving of pairing and intrinsic modes of excitation. In this theory, using the canonical transformation method with auxiliary collective variables,[7),8)] the pairing mode of excitation associated with the $J=0$-coupled quasi-particle pair is represented by the auxiliary bosons and the intrinsic mode of excitation characterized by the seniority quantum number is described in the quasi-particle state space independent of the quantum fluctuation of the pairing field. Thus, in this theory we are not faced with the above-mentioned difficulties.

The main purpose of this paper is to propose an alternative method which can give a rigorous expression for the coupling Hamiltonian between the pairing and intrinsic modes of excitation (a typical example of the latter is the quadrupole mode). The essence of this method is to introduce explicitly the concept of "ideal quasi-particles" which are independent of the pairing phase transition (from normal to BCS vacuum) and hence independent of the quantum fluctuation of the pairing field. It will be shown that the number of the ideal quasi-particles is equivalent to the seniority number. Accordingly the ideal quasi-particle can be regarded as substantiation of the concept of seniority. On the other hand, keeping the basic idea of Ref. 6), we can represent the pairing degree of freedom by boson operators. As is well known, the introduction of boson operators inevitably brings about the unphysical effect: Since there is nothing to prevent operating again and again on a state with a boson creation operator, the Pauli principle is eventually violated. However, in this method we are assured to be always in the physical subspace corresponding to the original fermion state space.

Whereas in Ref. 6) the Bogoliubov transformation was used from the outset, we here develop the method starting from the original nucleon operators. Accordingly we can deal with both normal and superconductive nuclei in a unified manner.

In § 2 the pairing and intrinsic degrees of freedom are defined through the quasi-spin formalism.[9] In § 3, extending the idea of the boson expansion method of Marumori and Yamamura,[10),11)] we transcribe the nucleon system into the "ideal boson-quasi-particle space" composed of the ideal quasi-particles and the pairing bosons. Here, only the pairing degree of freedom is represented by the boson operators and the intrinsic degree of freedom is explicitly treated in terms of the ideal quasi-particle operators. In § 4 the relation between this method and the canonical transformation method of Marumori[7] used in Ref. 6) will be clarified. In § 5, as a simple illustration, we deal with the superconducting system by introducing the coherent state of pairing bosons and discuss the relation between the ideal quasi-particle and the conventional quasi-particle defined by the Bogoliubov transformation.

§ 2. Pairing and intrinsic degrees of freedom in quasi-spin space

2-1. *Quasi-spin space*

Let us define the quasi-spin operators of the single-particle orbit a as

$$\hat{S}_+(a)=\sqrt{\frac{\Omega_a}{2}}\sum_{m_{\alpha_1}m_{\alpha_2}}\langle j_a m_{\alpha_1} j_a m_{\alpha_2}|00\rangle c^\dagger_{\alpha_1}c^\dagger_{\alpha_2},$$

$$\hat{S}_-(a)=\sqrt{\frac{\Omega_a}{2}}\sum_{m_{\alpha_1}m_{\alpha_2}}\langle j_a m_{\alpha_1} j_a m_{\alpha_2}|00\rangle c_{\alpha_2}c_{\alpha_1},$$

$$\hat{S}_0(a)=\frac{1}{2}\Big(\sum_{m_\alpha}c_\alpha^\dagger c_\alpha-\Omega_a\Big),\quad \Omega_a\equiv j_a+\frac{1}{2}, \tag{2·1}$$

where $c_\alpha^\dagger$ and c_α are the creation and annihilation operators of a nucleon in the single-particle state α.*) These operators then satisfy the same commutation relations as those of the angular-momentum operators:

$$[\hat{S}_+(a),\hat{S}_-(a)]=2\hat{S}_0(a),\quad [\hat{S}_0(a),\hat{S}_\pm(a)]=\pm\hat{S}_\pm(a). \tag{2·2}$$

The state vectors are specified by the quantum numbers $S(a)$ and $S_0(a)$, which are the eigenvalues of the quasi-spin $\hat{\boldsymbol{S}}(a)^2=\hat{S}_+(a)\hat{S}_-(a)+\hat{S}_0(a)^2-\hat{S}_0(a)$ and its projection $\hat{S}_0(a)$, respectively. They span the quasi-spin subspace of the orbit a:

$$\{|S(a),S_0(a)\rangle;\ |S_0(a)|\leqq S(a)\}. \tag{2·3}$$

The physical meanings of the quantum numbers $S(a)$ and $S_0(a)$ are known to be related simply to the seniority number and the nucleon number, respectively, through the relations

$$S(a)=\tfrac{1}{2}(\Omega_a-\nu_a)\quad\text{and}\quad S_0(a)=\tfrac{1}{2}(n_a-\Omega_a), \tag{2·4}$$

where ν_a and n_a stand for the seniority number and the nucleon number in the orbit a, respectively.

With the quasi-spin operators (2·1) we can define irreducible tensor operators in the quasi-spin subspace of the orbit a, as usual, by the commutation relations

$$\begin{aligned}&[\hat{S}_0(a),T_{kq}(a)]=qT_{kq}(a),\\ &[\hat{S}_\pm(a),T_{kq}(a)]=\sqrt{(k\mp q)(k\pm q+1)}\,T_{k,q\pm1}(a),\end{aligned} \tag{2·5}$$

where $T_{kq}(a)$ is the q-component of an irreducible tensor of rank k. The single-nucleon operators $c_\alpha^\dagger$ and $c_{\bar\alpha}$ are then regarded as spinors in the quasi-spin subspace:

$$T_{1/2,1/2}(\alpha)=c_\alpha^\dagger,\quad T_{1/2,-1/2}(\alpha)=c_{\bar\alpha}\equiv(-)^{j_a-m_\alpha}c_{\bar\alpha}. \tag{2·6}$$

Using the Wigner-Eckart theorem, we thus obtain the following useful relations

*) In this paper we adopt the spherical j-j coupling shell model and use the following notations: $\alpha=\{n_a, l_a, j_a, m_\alpha\}$, $\bar\alpha=\{n_a, l_a, j_a, -m_\alpha\}$, $a=\{n_a, l_a, j_a\}$ and $f(\bar\alpha)=(-)^{j_a-m_\alpha}f(\bar\alpha)$, where $f(\alpha)$ is an arbitrary function of α. The subscript $i=1, 2, \cdots$ of α is used for distinguishing different single-particle states within the same orbit a.

for the matrix elements of the irreducible tensors:[9]

$$\langle S(a), S_0(a)|T_{kq}(a)|S'(a), S_0'(a)\rangle = \frac{\langle S'(a)\, S_0'(a)\, kq|S(a)\, S_0(a)\rangle}{\langle S'(a)\, S_0'''(a)\, kq'|S(a)\, S_0''(a)\rangle}\langle S(a), S_0''(a)|T_{kq'}(a)|S'(a), S_0'''(a)\rangle . \tag{2·7}$$

Since the quasi-spin operators in different orbits commute with each other, the quasi-spin space for the general many j-shell case is simply expressed as the direct product composed of the quasi-spin subspace of each orbit. Therefore, from now on to § 4, we discuss the case of a single j-shell and omit the subscript a for the simplicity of notation.

2-2. *Definition of pairing and intrinsic degrees of freedom*

With the use of quasi-spin quantum numbers S and S_0, state vectors in the nucleon state space are generally denoted as $|S, S_0; \Gamma\rangle$, where Γ denotes a set of other quantum numbers such as ordinary angular momentum. Here it should be noted that the quasi-spin operators $\hat{\mathbf{S}}^2$ and $\hat{S}_0$ commute with the ordinary angular-momentum operators $\hat{J}_\pm$ and $\hat{J}_0$. Now by the definition of the state $|S, S_0=-S; \Gamma\rangle$ we obtain

$$\hat{S}_-|S, S_0=-S; \Gamma\rangle=0 , \tag{2·8}$$

which means that there is no $J=0$-coupled nucleon pair in this state. Equation (2·4), therefore, implies that the seniority number ν coincides with the nucleon number n in this state. Following Ref. 6), we hereafter say that a class of states $|S, S_0=-S; \Gamma\rangle$ involves only the "intrinsic" degree of freedom. On the other hand, a class of states $|S=\Omega/2, S_0; \Gamma\rangle$ consists of only $J=0$-coupled nucleon pairs, i.e., involves only the "pairing" degree of freedom. In general, the states $|S\neq\Omega/2, S_0\neq -S; \Gamma\rangle$ involve both "intrinsic" and "pairing" degrees of freedom.

Needless to say, the nucleon vacuum $|\mathrm{vac}\rangle$ is the state with $n=\nu=0$ and is given by

$$|\mathrm{vac}\rangle=|S=\Omega/2, S_0=-\Omega/2; \Gamma_0\rangle. \tag{2·9}$$

§ 3. Transcription of the nucleon system into the "ideal boson-quasi-particle space"

3-1. *Introduction of "ideal boson-quasi-particle space"*

In order to separate uniquely the pairing and intrinsic degrees of freedom in the nucleon state space, we first introduce the "ideal boson-quasi-particle space" and transcribe the original nucleon state space into this space. The basis vector of the "ideal boson-quasi-particle space" is defined as the direct product state composed of the "intrinsic" state $|S, \Gamma\rangle\!\rangle$ and pairing boson state $|N)\!)$:

$$|S, S_0\equiv -S+N; \Gamma\rangle\!\rangle\equiv|S, \Gamma\rangle\!\rangle\cdot|N)\!), \tag{3·1}$$

where

$$|N\rangle\!\rangle \equiv \frac{1}{\sqrt{N!}}(\boldsymbol{b}^{\dagger})^{N}|0\rangle\!\rangle, \quad \boldsymbol{b}|0\rangle\!\rangle = 0 . \tag{3·2}$$

Here the boson operators $\boldsymbol{b}^{\dagger}$ and $\boldsymbol{b}$ are introduced to represent the motion of $J=0$-coupled nucleon pairs and the intrinsic state $|S, \Gamma\rangle\!\rangle$ is introduced to represent the original nucleon state $|S, S_0=-S; \Gamma\rangle$. The space spanned by the intrinsic states is called "intrinsic space" and the space spanned by the pairing boson states is called "pairing space". Thus, the "ideal boson-quasi-particle space" is the direct product of these spaces and is spanned by the set of states

$$\{|S, S_0 \equiv -S+N; \Gamma\rangle\!\rangle; S=0, 1/2, \cdots, \Omega/2 \text{ and } N=0, 1, 2, \cdots \infty\}. \tag{3·3}$$

The original fermion space spanned by the nucleon states $|S, S_0; \Gamma\rangle$ is mapped into the physical subspace of the ideal boson-quasi-particle space by the following T-transformation:

$$T=\sum_{S=0}^{\Omega/2}\sum_{\Gamma}\sum_{S_0=-S}^{S}|S, S_0; \Gamma\rangle\!\rangle\langle S, S_0; \Gamma| . \tag{3·4}$$

From the structure of this transformation, it is obvious that we have a one-to-one correspondence between the original nucleon states and the direct product states $|S, S_0; \Gamma\rangle\!\rangle$ with $|S_0| \leqq S$ belonging to the physical subspace in the ideal boson-quasi-particle space, i.e.,

$$|S, S_0; \Gamma\rangle\!\rangle = T|S, S_0; \Gamma\rangle. \quad (|S_0| \leqq S) \tag{3·5}$$

The T-transformation satisfies the following properties:

$$T^{\dagger}T=\sum_{S=0}^{\Omega/2}\sum_{\Gamma}\sum_{S_0=-S}^{S}|S, S_0; \Gamma\rangle\langle S, S_0; \Gamma| = 1 \tag{3·6}$$

in the nucleon state space, and

$$TT^{\dagger}=\sum_{S=0}^{\Omega/2}\sum_{\Gamma}\sum_{S_0=-S}^{S}|S, S_0; \Gamma\rangle\!\rangle\langle\!\langle S, S_0; \Gamma| \equiv \boldsymbol{P}_{\hat{S}} , \tag{3·7}$$

where $\boldsymbol{P}_{\hat{S}}$ is the projection operator into the physical subspace in the ideal boson-quasi-particle space. It is convenient to rewrite $\boldsymbol{P}_{\hat{S}}$ as

$$\boldsymbol{P}_{\hat{S}}=\sum_{S=0}^{\Omega/2}\sum_{\Gamma}\boldsymbol{P}_{S}|S, \Gamma\rangle\!\rangle\langle\!\langle S, \Gamma| \tag{3·8}$$

with

$$\boldsymbol{P}_{S}=\sum_{N=0}^{2S}|N\rangle\!\rangle\langle\!\langle N| . \tag{3·9}$$

In this form, $\boldsymbol{P}_{\hat{S}}$ can be regarded as the projector operating first to the intrinsic states $|S, \Gamma\rangle\!\rangle$ and giving the "eigenvalue" $\boldsymbol{P}_{s}$ which then operates to the pairing space.

From the property (3·6), it is clear that any operator A in the nucleon state

space is transcribed into the operator $\boldsymbol{A}$ in the ideal boson-quasi-particle space as

$$A\to\boldsymbol{A}\equiv TAT^{\dagger}$$
$$=\sum_{S,S'=0}^{\Omega/2}\sum_{\Gamma\Gamma'}\sum_{S_0=-S}^{S}\sum_{S_0'=-S'}^{S'}\langle S,S_0;\Gamma|A|S',S_0';\Gamma'\rangle|S,S_0;\Gamma\rangle\!\rangle\langle\!\langle S',S_0';\Gamma'|. \quad (3\cdot10)$$

3-2. *Transcription of single-nucleon operators*

Now we perform the transcription of single-nucleon operators $c_\alpha^{\dagger}$ into the ideal boson-quasi-particle space. This is done in the following way:

$$\boldsymbol{c}_\alpha^{\dagger}\equiv Tc_\alpha^{\dagger}T^{\dagger}$$
$$=\sum_{S=0}^{\Omega/2-1/2}\sum_{\Gamma\Gamma'}\sum_{S_0=-S}^{S}\langle S,S_0;\Gamma|c_\alpha^{\dagger}|S+1/2,S_0-1/2;\Gamma'\rangle|S,S_0;\Gamma\rangle\!\rangle$$
$$\times\langle\!\langle S+1/2,S_0-1/2;\Gamma'|$$
$$+\sum_{S=1/2}^{\Omega/2}\sum_{\Gamma\Gamma'}\sum_{S_0=-S+1}^{S}\langle S,S_0;\Gamma|c_\alpha^{\dagger}|S-1/2,S_0-1/2;\Gamma'\rangle|S,S_0;\Gamma\rangle\!\rangle$$
$$\times\langle\!\langle S-1/2,S_0-1/2;\Gamma'|, \quad (3\cdot11)$$

where we have used the quasi-spin spinor property of the operator $c_\alpha^{\dagger}$. To extract the pairing degree of freedom from the above matrix elements, we can utilize the formula (2·7) and obtain

$$\langle S,S_0;\Gamma|c_\alpha^{\dagger}|S+1/2,S_0-1/2;\Gamma'\rangle$$
$$=\sqrt{\frac{S-S_0+1}{2S+1}}\langle S,-S;\Gamma|c_\alpha^{\dagger}|S+1/2,-S-1/2;\Gamma'\rangle,$$
$$\langle S,S_0;\Gamma|c_\alpha^{\dagger}|S-1/2,S_0-1/2;\Gamma'\rangle$$
$$=\sqrt{\frac{S+S_0}{2S}}\langle S,-S;\Gamma|c_{\tilde{\alpha}}|S-1/2,-S+1/2;\Gamma'\rangle,$$

in which only the matrix elements of $c_\alpha^{\dagger}$ and $c_{\tilde{\alpha}}$ between the states satisfying the condition $S_0=-S$ appear. Consequently, Eq. (3·11) may be rewritten as

$$\boldsymbol{c}_\alpha^{\dagger}=\sum_{S=0}^{\Omega/2-1/2}\sum_{\Gamma\Gamma'}\sum_{N=0}^{2S}|N\rangle\!\rangle\langle\!\langle N|\cdot|S,\Gamma\rangle\!\rangle\langle S,-S;\Gamma|c_\alpha^{\dagger}|S+1/2,-S-1/2;\Gamma'\rangle$$
$$\times\langle\!\langle S+1/2,\Gamma'|\sqrt{1-\frac{N}{2S+1}}$$
$$+\sum_{S=1/2}^{\Omega/2}\sum_{\Gamma\Gamma'}\sum_{N=1}^{2S}|N\rangle\!\rangle\langle\!\langle N-1|\sqrt{\frac{N}{2S}}|S,\Gamma\rangle\!\rangle$$
$$\times\langle S,-S;\Gamma|c_{\tilde{\alpha}}|S-1/2,-S+1/2;\Gamma'\rangle\langle\!\langle S-1/2,\Gamma'|,$$

where we have used the definition $S_0\equiv-S+N$ (see (3·1)). Let us here replace the boson number N in the first term by the operator $\boldsymbol{b}^{\dagger}\boldsymbol{b}$ and $\langle\!\langle N-1|\sqrt{N}$ in the second term by $\langle\!\langle N|\boldsymbol{b}^{\dagger}$. Furthermore let us define the "quasi-spin operator" $\hat{S}$ operating on the intrinsic states through

$$\hat{S}|S,\Gamma\rangle\!\rangle=S|S,\Gamma\rangle\!\rangle. \quad (3\cdot12)$$

Then, making use of the projection operator (3·8), we finally arrive at the important result:

$$c_\alpha^\dagger = P_{\hat{S}} \left\{ a_\alpha^\dagger \sqrt{1 - \frac{b^\dagger b}{2\hat{S}}} + \frac{b^\dagger}{\sqrt{2\hat{S}}} a_{\tilde{\alpha}} \right\} . \tag{3·13a}$$

In the same way, we obtain

$$\begin{aligned} c_{\tilde{\alpha}} &\equiv T c_{\tilde{\alpha}} T^\dagger \\ &= \left\{ -a_\alpha^\dagger \frac{b}{\sqrt{2\hat{S}}} + \sqrt{1 - \frac{b^\dagger b}{2\hat{S}}} a_{\tilde{\alpha}} \right\} P_{\hat{S}} = (c_{\tilde{\alpha}}^\dagger)^\dagger . \end{aligned} \tag{3·13b}$$

Here we have introduced the creation and annihilation operators $a_\alpha^\dagger$ and $a_{\tilde{\alpha}}$ defined in the intrinsic space as

$$\begin{aligned} a_\alpha^\dagger &\equiv T_{\text{in}} c_\alpha^\dagger T_{\text{in}}^\dagger , \\ a_{\tilde{\alpha}} &\equiv T_{\text{in}} c_{\tilde{\alpha}} T_{\text{in}}^\dagger = (a_{\tilde{\alpha}}^\dagger)^\dagger \end{aligned} \tag{3·14}$$

with

$$T_{\text{in}} \equiv \sum_{S=0}^{\Omega/2} \sum_{\Gamma} |S, \Gamma\rangle\langle S, S_0 = -S; \Gamma| . \tag{3·15}$$

3-3. *Properties of the ideal quasi-particle operators $a_\alpha^\dagger$ and $a_{\tilde{\alpha}}$*

Using the similar procedure to in the preceding subsection, we can prove the following "anticommutation relations" for the operators $a_\alpha^\dagger$ and a_α defined by (3·14):

$$\{a_\alpha^\dagger, a_{\alpha'}^\dagger\}_+ = \{a_\alpha, a_{\alpha'}\}_+ = 0 , \tag{3·16a}$$

$$\{a_\alpha, a_{\alpha'}^\dagger\}_+ = \delta_{\alpha\alpha'} - a_{\tilde{\alpha}}^\dagger \frac{1}{2\hat{S}} a_{\tilde{\alpha}'} . \tag{3·16b}$$

We can also show that the quasi-spin operator $\hat{S}$ defined by (3·12) is explicitly written in terms of the number operator of the "particles" $a_\alpha^\dagger$ and a_α as

$$2\hat{S} = \Omega - \sum_{m_\alpha} a_\alpha^\dagger a_\alpha \equiv \Omega - \hat{n} . \tag{3·17}$$

This relation implies that the number of the "particles", $a_\alpha^\dagger$ and $a_{\tilde{\alpha}}$, just coincides with the seniority number ν. Hence, we hereafter call these "particles" "ideal quasi-particles". The ideal quasi-particle operators possess all the properties necessary for substantiation of the concept of seniority:

1) They cannot form a $J=0$-coupled pair,

$$\sum_{m_\alpha} a_\alpha^\dagger a_{\tilde{\alpha}}^\dagger = 0 . \tag{3·18}$$

2) The number of their product cannot exceed Ω, i.e.,

$$a_{\alpha_1}^\dagger a_{\alpha_2}^\dagger \cdots a_{\alpha_n}^\dagger = 0 \quad \text{for} \quad n > \Omega . \tag{3·19}$$

3) They transfer a definite quasi-spin, i.e., senority,

$$[\hat{S}, \boldsymbol{a}_\alpha^\dagger] = -\tfrac{1}{2}\boldsymbol{a}_\alpha^\dagger\,, \quad [\hat{S}, \boldsymbol{a}_{\tilde{\alpha}}] = \tfrac{1}{2}\boldsymbol{a}_{\tilde{\alpha}}\,. \tag{3·20}$$

Here it should be noted that the explicit knowledge of the intrinsic states $|S, \Gamma\rangle\!\rangle$ is unnecessary in deriving Eqs. (3·16)$\sim$(3·20). Furthermore, once these equations are set up, we can construct the intrinsic states from the operators $\boldsymbol{a}^\dagger$, without using the defining equations (3·14) and (3·15). This is shown in § 3-5.

3-4. *Transcription of nucleon pair operators*

Let us see how the products of nucleon operators $c_\alpha^\dagger$ and c_α are transcribed. From Eq. (3·6) we have in general

$$T(AB)T^\dagger = TAT^\dagger \cdot TBT^\dagger\,, \tag{3·21}$$

where A and B are arbitrary nucleon operators. Therefore, all necessary expressions can be derived *directly* from the expression (3·13); for example, we obtain

$$\begin{aligned} T\hat{S}_+T^\dagger &= \tfrac{1}{2}\sum_{m_\alpha} \boldsymbol{c}_\alpha^\dagger \boldsymbol{c}_{\tilde{\alpha}}^\dagger = \boldsymbol{P}_{\hat{S}}\boldsymbol{b}^\dagger\sqrt{2\hat{S}-\boldsymbol{b}^\dagger\boldsymbol{b}}\,. \\ T\hat{S}_-T^\dagger &= \tfrac{1}{2}\sum_{m_\alpha} \boldsymbol{c}_{\tilde{\alpha}}\boldsymbol{c}_\alpha = \sqrt{2\hat{S}-\boldsymbol{b}^\dagger\boldsymbol{b}}\cdot\boldsymbol{b}\boldsymbol{P}_{\hat{S}}\,, \end{aligned} \tag{3·22}$$

and for the nucleon number operator

$$T\Big(\sum_{m_\alpha} c_\alpha^\dagger c_\alpha\Big)T^\dagger = \sum_{m_\alpha} \boldsymbol{c}_\alpha^\dagger \boldsymbol{c}_\alpha = \boldsymbol{P}_{\hat{S}}(\hat{\boldsymbol{n}} + 2\boldsymbol{b}^\dagger\boldsymbol{b})\,. \tag{3·23}$$

Here we have used the following properties of $\boldsymbol{P}_{\hat{S}}$:

$$[\boldsymbol{P}_{\hat{S}}, \boldsymbol{b}^\dagger\boldsymbol{b}] = [\boldsymbol{P}_{\hat{S}}, \hat{S}] = 0\,, \tag{3·24}$$

$$\boldsymbol{a}_\alpha^\dagger\boldsymbol{P}_{\hat{S}} = \boldsymbol{P}_{\hat{S}+1/2}\boldsymbol{a}_\alpha^\dagger\,, \quad \boldsymbol{a}_{\tilde{\alpha}}\boldsymbol{P}_{\hat{S}} = \boldsymbol{P}_{\hat{S}-1/2}\boldsymbol{a}_{\tilde{\alpha}}\,, \tag{3·25}$$

$$\boldsymbol{b}^\dagger\boldsymbol{P}_{\hat{S}} = \boldsymbol{P}_{\hat{S}+1/2}\boldsymbol{b}^\dagger\,, \quad \boldsymbol{b}\boldsymbol{P}_{\hat{S}} = \boldsymbol{P}_{\hat{S}-1/2}\boldsymbol{b} \tag{3·26}$$

and

$$\boldsymbol{P}_{\hat{S}}\boldsymbol{P}_{\hat{S}+k/2} = \begin{cases} \boldsymbol{P}_{\hat{S}} & (k \geqq 0) \\ \boldsymbol{P}_{\hat{S}+k/2}\,, & (k < 0) \end{cases} \tag{3·27}$$

where

$$\begin{aligned} \boldsymbol{P}_{\hat{S}+k/2} &\equiv \sum_{S=0}^{\Omega/2}\sum_{\Gamma} \boldsymbol{P}_{S+k/2}|S, \Gamma\rangle\!\rangle\langle\!\langle S, \Gamma| \\ &= \sum_{S=0}^{\Omega/2}\sum_{\Gamma}\sum_{S_0=-S}^{S+k} |S, S_0; \Gamma\rangle\!\rangle\langle\!\langle S, S_0; \Gamma|\,, \end{aligned} \tag{3·28}$$

k being an integer.

Formal structures of Eqs. (3·13), (3·22) and (3·23) are very similar to those given by Marshalek[12] in the boson expansion method for odd and even nuclear systems. However, it should be emphasized that the number of "ideal quasi-particles" is here allowed to change from zero up to Ω, whereas in the boson

expansion method the number of "odd particle" is restricted to zero or one. This is because only the pairing degree of freedom (associated with the $J=0$-coupled pairs) is represented by boson operators in our case.

3-5. *Structure of the intrinsic space*

Let us see the structure of the intrinsic space more explicitly. The nucleon vacuum defined by (2·9) is mapped by the T-transformation as

$$|\mathrm{vac}\rangle\!\rangle \equiv T|\mathrm{vac}\rangle = |S=\Omega/2, \Gamma_0\rangle\!\rangle |N=0\rangle\!\rangle \equiv |0\rangle\!\rangle \cdot |0\rangle\!\rangle , \tag{3·29}$$

where $|0\rangle\!\rangle$ and $|0\rangle\!\rangle$ represent the vacua for the ideal quasi-particles and pairing bosons, respectively;

$$\boldsymbol{a}_\alpha |0\rangle\!\rangle = 0 , \quad \boldsymbol{b}|0\rangle\!\rangle = 0 . \tag{3·30}$$

Using the property (3·21) of the T-transformation, any nucleon state $c^\dagger_{\alpha_1} c^\dagger_{\alpha_2} \cdots c^\dagger_{\alpha_n}|\mathrm{vac}\rangle$ is then transcribed into the state $\boldsymbol{c}^\dagger_{\alpha_1} \boldsymbol{c}^\dagger_{\alpha_2} \cdots \boldsymbol{c}^\dagger_{\alpha_n}|\mathrm{vac}\rangle\!\rangle$. With the aid of the expression (3·13) for the single-nucleon operator $\boldsymbol{c}_\alpha{}^\dagger$, the latter state can be represented as a linear combination of the product states

$$|k; \alpha_1\alpha_2\cdots\alpha_k\rangle\!\rangle |N\rangle\!\rangle \equiv \frac{1}{\sqrt{k!}} \boldsymbol{a}^\dagger_{\alpha_1}\boldsymbol{a}^\dagger_{\alpha_2}\cdots\boldsymbol{a}^\dagger_{\alpha_k}|0\rangle\!\rangle \cdot |N\rangle\!\rangle \tag{3·31}$$

with $k=n-2N\geqq 0$ and $0\leqq N\leqq\Omega$. Here $|N\rangle\!\rangle$ denote the pairing boson states which are already orthonormalized.

In order to elucidate the physical meaning of the intrinsic states $|k; \alpha_1\alpha_2\cdots\alpha_k\rangle\!\rangle$, let us define the overlap $\mathcal{N}_k$ as

$$\mathcal{N}_k(\alpha_1'\alpha_2'\cdots\alpha_k'; \alpha_1\alpha_2\cdots\alpha_k) \equiv \langle\!\langle k; \alpha_1'\alpha_2'\cdots\alpha_k'|k; \alpha_1\alpha_2\cdots\alpha_k\rangle\!\rangle . \tag{3·32}$$

As is evident from (3·16a) and (3·18), $\mathcal{N}_k$ is an antisymmetric function with respect to $(\alpha_1\alpha_2\cdots\alpha_k)$ and $(\alpha_1'\alpha_2'\cdots\alpha_k')$ having the property

$$\sum_{m_\alpha} \mathcal{N}_k(\alpha_1'\alpha_2'\cdots\alpha_k'; \alpha\tilde{\alpha}\alpha_3\alpha_4\cdots\alpha_k) = 0 . \tag{3·33}$$

From the "anticommutation relations" (3·16), the following relation is derived by mathematical induction:

$$\begin{aligned}\boldsymbol{a}_\alpha\boldsymbol{a}^\dagger_{\alpha_1}\boldsymbol{a}^\dagger_{\alpha_2}\cdots\boldsymbol{a}^\dagger_{\alpha_k} &= (-)^k\boldsymbol{a}^\dagger_{\alpha_1}\boldsymbol{a}^\dagger_{\alpha_2}\cdots\boldsymbol{a}^\dagger_{\alpha_k}\boldsymbol{a}_\alpha + k\mathcal{A}(\alpha_1\alpha_2\cdots\alpha_k)\delta_{\alpha\alpha_1}\boldsymbol{a}^\dagger_{\alpha_2}\boldsymbol{a}^\dagger_{\alpha_3}\cdots\boldsymbol{a}^\dagger_{\alpha_k} \\ &\quad -\boldsymbol{a}_{\tilde{\alpha}}{}^\dagger\frac{1}{2\hat{S}}\mathcal{A}(\alpha_1\alpha_2\cdots\alpha_k)\left\{\frac{k(k-1)}{2}\delta_{\tilde{\alpha}_1\alpha_2}\boldsymbol{a}^\dagger_{\alpha_3}\boldsymbol{a}^\dagger_{\alpha_4}\cdots\boldsymbol{a}^\dagger_{\alpha_k} + k\boldsymbol{a}^\dagger_{\alpha_1}\boldsymbol{a}^\dagger_{\alpha_2}\cdots\boldsymbol{a}^\dagger_{\alpha_{k-1}}\boldsymbol{a}_{\tilde{\alpha}_k}\right\},\end{aligned} \tag{3·34}$$

where $\mathcal{A}$ stands for the antisymmetrizer defined by

$$\mathcal{A}(\alpha_1\alpha_2\cdots\alpha_k)f(\alpha_1\alpha_2\cdots\alpha_k) = \frac{1}{k!}\sum_P (-)^P Pf(\alpha_1\alpha_2\cdots\alpha_k) \tag{3·35}$$

with $\sum_P$ denoting the sum over all permutation P with respect to $(\alpha_1\alpha_2\cdots\alpha_k)$, and $(-)^P$ the parity of the permutation. Substituting (3·34) into the definition (3·32), we obtain the recursion relation for $\mathcal{N}_k$:

$$\mathcal{N}_k(\alpha_1'\alpha_2'\cdots\alpha_k';\,\alpha_1\alpha_2\cdots\alpha_k)$$
$$=\mathcal{A}(\alpha_1\alpha_2\cdots\alpha_k)\Big[\delta_{\alpha_1\alpha_1'}\mathcal{N}_{k-1}(\alpha_2'\alpha_3'\cdots\alpha_k';\,\alpha_2\alpha_3\cdots\alpha_k)$$
$$-\frac{k-1}{2(\Omega+2-k)}\delta_{\tilde{\alpha}_1\alpha_2}\mathcal{N}_{k-1}(\alpha_2'\alpha_3'\cdots\alpha_k';\,\tilde{\alpha}_1'\alpha_3\cdots\alpha_k)\Big]. \qquad (3\cdot36)$$

From this recursion relation we obtain the explicit expressions for the overlap $\mathcal{N}_k$; for example,

$$\mathcal{N}_1(\alpha_1';\,\alpha_1)=\delta_{\alpha_1\alpha_1'},$$
$$\mathcal{N}_2(\alpha_1'\alpha_2';\,\alpha_1\alpha_2)=\mathcal{A}(\alpha_1\alpha_2)\mathcal{A}(\alpha_1'\alpha_2')\Big\{\delta_{\alpha_1\alpha_1'}\delta_{\alpha_2\alpha_2'}-\frac{1}{2\Omega}\delta_{\tilde{\alpha}_1\alpha_2}\delta_{\tilde{\alpha}_1'\alpha_2'}\Big\},$$
$$\mathcal{N}_3(\alpha_1'\alpha_2'\alpha_3';\,\alpha_1\alpha_2\alpha_3)=\mathcal{A}(\alpha_1\alpha_2\alpha_3)\mathcal{A}(\alpha_1'\alpha_2'\alpha_3')\Big\{\delta_{\alpha_1\alpha_1'}\delta_{\alpha_2\alpha_2'}\delta_{\alpha_3\alpha_3'}$$
$$-\frac{3}{2(\Omega-1)}\delta_{\tilde{\alpha}_1\alpha_2}\delta_{\tilde{\alpha}_1'\alpha_2'}\delta_{\alpha_3\alpha_3'}\Big\},$$
$$\mathcal{N}_4(\alpha_1'\alpha_2'\alpha_3'\alpha_4';\,\alpha_1\alpha_2\alpha_3\alpha_4)=\mathcal{A}(\alpha_1\alpha_2\alpha_3\alpha_4)\mathcal{A}(\alpha_1'\alpha_2'\alpha_3'\alpha_4')\Big\{\delta_{\alpha_1\alpha_1'}\delta_{\alpha_2\alpha_2'}\delta_{\alpha_3\alpha_3'}\delta_{\alpha_4\alpha_4'}$$
$$-\frac{3}{\Omega-2}\delta_{\tilde{\alpha}_1\alpha_2}\delta_{\tilde{\alpha}_1'\alpha_2'}\delta_{\alpha_3\alpha_3'}\delta_{\alpha_4\alpha_4'}+\frac{3}{4(\Omega-1)(\Omega-2)}\delta_{\tilde{\alpha}_1\alpha_2}\delta_{\tilde{\alpha}_3\alpha_4}\delta_{\tilde{\alpha}_1'\alpha_2'}\delta_{\tilde{\alpha}_3'\alpha_4'}\Big\},$$
etc. $\qquad (3\cdot37)$

With the aid of (3·36), we can furthermore prove the following relation by induction:

$$\sum_{\alpha_1''\alpha_2''\cdots\alpha_k''}\mathcal{N}_k(\alpha_1'\alpha_2'\cdots\alpha_k';\,\alpha_1''\alpha_2''\cdots\alpha_k'')\mathcal{N}_k(\alpha_1''\alpha_2''\cdots\alpha_k'';\,\alpha_1\alpha_2\cdots\alpha_k)$$
$$=\mathcal{N}_k(\alpha_1'\alpha_2'\cdots\alpha_k';\,\alpha_1\alpha_2\cdots\alpha_k). \qquad (3\cdot38)$$

This indicates that the overlap $\mathcal{N}_k$ are nothing but the matrix elements of the projection operator $\boldsymbol{P}^{\mu}$ which removes all the $J=0$-coupled components from the k particle states. In fact, the coupled-angular-momentum representations of Eqs. (3·37) exactly coincide with the projection operators given in Ref. 13). Therefore, the orthonormal basis of the intrinsic space is obtained by diagonalizing the overlap $\mathcal{N}_k$; the eigenvector with the eigenvalue $+1$ is the ordinary coefficients of fractional parentage in the seniority coupling scheme.

Now it is easily seen from Eqs. (3·33), (3·34) and (3·36) that

$$\boldsymbol{P}^{\mu}(\boldsymbol{c}^{\dagger}_{\alpha_1}\boldsymbol{c}^{\dagger}_{\alpha_2}\cdots\boldsymbol{c}^{\dagger}_{\alpha_k})|\mathrm{vac}\rangle\!\rangle$$
$$\equiv\sum_{\alpha_1'\alpha_2'\cdots\alpha_k'}\mathcal{N}_k(\alpha_1\alpha_2\cdots\alpha_k;\,\alpha_1'\alpha_2'\cdots\alpha_k')\boldsymbol{c}^{\dagger}_{\alpha_1'}\boldsymbol{c}^{\dagger}_{\alpha_2'}\cdots\boldsymbol{c}^{\dagger}_{\alpha_k'}|\mathrm{vac}\rangle\!\rangle$$
$$=\boldsymbol{a}^{\dagger}_{\alpha_1}\boldsymbol{a}^{\dagger}_{\alpha_2}\cdots\boldsymbol{a}^{\dagger}_{\alpha_k}|\mathrm{vac}\rangle\!\rangle. \qquad (3\cdot39)$$

This relation shows that the k ideal quasi-particle state is equivalent to the nucleon state projected to have a definite seniority $\alpha=k$.

§ 4. Relation to the canonical transformation method with auxiliary variables

In this section we show the relation between the method proposed in § 3 and the canonical transformation method with auxiliary variables used in Ref. 6).*)

4-1. *Canonical transformation U into collective representation*

In the use of the canonical transformation method with auxiliary variables, we first introduce boson operators $b^\dagger$ and b *in the original fermion space* and characterize the state vectors in the quasi-spin space by

$$|S, S_0=-S+N\rangle=\frac{1}{\sqrt{N!}}(b^+)^N|S, S_0=-S\rangle\,, \tag{4·1}$$

$$b|S, S_0=-S\rangle=0\,. \tag{4·2}$$

As is discussed in Ref. 6), such an introduction of the boson operators is made in terms of the Holstein-Primakoff representation,[14] but inevitably requires the extension of the quasi-spin space in such a way that the allowed values of S_0 become infinite:

$$\{|S, S_0\rangle;\ S_0=-S, -S+1, \cdots, +\infty\}. \tag{4·3}$$

Secondly, we introduce redundant bosons (i.e., auxiliary bosons) $\boldsymbol{b}^\dagger$ and $\boldsymbol{b}$ which are independent of the nucleon operators $(c_\alpha^\dagger, c_\alpha)$ *and* the boson operators $(b^\dagger, b)$:

$$[\boldsymbol{b}^\dagger, c_\alpha^\dagger]=[\boldsymbol{b}^\dagger, c_\alpha]=[\boldsymbol{b}^\dagger, b^\dagger]=[\boldsymbol{b}^\dagger, b]=0\,. \tag{4·4}$$

In order to compensate the over-completeness in the degrees of freedom due to the introduction of the auxiliary bosons, we impose on the state vectors a supplementary condition

$$\boldsymbol{b}^\dagger\boldsymbol{b}|\Psi\rangle=0\,, \tag{4·5}$$

which physically implies that we are only considering the subspace with no auxiliary bosons.

At this stage, let us define the following canonical transformation:**)

$$U=\exp\frac{\pi}{2}(\boldsymbol{b}^\dagger b-b^\dagger\boldsymbol{b})\,. \tag{4·6}$$

The following relations are then easily derived:

---

*) In this paper the boson operators represent the $J=0$-coupled nucleon pairs, whereas in Ref. 6) they are used for representing the $J=0$-coupled Bogoliubov quasi-particle pairs. Needless to say, the proof given in this section holds regardless of such a difference.

**) The equivalence between the U of (4·6) and the $U_{\rm col}$ of Ref. 6) is shown in the Appendix.

$$Ub^{+}U^{-1}=\boldsymbol{b}^{+}, \quad UbU^{-1}=\boldsymbol{b},$$
$$U\boldsymbol{b}^{+}U^{-1}=-b^{+}, \quad U\boldsymbol{b}U^{-1}=-b. \tag{4·7}$$

This implies that, in the representation after the canonical transformation which we call "collective representation", the boson operators $(b^{\dagger}, b)$ are completely replaced by the auxiliary bosons $(\boldsymbol{b}^{\dagger}, \boldsymbol{b})$. On the other hand, Eq. (4·5) becomes after the canonical transformation as

$$b^{\dagger}b|\Psi)=0, \quad |\Psi)=U|\Psi\rangle. \tag{4·8}$$

By comparing this supplementary condition with Eq. (4·2), we can see that in the collective representation the degree of freedom associated with the nucleon operators merely describes the intrinsic modes of the system (recall the definition of intrinsic modes in § 2-2). Thus, the Hilbert space in this representation may be characterized as the direct product of the boson space (associated with the auxiliary bosons $\boldsymbol{b}^{\dagger}$ and $\boldsymbol{b}$) and the intrinsic space composed of the "intrinsic" states $|S, S_0=-S\rangle$; The basis vectors can be represented as

$$|S, S_0=-S+N)\equiv|N\rangle\!\rangle\cdot|S, S_0=-S\rangle=\frac{1}{\sqrt{N!}}(\boldsymbol{b}^{\dagger})^{N}|0\rangle\!\rangle\cdot|S, S_0=-S\rangle. \tag{4·9}$$

By identifying the auxiliary bosons $\boldsymbol{b}^{\dagger}$ with those introduced in § 3, we can here notice the similarity between these basis vectors and those defined by (3·1) in the "ideal boson-quasi-particle space".

An arbitrary nucleon operator A is transformed by U as follows:

$$UAU^{-1}=\sum_{k,l=0}^{\infty}A_{kl}^{\mathrm{in}}\frac{(\boldsymbol{b}^{\dagger})^{k}}{k!}\cdot\frac{(-\boldsymbol{b})^{l}}{l!}, \tag{4·10}$$

where

$$A_{kl}^{\mathrm{in}}=([\underbrace{b, [b, \cdots [b}_{k}, [\underbrace{b^{\dagger}, [b^{\dagger}, \cdots [b^{\dagger}}_{l}, A]]\cdots])^{\mathrm{in}}. \tag{4·11}$$

Here the upper index "in" denotes that the degree of freedom associated with the boson operators $(b^{\dagger}, b)$ is completely removed from the operator in the parenthesis. Explicitly, it is written down as follows:

$$(O)^{\mathrm{in}}=\sum_{m,n=0}^{\infty}\frac{(-b^{\dagger})^{m}}{m!}[\underbrace{b, [b, \cdots [b}_{m}, [\underbrace{b^{\dagger}, [b^{\dagger}, \cdots [b^{\dagger}}_{n}, O]]\cdots]\frac{(b)^{n}}{n!}, \tag{4·12}$$

where O stands for an arbitrary nucleon operator. In fact, we can directly prove that

$$[(O)^{\mathrm{in}}, b^{\dagger}]=[(O)^{\mathrm{in}}, b]=0. \tag{4·13}$$

Therefore, carrying out the inverse transformation to (4·10), we obtain

$$A=U^{-1}(UAU^{-1})U=\sum_{k,l=0}^{\infty}A_{kl}^{\mathrm{in}}\frac{(b^{\dagger})^{k}}{k!}\cdot\frac{(-b)^{l}}{l!}. \tag{4·14}$$

4-2. *Relation between the T- and U-transformations*

With the aid of Eqs. (4·1) and (4·14), we can rewrite the transcribed form of an arbitrary nucleon operator A as follows:

$$TAT^{\dagger}=\sum_{S,S'=0}^{\Omega/2}\sum_{\Gamma\Gamma'}\sum_{N=0}^{2S}\sum_{N'=0}^{2S'}|S,\Gamma\rangle\rangle|N\rangle\rangle \times\langle S,-S;\Gamma|\frac{(b)^N}{\sqrt{N!}}\sum_{k,l=0}^{\infty}A^{\mathrm{in}}_{kl}\frac{(b^{\dagger})^k}{k!}\frac{(-b)^l}{l!}\frac{(b^{\dagger})^{N'}}{\sqrt{N'!}}|S',-S';\Gamma'\rangle\langle\langle S',\Gamma'|\langle\langle N'| . \tag{4·15}$$

Here we have used the fact that the set of quantum numbers Γ specifying the nucleon state together with the quasi-spin quantum numbers S and S_0 is not affected at all by the U-transformation. In the matrix element of Eq. (4·15), let us extract the part dependent on $b^{\dagger}$ and b, and replace it with the matrix element $\langle\langle N|(\boldsymbol{b}^{\dagger})^k(-\boldsymbol{b})^l|N'\rangle\rangle/k!l!$. Then Eq. (4·15) becomes

$$\begin{aligned}TAT^{\dagger}&=\sum_{S,S'=0}^{\Omega/2}\sum_{\Gamma,\Gamma'}\sum_{k,l=0}^{\infty}|S,\Gamma\rangle\rangle\langle S,-S;\Gamma|A^{\mathrm{in}}_{kl}|S',-S';\Gamma'\rangle\langle\langle S',\Gamma'| \\ &\quad\times\sum_{N=0}^{2S}\sum_{N'=0}^{2S'}|N\rangle\rangle\langle\langle N|\frac{(\boldsymbol{b}^{\dagger})^k}{k!}\cdot\frac{(-\boldsymbol{b})^l}{l!}|N'\rangle\rangle\langle\langle N'| \\ &=\sum_{S,S'=0}^{\Omega/2}\sum_{\Gamma\Gamma'}\boldsymbol{P}_S|S,\Gamma\rangle\rangle\langle S,-S;\Gamma|UAU^{-1}|S',-S';\Gamma'\rangle\langle\langle S',\Gamma'|\boldsymbol{P}_{S'} \\ &=\boldsymbol{P}_{\hat{S}}T_{\mathrm{in}}(UAU^{-1})T^{\dagger}_{\mathrm{in}}\boldsymbol{P}_{\hat{S}}\,,\end{aligned} \tag{4·16}$$

where we have used Eq. (4·10) and the projection operators $\boldsymbol{P}_{\hat{S}}$ and $\boldsymbol{P}_S$ are defined by (3·8) and (3·9), respectively. In this equation, T_{in} is defined by (3·15) and merely denotes the one-to-one correspondence between the intrinsic state $|S,\Gamma\rangle\rangle$ and the nucleon state $|S,-S;\Gamma\rangle$. Note here that, in the transformed operator UAU^{-1}, the pairing degree of freedom is completely replaced by the auxiliary bosons. Thus the T-transformation is equivalent to the U-transformation, aside from the fact that the former automatically cuts down the "unphysical states" with $N>2S$ in the pairing boson space. Here it may be worth emphasizing that in the use of the T-transformation it is unnecessary to introduce the boson operators $b^{\dagger}$ and b *in the original fermion space.*

§ 5. BCS approximation and pairing vibrational modes

5-1. *Relation between the Bogoliubov quasi-particle and the ideal quasi-particle*

It is very important to clarify the similarities and differences between the conventional Bogoliubov quasi-particle and the ideal quasi-particle defined by (3·14). For this purpose, let us consider the superconductive nuclei in which pairing phase transition takes place. In this case, we replace the pairing boson operators $\boldsymbol{b}_a^{\dagger}$

and $\boldsymbol{b}_a$ with their expectation values in the pairing space as follows:*)

$$\boldsymbol{b}_a^\dagger \to \langle \boldsymbol{b}_a^\dagger \rangle = \sqrt{2\hat{S}_a} v_a ,$$
$$\boldsymbol{b}_a \to \langle \boldsymbol{b}_a \rangle = \sqrt{2\hat{S}_a} v_a , \qquad (5\cdot1)$$

where v_a is a parameter. This means that we are considering the coherent state of pairing bosons as the ground state in the pairing space. In (5·1) we have expressed the expectation values as dependent on the quasi-spin operators $\hat{S}_a$ so that we can include the blocking effect due to the excitation of ideal quasi-particles. (Note that $\hat{S}_a$ operates on the *intrinsic* states.) If we neglect the projection operator $\boldsymbol{P}_{\hat{S}}$, the expression (3·13) for the single-nucleon operators in the "ideal boson-quasi-particle space" is reduced to

$$\boldsymbol{c}_\alpha^\dagger = \sqrt{1-v_a^2}\boldsymbol{a}_\alpha^\dagger + v_a \boldsymbol{a}_{\bar{\alpha}} ,$$
$$\boldsymbol{c}_{\bar{\alpha}} = -v_a \boldsymbol{a}_\alpha^\dagger + \sqrt{1-v_a^2}\boldsymbol{a}_{\bar{\alpha}} , \qquad (5\cdot2)$$

which is just the same form as the Bogoliubov transformation.

In spite of the above-mentioned similarity to the Bogoliubov transformation, the following difference should be emphasized: In our case, the symmetry breaking due to the pairing phase transition takes place only in the pairing space so that *the concept of ideal quasi-particle is completely independent of the phase transition.*

As is well known, one of the important motives for introducing the quasi-particle basis in the BCS theory is to characterize the excited states in terms of the seniority number in such a way that the number of quasi-particles is equivalent to the seniority. In a rigorous sense, however, the quasi-particle defined by the Bogoliubov transformation *cannot* be regarded as carrying a definite seniority. This is because the Bogoliubov quasi-particle can form a $J=0$-coupled pair which carries no seniority number and represents the fluctuation of the pairing field. On the other hand, the ideal quasi-particle introduced in this paper is completely independent of the fluctuation of the pairing field. Hence they are forbidden to form a $J=0$-coupled pair (recall Eq. (3·18)). Thus the ideal quasi-particle can be regarded, *in a rigorous sense*, as substantiation of the seniority concept.

5-2. *Pairing vibrational modes*

In order to illustrate simply how we treat the dynamical problems, we here take up the case of the conventional pairing Hamiltonian. A more general case will be treated in a forthcoming paper. The pairing Hamiltonian is given by

$$H = \sum_\alpha (\epsilon_a - \lambda) c_\alpha^\dagger c_\alpha - G \sum_{ab} \hat{S}_+(a)\hat{S}_-(b) , \qquad (5\cdot3)$$

where ϵ_a, λ and G denote the single-particle energy, the chemical potential and the

*) In this section we deal with the case of many j-shell. Therefore subscripts $a, b, \cdots$ are used for distinguishing different orbits. It is easily seen that the ideal quasi-particles in different orbits obey the ordinary anticommutation relations.

strength of the pairing force, respectively.

After the transcription into the ideal boson-quasi-particle space, the pairing Hamiltonian becomes

$$H \to THT^{\dagger} = \boldsymbol{P}_{\hat{S}} \boldsymbol{H} \boldsymbol{P}_{\hat{S}} ,$$

$$\boldsymbol{H} = \sum_{a} (\epsilon_a - \lambda) \{\hat{\boldsymbol{n}}_a + 2\boldsymbol{b}_a^{\dagger}\boldsymbol{b}_a\} - G \sum_{ab} \boldsymbol{b}_a^{\dagger} \sqrt{2\hat{S}_a - \boldsymbol{b}_a^{\dagger}\boldsymbol{b}_a} \sqrt{2\hat{S}_b - \boldsymbol{b}_b^{\dagger}\boldsymbol{b}_b} \cdot \boldsymbol{b}_b , \quad (5\cdot4)$$

where $\hat{\boldsymbol{n}}_a \equiv \sum_{m_a} \boldsymbol{a}_{a}^{\dagger} \boldsymbol{a}_a$ and $2\hat{S}_a = \Omega_a - \hat{\boldsymbol{n}}_a$. To deal with the situation in which the pairing phase transition takes place, we adopt the following transformation introducing new boson operators $\boldsymbol{\beta}_a^{\dagger}$ and $\boldsymbol{\beta}_a$:*)

$$\boldsymbol{b}_a^{\dagger} = \sqrt{\Omega_a} v_a + \boldsymbol{\beta}_a^{\dagger} , \quad \boldsymbol{b}_a = \sqrt{\Omega_a} v_a + \boldsymbol{\beta}_a . \quad (5\cdot5)$$

It is clear that the new boson operators $(\boldsymbol{\beta}_a^{\dagger}, \boldsymbol{\beta}_a)$ represent the effect of the fluctuation of the pairing field. Let us expand the square root in (5·4) into the power series of $\Omega^{-1/2}$ and take up the terms in the Hamiltonian to the order of unity. Then we obtain

$$\boldsymbol{H} = W + \boldsymbol{H}_{\mathrm{intr}} + \boldsymbol{H}_{\mathrm{pair}} , \quad (5\cdot6)$$

$$W = \sum_{a} 2(\epsilon_a - \lambda) \Omega_a v_a^{2} - \Delta^2/G , \quad (5\cdot6a)$$

$$\boldsymbol{H}_{\mathrm{intr}} = \sum_{a} \left(\epsilon_a - \lambda + \frac{v_a}{u_a} \Delta \right) \hat{\boldsymbol{n}}_a , \quad (5\cdot6b)$$

$$\boldsymbol{H}_{\mathrm{pair}} = \boldsymbol{H}_{\mathrm{pair}}^{(0)} + \boldsymbol{H}_{\mathrm{pair}}^{(1)} + \boldsymbol{H}_{\mathrm{pair}}^{(2)} , \quad (5\cdot6c)$$

$$\boldsymbol{H}_{\mathrm{pair}}^{(0)} = \sum_{a} \Big[2(\epsilon_a - \lambda) \boldsymbol{\beta}_a^{\dagger}\boldsymbol{\beta}_a + \frac{u_a v_a}{4u_a^{4}} \Delta \{ 2(4u_a^{2} + v_a^{2}) \boldsymbol{\beta}_a^{\dagger}\boldsymbol{\beta}_a + (2u_a^{2} + v_a^{2}) (\boldsymbol{\beta}_a^{\dagger}\boldsymbol{\beta}_a^{\dagger} + \boldsymbol{\beta}_a\boldsymbol{\beta}_a) \} \Big] , \quad (5\cdot6d)$$

$$\boldsymbol{H}_{\mathrm{pair}}^{(1)} = \sum_{a} \frac{\sqrt{\Omega_a}}{u_a} \{ 2u_a v_a (\epsilon_a - \lambda) - (u_a^{2} - v_a^{2}) \Delta \} (\boldsymbol{\beta}_a^{\dagger} + \boldsymbol{\beta}_a) , \quad (5\cdot6e)$$

$$\boldsymbol{H}_{\mathrm{pair}}^{(2)} = -G \sum_{ab} \frac{\sqrt{\Omega_a}}{2u_a} \cdot \frac{\sqrt{\Omega_b}}{2u_b} \{ (2u_a^{2} - v_a^{2}) \boldsymbol{\beta}_a^{\dagger} - v_a^{2} \boldsymbol{\beta}_a \} \times \{ (2u_b^{2} - v_b^{2}) \boldsymbol{\beta}_b - v_b^{2} \boldsymbol{\beta}_b^{\dagger} \} , \quad (5\cdot6f)$$

where $\Delta = G \sum_a \Omega_a u_a v_a$ and $u_a = \sqrt{1 - v_a^{2}}$. At this stage, we determine the parameters v_a so as to minimize the constant term W:

$$\frac{\partial W}{\partial v_a} = \frac{2\Omega_a}{u_a} \{ 2u_a v_a (\epsilon_a - \lambda) - (u_a^{2} - v_a^{2}) \Delta \} = 0 . \quad (5\cdot7)$$

This condition coincides with the one for eliminating the "dangerous term" $\boldsymbol{H}_{\mathrm{pair}}^{(1)}$

*) In Eq. (5·5) we can replace the constant term with $\sqrt{2\hat{S}_a} \cdot v_a$ as was done in (5·1). In this case we obtain the BCS equation and the pairing vibrational modes in which the blocking effect is already taken into account.[6]

and yields the ordinary BCS gap equation. Then $\boldsymbol{H}_{\text{intr}}$ becomes

$$\boldsymbol{H}_{\text{intr}}=\sum_a E_a\hat{\boldsymbol{n}}_a\,,\quad E_a=\sqrt{(\epsilon_a-\lambda)^2+\Delta^2}\,, \tag{5·8}$$

which implies that the energy of the ideal quasi-particle is the same as that of the Bogoliubov quasi-particle. Next, let us diagonalize $\boldsymbol{H}^{(0)}_{\text{pair}}$ by the following unitary transformation:

$$\begin{aligned}&\boldsymbol{\beta}_a^{\dagger}=\xi_a\boldsymbol{b}_a^{\dagger}+\eta_a\boldsymbol{b}_a\,,\\&\xi_a=\tfrac{1}{2}(u_a^{-1}+u_a)\,,\quad \eta_a=\tfrac{1}{2}(u_a^{-1}-u_a)\,.\end{aligned} \tag{5·9}$$

Then $\boldsymbol{H}^{(0)}_{\text{pair}}$ becomes to be

$$\boldsymbol{H}^{(0)}_{\text{pair}}=-\sum_a\frac{v_a^4}{2u_a^2}E_a+\sum_a 2E_a\boldsymbol{\beta}_a^{\dagger}\boldsymbol{\beta}_a\,, \tag{5·10}$$

and $\boldsymbol{H}^{(2)}_{\text{pair}}$ reduces to the form

$$\boldsymbol{H}^{(2)}_{\text{pair}}=-G\sum_{ab}\sqrt{\Omega_a}\sqrt{\Omega_b}\,\{u_a^2\boldsymbol{\beta}_a^{\dagger}-v_a^2\boldsymbol{\beta}_a\}\,\{u_b^2\boldsymbol{\beta}_b-v_b^2\boldsymbol{\beta}_b^{\dagger}\}\,, \tag{5·11}$$

which coincides with the conventional residual interaction generating the pairing vibrational modes in the RPA. In this way we obtain from $\boldsymbol{H}_{\text{pair}}$ the usual pairing vibrational modes including a special zero-energy solution, while the terms higher than the order of unity give the anharmonicity effects of the pairing vibrational modes and the coupling to the intrinsic modes represented by the ideal quasi-particle operators $(\boldsymbol{a}_\alpha^{\dagger},\boldsymbol{a}_\alpha)$.

§ 6. Concluding remarks

By introducing the concept of "ideal boson-quasi-particle space" we have achieved the exact separation of pairing and intrinsic degrees of freedom. In particular, we have obtained the closed expression of the single-nucleon operator in terms of the pairing bosons and the "ideal quasi-particles". Since the multiplication law is always assured in the T-transformation, any product of the nucleon operators can be transcribed in a systematic way into the ideal boson-quasi-particle space. Thus the interplay of the pairing and intrinsic modes of excitation can be explicitly treated in this space. Furthermore, since the concept of ideal quasi-particle is completely independent of the pairing phase transition, we can treat both the normal and superconducting systems in a unified way. This point will be concretely developed in a forthcoming paper.

In this paper, we have developed the method starting from the original nucleon operators and treated the superconducting system by introducing the coherent state of the pairing bosons. Of course, the method is also applicable to the case starting with the Bogoliubov quasi-particle. In this case we must transcribe the Bogoliubov quasi-particle into the ideal boson-quasi-particle space. Then we will again reach the concept of ideal quasi-particle. This point will also be discussed in a forthcom-

ing paper.

Acknowledgements

The authors would like to thank Prof. T. Marumori, Prof. M. Yamamura, Prof. K. Takada, Dr. A. Kuriyama and Dr. F. Sakata for valuable discussions. We are also grateful to the members of the nuclear theory group of Department of Physics, Kyoto University, for their interest in this work.

Appendix

The equivalence between the U defined by (4·6) and the canonical transformation U_{col} of Ref. 6) is seen as a special case of the following identities:

$$U(\theta) \equiv \exp\left(i\cdot\tan\frac{\theta}{2}\cdot pq\right)\exp(-i\cdot\sin\theta\cdot pq)\exp\left(i\cdot\tan\frac{\theta}{2}\cdot pq\right) \quad (\mathrm{A}\cdot 1\mathrm{a})$$

$$= \exp i\theta(pq - pq) \quad (\mathrm{A}\cdot 1\mathrm{b})$$

$$= \exp\theta(b^{\dagger}b - b^{\dagger}b) \quad (\mathrm{A}\cdot 1\mathrm{c})$$

$$= \exp\left(\tan\frac{\theta}{2}\cdot b^{\dagger}b\right)\exp(-\sin\theta\cdot b^{+}b)\exp\left(\tan\frac{\theta}{2}\cdot b^{\dagger}b\right), \quad (\mathrm{A}\cdot 1\mathrm{d})$$

where θ is a parameter and the canonical conjugate variables are related to the boson operators through

$$p = \frac{1}{\sqrt{2}}(b + b^{\dagger}), \quad q = \frac{i}{\sqrt{2}}(b - b^{\dagger}),$$

$$p = \frac{1}{\sqrt{2}}(b + b^{\dagger}), \quad q = \frac{i}{\sqrt{2}}(b - b^{\dagger}). \quad (\mathrm{A}\cdot 2)$$

For $\theta = \pi/2$, (A·1a) reduces to U_{col} of Ref. 6) while (A·1c) reduces to our U. It is interesting to note that $U(\theta)$ may be regarded as the operator generating the rotation 2θ around the y-axis in the abstract spin space composed of two kinds of boson.[15]

References

1) For example, J. Hadermann and A. C. Rester, Nucl. Phys. **A231** (1974), 120.
2) F. Sakata and T. Marumori, Genshikaku Kenkyu **20** (1975), 88 (in Japanese).
3) S. Iwasaki, T. Marumori, F. Sakata and K. Takada, Prog. Theor. Phys. **56** (1976), 1140.
4) S. Iwasaki, T. Marumori, F. Sakata and K. Takada, Prog. Theor. Phys. **56** (1976), 846.
5) D. R. Bes, R. A. Broglia, G. G. Dussel, R. Liotta and B. R. Mottelson, Phys. Letters **52B** (1974), 253.
   D. R. Bes, R. A. Broglia, G. G. Dussel and R. Liotta, Phys. Letters **56B** (1975), 109.
   D. R. Bes and R. A. Broglia, in *Problems of Vibrational Nuclei*, edited by G. Alaga, V. Paar and L. Šips (North Holland, Amsterdam, 1975), p. 1.
6) A. Kuriyama, T. Marumori, K. Matsuyanagi, F. Sakata and T. Suzuki, Prog. Theor. Phys.

Suppl. No. 58 (1975), 9, 184.
7) T. Marumori, J. Yukawa and R. Tanaka, Prog. Theor. Phys. **13** (1955), 442.
T. Marumori, Prog. Theor. Phys. **14** (1955), 608; **24** (1960), 331.
S. Hayakawa and T. Marumori, Prog. Theor. Phys. **18** (1957), 396.
8) T. Miyazima and T. Tamura, Prog. Theor. Phys. **15** (1956), 255.
F. Villars, Ann. Rev. Nucl. Sci. **7** (1957), 185.
9) R. D. Lawson and M. H. Macfarlane, Nucl. Phys. **66** (1965), 80.
M. Ichimura, *Progress in Nuclear Physics* (Pergamon Press), Vol. 10 (1969), p. 307.
10) T. Marumori, M. Yamamura and A. Tokunaga, Prog. Theor. Phys. **31** (1964), 1009.
11) M. Yamamura, Prog. Theor. Phys. **33** (1965), 199.
12) E. R. Marshalek, Nucl. Phys. **A224** (1974), 221.
13) A. Kuriyama, T. Marumori, K. Matsuyanagi and R. Okamoto, Prog. Theor. Phys. Suppl. No. 58 (1975), 32.
14) T. Holstein and H. Primakoff, Phys. Rev. **58** (1940), 1098.
15) J. Schwinger, in *Quantum Theory of Angular Momentum*, edited by L. Biedenharn and H. Van Dam (Academic Press, New York, 1965), p. 229.

Structure of Yrast Traps

T. Døssing. K. Neergård, K. Matsuyanagi, and Hsi-Chen Chang[a]
The Niels Bohr Institute, University of Copenhagen, DK-2100 Copenhagen Ø, Denmark
(Received 11 July 1977)

An "island" of isomeric states with high multiplicities found in a recent experiment are interpreted as "yrast traps" in deformed nuclei rotating around a symmetry axis. According to our interpretation, a group of trap states for neutron numbers around 82 and angular momenta below 40 is connected with the nuclear shell structure for weakly deformed potentials. A second group of traps situated in a more narrow region around neutron number 82 and with angular momentum around 50 is attributed to the occurence of shell structure for a ratio of axes 2:3.

Recently a search for high-spin isomeric states ("yrast traps") was reported[1] by a joint group from the Niels Bohr Institute and Gesellschaft für Schwerionenforschung. Several isomers with multiplicities between 8 and 20 were found, all belonging to nuclei situated in a specific part of the investigated area of the N-Z plane around the neutron number 82.

According to a suggestion[2] by Bohr and Mottelson, yrast traps may appear when, for certain values of the angular momentum, the single-particle potential becomes axially symmetric with respect to the spin direction. The reason is that, with this symmetry of the potential, there is no organization of the individual levels of the yrast region into rotational bands parallel to the yrast line. The electromagnetic transitions which carry off angular momentum have single-particle character. Under such circumstances a given configuration of the independent-particle system may be unable to decay through a transition with low multipolarity and in this way becomes a trap.

Numerical calculations based on this idea were carried out[3,4] by the Lund-Warsaw group. The present theoretical "search" for trap states is more extensive as to the set of nuclei and deformations considered and covers the experimentally investigated region.[1] We find as a result of this search new classes of traps connected with strongly oblate and weakly prolate shapes, which were not predicted in the earlier studies. We also attempt to get a deeper qualitative insight into the general structure of the trap configurations.

For most even nuclei in the experimentally investigated area we have calculated by the Strutinsky method[3,5,6] the energy at various angular momenta as a function of the deformation parameters β and γ. Our deformation space and parameters are the same as in Ref. 6. In particular, a Woods-Saxon single-particle potential was used.

From the results of this calculation we have extracted the difference between the minimal energy with restriction to shapes that rotate around the symmetry axis and the minimal energy for the total deformation space. The shapes with rotation around the symmetry axis included in the deformation space extend from weakly prolate shapes (ratio of axes 1.08:1) through the spherical shape to very strongly oblate shapes (ratio of axes 1:2.5). The energy differences calculated in this way are shown in Fig. 1 on a N-Z diagram for a number of angular momenta. In the white areas of the diagram the equilibrium shape corresponds to rotation around the symmetry axis; hence, for these values of N, Z, and I, traps are possible. We define a trap state in the same way as in Ref. 3, namely, as a state which cannot decay through an $E1$, $M1$, $E2$, or $M2$ single-particle transition. In addition we require that it be an yrast state. For all combinations of N, Z, and I within the white areas of Fig. 1 we search for independent-particle states which satisfy these conditions. The angular momenta of theoretical trap states found in this way are shown as encircled numbers in Fig. 1.

The theoretical traps fall into several groups with different deformation. For $I<40$ and neutron numbers 80, 84–88, and 114, the deformation is small ($\beta<0.15$). The shape is prolate for $N=80$ and 114, and oblate for $N=84$–88. The traps calculated by the Lund-Warsaw group[3,4] all belong to the small oblate deformation. For neutron numbers 82–84 we predict a number of traps belonging to a strongly oblate shape with ratio of axes approximately equal to 2:3 ($\beta\approx0.4$). This deformation comes into play only for $I>40$ and all theoretical traps with $I>40$ belong to it. The groups mentioned so far (except for $N=114$) build up an "island" of theoretical traps with $N=80$–88, $Z=62$–70, the contour of which approximately corresponds to that of the empirical "island."[1] Our model gives traps also in the adjacent odd-A nu-

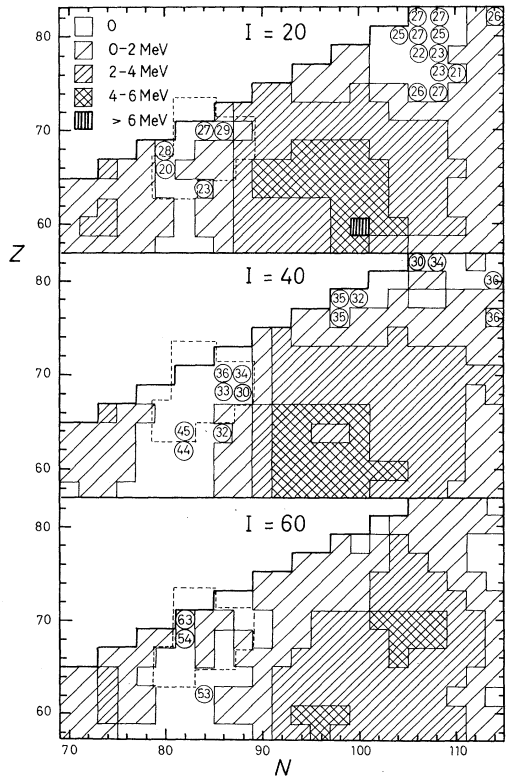

FIG. 1. Contour diagram of the minimal energy with restriction to shape that rotate around the symmetry axis measured relative to the minimal energy in the whole β-γ plane. This energy is shown for even-even nuclei and for the three values 20, 40, and 60 of the angular momentum. The encircled numbers are the spins of theoretical traps, grouped into the inervals $20 \leq I \leq 29$, $30 \leq I \leq 49$, and $I \geq 50$. The dashed line shows the approximate contour of the empirical "island" of isomers (Ref. 1) assuming that four neutrons were evaporated.

clei.

For neutron numbers 98–110 the deformation is oblate with $\beta \approx 0.25$. Some of the nuclei belonging to this group were investigated in the experiment, but no isomers were found. A possible reason is that when the hexadecapole degree of freedom is taken into account most of these nuclei may be found to have at the spin values considered a shape deviating from oblate symmetry. In fact, in calculations[7] for $I = 0$ the hexadecapole degree of freedom is decisive for producing prolate shapes of the W–Os nuclei.

The main pattern in the occurence of trap states can be understood in terms of simple systematic features of the single-particle spectrum. As a first example we consider the case of weakly oblate shapes ($N = 84$–88, $Z = 64$-70).

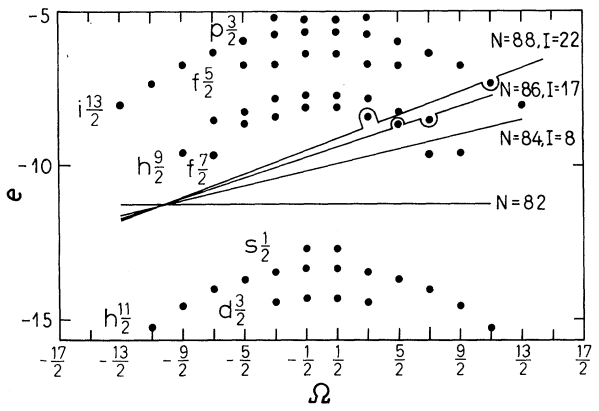

FIG. 2. Single-neutron energies e for the oblate deformation $\beta = 0.1$ vs the angular momentum Ω with respect to the symmetry axis. The quantum numbers given are those of the spherical level towards which each state converges in the limit of $\beta \to 0$. The neutron Fermi surfaces of the trap configurations in the region $N = 84$–88, $Z = 64$–70 are shown.

The single-particle energies for neutrons in the oblate potential with deformation $\beta = 0.1$ are plotted in Fig. 2 versus the angular-momentum projection. (Note that by definition Ω is the projection on the direction of the total angular momentum, and therefore the sum of single-particle Ω is equal to I.) In a corresponding plot for the spherical potential the dots would lie on horizontal lines labeled by the quantum numbers (nlj). Turning on an oblate deformation these lines are bent into a bell shape. Still, for the small deformation $\beta = 0.1$ a gap remains at $N = 82$.

Configurations with neutron numbers $N = 84$–86, 88 and increasing angular momentum can be obtained by filling particles into levels above the $N = 82$ gap. None of the configurations shown can decay with a single-particle transition without changing the angular momentum by at least three units. Hence they are trap configurations. The neutron configurations formed in this way are involved in the trap states for $N = 84$–88, $Z = 64$–70. They are composed of particles in high-Ω members of the subshells $f_{7/2}$, $h_{9/2}$, and $i_{13/2}$.

In order to have a trap state of the total nuclear system both the neutrons and the protons must be in trap configurations. The proton configurations for $Z = 64$–70 in the weakly oblate potential are built from particles in high-Ω $h_{11/2}$ states and holes in low-Ω $d_{5/2}$ states. Quite generally, when holes are involved in a trap configuration for an oblate shape they must have low Ω. (This rule may be inferred from a study of the neutron spectum in Fig. 2.)

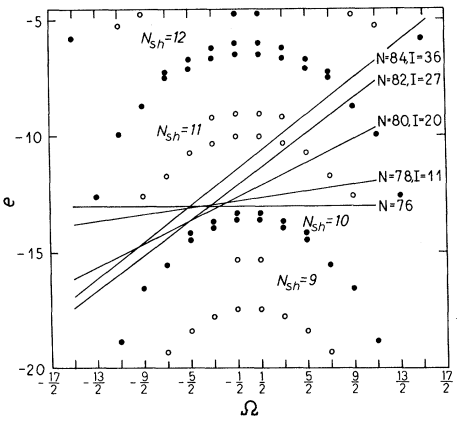

FIG. 3. Single-neutron energies for the oblate deformation $\beta = 0.40$. The closed points belong to even values of the shell quantum number N_{sh} and the open points to odd N_{sh}. The Fermi surfaces discussed in the text are shown.

For a prolate potential we can make a similar discussion exchanging the words "particle" and "hole." Prolate configurations involving high-Ω members of the $h_{11/2}$ and $i_{13/2}$ shells enter the traps with $N = 80$ and $N = 114$. Generally, however, the dominance of orbits with low j in the upper end of the major shells makes the prolate single-particle spectra less suitable for building traps.

The neutron configurations discussed above for the small oblate deformation have a structure similar to that of known isomers above ^{208}Pb composed of particles in aligned spherical orbits with large j. The special stability of these aligned configurations is usually discussed in terms of the properties of the residual interaction.[8]

It is worth noting that in fact the density distribution of such a configuration is oblate with symmetry axis along the direction of the total angular momentum. If holes are added to the aligned configuration the particle-hole interaction favors hole states having low density along the "equator" thus contributing to the oblateness of the total density. In the present model the special stability of this type of configurations results from the lowering of the energies of the high-Ω particles and low-Ω holes in an oblate potential. The relation between the two approaches will be further discussed in a separate publication.[9]

The trap states for $N = 82$ and 84, $Z = 62$–70, and $I \geq 44$ exhibit another single-particle structure of particular interest. These nuclei aquire at $I \approx 50$ a strongly oblate shape with a ratio of axes close to 2:3. The occurence of this deformation appears to be connected with the shell structure associated with the quantum number[10] $N_{sh} = 3n_z + 2n_\perp$, where n_z and $n_\perp$ are the usual asymptotic quantum numbers describing the number of oscillations parallel and perpendicular to the symmetry axis. As shown in Fig. 3, the neutron number $N = 76$ completes the $N_{sh} = 10$ shell, and above $N = 76$ we get trap configurations with $N = 78$, 80, 82, and 84, similar to those described above for the small oblate deformation. Among these, only the $N = 82$ and 84 configurations have a sufficient neutron spin to come into play at $I \approx 50$. They can, for $Z = 62$–70, combine with proton configurations analogous to those discussed above for the weakly oblate case being built from a few particles in high-Ω states with $N_{sh} = 11$ and 12, and several holes in low-Ω states with $N_{sh} = 10$.

The systematics of the 2:3 shell structure points to the possible existence of similar traps connected with the completion of other shells with even value of N_{sh}, for example, for nucleon numbers above 48 ($N_{sh} = 8$) or 114 ($N_{sh} = 12$).

We wish to express our gratitude to S. Bjørnholm, A. Bohr, S. Frauendorf, T. L. Khoo, B. R. Mottelson, J. Pedersen, and P. Vogel for valuable suggestions.

The work was supported by the Scientific Research Council of the Danish State and the Commemorative Association of the Japan World Exposition.

[a]Present and permanent address: Atomic Energy Institute, Academy of Science, Peking, China.

[1]J. Pedersen *et al.*, Phys. Rev. Lett. 39, 990 (1977).
[2]A. Bohr and B. R. Mottelson, Phys. Scr. 10A, 13 (1974).
[3]G. Andersson *et al.*, Nucl. Phys. A268, 205 (1976).
[4]M. Cerkaski *et al.*, Phys. Lett. 70B, 9 (1977).
[5]K. Neergård *et al.*, Nucl. Phys. A262, 61 (1976).
[6]K. Neergård *et al.*, Nucl. Phys. A287, 48 (1977).
[7]U. Götz *et al.*, Nucl. Phys. A192, 1 (1972).
[8]See, for example, J. Blomquist *et al.*, Phys. Rev. Lett. 38, 534 (1977), and references therein.
[9]K. Matsuyanagi and T. Døssing, to be published.
[10]A. Bohr and B. R. Mottelson, *Nuclear Structure* (Benjamin, New York, 1975), Vol. 2.

1.D.1:
1.D.2

Nuclear Physics **A307** (1978) 253–276; © *North-Holland Publishing Co., Amsterdam*

HIGH-SPIN ISOMERS IN Po, At AND Rn IN THE DEFORMED INDEPENDENT PARTICLE MODEL

K. MATSUYANAGI †, T. DØSSING †† and K. NEERGÅRD

The Niels Bohr Institute, University of Copenhagen, Blegdamsvej 17, DK-2100 Copenhagen, Denmark

Received 9 May 1978

(Revised 20 June 1978)

Abstract: The isomeric states in Po, At and Rn isotopes are described as independent particle states in a deformed potential which is symmetric with respect to the direction of the angular momentum. The known parts of the yrast lines of these nuclei are found to be well described by the model. In particular all observed isomeric states are reproduced as "traps". The variation of the shape along the yrast line is studied. In most of the nuclei considered a gradual rise of oblate deformation takes place. This can be understood from simple qualitative considerations. The relation of the present approach to a description within the spherical shell model with residual interactions is discussed.

1. Introduction

Within the last few years there has been a remarkable progress in the study of isomeric states with large angular momenta.

A classical example of such a state, known for about fifteen years [1]), is the 45 s isomer in ^{212}Po with spin and parity 16^+ or 18^+. Although the exact structure of this state remains uncertain, all suggested interpretations [2,3]) agree in so far as they involve an alignment of the angular momenta of the valence particles. Extensive experimental work carried out in the seventies has shown that the region of nuclei with a few particles or holes in excess of the double-closed-shell ^{208}Pb core is indeed rich in isomeric states with such a structure. The highest spin of an isomer in this category so far observed is $J = 30$, measured recently [4]) in ^{212}Rn.

Another group of high-spin isomers is constituted by the "K-isomers" observed in well-deformed nuclei. The 4 s and 31 y isomers [5]) in ^{178}Hf, which can be interpreted as respectively a $K^\pi = 8^-$ and a $K^\pi = 16^+$ band head, are classical examples of isomers of this kind. Also this family has been considerably extended within the last few years. Thus, the highest spin of an isomer in this category is now $J = 22$ measured [ref. [6])] in ^{176}Hf.

An important step forward was taken with the introduction of an experimental technique which enables one to scan a large area of the N-Z plane for the appearance

† On leave of absence from Department of Physics Kyoto University, Kyoto, Japan.
†† Present address: Max-Planck-Institut für Kernphysik, Heidelberg, West-Germany.

of high-spin isomeric states. Using this technique, Pedersen *et al.*, employing the facilities of the Gesellschaft für Schwerionenforschung, Darmstadt, were able to make the first experimental verification [7]) of the existence of an "island" of isomers with multiplicities 10–20 in the region of neutron deficient isotopes of light rare earth elements. [Some single isomers belonging to the island were found independently [26, 27]) by other groups.] The likelihood of the appearance of high-spin isomers in this region had been suggested earlier by Anderson *et al.* [8]) on the basis of calculations within a deformed independent particle model of yrast states.

In a previous paper [9]), we analysed the structure of the "trap configurations" described by the model of Anderson *et al.* This analysis revealed the close relationship between the presumable structure of most of the isomers of the Darmstadt experiment and that of the afore-mentioned isomers in the region of ^{208}Pb. It is therefore natural to raise the question to what extent the same model is able to reproduce the properties of these well-known isomers. An answer to this question is of obvious importance for the degree of confidence one could have in predictions based on this model in other regions of the periodic table.

In the present paper, we apply the independent particle model in a calculation of the yrast spectra of Po, At and Rn. Apart from examining the ability of the model in reproducing the experimental data, we aim at shedding light on the mutual relationships between angular momentum alignment, deformation and shell structure. In particular, we discuss the implications of the fact that in the independent particle model the isomers in the ^{208}Pb region have finite (but small) deformations. It will be shown that in fact the deformation energy is the factor which in this model stabilizes the isomeric configurations. The variation of the deformation along the yrast line is examined and interpreted in terms of simple qualitative considerations.

Conventionally, the spectroscopic properties of nuclei in the vicinity of ^{208}Pb are discussed in terms of the spherical shell model with residual interactions. Some calculations based on this approach have been able to account for the measured excitation energies with an accuracy which is extraordinary in nuclear physics. [See ref. [10]) and references therein.] The relation of the present approach to the spherical shell model is a recurrent theme in our paper.

In particular we attempt to identify the parts of the shell-model residual interaction energy which are taken into account through the deformation energy in the independent particle model.

Calculations similar to ours for the nucleus ^{212}Rn were performed [11]) by Leander. His detailed assumptions deviate somewhat from those employed in the present paper. Aberg has investigated [12]) the applicability of the deformed independent particle model to the description of the K-isomers in $^{172-180}$Hf.

2. Model

2.1. BASIC PRINCIPLES

The deformed independent particle model of yrast states in the regime of axial symmetry with respect to the direction of the angular momentum is discussed in detail in the original paper by Anderson *et al.* [8]). The extension of this model by inclusion of pairing was considered by Cerkashi *et al.* [13]). For completeness we give below a brief account of its basic principles. The explicit formulas may be found in the papers quoted above.

The model deals with independent particle configurations in an axially symmetric deformed potential. The sum of single-particle angular momenta along the symmetry axis is taken as a measure of the total angular momentum of the nucleus. The energy is calculated by the Strutinsky method [14]). In our case, this amounts to evaluating in the BCS approximation the independent particle plus pairing energy blocking the levels occupied by unpaired particles. From this the smooth energy of the ground-state configuration is subtracted and replaced by the liquid drop energy. As shown in ref. [25]) this is a correct procedure for the Woods-Saxon potential where the average increase of energy, as a function of the angular momentum, closely corresponds to a rigid rotation of a homogeneous ellipsoid with the same deformation.

The deformation is determined separately for each configuration so as to yield the minimal energy.

2.2. SINGLE-PARTICLE ENERGIES

As a model of the single-particle field we use the deformed Woods-Saxon potential as defined by Pashkevich [15]) with the parameters suggested by Pauli [16]). The deformation space is restricted to purely ellipsoidal shapes and is thus described by the single parameter $\varepsilon = 3(q-1)/(2q+1)$, where q denotes the ratio between the distance of the "poles" and the diameter of the "equator".

It is well known [16]) that in this model the empirical single-particle energies in ^{208}Pb are reproduced only with an accuracy of 1–2 MeV. Since the calculated yrast spectra are very sensitive to the single-particle energies, we modify in the vicinity of the $Z = 82$ and $N = 126$ gaps the Woods-Saxon energies so as to have for $\varepsilon = 0$ the empirical values. This is done by means of constant shifts independent of the deformation.

2.3. PAIRING FORCE

The strength parameters G_p and G_n of the pairing force are determined by the average gap method [14]) applied to the ground-state configuration of the nucleus considered. For the average gap we use the conventional value $\tilde{\Delta} = 12A^{-\frac{1}{2}}$ MeV.

2.4. LIQUID DROP MODEL

Following Myers and Swiatecki [17]) we use as expression for the liquid drop energy (in MeV)

$$E_{\mathrm{LD}} = 17.9439A^{\frac{2}{3}}\left(1-1.7826\left(\frac{N-Z}{A}\right)^2\right)(B_{\mathrm{S}}-1)+0.7053\frac{Z^2}{A^{\frac{1}{3}}}(B_{\mathrm{C}}-1), \qquad (2.1)$$

where B_{S} and B_{C} denote, respectively, the surface and the Coulomb potential energy in units of the spherical values assuming a homogeneous charge distribution bounded by a sharp ellipsoidal surface.

3. Application to the ^{208}Pb region

3.1. DEFORMATION AND DEFORMATION ENERGY

Fig. 1 shows for a couple of independent particle configurations the dependence of the energy on the deformation parameter ε. As examples we have chosen the configurations corresponding to two alternative interpretations of the 45 s isomer in ^{212}Po given in the literature. Thus for example the configuration indicated by $J^\pi = 16^+$ consists of the ^{208}Pb core plus two protons in the states emerging from the spherical orbitals $\mathrm{h}_{\frac{9}{2}}$, $m = \frac{7}{2}$ and $\frac{9}{2}$, and two neutrons in the states emerging from $\mathrm{g}_{\frac{9}{2}}$, $m = \frac{7}{2}$ and $\frac{9}{2}$. In other words it is equal in the limit $\varepsilon \to 0$ to the shell-model state [3]) $(\pi(\mathrm{h}_{\frac{9}{2}})^2\nu(\mathrm{g}_{\frac{9}{2}})^2)_{J^\pi M=16^+16}$. In a similar way the configuration indicated by $J^\pi = 18^+$ converges in the spherical limit into the shell-model state [2]) $(\pi(\mathrm{h}_{\frac{9}{2}})^2\nu(\mathrm{g}_{\frac{9}{2}}\mathrm{i}_{\frac{13}{2}}))_{J^\pi M=18^+18}$.

One sees in these examples various characteristic features. In both cases the equilibrium deformation is oblate and of the order $\varepsilon_0 \approx -0.03$ (respectively, $\varepsilon_0 = -0.025$ and $\varepsilon_0 = -0.035$ in the two cases). The energy gained by distorting

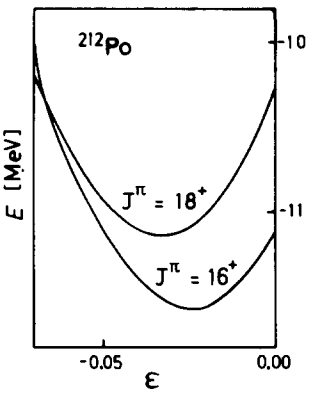

Fig. 1. Calculated energies of two possible configurations of the 45 s isomer in ^{212}Po plotted against deformation. The configurations are described in subsect. 3.1. Energies are measured relative to the energy of the spherical liquid drop.

the spherical shape by this amount is of the order 1 MeV (respectively 0.52 MeV and 0.88 MeV). These features may be qualitatively understood in terms of simple considerations related to Rainwater's arguments [18]) for the appearance of deformed shapes between the closed spherical shells.

If we neglect the pairing energy we can write in a good approximation for small deformations ($|\varepsilon| \lesssim 0.05$)

$$\begin{aligned} E^{(i)}_{\mathrm{def}}(\varepsilon) &= E^{(i)}(\varepsilon) - E^{(i)}(0) \\ &= (\sum_i C_i)\varepsilon + \tfrac{1}{2} C_0{}^{(i)} \varepsilon^2 . \end{aligned} \tag{3.1}$$

Here the first term involves a summation over the particles and holes of the configuration $\{i\}$ considered. The coefficients C_i are given by

$$C_i = \pm \left(\frac{\mathrm{d}e_i(\varepsilon)}{\mathrm{d}\varepsilon} \right)_{\varepsilon = 0} = \pm \alpha_{j_i} \left(\frac{m_i^2}{j_i(j_i+1)} - \tfrac{1}{3} \right), \tag{3.2}$$

where $e_i(\varepsilon)$ denotes the single-particle energy, and the upper and lower sign refers to respectively particles and holes. These expressions are valid since neither the smooth part of the independent particle energy in the ground-state configuration nor the liquid drop energy contribution to the linear term in the Taylor expansion of $E^{(i)}_{\mathrm{def}}(\varepsilon)$. In (3.2) m_i is the projection of the single-particle angular momentum on the symmetry axis, and j_i is the usual angular momentum quantum number in the limit $\varepsilon \to 0$. The factors α_j, which are related to the radial matrix elements of the gradient of the single-particle potential, have positive values of the order 30 MeV (see fig. 2). The coefficient $C_0^{(i)}$ has values of the order of 1–2 GeV, reflecting mainly the stiffness of the ^{208}Pb core. Thus for the doubly closed shell configuration $C_0 = 1.6$ GeV, while in aligned valence configurations (see below), the extra particles contribute typically 0.1–0.2 GeV.

From (3.1) we get the following expressions for the equilibrium deformation ε_0 and corresponding deformation energy $E_{\mathrm{def}}(\varepsilon_0)$:

$$\varepsilon_0 = -(\sum_i C_i)/C_0, \tag{3.3}$$

$$E_{\mathrm{def}}(\varepsilon_0) = -\tfrac{1}{2} C_0 \varepsilon_0^2 = -(\sum_i C_i)^2 / 2C_0 . \tag{3.4}$$

These expressions are seen to reproduce the sign and order of magnitude of both quantities found by the exact calculation.

The simple equations (3.2)–(3.4) enable one to make additional conclusions. Consider for definiteness a nucleus with a few particles in excess of the closed shells. A large total angular momentum is obtained in the aligned configurations, i.e. in configurations where the unpaired particles occupy within each subshell a number of states with the maximally possible values of m. The configurations in ^{212}Po considered above are examples of such aligned configurations. Using the valence particles the nucleus can build up in this way angular momenta up to a certain maximum.

In order to get higher values of the angular momentum it is necessary to involve particle-hole excitations of the core. The largest additional angular momentum due to a particle-hole pair is obtained when both the particle and the hole have large values of m. However, we see from (3.2) that this combination leads to a cancelation in the numerator of (3.4). Therefore such configurations tend to be non-yrast. From an energetical point of view it is more favorable to combine particles with large m and holes with $m \approx 0$.

The configurations composed of particles with large m and holes with $m \approx 0$ are therefore expected to play a significant role in the yrast spectra of nuclei with particles in excess of ^{208}Pb. From (3.3) we expect such configurations to have an oblate equilibrium deformation. Furthermore, since both the deformation and the angular momentum are increasing functions of the number of particle-hole pairs involved, the deformation is expected to increase along the yrast line. In nuclei below the closed shells we expect a similar trend, except that there the deformations are prolate. [This shows that the trends discussed above are genuine effects of the shell structure. Incidentally, the trend towards increasing oblate deformation with increasing angular momentum found in the nuclei above the closed shells resembles that of a classical liquid drop [19]). However, the contribution of the classical forces to the equilibration of the shape in these states is negligible.]

As shown in ref. [9]) the configurations giving rise to yrast traps for weakly deformed oblate shapes have exactly the afore-mentioned structure composed of aligned particles and holes with $m \approx 0$. In the examples considered in sect. 4 we shall see that indeed the yrast states of this kind are often traps. We define here a trap in the same way as in previous works [8]), namely as a configuration which cannot decay by an E1, M1, E2 or M2 single-particle transition. Usually, these yrast states are also, in the terminology of Andersson *et al.* [8]), "optimal", i.e. their configurations are obtained by occupying all single-particle states below a titled Fermi surface in the single-particle states below a titled Fermi surface in the plot of single-particle energies against m. (See e.g. fig. 8).

In the cases considered in sect. 4 the holes are often produced by emptying the $p_{\frac{1}{2}}$ neutron orbital. The large quadratic term in the dependence of the energy of this orbital on ε (see fig. 2) then enhances the trend towards oblate deformations, since it gives a negative contribution to the stiffness parameter $C_0^{(i)}$.

With increasing deformation the discussion in terms of particles and holes relative to the spherical closed shells gradually looses sense, and it becomes more relevant to consider the shell closures in the deformed potential like those with neutron numbers 124, 120 and 114, indicated in fig. 2. The emptying of the $p_{\frac{1}{2}}$ orbital mentioned above may thus alternatively be viewed as a transition to a regime of particle configurations relative to the neutron shell closure at $N = 124$. In a similar way the configurations with particles above the $N = 120$ and $N = 114$ gaps are expected to enter the yrast spectra of somewhat more neutron deficient nuclei than those considered in the present paper. The rather narrow gap at $\varepsilon \approx -0.3$ and $N = 114$ is

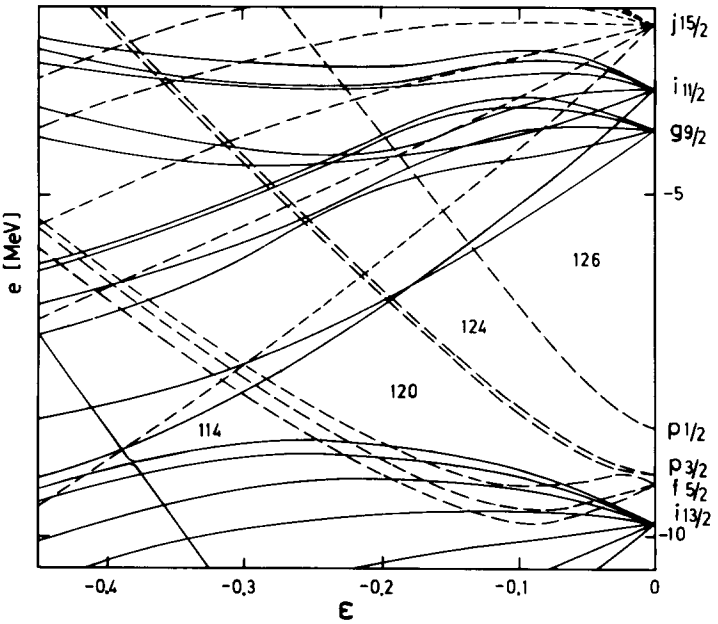

Fig. 2. Neutron single-particle energies in the Woods-Saxon potential.

analogous to the $N = 76$ gap discussed in ref. [9]). As shown there such deformed shell closures may give rise to trap configurations with a structure very similar to that discussed above. The consideration of such strongly deformed states is, however, beyond the scope of the present study.

3.2. ANGULAR MOMENTUM

Following the prescription of Andersson *et al.* [8]) we take the sum of single-particle angular momenta along the symmetry axis of the average potential as a measure of the total angular momentum of the system (cf. subsect. 2.1). This could correspond an interpretation of the states described by the model as band heads of rotational bands.

Evidently this interpretation is not meaningful for small deformations. This does not, however, cause any problems as far as aligned configurations are concerned.

Evidently this interpretation is not meaningful for small deformations. This does not, however, cause any problems as far as aligned configurations are concerned. In these configurations we have by definition $M \equiv \sum_i m_i = J_{\max}$, where $J_{\max}$ is the maximal angular momentum that can be built from the particles in the spherical subshells occupied in the limit $\varepsilon \to 0$. As seen in the examples discussed in the beginning of subsect. 3.1 the deformed configuration converges in this case into a spherical state with the good angular momentum $J = J_{\max} = M$.

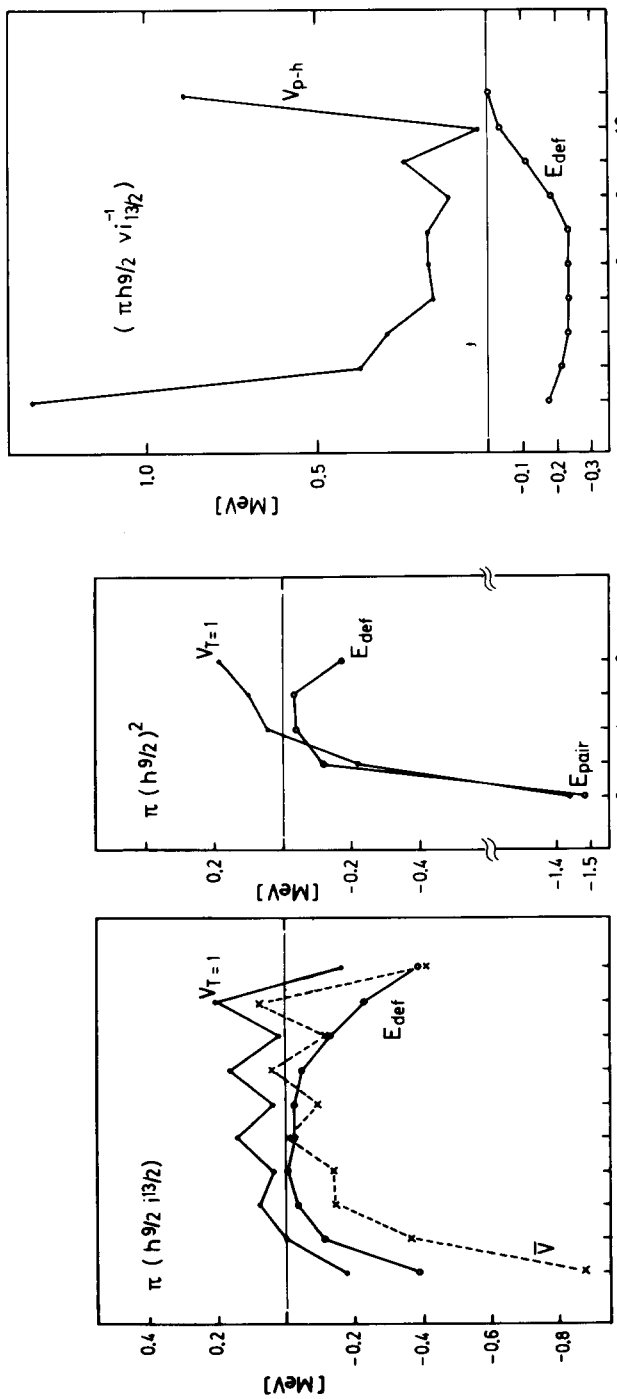

Fig. 3. Empirical matrix elements of the residual interaction according to Schiffer and True [20]) and calculated deformation energies E_{def} for some simple configurations. For details see subsect. 3.3. (a) The multiplet $\pi(h_{9/2}i_{13/2})$. The average matrix element $\bar{V}$ is defined by eq. (3.5). (b) The multiplet $\pi(h_{9/2})^2$. The point labelled "E_{pair}" shows the pairing energy in the spherical ground state of ^{210}Po. (c) The multiplet $\pi(h_{9/2})\nu(i_{13/2})^{-1}$.

The non-aligned configurations ($M < J_{max}$) have in the limit $\varepsilon \to 0$ wave functions corresponding to a distribution of J in the interval $M \leqq J \leqq J_{max}$. It cannot be generally assumed that the component with $J = M$ is the dominating component of this wave function. In some cases it even does not exist. Since, however, we consider in the following mostly states for which it causes no troubles to assume $J = M$, we adopt in the present paper this conventional assumption of the model considered. In the few cases where this leads to manifestly spurious results we make a comment.

3.3. DEFORMATION ENERGIES OF SIMPLE CONFIGURATIONS

In the absence of pairing the excitation energies calculated by our model in the limit $\varepsilon \to 0$ are equal to the unperturbed excitation energies of the spherical shell model. Hence, apart from a constant depending only on the nucleus considered, the deformation energy of a given configuration corresponds to the shell-model interaction energy. It is therefore interesting to make a comparison of these quantities.

In the present section we consider some simple two-particle and particle-hole configurations. Thus in fig. 3 we show the empirical interaction matrix elements in the shell-model configurations $\pi(h_{\frac{9}{2}})^2$, $\pi(h_{\frac{9}{2}} i_{\frac{13}{2}})$ and $\pi(h_{\frac{9}{2}})\nu(i_{\frac{13}{2}})^{-1}$ as extracted [20]) from the spectra of ^{210}Po and ^{208}Bi. For comparison the deformation energy at equilibrium of the corresponding independent particle configurations are also shown. (For $J < J_{max}$ the configuration with lowest energy built from states in the relevant subshells is taken.)

Obvious differences between the behaviour of the two quantities are seen in fig. 3. We notice in particular:

(i) The $T = 1$ interaction is generally weak, except in the pairing force channel $j_1 = j_2$, $J = 0$. Furthermore it has a repulsive component. The $T = 0$ interaction is much stronger and attractive. On the other hand, the deformation energy is practically charge independent. In particular it always has a minimum for $J = J_{max}$, even in the case $T = 1$, $j_1 = j_2$, in which case the shell-model interaction is maximally repulsive for $J = J_{max}$.

(ii) The particle-hole interaction in the multiplet $\pi(h_{\frac{9}{2}})\nu(i_{\frac{13}{2}})^{-1}$ is repulsive and strongly peaked at $J = J_{min}$ and $J = J_{max}$. The deformation energy has a weak variation and is (by definition) always negative.

(iii) The shell-model interaction energy exhibits when considered as a function of J a staggering, which has no counterpart in the deformation energy.

It is instructive, however, to consider the average of the $T = 0$ and $T = 1$ particle-particle interactions,

$$\bar{V} = \tfrac{1}{4}V_{T=0} + \tfrac{3}{4}V_{T=1} = \tfrac{1}{2}(V_{pp} + V_{pn}), \tag{3.5}$$

corresponding to the isoscalar part of the particle-hole interaction. The behaviour of $\bar{V}_J$ in the configuration $h_{\frac{9}{2}} i_{\frac{13}{2}}$ is shown in fig. 3a. Averaging out the staggering, the behaviour of $\bar{V}_J$ is seen to be amazingly close to that of $E_{def}(\varepsilon_0)$. In configurations other than $h_{\frac{9}{2}} i_{\frac{13}{2}}$ the situation is similar.

Making a somewhat ambitious extrapolation from these simple configurations one might expect the deformation energy to account for the major part of the shell-model interaction energy in configuration. which:

(i) Consist of aligned particles (holes) in a possible combination with holes (particles) with $m \approx 0$, so that the attraction between aligned particles is maximally exploited and the strongly repulsive channels of an aligned or anti-aligned particle and hole avoided. This is the typical structure of trap configurations.

(ii) Involve approximately equally many particles or holes of both kinds so that the isospin dependence of the shell-model residual interaction is averaged out. This situation is generally approached at higher angular momenta, since in this limit the particles of both kinds tend to contribute equally to the total spin.

In the examples studied in sect. 4 we shall see indeed a confirmation of these expectations.

It could be noticed that most of the left-out components of the two-body force are repulsive and therefore do not contribute to the stabilization of isomeric configurations.

3.4. PAIRING

Due to the blocking of unpaired levels in the BCS calculation the pairing gaps are rapidly decreasing functions of the angular momentum. For the nuclei considered in the present paper pairing is usually completely absent in configurations with seniority $\gtrsim 2$. Hence the essential role of pairing in our calculations consist in lowering the energy of configurations with seniority $\lesssim 2$ (typically the ground states) relative to the rest of the spectrum.

When present the pairing energy should be added to the deformation energies for a relevant comparison with the interaction energies in the spherical shell-model (see e.g. fig. 3b).

4. Examples

4.1. THE NUCLEI ^{209,210}Po AND ^{210,211}At

In figs. 4 and 5 we show a comparison between calculated and empirical yrast levels of the nuclei ^{209,210}Po and ^{210,211}At. The configurations are described in tables 1 and 2 in a notation indicating the number of states in each spherical subshell occupied in the limit $\varepsilon \to 0$. Paired particles or holes are indicated as occupying states in the first available subshell.

As seen from these configurations the yrast spectra of ^{209,210}Po and ^{210,211}At have a closely interrelated structure. It is therefore reasonable to encompass them in a common discussion.

In most cases the calculated and measured yrast energies agree within 100–200 keV. The considerably larger deviation found in a case like the $J = \frac{29}{2}$ state in ^{209}Po

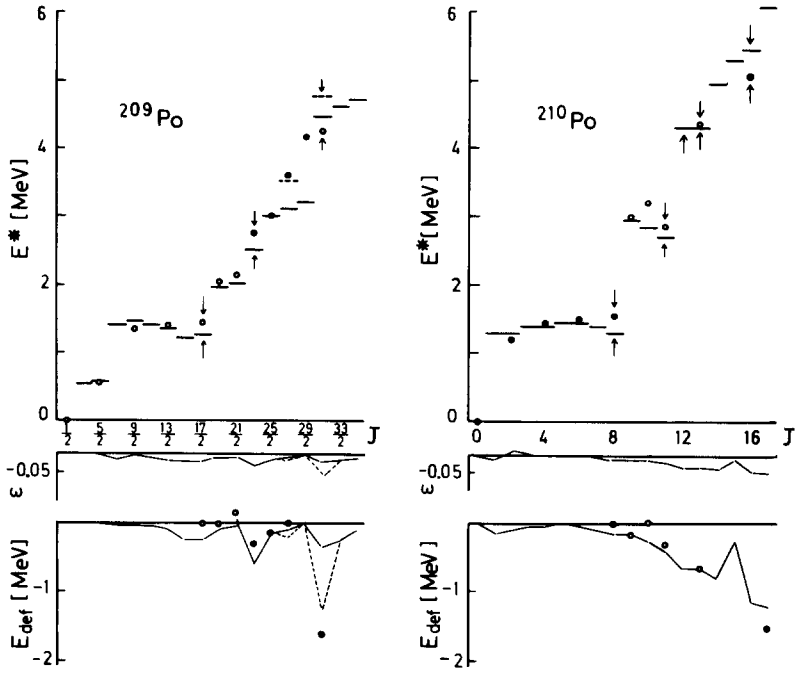

Fig. 4. Yrast levels in ^{209,210}Po. In the upper part of the figure, calculated excitation energies are indicated by horizontal bars and empirical excitation energies by open or filled circles for respectively odd and even parity. An arrow indicates a calculated trap or observed isomer. In cases where the probable configuration of the observed yrast state deviate from the calculated one the calculated excitation energy of the former configuration is shown by a dashed line. The deformations and deformation energies are displayed in the lower part of the figure. The empirical quantity shown together with the deformation energy is defined in subsect. 4.1. Empirical data from refs. [21,22]).

TABLE 1

Calculated yrast configurations [a,b]) in ^{209,210}Po

^{209}Po		^{210}Po	
$\frac{1}{2}^-$	$\pi(h_{9/2})^2\nu p_{1/2}^{-1}$	0^+–8^+	$\pi(h_{9/2})^2$
$\frac{3}{2}^-$	$\pi(h_{9/2})^2\nu p_{3/2}^{-1}$	9^-–11^-	$\pi(h_{9/2}i_{13/2})$
$\frac{5}{2}^-$	$\pi(h_{9/2})^2\nu f_{5/2}^{-1}$	12^-, 13^-	$\pi(h_{9/2})^2\nu(p_{1/2}^{-1}g_{9/2})$
$\frac{7}{2}^-$–$\frac{17}{2}^-$	$\pi(h_{9/2})^2\nu p_{1/2}^{-1}$	14^-	$\pi(h_{9/2})^2\nu(p_{1/2}^{-1}i_{11/2})$
$\frac{19}{2}^-$, $\frac{21}{2}^-$	$\pi(h_{9/2})^2\nu f_{5/2}^{-1}$	15^-	$\pi(h_{9/2})^2\nu(f_{5/2}^{-1}g_{9/2})$
$\frac{23}{2}^+$	$\pi(h_{9/2}i_{13/2})\nu p_{1/2}^{-1}$	16^+	$\pi(h_{9/2}i_{13/2})\nu(p_{1/2}^{-1}g_{9/2})$
$\frac{25}{2}^+$–$\frac{29}{2}^+$	$\pi(h_{9/2})^2\nu i_{13/2}^{-1}$	17^+	$\pi(h_{9/2}i_{13/2})\nu(p_{1/2}^{-1}i_{11/2})$
$(\frac{27}{2}^+)$	$\pi(h_{9/2}i_{13/2})\nu f_{5/2}^{-1}$		
$\frac{31}{2}^-$–$\frac{35}{2}^-$	$\pi(h_{9/2}i_{13/2})\nu i_{13/2}^{-1}$		
$(\frac{31}{2}^-)$	$\pi(h_{9/2}i_{13/2})\nu\{(p_{1/2})^{-2}g_{9/2}\}$		

[a]) The notation used to describe the configurations is explained in subsect. 4.1.

[b]) A spin and parity given in parenthesis correspond to a dashed line in fig. 3.

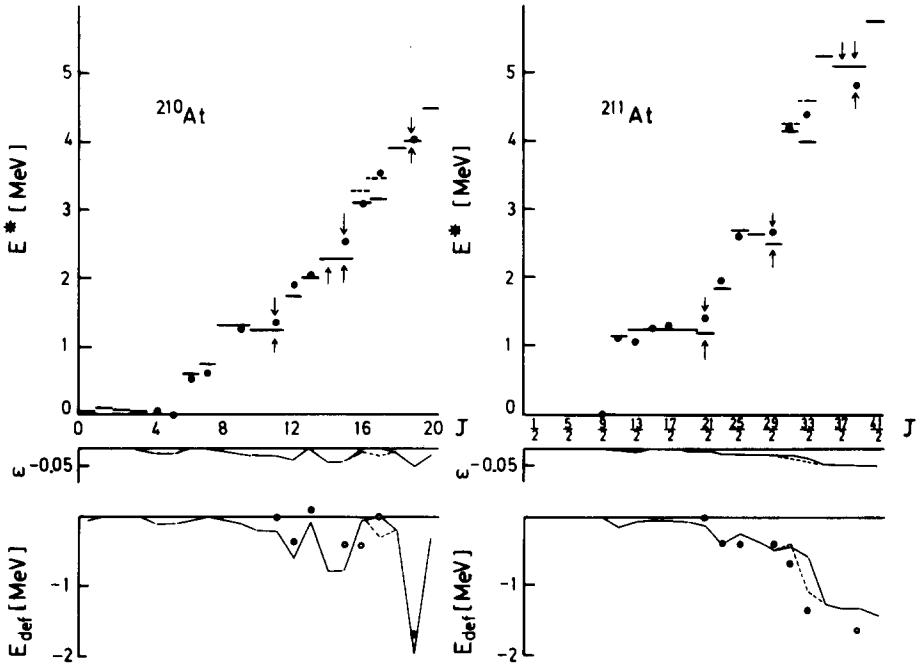

Fig. 5. Same as fig. 4 for ^{210,211}At. Empirical data from refs. [23,24]).

TABLE 2

Calculated yrast configurations [a]) in ^{210,211}At

	^{210}At		^{211}At
$4^+, 5^+$	$\pi(h_{9/2})^3\nu p_{1/2}^{-1}$	$\frac{1}{2}^- - \frac{21}{2}^-$	$\pi(h_{9/2})^3$
$6^+, 7^+$	$\pi(h_{9/2})^3\nu f_{5/2}^{-1}$	$\frac{23}{2}^-$	$\pi\{(h_{9/2})^2 f_{7/2}\}$
$8^+ - 11^+$	$\pi(h_{9/2})^3\nu p_{1/2}^{-1}$	$\frac{25}{2}^+ - \frac{29}{2}^+$	$\pi\{(h_{9/2})^2 i_{13/2}\}$
12^+	$\pi\{(h_{9/2})^2 f_{7/2}\}\nu p_{1/2}^{-1}$	$\frac{31}{2}^-, \frac{33}{2}^-$	$\pi\{(i_{13/2})^2 h_{9/2}\}$
13^+	$\pi\{h_{9/2})^3\nu f_{5/2}^{-1}$	$(\frac{31}{2}^+)$	$\pi(h_{9/2})^3\nu(p_{1/2}^{-1}g_{9/2})$
$14^-, 15^-$	$\pi\{(h_{9/2})^2 i_{13/2}\}\nu p_{1/2}^{-1}$	$(\frac{33}{2}^+)$	$\pi\{(h_{9/2})^2 f_{7/2}\}\nu(p_{1/2}^{-1}g_{9/2})$
$16^-, 17^-$	$\pi(h_{9/2})^3\nu i_{13/2}^{-1}$	$\frac{35}{2}^- - \frac{39}{2}^-$	$\pi\{(h_{9/2})^2 i_{13/2}\}\nu(p_{1/2}^{-1}g_{9/2})$
$(16^-, 17^-)$	$\pi\{(h_{9/2})^2 i_{13/2}\}\nu f_{5/2}^{-1}$	$\frac{41}{2}^-$	$\pi\{(h_{9/2})^2 i_{13/2}\}\nu(p_{1/2}^{-1}i_{11/2})$
18^-	$\pi\{(h_{9/2})^2 f_{7/2}\}\nu i_{13/2}^{-1}$		
19^+	$\pi\{(h_{9/2})^2 i_{13/2}\}(p_{1/2})^{-2}g_{9/2}\}$		
20^+	$\pi\{(h_{9/2})^2 i_{13/2}\}\nu i_{13/2}^{-1}$		

[a]) See comments [a, b]) to table 1.

is easily understood from the discussion of the proton-neutron particle-hole interaction in subsect. 3.3. A similar situation appears for the $J = \frac{33}{2}$ state in this nucleus and the $J = 17$ and $J = 20$ states in ^{210}At.

The $J = 1$, 3, 5 and 7 states in ^{210}Po and the $J = \frac{19}{2}$ state ^{211}At are manifestly spurious products of the model.

Several isomeric states are observed in these nuclei. All of them are reproduced as traps in our calculation. The calculated configurations of the $J = 12$ and $J = 13$ states in ^{210}Po correspond to respectively an anti-parallel or parallel coupling of the $p_{\frac{1}{2}}$ hole to the aligned particle configuration $(\pi(h_{\frac{9}{2}})^2\nu(g_{\frac{9}{2}}))_{25/2^+}$. The exact degeneracy of these configurations, which makes both of them traps according to our definition, is clearly a spurious effect of the model. From the trend of the empirical interaction matrix elements [20]) involving the neutron $p_{\frac{1}{2}}$ hole one would expect the actual energy of the $J = 12$ state to be somewhat higher than the $J = 13$ state. Similar remarks apply to the $J = 14$ and $J = 15$ states in ^{210}At.

The energy of isomeric states involving only valence protons or valence protons in combination with a single $p_{\frac{1}{2}}$ hole is generally underestimated by a few hundred keV. Clearly, this is a trend to be expected from the discussion in subsect. 3.2, since in these configurations most or all of the interacting pairs have $T = 1$, and the interaction in this channel is weak and partly repulsive.

In the lower parts of figs. 4 and 5 the calculated deformation energies of the yrast states are shown. The general trend seen in these figures is easily understood from the discussion in subsect. 3.1.

For the yrast states which have a well-established interpretation in the spherical shell model we show in figs. 4 and 5 for comparison with the calculated deformation energies the empirical interaction energy. Since only the relative values are relevant for such a comparison we have rather arbitrarily normalized the interaction energy of the first aligned configuration (e.g. the 8^+ state in ^{210}Po) to zero. Furthermore, we have subtracted for the configurations involving two holes in the neutron $p_{\frac{1}{2}}$ shell the empirical pairing energy of ^{206}Pb, $-B[^{206}\text{Pb}]+2B[^{207}\text{Pb}]-B[^{208}\text{Pb}] = -0.64$ MeV, where $B[\ ]$ denotes the binding energy.

It is obvious from this comparison that the deformation energy accounts for the main trend in the variation of the empirical interaction energy along the yrast line. In particular, the model is seen to account quite well for the order of magnitude ($\approx$ 1 MeV) of the amount of interaction energy gained by adding a neutron particle-hole pair to a given valence configuration (e.g. the relative energy of the $J = \frac{29}{2}$ and $J = \frac{39}{2}$ states in ^{211}At). However, the empirical value of this quantity tends to be generally about 0.5 MeV larger than calculated. We return in subsect. 4.3 to a discussion of this deviation.

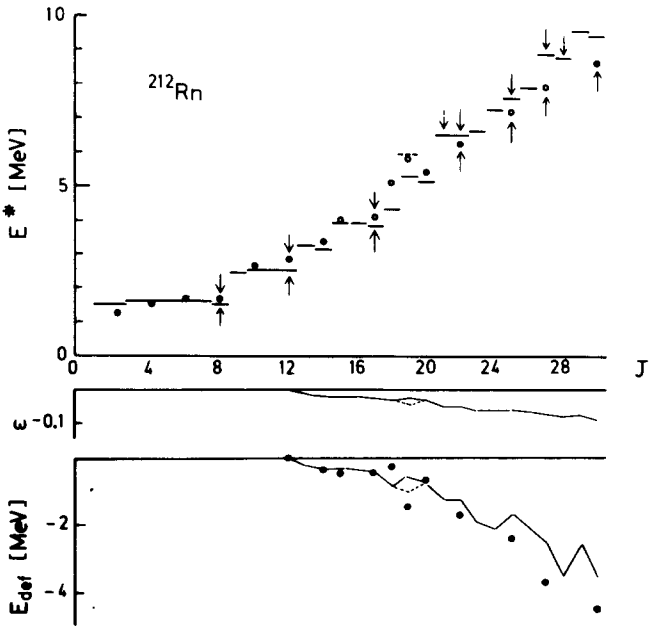

Fig. 6. Same as fig. 4 for ^{212}Rn. Empirical data from ref. [4]).

TABLE 3

Calculated yrast configurations [a]) in ^{212}Rn

^{212}Rn	
0^+–12^+	$\pi(h_{9/2})^4$
$13^+, 14^+$	$\pi\{(h_{9/2})^3 f_{7/2}\}$
15^-–17^-	$\pi\{(h_{9/2})^3 i_{13/2}\}$
18^-	$\pi\{(h_{9/2})^2 f_{7/2} i_{13/2}\}$
$19^+, 20^+$	$\pi\{(h_{9/2})^2 (i_{13/2})^2\}$
(19^-)	$\pi\{(h_{9/2})^3 f_{7/2}\}\nu(p_{1/2}^{-1} g_{9/2})$
$21^+, 22^+$	$\pi\{(h_{9/2})^3 i_{13/2}\}\nu(p_{1/2}^{-1} g_{9/2})$
23^+	$\pi\{(h_{9/2})^2 f_{7/2} i_{13/2}\}\nu(p_{1/2}^{-1} g_{9/2})$
24^+	$\pi\{(h_{9/2})^2 f_{7/2} i_{13/2}\}\nu(p_{1/2}^{-1} i_{11/2})$
25^-	$\pi\{(h_{9/2})^2 (i_{13/2})^2\}\nu(p_{1/2}^{-1} g_{9/2})$
26^-	$\pi\{(h_{9/2})^2 f_{7/2} i_{13/2}\}\nu(p_{1/2}^{-1} j_{15/2})$
27^-	$\pi\{(h_{9/2})^2 (i_{13/2})^2\}\nu(p_{1/2}^{-1} j_{15/2})$
27^-	$\pi\{(h_{9/2})^3 i_{13/2}\}\nu\{(p_{1/2})^{-2} g_{9/2} i_{11/2}\}$
28^-	$\pi\{(h_{9/2})^2 f_{7/2} i_{13/2}\}\nu\{(p_{1/2})^{-2} g_{9/2} i_{11/2}\}$
29^+	$\pi\{(h_{9/2})^3 i_{13/2}\}\nu\{(p_{1/2})^{-2} g_{9/2} j_{15/2}\}$
30^+	$\pi\{(h_{9/2})^2 f_{7/2} i_{13/2}\}\nu\{(p_{1/2})^{-2} g_{9/2} j_{15/2}\}$

[a]) See comments [a, b]) to table 1.

4.2. THE NUCLEUS ^{212}Rn

Data and calculated results for the nucleus ^{212}Rn are shown in fig. 6 and table 3.

In the yrast spectrum of this nucleus for $J \leqq 22$ we see all the same features as discussed above for the nuclei ^{209,210}Po and ^{210,211}At.

(i) The calculated and measured yrast energies agree in general within a few hundred keV.

(ii) The observed isomeric states are reproduced as yrast traps. Concerning the $J = 21$ state the situation is the same as for the $J = 12$ state in ^{210}Po.

(iii) The energy of the isomeric states involving only valence protons is generally underestimated.

(iv) The deformation energy accounts for the main trend in the variation along the yrast line of the empirical interaction energy.

(v) The gain of interaction energy due to an additional neutron particle-hole pair is underestimated by about 0.5 MeV. (See the relative energy of the $J = 17$ and $J = 22$ states.)

We shall discuss here in particular the structure of the three observed isomeric states [4]) with their suggested spins and parities of, respectively, 25^-, 27^- and 30^+.

For the 25^- state Horn *et al.* suggest the assignment $\pi((h_{\frac{9}{2}})^3 i_{\frac{13}{2}})\, \nu((p_{\frac{1}{2}})^{-1} j_{15/2})$. This configuration is found in our calculation 0.2 MeV above the yrast level. The experiment seems not, however, to rule out the calculated yrast configuration (table 3). This is a trap configuration provided we consider the M2 transition from the $i_{\frac{13}{2}}$ to the $f_{\frac{7}{2}}$ shell as *l*-forbidden due to the closeness to the spherical limit (see fig. 8).

For the 27^- and 30^+ states Horn *et al.* suggest configurations involving aligned particle-hole pairs like $\nu((i_{\frac{13}{2}})^{-1} g_{\frac{9}{2}})_{11^+}$ or $\nu((f_{\frac{5}{2}})^{-1} j_{15/2})_{10^+}$. Due to the repulsive

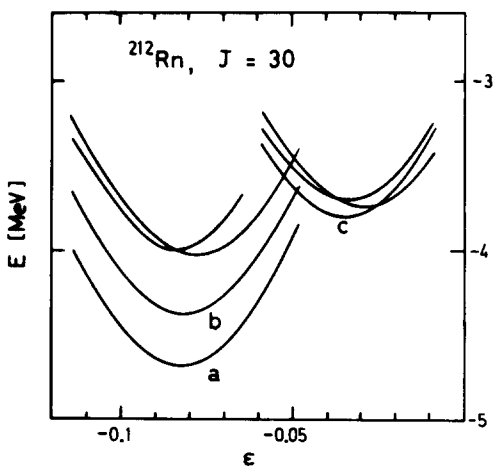

Fig. 7. Plot similar to fig. 1 for some configurations with $J = 30$ in ^{212}Rn. The configurations are: (a) $\pi\{(h_{9/2})^2 f_{7/2} i_{13/2}\} \nu\{(p_{1/2})^{-2} g_{9/2} j_{15/2}\}$, (b) $\pi\{(h_{9/2})^2 (i_{13/2})^2\} \nu\{(p_{1/2})^{-2} g_{9/2} i_{11/2}\}$, (c) $\pi\{(h_{9/2})^2 (i_{13/2})^2\}$ $\nu\{(i_{13/2})^{-1} g_{9/2}\}$.

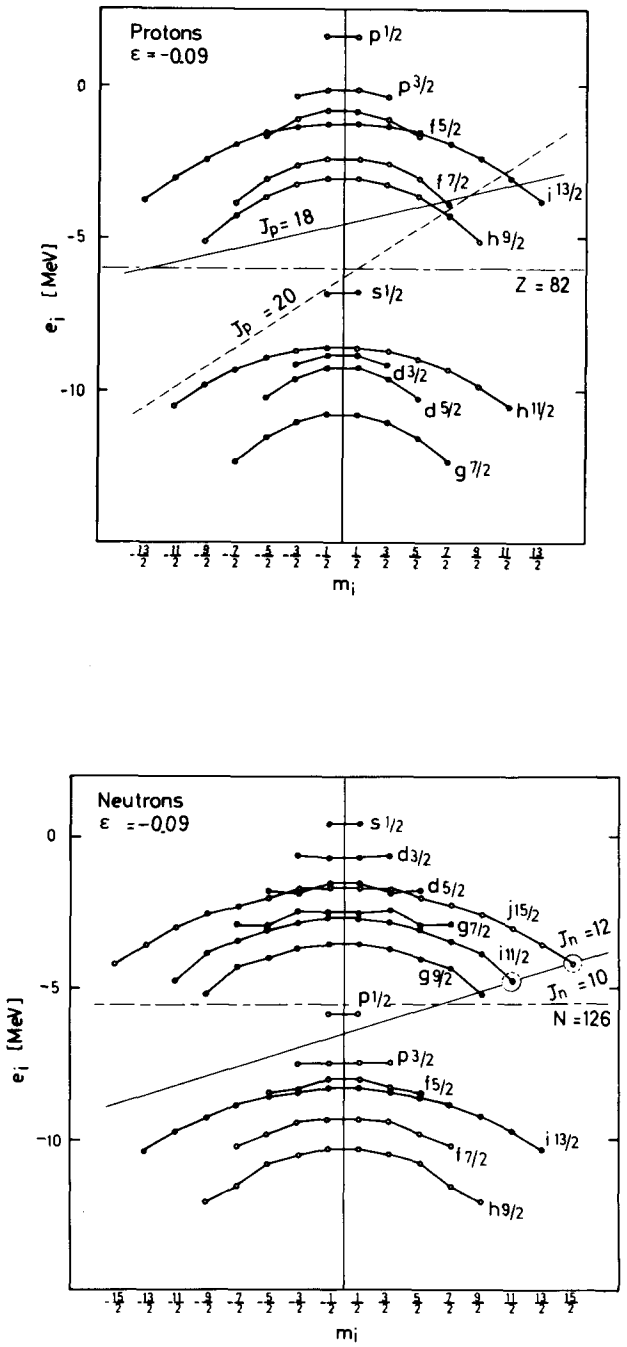

Fig. 8. The Fermi surfaces of the configurations (a) (solid) and (b) (dashed) of fig. 7 displayed in a plot of single-particle energies against m for $\varepsilon = -0.09$. The single-particle energies are those used in the calculations, cf. subsect. 2.2.

interaction between aligned particles and holes (cf. subsect. 3.3) the strong attraction in these configurations assumed by Horn *et al.* appears, however, somewhat unlikely. More probably these states involve 2p-2h excitations of the core.

It is seen, in fact, from table 3 that such configurations enter the yrast line just around $J = 27$. Thus the two configurations with this angular momentum listed in the table are practically degenerate. One of these is a 1p-1h configuration. The second is a 2p-2h configuration. While the former is not a trap the latter is. We consider therefore the 2p-2h configuration in table 3 as a likely candidate for the structure of the 27^- isomer.

As seen from fig. 7 the 2p-2h configurations with $J = 30$ have about 1 MeV lower equilibrium energies than the 1p-1h configurations with this spin. Fig. 8 displays the structure of the configurations labelled (a) and (b) in fig. 7.

The configuration (a) can decay by M2 to the calculated yrast trap at $J = 28$. Since $B(\mathrm{M2}; j_{15/2} \rightarrow i_{13/2})$ is known from ^{209}Pb we can estimate the half-life of this transition to be about 15 ns. Assuming that the actual energy distance between the $J = 28$ and $J = 30$ state is 35 % lower than calculated, the measured 152 ns E3 transition to the 27^- isomer would thus be able to compete with the M2 transition to the 28^- state.

The configuration (b) is a trap using the same criterion as applied above for the 25^- state, and it could thus be an alternative candidate for the structure of the observed 30^+ state.

Adopting these interpretations we see that the rules (i)–(v) formulated above remain valid considering configurations involving 2p-2h neutron excitations of the core. In particular the major part of the interaction energy in these configurations, -4 MeV, is seen to be accounted for as deformation energy. We see also that the tendency of our model to underestimate the gain of interaction energy due to an additional particle-hole pair by about 0.5 MeV, which was observed already in connection with the 1p-1h configurations, remains in the transition from the 1p-1h to the 2p-2h configurations. (Note that this supports the assignment of a 2p-2h configuration to the $J = 27$ yrast state.)

In the 2p-2h configurations we have $\varepsilon_0 \approx -0.1$. We are thus in these configurations approaching a region of deformations where rotational bands built on the isomeric states could be expected to exist.

4.3. SURVEY OF ISOMERS IN Po, At AND Rn

Table 4 gives a survey of calculated and measured excitation energies of observed isomeric states in the nuclei considered above. We have included in the table also the classical example of isomeric states in this mass region, the 45 s isomer in ^{212}Po. The $J^\pi = 16^+$ interpretation [3]) of the latter is adopted here. As mentioned above other interpretations involving $J^\pi = 18^+$ have been suggested in the literature [2]). (See also the discussion of fig. 1 in subsect. 3.1.) While the $J^\pi = 16^+$ configuration

TABLE 4

Observed isomers in isotopes of Po, At and Rn

	J^π	Configuration [a]	E^*_{exp} [b]	E^*_{cal} [c]	E_{int} [d]	E_{def} [e]
^{209}Po	$\frac{17}{2}^-$	$\pi(h_{9/2})^2 \nu p^{-1}_{1/2}$	1.47	1.23	0.0	−0.26
	$\frac{23}{2}^+$	$\pi(h_{9/2} i_{13/2}) \nu p^{-1}_{1/2}$	2.77	2.52	−0.30	−0.60
	$\frac{31}{2}^-$	$\pi(h_{9/2} i_{13/2}) \nu\{(p_{1/2})^{-2} g_{9/2}\}$	4.27	4.76	−1.61	−1.30
^{210}Po	8^+	$\pi(h_{9/2})^2$	1.56	1.31	0.0	−0.17
	11^-	$\pi(h_{9/2} i_{13/2})$	2.85	2.71	−0.31	−0.39
	13^-	$\pi(h_{9/2})^2 \nu(p^{-1}_{1/2} g_{9/2})$	4.37	4.30	−0.63	−0.64
	16^+	$\pi(h_{9/2} i_{13/2}) \nu(p^{-1}_{1/2} g_{9/2})$	5.06	5.46	−1.54	−1.13
^{212}Po	16^+	$\pi(h_{9/2})^2 \nu(g_{9/2})^2$	2.93	2.44		−0.52
^{210}At	11^+	$\pi(h_{9/2})^3 \nu p^{-1}_{1/2}$	1.36	1.23	0.0	−0.20
	15^-	$\pi\{(h_{9/2})^2 i_{13/2}\} \nu p^{-1}_{1/2}$	2.55	2.30	−0.41	−0.78
	19^+	$\pi\{(h_{9/2})^2 i_{13/2}\} \nu\{(p_{1/2})^{-2} g_{9/2}\}$	4.03	4.01	−1.74	−1.99
^{211}At	$\frac{21}{2}^-$	$\pi(h_{9/2})^3$	1.42	1.21	0.0	−0.13
	$\frac{29}{2}^+$	$\pi\{(h_{9/2})^2 i_{13/2}\}$	2.64	2.48	−0.38	−0.50
	$\frac{39}{2}^-$	$\pi\{(h_{9/2})^2 i_{13/2}\} \nu(p^{-1}_{1/2} g_{9/2})$	4.82	5.11	−1.64	−1.37
^{212}Rn	8^+	$\pi(h_{9/2})^4$	1.67	1.53		−0.06
	12^+	$\pi(h_{9/2})^4$	2.86	2.50	0.0	−0.05
	17^-	$\pi\{(h_{9/2})^3 i_{13/2}\}$	4.04	3.78	−0.42	−0.44
	22^+	$\pi\{(h_{9/2})^3 i_{13/2}\} \nu(p^{-1}_{1/2} g_{9/2})$	6.18	6.45	−1.72	−1.26
	25^-	$\pi\{(h_{9/2})^2 (i_{13/2})^2\} \nu(p^{-1}_{1/2} g_{9/2})$	7.11	7.51	−2.39	−1.68
	27^-	$\pi\{(h_{9/2})^3 i_{13/2}\} \nu\{(p_{1/2})^{-2} g_{1/2} i_{11/2}\}$	7.85	8.82	−3.63	−2.52
	30^+	$\pi\{(h_{9/2})^2 f_{7/2} i_{13/2}\} \nu\{(p_{1/2})^{-2} g_{9/2} j_{15/2}\}$	8.55	9.34	−4.47	−3.54

[a]) See comment [a]) to table 1.
[b]) Observed excitation energy.
[c]) Calculated excitation energy.
[d]) Empirical quantity defined in subsect. 4.1.
[e]) Calculated deformation energy.

with the structure indicated in table 4 is a trap in our calculation the configuration with $J^\pi = 18^+$ is not.

Some general trends already discussed in subsects. 4.1 and 4.2 are very clearly displayed in table 4. Thus we can distinguish isomers having a valence configuration of the type $\pi(h_{\frac{9}{2}})^n \nu(p_{\frac{1}{2}})^{-m}$ or $\pi((h_{\frac{9}{2}})^{n-1} i_{\frac{13}{2}}) \nu(p_{\frac{1}{2}})^{-m}$ and core-excited isomers obtained from these by adding one or two particle-hole pairs of the type $\nu((p_{\frac{1}{2}})^{-1} g_{\frac{9}{2}})$ or $\nu((p_{\frac{1}{2}})^{-1} j_{15/2})$.

The excitation energies of the isomeric states are generally well reproduced by our model. This means that the relative shell-model interactions energies in these configurations are accounted for mainly by the differences in deformation energy. (Only the 8^+ isomer in ^{212}Rn has some pairing.) In this way the expectations formulated at the end of subsect. 3.3 are seen to be confirmed by the detailed calculations.

TABLE 5

Predicted yrast traps with $J < 40$ in isotopes of Po, At and Rn

	J^π	E^*_{cal} [a])	Configuration [b])
^{212}Po	19^-	3.74	$\pi(h_{9/2}i_{13/2})\nu(g_{9/2})^2$
	29^-	7.33	$\pi(h_{9/2}i_{13/2})\nu(p^{-1}_{1/2}g_{9/2}i_{11/2}j_{15/2})$
^{211}At	$\frac{49}{2}^+$	7.45	$\pi\{(h_{9/2})^2i_{13/2}\}\nu\{(p_{1/2})^{-2}g_{9/2}i_{11/2}\}$
	$\frac{65}{2}^+$	11.04	$\pi\{(h_{9/2})^2i_{13/2}\}\nu\{(p_{1/2})^{-2}f^{-1}_{5/2}g_{9/2}i_{11/2}j_{15/2}\}$
^{213}At	$\frac{45}{2}^+$	3.36	$\pi\{(h_{9/2})^2i_{13/2}\}\nu(g_{9/2})^2$
	$\frac{65}{2}^+$	6.80	$\pi\{(h_{9/2})^2i_{13/2}\}\nu(p^{-1}_{1/2}g_{9/2}i_{11/2}j_{15/2})$
	$\frac{71}{2}^-$	8.60	$\pi\{(h_{9/2})^2i_{13/2}\}\nu\{(p_{1/2})^{-2}(g_{9/2})^2i_{11/2}j_{15/2}\}$
^{210}Rn	37^-	12.18	$\pi\{(h_{9/2})^2f_{7/2}i_{13/2}\}\nu\{(p_{1/2})^{-2}(f_{5/2})^{-3}g_{9/2}i_{11/2}j_{15/2}\}$
^{212}Rn	35^-	12.40	$\pi\{(h_{9/2})^2f_{7/2}i_{13/2}\}\nu\{(p_{1/2})^{-2}f^{-1}_{5/2}g_{9/2}i_{11/2}j_{15/2}\}$
^{214}Rn	19^-	3.68	$\pi\{(h_{9/2})^3i_{13/2}\}\nu(g_{9/2})^2$
	20^+	3.71	$\pi(h_{9/2})^4\nu(g_{9/2})^2$
	25^-	4.77	$\pi\{(h_{9/2})^3i_{13/2}\}\nu(g_{9/2})^2$
	35^-	8.17	$\pi\{(h_{9/2})^3i_{13/2}\}\nu(p^{-1}_{1/2}g_{9/2}i_{11/2}j_{15/2})$
	36^-	8.21	$\pi\{(h_{9/2})^2f_{7/2}i_{13/2}\}\nu(p^{-1}_{1/2}g_{9/2}i_{11/2}j_{15/2})$
	39^+	9.87	$\pi\{(h_{9/2})^2f_{7/2}i_{13/2}\}\nu\{(p_{1/2})^{-2}(g_{9/2})^2i_{11/2}j_{15/2}\}$
^{216}Rn	21^-	3.22	$\pi(h_{9/2})^4\nu\{(g_{9/2})^2i_{11/2}j_{15/2}\}$
	24^+	4.16	$\pi(h_{9/2})^4\nu\{(g_{9/2})^3i_{11/2}\}$
	27^-	4.73	$\pi(h_{9/2})^4\nu\{(g_{9/2})^2i_{11/2}j_{15/2}\}$
	30^+	5.50	$\pi\{(h_{9/2})^3f_{7/2}\}\nu\{(g_{9/2})^3i_{11/2}\}$
	31^+	5.30	$\pi\{(h_{9/2})^3i_{13/2}\}\nu\{(g_{9/2})^2i_{11/2}j_{15/2}\}$
	33^-	6.07	$\pi\{(h_{9/2})^3i_{13/2}\}\nu\{(g_{9/2})^3i_{11/2}\}$
	35^-	6.13	$\pi\{(h_{9/2})^3f_{7/2}\}\nu\{(g_{9/2})^2i_{11/2}j_{15/2}\}$
	38^+	6.66	$\pi\{(h_{9/2})^3i_{13/2}\}\nu\{(g_{9/2})^2i_{11/2}j_{15/2}\}$
	39^+	6.73	$\pi\{(h_{9/2})^2f_{7/2}i_{13/2}\}\nu\{(g_{9/2})^2i_{11/2}j_{15/2}\}$

[a]) Calculated excitation energy.
[b]) See comment [a]) to table 1.

The agreement between theory and experiment is particularly good when we consider the relative energies within each group of isomers mentioned above, valence configuration, 1p-1h states, and 2p-2h states. The typical deformation energy in each of these groups is respectively -0.5, -1.5 and -4 MeV. As mentioned already the empirical difference in interaction energy between the groups tends to be about 0.5 MeV larger than given by these numbers. Several effects may contribute to this deviation.

(i) It is well known [14]) that the absolute value of the shell correction energy of ^{208}Pb as calculated by the Strutinsky method using empirical single-particle levels is about 50 % larger than measured. The origin of this discrepancy is not well understood. (See the detailed discussion in ref. [14]).) It seems likely, however, that the too strong binding of ^{208}Pb implies that we have also a too large stiffness of the double-closed-shell core. As it follows immediately from the discussion in subsect. 3.1, this

would involve the observed trend of a too small gain of interaction energy per added particle-hole pair. If this explanation is correct we also expect that our calculated deformations are somewhat too small.

(ii) From the discussion in subsect. 3.3 we expect the deformation energy to account for the interaction energy due to an average residual interaction like $\bar{V}$ defined by (3.5). In the valence configurations we have, however, a surplus of $T = 1$ bonds between the particles. This was mentioned already in subsect. 4.1 as a likely explanation of the underestimate of the energies of these configurations. In the core-excited configurations there is an opposite tendency. Hence the actual gain of interaction energy per particle-hole pair should be larger than given by the average interaction.

(iii) The configuration $\nu((p_{\frac{1}{2}})^{-1}g_{\frac{9}{2}})_{5^-}$ is the main component of the collective 5^- state in ^{208}Pb, which is shifted 0.25 MeV below the particle-hole energy.

(iv) In the configuration $\nu((p_{\frac{1}{2}})^{-2}g_{\frac{9}{2}})_{\frac{9}{2}^+}$ the pairing energy vanishes for $\varepsilon \approx -0.05$ due to the rapid rise of the energy of the $p_{\frac{1}{2}}$ state with increasing deformation. (See fig. 2.) A more accurate treatment of pairing might change this picture.

In fig. 5, we have listed some additional isomers predicted as traps in our model. In particular the nucleus ^{216}Rn with four protons and four neutrons outside the closed shells seems to provide very rich possibilities for producing isomeric states with relatively high spin ($I \approx 40$) and low excitation energy ($E^* \approx 7$ MeV).

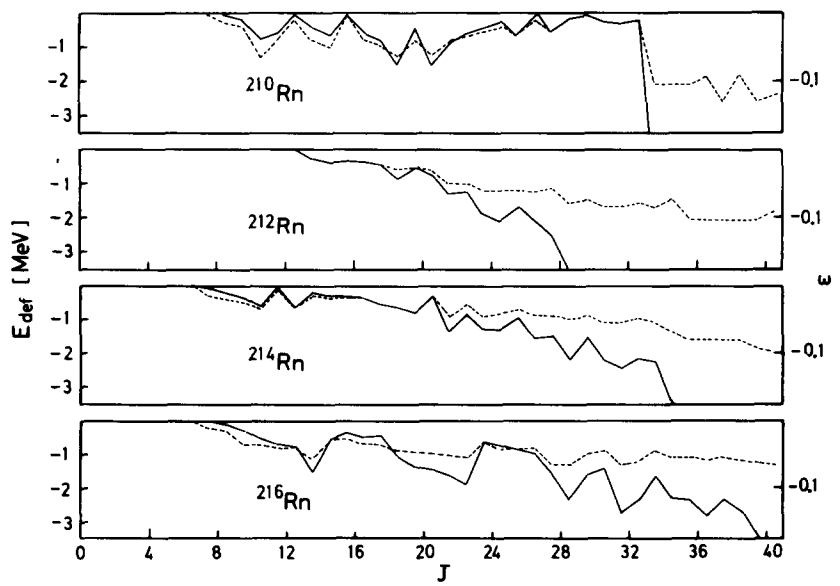

Fig. 9. Equilibrium deformations (dashed line) and deformation energies (solid line) along the yrast line of $^{210-216}$Rn.

4.4. RISE OF OBLATE DEFORMATION – THE EVEN Rn ISOTOPES

As an instructive example of the features discussed in subsect. 3.1 we show in fig. 9 the calculated deformations and deformation energies in the yrast states of the even isotopes $^{210-216}$Rn.

The yrast line of ^{216}Rn is characterized by a gradually increasing oblateness (from $\varepsilon = 0$ for $J = 0$ to $\varepsilon \approx -0.07$ for $J = 40$). Going from ^{216}Rn to the neutron closed shell nucleus ^{212}Rn, the slope gets steeper. This is because a smaller maximal angular momentum can be built up by aligning the valence particles ($J \approx 20$ in ^{212}Rn as compared with $J \approx 40$ in ^{216}Rn), and therefore excitations of the neutron core enter the yrast configurations at a lower angular momentum.

In contrast to $^{212-216}$Rn the nucleus ^{210}Rn with two neutron holes does not display a steady variation of the yrast deformation. This is because neutron configurations with holes in the large-j orbital $i_{\frac{13}{2}}$ intervene into the yrast line involving a tendency towards prolate deformations. Thus, we have in this nucleus competing trends in the proton and neutron parts of the system. However, the maximal angular momentum which can be built from the six valence particles and holes is equal to 33. Therefore, around this value of J particle-hole excitations start to take place. These enhance the "particle character" of the system and consequently we get from this point a development similar to that of the heavier isotopes.

5. Relation of the present approach to a shell-model description

Some of the isomeric states discussed above have been interpreted previously in terms of calculations based on the spherical shell model with residual interactions. In particular, calculations of this kind using empirical matrix elements of the interaction have proved extremely successful in reproducing the excitation energies in these and other cases. [See ref. [10]) and references therin.]

We have seen above that the major part of the interaction energy in the isomeric states can be understood within the independent particle model as a deformation energy associated with a (in most cases relatively small) quadrupole distortion of the single-particle potential. This is not really surprising when we consider the typical structure of the isomeric configurations and the mechanism giving rise, from a shell-model point of view, to the appearance of a deformation of the nuclear shape.

As usual we discuss for definiteness the case of nuclei with a few particles outside the closed shells, i.e. the case characterized by oblate deformations. As shown by several authors (see references in the review by Schiffer and True [20])), the residual interaction between two such particles is characterized by the angle θ between their angular momentum vectors. Thus in particular the $T = 0$ interaction is strongly attractive for values of this angle approaching 0 and π. Examples of this feature are seen in figs. 3a and b. Since the angles $\theta = 0$ and $\theta = \pi$ correspond to maximal overlaps of the density distributions in the interacting orbitals, this behaviour of the matrix elements is the typical signature of a short-range attractive interaction.

Obviously, it leads to a stabilization of high-spin configurations composed of particles with aligned angular momenta.

The density distribution of such an aligned configuration is oblate, and the symmetry axis of the oblate shape is parallel to the direction of the total angular momentum. If holes are added to the aligned configuration, the orientation of their angular momenta giving the most stable configurations is that perpendicular to this direction. Thus, in the most stable configurations involving holes, these cooperate in making the total density distribution oblate.

It is seen that the configurations which are most stabilized by the residual interaction are just those with the typical structure of traps described in subsect. 3.1, and that quite generally these configurations have an oblate density distribution. The polarization of the core induced by the short-range attraction between valence and core nucleons enhances the oblate deformation. The mean field is then also oblate. Since, as it was seen in subsect. 3.1, the same configurations are stabilized by an oblate distortion of the single-particle potential we have in these configurations a good approximation to self-consistency. This implies, however, that a major part of the interaction energy is absorbed in the Hartree-Fock energy and therefore also in the Strutinsky renormalized independent particle energy, which according to the energy theorem [14]) may be considered as an approximation to the Hartree-Fock energy.

As seen in sect. 4, the yrast lines of the isotopes of Po, At and Rn considered are characterized by a growth of the oblate deformation with increasing angular momentum. With increasing deformation the shell-model description of the yrast states must be expected to become increasingly complicated due to configuration mixing. This is particularly the case for configurations involving the single-particle state emerging from the $\nu p_{\frac{1}{2}}$ orbital. Already at small deformations, $\varepsilon \approx -0.05$, this state contains large components of the states $\nu p_{\frac{3}{2}}$ and $\nu f_{\frac{5}{2}}$, and its structure is best described by the asymptotic quantum numbers.

It seems that with the present experimental capacity one is about to reach a region of deformations where such difficulties of the shell-model approach might be expected to become serious. The advantage of the deformed independent particle model in spite of its minor accuracy in the regime of very small distortions from the spherical shape is that it can be used for all deformations, from the smallest ones discussed in the present paper to the largest, being of the same order of magnitude as the prolate deformations encountered in the fission process. In addition it provides a stimulatingly simple physical picture [9]) of the structure of yrast traps in this entire range of deformations.

6. Summary

Considering the independent particle model of yrast states in the regime of axial symmetry with respect to the direction of the angular momentum we have studied.

the yrast spectra of isotopes of Po, At and Rn. With the exception of some well-understood cases of larger deviations the model was found to reproduce the empirical excitation energies in the lower part of the yrast line within an accuracy of the order of a few hundred keV. In particular, the energies of all isomeric states are well reproduced, and all of them correspond to calculated traps.

The deformation energies of isomers involving 2p-2h excitations of the core tend to be underestimated by about 1 MeV out of a total deformation energy $E_{\text{def}} \approx -4$ MeV. Possible reasons of this were discussed in subsect. 4.3.

The recently observed isomers in ^{212}Rn with $J^{\pi} = 25^{-}$, 27^{-} and 30^{+} were interpreted in subsect. 4.2 within our model.

In most of the nuclei studied we find a gradual increase of oblate deformation along the yrast line. This feature may be understood from simple arguments considered in subsect. 3.1.

Special attention has been payed to the relation between our model and the spherical shell model. It has been shown that the deformation energy associated with a quadrupole distortion of the single-particle potential accounts for the major part of the shell-model interaction energy in the isomeric configurations. A qualitative understanding of this result is furnished by the considerations made in subsect. 3.3 and sect. 5.

We acknowledge discussions with staff members and guests at the Niels Bohr Institute and NORDITA, particularly Aage Bohr, Sven Bjørnholm, and B. R. Mottelson. One of us (K.M.) is indebted to the Nishina Memorial Foundation, the Scientific Research Council of the Danish State, and the Commemorative Association of the Japan World Exposition for financial support.

References

1) I. Perlman *et al.*, Phys. Rev. **127** (1962) 917
2) N. K. Glendenning and K. Harada, Nucl. Phys. **72** (1965) 481
3) B. L. Birbrair, Phys. Lett. **34B** (1971) 558
4) D. Horn *et al.*, Phys. Rev. Lett. **39** (1977) 389
5) R. G. Helmer and C. W. Reich, Nucl. Phys. **A114** (1968) 649
6) T. L. Khoo, F. M. Bernthal, R. G. H. Robertson and R. A. Warner, Phys. Rev. Lett. **37** (1976) 823
7) J. Pedersen *et al.*, Phys. Rev. Lett. **39** (1977) 990
8) G. Andersson *et al.*, Nucl. Phys. **A268** (1976) 205
9) T. Døssing, K. Neergård, K. Matsuyanagi and Hs.-Ch. Chang, Phys. Rev. Lett. **39** (1977) 1395
10) J. Blomquist *et al.*, Phys. Rev. Lett. **38** (1977) 534
11) G. Leander, private communication
12) S. Åberg, preprint 1977
13) M. Cerkashi *et al.*, Phys. Lett. **70B** (1977) 9
14) M. Brack *et al.*, Rev. Mod. Phys. **44** (1972) 320
15) V. V. Pashkevich and V. M. Strutinsky, Sov. J. Nucl. Phys. **9** (1969) 35
16) H. C. Pauli, Phys. Reports **7** (1973) 35
17) W. D. Myers and W. J. Swiatecki, Ark. Fys. **36** (1967) 343
18) J. Rainwater, Phys. Rev. **79** (1950) 434
19) S. Cohen, F. Plasil and J. Swiatecki, Ann. of Phys. **82** (1974) 557

20) J. P. Schiffer and W. W. True, Rev. Mod. Phys. **48** (1976) 191
21) I. Bergström, J. Blomqvist, C. J. Herrlander and K. Wikström, Physica Scripta **10** (1974) 287
22) B. Fant, Physica Scripta **4** (1971) 175
23) V. Rahkohnen, I. Bergström, J. Blomquist and O. Knuuttila, Z. Phys. **A284** (1978) 357
24) K. H. Maier, J. R. Leigh, F. Pühlhofer and R. M. Diamond, Phys. Lett. **35B** (1971) 401
25) K. Neergård, H. Toki, M. Ploszajczak and A. Faessler, Nucl. Phys. **A287** (1977) 48
26) A. M. Stefanini, P. Kleinheinz and M. R. Maier, Phys. Lett. **62B** (1976) 405
27) R. Broda *et al.*, Z. Phys. **A285** (1978) 423

Progress of Theoretical Physics, Vol. 61, No. 6, June 1979

Dynamical Interplay of Pairing and Quadrupole Modes in Transitional Nuclei. I

Tōru SUZUKI,† Masahiko FUYUKI* and Kenichi MATSUYANAGI*

Research Institute for Fundamental Physics
Kyoto University, Kyoto 606
**Department of Physics, Kyoto University, Kyoto 606*

(Received October 21, 1978)

Using the single j-shell model with the pairing plus quadrupole force, we show that
1) the transition from vibrational to rotational excitation structure can be reproduced within the collective model space built up from the $J=0$- and $J=2$- coupled nucleon pairs,
2) change of the monopole pair field due to many-quasiparticle excitations does accelerate the transition; this fact indicates the importance of taking explicit account of the coupling between pairing rotation and many-phonon excitations in transitional nuclei.

§ 1. Introduction

In the conventional approach to the anharmonicity effects associated with low-frequency quadrupole phonon modes, one first introduces the quasiparticle representation through Bogoliubov transformation. Absorbing in this way the correlation responsible for the Cooper pairing into the static pair field, one then treats the anharmonicity effects as interactions between quadrupole phonons. The physical picture implicitly assumed in this approach is that the static pair field is stable enough not to be drastically affected by the phonon excitations (which are built up from quasiparticle excitations). Namely, phonon-phonon interactions are treated on the assumption that the change of pair field due to the phonon excitations is negligible.

This assumption cannot be justified, however, in a situation where the number of quasiparticles v composing phonons is no longer a small fraction of Ω, where Ω is the effective pair-degeneracy of the valence shell. This is because the BCS approximation is justified only when $O(v/\Omega) \ll 1$. Hence, in such a situation, one should expect dynamical couplings between pairing and quadrupole modes of excitation.

In fact, recent studies on the anharmonicity effects appear to indicate the necessity of dynamical treatment of their couplings. In the superconducting nuclei, the couplings may be classified into two kinds;

1) coupling between pairing vibrations and quadrupole phonons,
2) coupling between pairing rotations and quadrupole phonons.

Recently, Iwasaki, Marumori, Sakata and Takada[1),2)] have shown that the former

† Present address: Institut für Kernphysik, Kernforschungsanlage Jülich, D-5170 Jülich, West Germany.

effect is indeed very strong already at the two-phonon 0^+ states. On the other hand, taking the latter effect into account is equivalent to restore the symmetry (nucleon-number conservation) broken by the BCS approximation.[3] Although we already know that the broken symmetry is restored in the RPA order,[4] no investigation has been done up to now for the case of treating anharmonicity effects associated with many-phonon excitations.

In this series of papers, we investigate the role of dynamical couplings between pairing and quadrupole modes in characterizing the excitation structure of transitional nuclei. Special effort will be put on restoring the symmetry broken in the BCS approximation. In this first paper, we adopt the single j-shell model with the pairing plus quadrupole (P+QQ) force.[5] Although the model is schematic, it is useful for the present purpose in the following reasons:

1) The model is able to reproduce the transition from vibrational to rotational excitation structures.
2) The coupling effect between quadrupole phonons and pairing rotations may be evaluated exactly, since there is no pairing vibration mode in this case.

In § 2, a model for collective quadrupole excitations is formulated in the nucleon-number conserving representation. In this model, the low-frequency collective dynamics are assumed to be well described in terms of the nucleon-pair operators with $J=0$ and $J=2$.*) The formulation of model is based on a combined use of the "quantized" Bogoliubov transformation proposed in Ref. 6) and the method for describing many-phonon states proposed by Holzwarth, Janssen and Jolos,[7] and Iwasaki, Sakata and Takada.[8]

In § 3, adopting an additional approximation which leads to the $SU(6)$ scheme of Janssen, Jolos and Dönau,[9] we transcribe the model into boson representation. The resulting boson representation bears a resemblance to the sd-boson model of Arima and Iachello.[10] In § 4, we first show that our model is capable of reproducing the basic pattern of the transition from vibrational to rotational excitations. Then, the result of number-conserving treatment is compared with that of BCS approximation. The comparison will exhibit a dramatic effect of blocking (associated with phonon excitations) to the pair field.[11]

In a succeeding paper,[12] we shall present a more systematic analysis of band structure in the transitional region. There, the coupling between phonon excitations and pairing rotations will be explicitly treated in the quasiparticle representation.

§ 2. Formulation of model

2.1. *Basic assumption*

Let us first define the nucleon-pair operators as

*) A similar idea has also been developed by Arima et al.[18)~20)] in their attempt to give a microscopic foundation of the phenomenological sd-boson model.[10]

$$A^{\dagger}_{J\mu}=\frac{1}{\sqrt{2}}\sum_{m_1m_2}\langle jm_1jm_2|J\mu\rangle c^{\dagger}_{jm_1}c^{\dagger}_{jm_2}\,, \tag{2·1a}$$

$$B^{\dagger}_{J\mu}=-\sum_{m_1m_2}\langle jm_1jm_2|J\mu\rangle c^{\dagger}_{jm_1}c_{j-m_2}(-)^{j-m_2}\,. \tag{2·1b}$$

The operators $B^{\dagger}_{J\mu}$ with $J=0, 1$ and 2 have simple physical meanings as

$$\hat{\mathcal{N}}=\sqrt{2\Omega}B^{\dagger}_{00}\,, \quad \text{(nucleon number)} \tag{2·2a}$$

$$\hat{J}_{\mu}=\sqrt{\frac{\Omega(2\Omega-1)(2\Omega+1)}{6}}B^{\dagger}_{1\mu}\,, \quad \text{(angular momentum)} \tag{2·2b}$$

$$\hat{Q}_{\mu}=q\cdot B^{\dagger}_{2\mu}\,, \quad \text{(quadrupole moment)} \tag{2·2c}$$

where $\Omega=j+1/2$ and $q=\langle j\|r^2Y_2\|j\rangle/\sqrt{5}$.

As is well known, nuclear superconductivity implies a condensation of the $J=0$-coupled nucleon pairs, so that the state vector of $\mathcal{N}=$even nucleon system is written in the form $(A^{\dagger}_{J=0})^{\mathcal{N}/2}|0\rangle$. Condensation of the $J=2$-coupled nucleon pairs may occur in association with the action of quadrupole field, as is expected from the commutation relation $[B^{\dagger}_{2\mu}, A^{\dagger}_{00}]=\sqrt{2/\Omega}A^{\dagger}_{2\mu}$. A competition of pairing and quadrupole correlations in nuclei might therefore suggest a condensate of the form $(A^{\dagger}_{J=0}+\beta A^{\dagger}_{J=2})^{\mathcal{N}/2}|0\rangle$, or more generally $\sum C_{n_1n_2}|n_1n_2\rangle$ with

$$|n_1n_2\rangle=\frac{1}{\sqrt{n_1!\,n_2!}}(A^{\dagger}_{J=0})^{n_1}(A^{\dagger}_{J=2})^{n_2}|0\rangle\,. \quad (n_1+n_2=\mathcal{N}/2) \tag{2·3}$$

This is, however, not self-evident, because higher multipoles with $J\geq 4$ might play important roles with increasing quadrupole correlation. Nevertheless, it is tempting to assume that the state vectors of collective model space are explicitly constructed as in (2·3) in terms of only nucleon-pair operators with $J=0$ and $J=2$. This is the basic assumption of the model we are going to consider.

The direct use of state vectors of the form (2·3) is not convenient, since they are highly non-orthogonal: Because of the Pauli principle, the $J=2$-coupled pair operators themselves do not uniquely represent the quadrupole degree of freedom. Thus, we have to construct our model space so that the pairing and quadrupole degrees of freedom are precisely specified. This is readily achieved by adopting the well-known quasi-spin formalism.[13] As we shall see in the following, this formalism leads us to the concept of pairing and intrinsic subspaces in the quasi-spin space.

2.2. *Pairing and intrinsic degrees of freedom in quasi-spin space*

The operators $\hat{S}_+=\sqrt{\Omega}A^{\dagger}_{00}$, $\hat{S}_-=\sqrt{\Omega}A_{00}$ and $\hat{S}_0=\frac{1}{2}(\hat{\mathcal{N}}-\Omega)$ are known to satisfy the quasi-spin algebra. With the use of quasi-spin quantum numbers, S and S_0, we can denote any nucleon state as $|S, S_0; \Gamma\rangle$, where Γ stands for a set of other quantum numbers such as ordinary angular momentum JM. A class of states $|S, S_0=-S; \Gamma\rangle$ has a special physical meaning, since

$$\hat{S}_-|S, S_0=-S; \Gamma\rangle=0\,, \tag{2·4}$$

which implies that there is no $J=0$-coupled nucleon pair in this class of states. Racah's seniority v is equivalent to the nucleon number of the state $|S, S_0=-S; \Gamma\rangle$. Starting with these states we can readily construct all nucleon states as

$$|S, S_0=-S+p; \Gamma\rangle=\sqrt{\frac{(2S-p)!}{(2S)!\,p!}}(\hat{S}_+)^p|S, S_0=-S; \Gamma\rangle\,, \quad (p=0, 1, \cdots, 2S) \tag{2·5}$$

the nucleon number of which is given by $\mathcal{N}=v+2p$. Thus, the quasi-spin quantum numbers, S and S_0, are simply related to the seniority and nucleon numbers by

$$S=\tfrac{1}{2}(\Omega-v) \quad \text{and} \quad S_0=\tfrac{1}{2}(\mathcal{N}-\Omega)\,. \tag{2·6}$$

Following Ref. 14), we call the modes which transfer the seniority quantum number "intrinsic" modes. On the other hand, the modes which transfer no seniority are called "pairing" modes. The above procedure itself suggests that we can transcribe the nucleon state space into an ideal space in which the interplay of intrinsic and pairing modes is explicitly visualized.

2.3. *Transcription of nucleon system into "ideal boson-quasiparticle space"*

Let us introduce direct-product states $|S, \Gamma\rangle|p)$ so that these states keep the following correspondence to the original nucleon states,

$$|S, \Gamma\rangle|p) \leftrightarrow |S, S_0=-S+p; \Gamma\rangle\,, \tag{2·7}$$

where $|p)$ denotes the pairing-boson state defined by

$$|p)=\frac{1}{\sqrt{p!}}(\boldsymbol{b}^\dagger)^p|0), \quad \boldsymbol{b}|0)=0\,. \tag{2·8}$$

The boson operators, $\boldsymbol{b}^\dagger$ and $\boldsymbol{b}$, represent the pairing modes and correspond to the $J=0$-coupled nucleon pairs, $A^\dagger_{00}$ and A_{00}. The intrinsic state $|S, \Gamma\rangle$ in (2·7) has been introduced to represent the original nucleon state $|S, S_0=-S; \Gamma\rangle$. We shall call the space spanned by the direct-product states $|S; \Gamma\rangle|p)$ "ideal boson-quasiparticle space". As shown in Ref. 6) the original nucleon operators are then transcribed into the ideal space as

$$\left.\begin{aligned} c^\dagger_{jm} &\to \boldsymbol{a}^\dagger_{jm}\hat{u}+\hat{v}^\dagger\boldsymbol{a}_{\tilde{jm}}\,, \\ c_{jm} &\to \hat{u}\boldsymbol{a}_{jm}+\boldsymbol{a}^\dagger_{\tilde{jm}}\hat{v}\,, \end{aligned}\right\} \tag{2·9}$$

where

$$\hat{u}=\sqrt{1-\frac{\boldsymbol{b}^\dagger\boldsymbol{b}}{2\hat{S}}}\,, \quad \hat{v}=\frac{\boldsymbol{b}}{\sqrt{2\hat{S}}}\,, \tag{2·10}$$

$$2\hat{S}=\Omega-\sum_m \boldsymbol{a}^\dagger_{jm}\boldsymbol{a}_{jm}\equiv\Omega-\hat{\boldsymbol{n}}\,, \tag{2·11}$$

and $a_{j\tilde{m}} \equiv a_{j-m}(-)^{j-m}$. Note that $\hat{u}^\dagger\hat{u}+\hat{v}^\dagger\hat{v}=1$. The intrinsic operators $(a^\dagger_{jm}, a_{jm})$ which we call "ideal quasiparticles" satisfy the following "anticommutation relations":

$$\{a^\dagger_{jm}, a^\dagger_{jm'}\} = \{a_{jm}, a_{jm'}\} = 0\,,$$

$$\{a_{jm}, a^\dagger_{jm'}\} = \delta_{mm'} - \frac{1}{2\hat{S}+1} a^\dagger_{j\tilde{m}} a_{j\tilde{m}'}\,, \tag{2·12}$$

and 1) vanish identically if they couple to a pair of $J=0$, 2) vanish if their number exceeds Ω, 3) transfer the seniority quantum number by one unit. The ideal quasiparticles may be regarded as a field-theoretical embodiment of the seniority concept. In fact, the k-ideal quasiparticle state is equivalent[6] to the nucleon state projected to have a definite seniority $v=k$.*) We can thus explicitly construct the intrinsic state $|S;\Gamma\rangle$ in terms of the operators $a^\dagger_{jm}$ and a_{jm}.

It is interesting to note that (2·9) takes the same form as the Bogoliubov transformation if we replace the pairing bosons, $b^\dagger$ and b, with c-numbers. In this sense we may call this transformation "quantized" Bogoliubov transformation.

By making use of (2·9), we can transcribe the nucleon-pair operators into the "ideal boson-quasiparticle space" as

$$A^\dagger_{J\mu} \to \sqrt{\Omega}\,\delta_{J0}\delta_{\mu 0}\hat{v}^\dagger\hat{u} - \sqrt{2}\,\hat{v}^\dagger\hat{u}B^\dagger_{J\mu} + A^\dagger_{J\mu}\hat{u}'\hat{u} - \hat{v}'^\dagger\hat{v}^\dagger A_{J\tilde{\mu}}\,, \quad (J=\text{even}) \tag{2·13}$$

$$B^\dagger_{J\mu} \to \sqrt{2\Omega}\,\delta_{J0}\delta_{\mu 0}\hat{v}^\dagger\hat{v} + (\hat{u}\hat{u} - \hat{v}^\dagger\hat{v})B^\dagger_{J\mu} + \sqrt{2}\,A^\dagger_{J\mu}\hat{u}'\hat{v} + \sqrt{2}\,\hat{v}^\dagger\hat{u}'A_{J\tilde{\mu}} \quad (J=\text{even}) \tag{2·14}$$

and

$$B^\dagger_{J\mu} \to B^\dagger_{J\mu} \quad \text{for} \quad J=\text{odd}\,, \tag{2·15}$$

where $\hat{u}$ and $\hat{v}$ are defined by (2·10) and

$$\hat{u}' = \sqrt{1 - \frac{b^\dagger b}{2\hat{S}-1}} \quad \text{and} \quad \hat{v}' = \frac{b}{\sqrt{2\hat{S}-1}}\,. \tag{2·16}$$

The operators, $A^\dagger_{J\mu}$, $A_{J\mu}$ and $B^\dagger_{J\mu}$, appearing in Eqs. (2·13)$\sim$(2·15) are the pair operators acting in the intrinsic space;

$$A^\dagger_{J\mu} = \frac{1}{\sqrt{2}} \sum_{m_1 m_2} \langle jm_1 jm_2 | J\mu\rangle a^\dagger_{jm_1} a^\dagger_{jm_2}\,, \tag{2·17a}$$

$$B^\dagger_{J\mu} = -\sum_{m_1 m_2} \langle jm_1 jm_2 | J\mu\rangle a^\dagger_{jm_1} a_{j\tilde{m}_2}\,. \tag{2·17b}$$

2.4. *Collective quadrupole subspace in the intrinsic space*

The formulation presented above is exact. We now introduce collective quad-

*) Consequently, we have no need of the seniority-projection operator used by Arima et al.[18)~20)]

rupole subspace *in the intrinsic space.* This collective subspace is built up from the quadrupole pair operators $A^{\dagger}_{2\mu}$, defined by (2·17a), which transfer the seniority quantum number by two units;

$$|n\alpha JM\rangle_{\text{unnorm}}=\frac{1}{\sqrt{n!}}(A_2^{\dagger})^n_{\alpha JM}|0\rangle\,, \tag{2·18}$$

where α denotes a set of quantum numbers necessary to classify these states. We call these states "many-phonon states".

Our model space is thus spanned by the direct-product states $|p)\cdot|n\alpha JM\rangle_{\text{unnorm}}$,

$$|p)\cdot|n\alpha JM\rangle_{\text{unnorm}}=\frac{1}{\sqrt{p!\,n!}}(b^{\dagger})^p(A_2^{\dagger})^n_{\alpha JM}|0)\cdot|0\rangle\,, \tag{2·19}$$

the nucleon numbers of which are given by $\mathcal{N}=2(p+n)$. We call this model space "collective subspace". Since the treatment of the pairing boson $(b^{\dagger}, b)$ is trivial, let us discuss how to calculate the matrix elements of physical interest in the collective quadrupole subspace defined by (2·18). For this purpose let us adopt the method of Holzwarth et al.[7] which corresponds to the first-order approximation of Ref. 8). We, however, replace the ordinary fermion anticommutation relation with (2·12), since the collective quadrupole subspace has been defined in the intrinsic space. The use of (2·12) guarantees the orthogonality of the many-phonon states to the pairing space.

First, we note that the many-phonon states (2·18) are neither normalized nor orthogonalized. Therefore, we have to diagonalize the norm matrix in principle. However, as shown in Ref. 15), the many-phonon states satisfy the orthogonality property very well when they are classified by the representation of the group $O(5)$, i.e., in terms of $\alpha=(\nu,\gamma)$ where ν is the boson seniority and γ an additional quantum number. Thus, our task is reduced to calculating the normalization constants

$$\mathcal{N}_{n\alpha J}\equiv\langle n\alpha JM|n\alpha JM\rangle_{\text{unnorm}}\,. \tag{2·20}$$

The recursion relation for $\mathcal{N}_{n\alpha J}$ is obtained[7),15)] as

$$\begin{aligned}\mathcal{N}_{n\alpha J}=&\sum_{\alpha' J'}(d^{n-1}(\alpha' J')\,d|\}\,d^n\alpha J)^2\mathcal{N}_{n-1,\alpha' J'}\\&\times[1-\tfrac{1}{2}\{F(n\alpha J)-F(n-1,\alpha' J')\}],\end{aligned} \tag{2·21}$$

where

$$\begin{aligned}F(n\alpha J)=&\left(\frac{1}{5}C_0-\frac{2}{7}C_2+\frac{3}{35}C_4\right)(n-\nu)\,(n+\nu+3)\\&+\left(\frac{4}{7}C_2+\frac{3}{7}C_4\right)\cdot n\,(n-1)\\&-\frac{1}{7}(C_2-C_4)\,\{J\,(J+1)-6n\}\end{aligned} \tag{2·22}$$

and $(d^{n-1}(\alpha' J')\, d|\}\, d^n \alpha J)$ is the cfp for quadrupole bosons. In (2·22), $C_{\lambda=0,2,4}$ are important quantities which measure the deviation of two-phonon norms from unity;

$$C_\lambda \equiv 1 - \langle n=2, \lambda\mu | n=2, \lambda\mu \rangle_{\text{unnorm}}\,, \quad (\lambda = 0, 2 \text{ and } 4) \tag{2·23}$$

where $|n=2, \lambda\mu\rangle_{\text{unnorm}}$ are the unnormalized two-phonon states with angular momentum $\lambda\mu$. The explicit expression for C_λ is

$$C_\lambda = 50 \begin{Bmatrix} j & j & 2 \\ j & j & 2 \\ 2 & 2 & \lambda \end{Bmatrix} + (1-\delta_{\lambda 0}) \frac{100}{\Omega - 2} \begin{Bmatrix} \lambda & 2 & 2 \\ j & j & j \end{Bmatrix}^2 + \delta_{\lambda 0} \frac{5}{\Omega(\Omega-1)}\,. \tag{2·24}$$

Once we have calculated the normalization constants with the help of recursion relation (2·21), matrix elements of "phonon" operator $A^\dagger_{2\mu}$ are immediately given as

$$\begin{aligned} &\langle n\alpha J \| A_2^\dagger \| n-1, \alpha' J' \rangle \\ &\quad = \sqrt{n}\, \sqrt{2J+1}\, (d^{n-1}(\alpha' J')\, d|\}\, d^n \alpha J) \sqrt{\mathcal{N}_{n\alpha J} / \mathcal{N}_{n-1,\alpha' J'}}\,, \end{aligned} \tag{2·25}$$

where $|n\alpha JM\rangle$ are the normalized many-phonon states,

$$|n\alpha JM\rangle = \mathcal{N}^{-1/2}_{n\alpha J} |n\alpha JM\rangle_{\text{unnorm}}\,. \tag{2·26}$$

In the same way, we obtain

$$\begin{aligned} &\langle n\alpha J \| B_L^\dagger \| n\alpha' J' \rangle \\ &\quad = -5(-)^L \sqrt{(2L+1)(2J+1)(2J'+1)} \begin{Bmatrix} 2 & 2 & L \\ j & j & j \end{Bmatrix} \left(\sqrt{\frac{\mathcal{N}_{n\alpha J}}{\mathcal{N}_{n\alpha' J'}}} + \sqrt{\frac{\mathcal{N}_{n\alpha' J'}}{\mathcal{N}_{n\alpha J}}} \right) \\ &\qquad \times n \sum_{\alpha'' J''} (-)^{L+J+J''} \begin{Bmatrix} 2 & 2 & L \\ J & J' & J'' \end{Bmatrix} (d^{n-1}(\alpha'' J'')\, d|\}\, d^n \alpha J) \\ &\qquad \times (d^{n-1}(\alpha'' J'')\, d|\}\, d^n \alpha' J')\,. \quad (L = 0, 1, 2, 3 \text{ and } 4) \end{aligned} \tag{2·27}$$

2.5. *Transcribed Hamiltonian*

Let us now introduce the P+QQ Hamiltonian,

$$H = H_0 + H_P + H_{QQ}\,, \tag{2·28}$$

$$H_0 = (\epsilon - \lambda) \sum_m c^\dagger_{jm} c_{jm} = (\epsilon - \lambda) \sqrt{2\Omega} B^\dagger_{00}\,, \tag{2·28a}$$

$$H_P = -G \hat{S}_+ \hat{S}_- = -G\Omega A^\dagger_{00} A_{00}\,, \tag{2·28b}$$

$$H_{QQ} = -\tfrac{1}{2} \chi \sum_\mu \hat{Q}^\dagger_\mu \hat{Q}_\mu = -\tfrac{1}{2} \chi q^2 \sum_\mu B^\dagger_{2\mu} B_{2\mu}\,, \tag{2·28c}$$

where λ is the chemical potential. After the "quantized" Bogoliubov transformation (2·9) into the ideal boson-quasiparticle space, the P+QQ Hamiltonian becomes

$$H\to \boldsymbol{H}=\boldsymbol{H}_0+\boldsymbol{H}_P+\boldsymbol{H}_{QQ}\,, \tag{2·29}$$

$$\boldsymbol{H}_0=(\epsilon-\lambda)\cdot(\hat{\boldsymbol{n}}+2\boldsymbol{b}^\dagger\boldsymbol{b})\,, \tag{2·29a}$$

$$\boldsymbol{H}_P=-G\Omega\boldsymbol{b}^\dagger\boldsymbol{b}+G\boldsymbol{b}^\dagger\boldsymbol{b}^\dagger\boldsymbol{b}\boldsymbol{b}+G\hat{\boldsymbol{n}}\boldsymbol{b}^\dagger\boldsymbol{b}\,, \tag{2·29b}$$

$$\boldsymbol{H}_{QQ}=\boldsymbol{H}_{QQ}^{X}+\boldsymbol{H}_{QQ}^{Y}+\boldsymbol{H}_{QQ}^{V}\,, \tag{2·29c}$$

$$\boldsymbol{H}_{QQ}^{X}=-2\chi q^2(\hat{v}^\dagger\hat{u}')\sum_\mu \boldsymbol{A}_{2\mu}^\dagger\boldsymbol{A}_{2\mu}(\hat{u}'\hat{v})\,, \tag{2·29d}$$

$$\boldsymbol{H}_{QQ}^{Y}=-\sqrt{2}\,\chi q^2\{(\hat{u}\hat{u}-\hat{v}^\dagger\hat{v})\sum_\mu \boldsymbol{A}_{2\mu}^\dagger\boldsymbol{B}_{2\mu}(\hat{u}'\hat{v})+\text{h.c.}\}\,, \tag{2·29e}$$

$$\boldsymbol{H}_{QQ}^{V}=-\chi q^2\sum_\mu\{\boldsymbol{A}_{2\mu}^\dagger(\hat{u}'\hat{v})\boldsymbol{A}_{2\tilde{\mu}}^\dagger(\hat{u}'\hat{v})+\text{h.c.}\}\,, \tag{2·29f}$$

where the recoupling terms of the quadrupole force are neglected. Note that the above expression reduces to the ordinary quasiparticle Hamiltonian if we replace the operators $\hat{u}$, $\hat{u}'$ and $\hat{v}$ with c-numbers; i.e., $\hat{u}\to u$, $\hat{u}'\to u$, $\hat{v}\to v$.*) The operators, $\hat{u}$ and $\hat{v}$ in (2·29d)$\sim$(2·29f), bring about dynamical couplings of the pairing modes to the quadrupole modes. They are diagonal with respect to the number of ideal quasiparticles $\hat{\boldsymbol{n}}=\sum_m \boldsymbol{a}_{jm}^\dagger\boldsymbol{a}_{jm}$.

It is convenient to define the intrinsic Hamiltonian in the following manner:

$$\hat{h}_0+\hat{h}_X=(\epsilon-\lambda)\hat{\boldsymbol{n}}-2\chi q^2\sum_\mu \boldsymbol{A}_{2\mu}^\dagger\boldsymbol{A}_{2\mu}\,, \tag{2·30a}$$

$$\hat{h}_Y=-\sqrt{2}\,\chi q^2\sum_\mu\{\boldsymbol{A}_{2\mu}^\dagger\boldsymbol{B}_{2\mu}+\text{h.c.}\}\,, \tag{2·30b}$$

$$\hat{h}_V=-\chi q^2\sum_\mu\{\boldsymbol{A}_{2\mu}^\dagger\boldsymbol{A}_{2\tilde{\mu}}^\dagger+\text{h.c.}\}\,. \tag{2·30c}$$

Their matrix elements in the intrinsic space are easily calculated by adopting the same procedure as in 2.4;

$$\begin{aligned}&\langle n\alpha JM|(\hat{h}_0+\hat{h}_X)|n\alpha' JM\rangle\\&\quad=n\omega\delta_{\alpha\alpha'}+\tfrac{1}{2}n(n-1)\delta_{\alpha\alpha'}\sum_{\alpha''J''}\sum_\lambda C_X(\lambda)(d^{n-2}(\alpha''J'')d^2(\lambda)|\}d^n\alpha J)^2\,,\end{aligned} \tag{2·31a}$$

$$\begin{aligned}&\langle n\alpha JM|\hat{h}_Y|n-1,\alpha' JM\rangle\\&\quad=(n-1)\sqrt{n}\,C_Y\sqrt{\mathcal{N}_{n\alpha J}/\mathcal{N}_{n-1,\alpha' J}}\sum_{\alpha''J''}(d^{n-2}(\alpha''J'')d|\}d^{n-1}\alpha' J)\\&\qquad\times(d^{n-2}(\alpha''J'')d^2(\lambda=2)|\}d^n\alpha J)\,,\end{aligned} \tag{2·31b}$$

$$\begin{aligned}&\langle n\alpha JM|\hat{h}_V|n-2,\alpha' JM\rangle\\&\quad=\sqrt{n(n-1)}\,C_V\sqrt{\mathcal{N}_{n\alpha J}/\mathcal{N}_{n-2,\alpha' J}}\cdot(d^{n-2}(\alpha' J)d^2(\lambda=0)|\}d^n\alpha J)\,,\end{aligned} \tag{2·31c}$$

where

*) This is equivalent to the replacement $\boldsymbol{b}^\dagger\to\sqrt{2\hat{S}}\,v$. By furthermore replacing the operator $\sqrt{2\hat{S}}$ with $\sqrt{\Omega}$, i.e., with its expectation value in the seniority-zero state, we obtain the ordinary BCS approximation. If a finite-seniority state is used instead of the above in the latter step, we obtain the blocking BCS approximation.

$$\omega=2(\epsilon-\lambda)-2\chi q^2, \tag{2·32a}$$

$$C_X(\lambda)=4\chi q^2 C_\lambda-\frac{2000}{1-C_\lambda}\chi q^2\sum_{L\geq 4}(2L+1)\left[\begin{Bmatrix} j & j & L\\ j & j & 2\\ 2 & 2 & \lambda\end{Bmatrix}\right.$$
$$\left.+(1-\delta_{\lambda 0})\frac{2}{\Omega-2}\begin{Bmatrix} L & 2 & \lambda\\ j & j & j\end{Bmatrix}\begin{Bmatrix} 2 & 2 & \lambda\\ j & j & j\end{Bmatrix}\right]^2, \tag{2·32b}$$

$$C_Y=10\sqrt{2}\,\chi q^2\begin{Bmatrix} 2 & 2 & 2\\ j & j & j\end{Bmatrix}-\frac{100\sqrt{2}}{1-C_{\lambda=2}}\chi q^2\sum_{L\geq 4}(2L+1)\begin{Bmatrix} L & 2 & 2\\ j & j & j\end{Bmatrix}$$
$$\times\left[\begin{Bmatrix} j & j & L\\ j & j & 2\\ 2 & 2 & 2\end{Bmatrix}+\frac{2}{\Omega-2}\begin{Bmatrix} L & 2 & 2\\ j & j & j\end{Bmatrix}\begin{Bmatrix} 2 & 2 & 2\\ j & j & j\end{Bmatrix}\right], \tag{2·32c}$$

$$C_V=-\sqrt{5}\,\chi q^2. \tag{2·32d}$$

§ 3. Boson representation

3.1. *Mapping of collective quadrupole subspace onto boson space*

Corresponding to the fermion many-phonon states (2·26), let us introduce the normalized boson states as

$$|n\alpha JM)=\frac{1}{\sqrt{n!}}(d^\dagger)^n_{\alpha JM}|0), \tag{3·1}$$

where $d_\mu^\dagger$ are the quadrupole boson operators with magnetic quantum numbers μ. Then, a guiding principle[16] to find boson representation of the fermion operators is to establish the one-to-one correspondence between the matrix elements in fermion space and those in boson space. One may notice that the reduced matrix elements of pair operators, (2·25) and (2·27), are rewritten as

$$\langle n\alpha J\|\boldsymbol{A}_2^\dagger\|n-1,\alpha' J'\rangle=(n\alpha J\|d^\dagger\|n-1,\alpha' J')\sqrt{\mathcal{N}_{n\alpha J}/\mathcal{N}_{n-1,\alpha' J'}}, \tag{3·2}$$

$$\langle n\alpha J\|\boldsymbol{B}_L^\dagger\|n\alpha' J'\rangle=-5(-)^L\begin{Bmatrix} 2 & 2 & L\\ j & j & j\end{Bmatrix}\left(\sqrt{\frac{\mathcal{N}_{n\alpha J}}{\mathcal{N}_{n\alpha' J'}}}+\sqrt{\frac{\mathcal{N}_{n\alpha' J'}}{\mathcal{N}_{n\alpha J}}}\right)$$
$$\times(n\alpha J\|(d^\dagger d)_L\|n\alpha' J'). \tag{3·3}$$

The matrix elements of the intrinsic Hamiltonian listed in Eq. (2·31) are also rewritten in a similar manner. Thus, one can easily obtain boson representation in the same way as was performed by Lie and Holzwarth.[17]

3.2. *SU(6) approximation*

In general, boson representation of fermion operators takes a form expanded in terms of boson creation and annihilation operators. However, one can perform an approximate summing up of all orders of the expansion.

Let us consider the recursion relation (2·21) for the fermion norm. Then,

we notice that

$$F(n\alpha J)=C\cdot n(n-1), \tag{3·4}$$

if $C_0=C_2=C_4\equiv C$. Namely, in this case $F(n\alpha J)$ is independent of both α and J. Hence we obtain[7),8)]

$$\mathcal{N}_{n\alpha J}=\prod_{m=1}^{n}\{1-(m-1)C\}. \tag{3·5}$$

Inserting this into (3·2) and (3·3), we see that

$$\boldsymbol{A}^{\dagger}_{2\mu}\to d_{\mu}^{\dagger}\sqrt{1-C\hat{n}_d}, \tag{3·6}$$

$$\boldsymbol{B}^{\dagger}_{L\mu}\to -10(-)^{L}\begin{Bmatrix}2 & 2 & L\\ j & j & j\end{Bmatrix}(d^{\dagger}d)_{L\mu}, \tag{3·7}$$

where $\hat{n}_d=\sum_{\mu}d_{\mu}^{\dagger}d_{\mu}$. The approximation $C_0=C_2=C_4$ thus leads to the $SU(6)$ boson model of Janssen, Jolos and Dönau.[9)] Now, the exact calculation[8)] for the two-phonon norm indicates that $C_2\approx C_4\approx 2/\Omega$. Combining with the fact that the maximum number of d-bosons should be $\Omega/2$, the half of the maximal possible fermion seniority, it seems quite reasonable to take $C=2/\Omega$. Although realistic calculations[15)] indicate considerably larger values for C_0 than C_2 and C_4, we adopt in the following the approximation (3·5) with $C=2/\Omega$ for simplicity.

3.3. *sd-boson representation*

Once we adopt the approximation (3·5), it is straightforward to transcribe the model formulated in § 2 into the language of the *sd*-boson model of Arima and Iachello:[10)] By changing the notation of our pairing boson $(\boldsymbol{b}^{\dagger},\boldsymbol{b})$ into the s-boson $(s^{\dagger},s)$ and noting that $\hat{\boldsymbol{n}}=2\hat{n}_d$, one can express the nucleon-pair operators as*)

$$\begin{aligned}A^{\dagger}_{2\mu}\to\mathring{A}^{\dagger}_{2\mu}=&\sqrt{\frac{(\Omega-\Pi-\hat{n}_d+1)(\Omega-\Pi-\hat{n}_d+2)}{\Omega(\Omega-2\hat{n}_d+1)}}d_{\mu}^{\dagger}\\&+10\sqrt{2}\begin{Bmatrix}2 & 2 & 2\\ j & j & j\end{Bmatrix}\sqrt{\frac{\Omega-\Pi-\hat{n}_d+1}{\Omega-2\hat{n}_d}}s^{\dagger}(d^{\dagger}d)_{2\mu}\\&-\frac{1}{\sqrt{\Omega(\Omega-2\hat{n}_d-1)}}(s^{\dagger}s^{\dagger})d_{\tilde{\mu}},\end{aligned} \tag{3·8}$$

$$\begin{aligned}B^{\dagger}_{L\mu}\to\mathring{B}^{\dagger}_{L\mu}=&\left\{\sqrt{\frac{2(\Omega-\Pi-\hat{n}_d+1)}{\Omega(\Omega-2\hat{n}_d+1)}}(d^{\dagger}s)_{2\mu}+(s^{\dagger}d)_{\tilde{2}\mu}\sqrt{\frac{2(\Omega-\Pi-\hat{n}_d+1)}{\Omega(\Omega-2\hat{n}_d+1)}}\right\}\delta_{L2}\\&-10(-)^{L}\begin{Bmatrix}2 & 2 & L\\ j & j & j\end{Bmatrix}\frac{(\Omega-\Pi-\hat{n}_d)-(-)^{L}(\Pi-\hat{n}_d)}{\Omega-2\hat{n}_d}(d^{\dagger}d)_{L\mu},\\&(L=1,2,3\text{ and }4)\end{aligned} \tag{3·9}$$

*) Recently, Otsuka et al.[19),20)] have derived a boson representation through a similar procedure. It is interesting to note that they also obtained[19)] the same expression as (3·9), though they adopted somewhat different approximation scheme for the matrix elements in the intrinsic space.

where

$$\hat{n}_d=\sum_\mu d_\mu^\dagger d_\mu,\quad \hat{n}_s=s^\dagger s,\quad \hat{n}_s+\hat{n}_d=\Pi \tag{3·10}$$

with Π being half of the nucleon number $\mathcal{N}$ of the final state, i.e., $\Pi=\mathcal{N}/2$. The square-root operators in the above expressions come from the $\hat{u}$ and $\hat{v}$ operators involved in the expressions (2·13) and (2·14). Together with the s-bosons, they represent the blocking effects to the pair field due to the presence of d-bosons. It is interesting to note that, in the final expressions (3·8) and (3·9), the square-root operator $\sqrt{1-(2/\Omega)\hat{n}_d}$ in (3·6) has exactly cancelled out the same operator contained in the denominator of the $\hat{u}$ and $\hat{v}$ operators.

The P+QQ Hamiltonian takes the following form:

$$\begin{aligned}H\to\mathring{H}=&\omega_s\hat{n}_s+G\hat{n}_s\hat{n}_s+2G\hat{n}_d\cdot\hat{n}_s\\&+\hat{\omega}_d\hat{n}_d+\tfrac{1}{2}\sum_{\lambda\mu}\hat{f}_X(\lambda)\,(d^\dagger d^\dagger)_{\lambda\mu}(dd)_{\lambda\mu}\\&+\{\hat{f}_Y\sum_\mu(d^\dagger d^\dagger)_{2\mu}(ds)_{2\mu}+\text{h.c.}\}\\&+\{\hat{f}_V(d^\dagger d^\dagger)_{00}(ss)_{00}+\text{h.c.}\},\end{aligned}\tag{3·11}$$

where

$$\omega_s=2(\epsilon-\lambda)-G(\Omega+1), \tag{3·11a}$$

$$\hat{\omega}_d=2(\epsilon-\lambda)-2\chi q^2\frac{(\Pi-\hat{n}_d)(\Omega-\Pi-\hat{n}_d)}{(\Omega-2\hat{n}_d)(\Omega-2\hat{n}_d-1)}, \tag{3·11b}$$

$$\hat{f}(\lambda)_X=C_X(\lambda)\cdot\frac{(\Pi-\hat{n}_d)(\Omega-\Pi-\hat{n}_d)}{(\Omega-2\hat{n}_d)(\Omega-2\hat{n}_d-1)}, \tag{3·11c}$$

$$\hat{f}_Y=C_Y\cdot\frac{(\Omega-\Pi)-\Pi}{\Omega-2\hat{n}_d}\sqrt{\frac{\Omega-\Pi-\hat{n}_d+1}{\Omega(\Omega-2\hat{n}_d+1)}}, \tag{3·11d}$$

$$\hat{f}_V=C_V\cdot\sqrt{\frac{(\Omega-\Pi-\hat{n}_d+1)(\Omega-\Pi-\hat{n}_d+2)}{\Omega^2(\Omega-2\hat{n}_d+1)(\Omega-2\hat{n}_d+3)}}. \tag{3·11e}$$

This expression has been obtained by directly making the mapping of the intrinsic Hamiltonian (2·30) into the d-boson space, and not via the repeated use of the expressions (3·8) and (3·9) for the nucleon-pair operators. This is in accord with the spirit of the modified Marumori method developed by Lie and Holzwarth.[16]

The expression (3·11) is convenient because it shows the relation to the conventional quasiparticle picture in a transparent way. Indeed, by replacing the s-bosons with c-numbers and neglecting $\hat{n}_d$ in the square-root operators, we can regard the d-bosons as corresponding to the conventional quasiparticle pairs with $J^\pi=2^+$. It is interesting to notice that the energy of d-boson ($J=2$-coupled pair) manifests itself as an *operator* $\hat{\omega}_d$ in the nucleon-number conserving representation; namely, the "unperturbed energy term" $\hat{\omega}_d\hat{n}_d$ in effect involves an interaction be-

tween s- and d-boson (rewrite (3·11b) using $\Pi-\hat{n}_d=\hat{n}_s$). Thus, our d-boson is not correlated at all in the two-particle system; the d-boson can be viewed as a correlated pair only when one goes to many-particle system.

In the same sense, the interactions between d-bosons in (3·11) are in fact the many-body interactions *mediated* by the s-bosons. Hence, it is impossible to fully express the quadrupole force between like nucleons as two-body interactions (between bosons) *with constant coupling strengths*. In this sense, the present model should be distinguished from the phenomenological sd-boson model of Arima and Iachello.[10]

§ 4. Numerical examples

The Hamiltonian (3·11) has been diagonalized within the sd-boson space $\{(1/\sqrt{n_s!n_d!})\,(s^\dagger)^{n_s}(d^\dagger)^{n_d}_{\alpha JM}|0)\,;\,n_s+n_d=\Pi=\mathcal{N}/2\}$. Typical examples are shown in Fig. 1(a), Fig. 2 and Fig. 3(a). It is seen that the model under consideration produces a gradual change, as a function of χq^2, of excitation spectrum from vibrational to rotational pattern (Fig. 1(a) and Fig. 2). In particular, a formation of excited band structure with $J^\pi=2^+, 3^+, 4^+, \cdots$ is exhibited in Fig. 3(a). On the other hand, if one makes the BCS approximation (replacement of the $\hat{u}$, $\hat{v}$ operators with c-numbers), then it becomes hard to reproduce the rotation-like excitations and the formation of band structure (see Fig. 1(b), Fig. 2 and Fig. 3(b)).

Two important effects, which are lost due to the BCS approximation and are responsible for the above-mentioned difference, may be found when one examines the structure of (2·29) or (3·11):

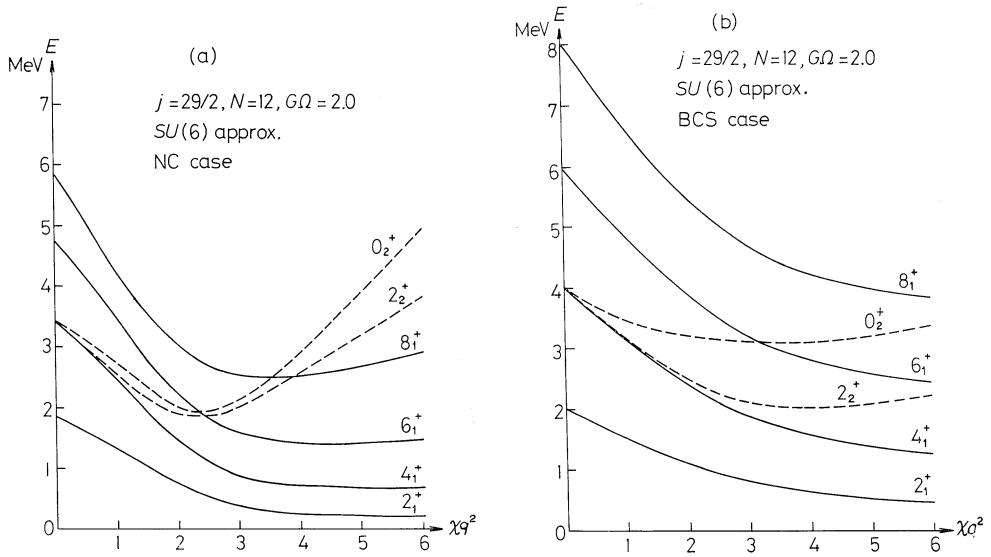

(continued)

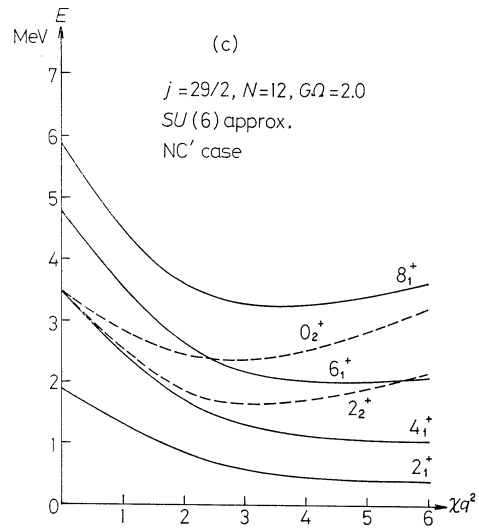

Fig. 1. Calculated energy eigenvalues for the yrast and the second 0^+, 2^+ states for $j=29/2$ and nucleon number $\mathcal{N}=12$ system, as functions of the quadrupole force strength χq^2. Pairing force strength G is fixed at $2/\Omega=0.133$ which corresponds to the quasiparticle energy of 1 MeV in the BCS approximation. Many-phonon norm matrices are evaluated under the $SU(6)$ approximation. (a) The case where the pairing force and the operators $\hat{u}$, $\hat{v}$ in the quadrupole force (Eqs. (2·29)) are exactly evaluated. (NC case) (b) The case where the pairing field is fixed at the seniority-zero state. In this case, pairing bosons $\boldsymbol{b}^+$, $\boldsymbol{b}$ and $\hat{u}$, $\hat{v}$ operators in Eqs. (2·29) are replaced by c-numbers. (BCS case) (c) The case where only the factor $\hat{u}^\dagger\hat{u}-\hat{v}^\dagger\hat{v}$ in $\boldsymbol{H}^Y_{QQ}$ (Eq. (2·29e)) is replaced by c-number. Other factors dependent on the pairing variables are exactly evaluated. (NC′ case)

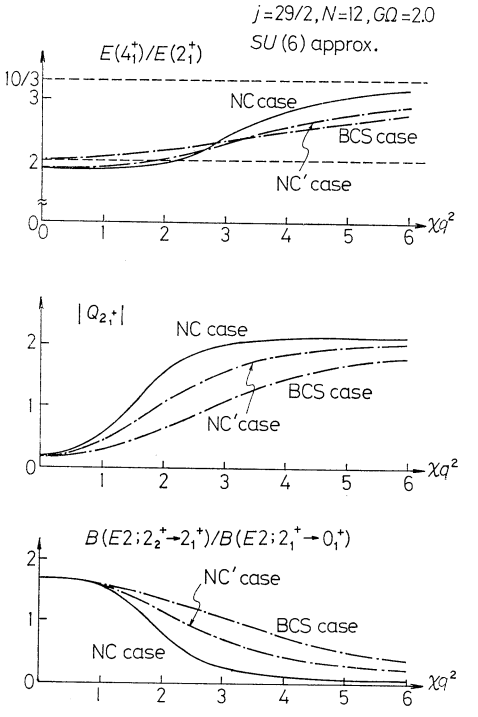

Fig. 2. Various quantities which characterize the band structure, as functions of the quadrupole force strength χq^2: excitation energy ratio $E(4_1^+)/E(2_1^+)$: absolute value of the spectroscopic quadrupole moment for the first 2^+ state (arbitrary unit): ratio of the reduced transition probabilities $B(E2;\ 2_2^+\to 2_1^+)/B(E2;\ 2_1^+\to 0_1^+)$. Adopted parameters are the same as in Fig. 1.

1) The operators, $\hat{u}$ and $\hat{v}$, appear in the Hamiltonian as products $\hat{u}\hat{v}$ or $(\hat{u}\hat{u}-\hat{v}^\dagger\hat{v})$. The product $\hat{u}\hat{v}$ depends rather weakly on the d-boson number (fermion seniority), while $(\hat{u}\hat{u}-\hat{v}^\dagger\hat{v})$ depends strongly. Consequently, effects of the Y-type interaction, which accompanies $(\hat{u}\hat{u}-\hat{v}^\dagger\hat{v})$ and is written as $\hat{f}_Y\sum_\mu(d^\dagger d^\dagger)_{2\mu}(ds)_{2\mu}$ in

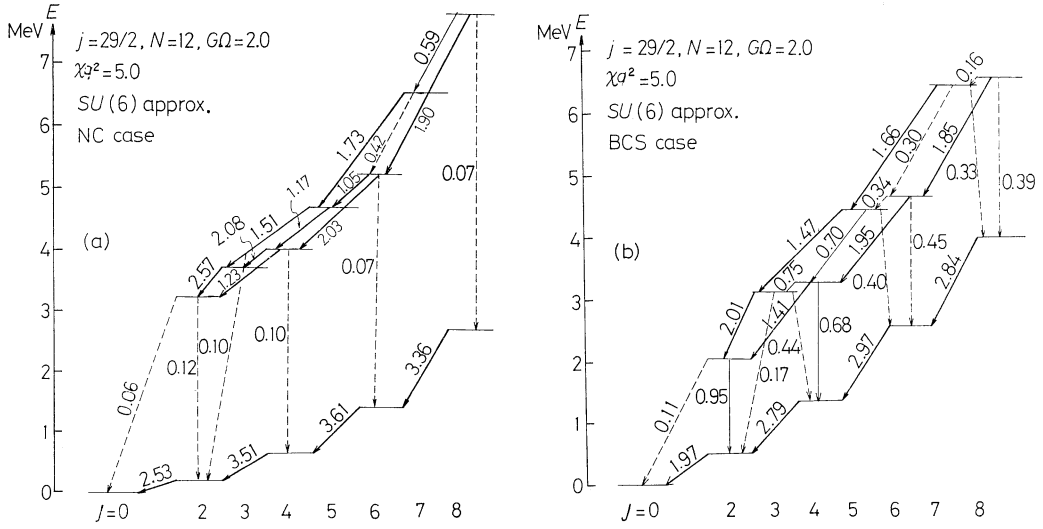

Fig. 3. Excitation energy versus angular momentum for the yrast and yrare states. Quadrupole force strength χq^2 is fixed at 5.0. Other parameters are the same as in Fig. 1. Numbers on the arrows denote the $B(E2)$ values in unit of $B(E2; 2^+ \to 0^+)$ value in the Tamm-Dancoff approximation. (a) NC case. (b) BCS case.

the boson Hamiltonian (3·11), increase with increasing d-boson number (note the denominator of $\hat{f}_Y$ given by (3·11d)). This enhancement of the Y-type interaction results from the blocking effect to the pair field and is neglected in the BCS approximation. The importance of keeping the operator form of $\hat{f}_Y$ is seen by comparing Fig. 1(a) with Fig. 1(c). In the latter calculation, the operator $\hat{u}\hat{u} - \hat{v}^\dagger\hat{v} = (\Omega - 2\Pi)/(\Omega - 2\hat{n}_d)$ in $\hat{f}_Y$ is replaced by the constant $(u^2 - v^2) = (\Omega - 2\Pi)/\Omega$.

2) In the BCS approximation, unperturbed energies for the many-phonon states are considerably overestimated mainly due to the neglect of a decrease of the pairing correlation with increasing fermion seniority.

Thus, the numerical examples presented here clearly indicate the necessity of taking explicit account of the change of pair field due to many-phonon excitations, which has been neglected in the conventional quasiparticle description.

Acknowledgements

One of us (K.M.) would like to thank Professor A. Bohr and Professor R. Broglia for valuable comments and discussions during his stay at the Niels Bohr Institute. He also acknowledges the fellowships from the Scientific Research Council of Danish State and the Nishina Memorial Foundation, while T.S. is indebted to the Yukawa Foundation for financial aid. Numerical calculations were carried out by using the FACOM M-190 at the Data Processing Center of Kyoto University.

References

1) S. Iwasaki, T. Marumori, F. Sakata and K. Takada, Prog. Theor. Phys. **56** (1976), 1140.
2) F. Sakata, S. Iwasaki, T. Marumori and K. Takada, Z. Phys. **A286** (1978), 195.
3) D. R. Bès and R. A. Broglia, *Proceedings of the International School of Physics, "Enrico Fermi"*, course LXIX (1977), p. 55.
4) E. R. Marshalek and J. Weneser, Ann. of Phys. **53** (1969), 569.
5) D. R. Bès and R. A. Sorensen, *The Pairing-Plus-Quadrupole Model, Advances in Nuclear Physics* (Plenum Press), vol. 2 (1969), p. 129.
6) T. Suzuki and K. Matsuyanagi, Prog. Theor. Phys. **56** (1976), 1156.
7) G. Holzwarth, D. Janssen and R. V. Jolos, Nucl. Phys. **A261** (1976), 1.
8) S. Iwasaki, F. Sakata and K. Takada, Prog. Theor. Phys. **57** (1977), 1289.
9) D. Janssen, R. V. Jolos and F. Dönau, Yadern Fiz. **22** (1975), 965; Soviet J. Nucl. Phys. **22** (1976), 503; Nucl. Phys. **A224** (1974), 93.
   R. V. Jolos and D. Janssen, Fiz. Elem. Chastits At. Yadra 8 (1977), 330; Soviet J. Part. Nucl. 8 (1977), 138.
10) A. Arima and F. Iachello, Ann. of Phys. **99** (1976), 253; **111** (1978), 201.
11) T. Suzuki, *Proceedings of the International Conference on Nuclear Structure—contributed papers—Tokyo 1977*, p. 84.
12) T. Suzuki, M. Fuyuki and K. Matsuyanagi, RIFP-359, submitted to Prog. Theor. Phys.
13) For instance, see, A. Arima and M. Ichimura, Prog. Theor. Phys. **36** (1966), 296.
14) A. Kuriyama, T. Marumori, K. Matsuyanagi, F. Sakata and T. Suzuki, Prog. Theor. Phys. Suppl. No. 58 (1975), 9.
15) T. Suzuki, M. Fuyuki and K. Matsuyanagi, Prog. Theor. Phys. **61** (1979), 1082.
16) T. Marumori, M. Yamamura and A. Tokunaga, Prog. Theor. Phys. **31** (1964), 1009.
17) S. G. Lie and G. Holzwarth, Phys. Rev. **C12** (1975), 1035.
18) A. Arima, *Proceedings of the Colloque Franco-Japonais and INS Symposium, Dogashima and Tokyo 1976*, p. 90.
19) T. Otsuka, A. Arima, F. Iachello and I. Talmi, Phys. Letters **76B** (1978), 139.
20) T. Otsuka, A. Arima and F. Iachello, Nucl. Phys. **A309** (1978), 1.

Progress of Theoretical Physics, Vol. 62, No. 3, September 1979

Dynamical Interplay of Pairing and Quadrupole Modes in Transitional Nuclei. II

Tōru SUZUKI,† Masahiko FUYUKI* and Kenichi MATSUYANAGI*

Research Institute for Fundamental Physics
Kyoto University, Kyoto 606
**Department of Physics, Kyoto University, Kyoto 606*

(Received March 27, 1979)

We develop a microscopic method to treat the mode-mode couplings between many-quasiparticle excitations and pairing rotations. The canonical transformation method with auxiliary number- and angle-variables is employed to extract the pairing rotational degree of freedom without violating the Pauli principle. In the case of single j-shell, the mode-mode couplings can be treated exactly, the analytical expressions of which are used to test the convergence of the perturbative expansion of the couplings in terms of $1/\Omega$.

§ 1. Introduction

In a preceding paper,[1] referred to as I, we suggested the importance of taking explicit account of the couplings between pairing rotations and quadrupole modes of excitation in transitional nuclei. Characteristic properties of the pairing plus quadrupole (P+QQ) force model were analyzed in I for the case of single j-shell. This was done by using the nucleon-number conserving basis states, without explicit reference to the concept of pairing rotations. In this paper, we consider the same model by starting with the quasiparticle representation, and develop a microscopic method to explicitly treat the dynamical couplings between pairing rotations and many-quasiparticle excitations (which are responsible for the quadrupole modes).

The pairing rotation is a collective mode to restore the nucleon-number conservation (the gauge invariance) broken by the deformation of the pair field, while the quasiparticle mode is a single-particle mode in the deformed pair potential.[2)~4)] Thus, the mode-mode coupling under consideration may be formulated in a manner quite analogous to the (phenomenological) particle-rotor model for the collective rotations in the ordinary coordinate space. For the latter case, there are already some attempts[5),6)] to the microscopic description of the particle-rotor couplings, in which the collective rotation is described as a special zero-energy mode[7)~9)] associated with the spontaneous breakdown of rotational symmetry in the Nilsson potential. On the other hand, the microscopic description of the pairing

† Present address: Institut für Kernphysik, Kernforschungsanlage Jülich, D-5170 Jülich, West Germany.

rotation has been considered by several authors[10)~13)] for the case where residual interactions do not change the seniority quantum numbers, i.e., for the case where there is no dynamical coupling to the quadrupole modes of excitation. Thus, we develop in this paper a microscopic formulation of the pairing rotation such that the dynamical couplings of this kind can be treated in a simple and systematic way. This formulation of the two-dimensional rotation in gauge space, in turn, may shed a light on the problems of particle-rotor couplings in the ordinary coordinate space.

In § 2 we introduce exact number- and angle-operators to describe the pairing rotation, and compare the RPA treatment with the exact one. We then derive in § 3 an effective Hamiltonian and effective operators for the model space in which state vectors take the same form as those in the particle-rotor model. In this derivation, the canonical transformation method with auxiliary variables[14),15)] is used; hence, there is no overcompleteness in the degrees of freedom and no violation of the Pauli principle in this formulation. Namely, the intrinsic modes (quasiparticle excitations) are exactly orthogonal to the pairing rotational mode. In the case of single j-shell, the diagonalization of the mode-mode coupling Hamiltonian leads to the results which are completely the same as those given in I where nucleon-number conserving representation was adopted. On the other hand, in the general many j-shell case, the pairing vibrational modes come into play in addition to the pairing rotations under consideration. In this general case to be treated in a succeeding paper, we shall adopt a perturbative expansion of the mode-mode couplings in terms of the expansion parameter $1/\Omega$, where Ω is the effective pair-degeneracy of the valence shell. Thus, we present in § 4 some numerical examples for the single j-shell which suggest a fast convergence of such an expansion.

§ 2. Pairing rotation, number- and angle-operators

2.1. *Division of monopole boson into static- and fluctuating-parts*

We consider a condensate of the monopole bosons, which corresponds to a condensate of the $J=0$-coupled nucleon pairs. Thus, it is convenient to divide the monopole bosons $(\boldsymbol{b}^\dagger, \boldsymbol{b})$ into static- and fluctuating-parts as

$$\begin{aligned} \boldsymbol{b}^\dagger &= \sqrt{\Omega}\, v + \tilde{\boldsymbol{b}}^\dagger , \\ \boldsymbol{b} &= \sqrt{\Omega}\, v + \tilde{\boldsymbol{b}} , \end{aligned} \tag{2·1}$$

where v is a real parameter to be determined later, and $(\tilde{\boldsymbol{b}}^\dagger, \tilde{\boldsymbol{b}})$ are the boson operators representing the fluctuation of the deformed pair field. Equation (2·1) implies an introduction of the coherent state $|\mathrm{coh})$ satisfying the property

$$\tilde{\boldsymbol{b}}|\mathrm{coh}) = 0 . \tag{2·2}$$

Inserting (2·1) into the pairing Hamiltonian expressed in the ideal boson-quasipar-

ticle space, (I·2·29),*) we obtain

$$\begin{aligned} \boldsymbol{H}_0+\boldsymbol{H}_{\mathrm{P}} &= W+\{(\varepsilon-\lambda)+G\Omega v^2\}\hat{\boldsymbol{n}} \\ &\quad +\{2(\epsilon-\lambda)-G\Omega(u^2-v^2)\}\tilde{\boldsymbol{N}} \\ &\quad +G\tilde{\boldsymbol{N}}^2+G\hat{\boldsymbol{n}}\tilde{\boldsymbol{N}}\,, \end{aligned} \tag{2·3}$$

where $u^2+v^2=1$, $\Omega=j+1/2$, and

$$W=2(\epsilon-\lambda)\Omega v^2-G\Omega^2u^2v^2, \tag{2·4}$$

$$\tilde{\boldsymbol{N}}=\sqrt{\Omega}\,v(\tilde{\boldsymbol{b}}^\dagger+\tilde{\boldsymbol{b}})+\tilde{\boldsymbol{b}}^\dagger\tilde{\boldsymbol{b}}\,. \tag{2·5}$$

Obviously, the pairing Hamiltonian can be written entirely in terms of the ideal-quasiparticle-number operator $\hat{\boldsymbol{n}}$ and the boson-number-fluctuation operator $\tilde{\boldsymbol{N}}=\boldsymbol{b}^\dagger\boldsymbol{b}-\Omega v^2\equiv\hat{\boldsymbol{N}}-\Omega v^2$.

The parameter v and the chemical potential λ in (2·3) are determined as usual by the conditions $\partial W/\partial v=0$ (which is equivalent to eliminating the dangerous term linear in $\tilde{\boldsymbol{N}}$) and

$$(\mathrm{coh}|\hat{\boldsymbol{N}}|\mathrm{coh})=\Omega v^2=\Pi\,, \tag{2·6}$$

where Π is half of the nucleon number $\mathcal{N}$, i.e., $\Pi=\mathcal{N}/2$. Then, the pairing Hamiltonian becomes

$$\boldsymbol{H}_0+\boldsymbol{H}_{\mathrm{P}}=W+E\hat{\boldsymbol{n}}+G\tilde{\boldsymbol{N}}^2+G\hat{\boldsymbol{n}}\tilde{\boldsymbol{N}} \tag{2·7}$$

with

$$E=\sqrt{(\epsilon-\lambda)^2+\Delta^2}=\tfrac{1}{2}G\Omega\,, \quad \text{(quasiparticle energy)} \tag{2·8}$$

$$\Delta=G\Omega uv\,. \quad \text{(energy gap)} \tag{2·9}$$

2.2. *Pairing rotation under the RPA*

In this subsection, we briefly review the concept of pairing rotation defined under the RPA. To make the connection to the conventional formulation[4] transparent, we introduce new boson operators $(\beta^\dagger,\beta)$ through[16]

$$\begin{aligned} \tilde{\boldsymbol{b}}^\dagger+\tilde{\boldsymbol{b}} &= u(\beta^\dagger+\beta)\,, \\ \tilde{\boldsymbol{b}}^\dagger-\tilde{\boldsymbol{b}} &= u^{-1}(\beta^\dagger-\beta)\,. \end{aligned} \tag{2·10}$$

The vacuum for the β-boson is related to the coherent state by

$$|\phi_0)=\exp\tfrac{1}{2}\ln u\cdot(\tilde{\boldsymbol{b}}^\dagger\tilde{\boldsymbol{b}}^\dagger-\tilde{\boldsymbol{b}}\tilde{\boldsymbol{b}})\,|\mathrm{coh})\,, \qquad \beta|\phi_0)=0\,. \tag{2·11}$$

*) We cite the equations in Ref. 1) by adding I to the first place of the equation number. In Ref. 1) are also given full accounts of the notations adopted in this paper. Note that the Hartree-Fock contribution of the pairing force is dropped in the expression (2·3).

Expanding (2·7) in terms of the small parameter $\Omega^{-1/2}$ and retaining the terms up to the order unity,*) we obtain

$$\boldsymbol{H}_0+\boldsymbol{H}_{\mathrm{P}}^{(0)}=W+E\hat{n}$$
$$+2E\beta^{\dagger}\beta-G\Omega\,(u^4+v^4)\,\beta^{\dagger}\beta+G\Omega u^2v^2\,(\beta^{\dagger}\beta^{\dagger}+\beta\beta)\,. \qquad (2\cdot12)$$

This is nothing but the pairing Hamiltonian in the RPA, and the β-boson corresponds to the $J=0$-coupled quasiparticle pair in the conventional description. It is well known that the RPA treatment of (2·12) results in a special eigenmode with zero-energy, called pairing rotation. In order to correctly obtain the rotational energy, the number- and angle-operators, $\tilde{\boldsymbol{N}}^{(0)}$ and $\hat{\boldsymbol{\Phi}}^{(0)}$, are introduced through a set of equations,

$$[\hat{\boldsymbol{\Phi}}^{(0)},\,\tilde{\boldsymbol{N}}^{(0)}]=i\,, \qquad (2\cdot13a)$$

$$[\boldsymbol{H}_0+\boldsymbol{H}_{\mathrm{P}}^{(0)},\,\tilde{\boldsymbol{N}}^{(0)}]=0\,, \qquad (2\cdot13b)$$

$$[\boldsymbol{H}_0+\boldsymbol{H}_{\mathrm{P}}^{(0)},\,i\hat{\boldsymbol{\Phi}}^{(0)}]=\frac{1}{\mathcal{J}}\tilde{\boldsymbol{N}}^{(0)}\,. \qquad (2\cdot13c)$$

The solution of this set of equations is

$$\tilde{\boldsymbol{N}}^{(0)}=\sqrt{\Omega}\,uv\,(\beta^{\dagger}+\beta)\,, \qquad (2\cdot14a)$$

$$\hat{\boldsymbol{\Phi}}^{(0)}=\frac{1}{2i\sqrt{\Omega}\,uv}\,(\beta^{\dagger}-\beta)\,, \qquad (2\cdot14b)$$

and $\mathcal{J}=1/2G$. Then, (2·12) is written as

$$\boldsymbol{H}_0+\boldsymbol{H}_{\mathrm{P}}^{(0)}=W+E\hat{n}+\frac{1}{2\mathcal{J}}\,(\tilde{\boldsymbol{N}}^{(0)})^2\,. \qquad (2\cdot15)$$

The last term of (2·15) represents the energy of the pairing rotation. The RPA ground state $|\Psi_0^{(0)})$ may be determined by the condition

$$\tilde{\boldsymbol{N}}^{(0)}|\Psi_0^{(0)})=0\,, \qquad (2\cdot16)$$

which leads to the solution of the form[9),12)]

$$|\Psi_0^{(0)})=\mathcal{N}_{\mathrm{RPA}}^{-1/2}\,c^{-1/2\beta^{\dagger}\beta^{\dagger}}|\phi_0)=\mathcal{N}_{\mathrm{RPA}}^{-1/2}\,c^{-1/2\tilde{b}^{\dagger}\tilde{b}^{\dagger}}|\mathrm{coh})\,. \qquad (2\cdot17)$$

The condition (2·16) is required in order that $|\Psi_0^{(0)})$ should be consistent with the fact that the RPA treatment of the pairing Hamiltonian restores the nucleon-number conservation broken by the BCS approximation. However, the normalization factor $\mathcal{N}_{\mathrm{RPA}}$ in (2·17) diverges, which has been known to be the main difficulty of the RPA.[9),12)]

*) We regard $G\Omega$ as order unity.

2.3. *Exact number- and angle-operators*

In order to go beyond the RPA and to describe the quasiparticle-pairing rotation couplings, let us now introduce exact number- and angle-operators as*)

$$\hat{\Pi}=\frac{1}{2}\sum_{m}c_{jm}^{\dagger}c_{jm}=\boldsymbol{b}^{\dagger}\boldsymbol{b}+\frac{1}{2}\hat{\boldsymbol{n}}=\hat{\boldsymbol{N}}+\frac{1}{2}\hat{\boldsymbol{n}}\,, \tag{2·18}$$

$$e^{i\hat{\Phi}}=\hat{S}_{+}\frac{1}{\sqrt{\hat{S}_{-}\hat{S}_{+}}}=\boldsymbol{b}^{\dagger}\frac{1}{\sqrt{\boldsymbol{b}\boldsymbol{b}^{\dagger}}}\,, \tag{2·19}$$

which satisfy the commutation relation

$$[\hat{\Pi},\,e^{i\hat{\Phi}}]=e^{i\hat{\Phi}}\,. \tag{2·20}$$

Note that $\hat{\Pi}$ is the sum of the monopole-boson number $\hat{\boldsymbol{N}}$ and the pair-number of ideal quasiparticles $\frac{1}{2}\hat{\boldsymbol{n}}$, while $e^{i\hat{\Phi}}$ depends only upon the monopole-boson degree of freedom. One may formally write the angle operator $\hat{\Phi}$ as[13]

$$\hat{\Phi}=\frac{1}{2i}\{\ln\boldsymbol{b}^{\dagger}-\ln\boldsymbol{b}\}\,, \tag{2·21}$$

$$[\hat{\Phi},\,\hat{\Pi}]=i\,. \tag{2·22}$$

Once the deformation of the pair field takes place, the angle-operator $\hat{\Phi}$, (2·21), acquires a definite physical meaning. Indeed, inserting (2·1) into (2·21), one can in this case expand $\hat{\Phi}$ in terms of $\Omega^{-1/2}$ as follows:[13]

$$\begin{aligned}\hat{\Phi}&=\frac{1}{2i}\left\{\ln\left(1+\frac{\tilde{\boldsymbol{b}}^{+}}{\sqrt{\Omega}\,v}\right)-\ln\left(1+\frac{\tilde{\boldsymbol{b}}}{\sqrt{\Omega}\,v}\right)\right\}\\&=\frac{1}{2i\sqrt{\Omega}\,v}(\tilde{\boldsymbol{b}}^{\dagger}-\tilde{\boldsymbol{b}})-\frac{1}{4i\Omega v^{2}}(\tilde{\boldsymbol{b}}^{\dagger}\tilde{\boldsymbol{b}}^{\dagger}-\tilde{\boldsymbol{b}}\tilde{\boldsymbol{b}})\\&\quad+\frac{1}{6i\Omega\sqrt{\Omega}\,v^{3}}(\tilde{\boldsymbol{b}}^{\dagger}\tilde{\boldsymbol{b}}^{\dagger}\tilde{\boldsymbol{b}}^{\dagger}-\tilde{\boldsymbol{b}}\tilde{\boldsymbol{b}}\tilde{\boldsymbol{b}})+\cdots\\&=\hat{\Phi}^{(0)}+\text{higher order terms.}\end{aligned} \tag{2·23}$$

In the same way, we obtain

$$\hat{\Pi}=\Pi+\tilde{\boldsymbol{N}}+\tfrac{1}{2}\boldsymbol{n}\,, \tag{2·24}$$

$$\tilde{\boldsymbol{N}}=\tilde{\boldsymbol{N}}^{(0)}+\tilde{\boldsymbol{b}}^{\dagger}\tilde{\boldsymbol{b}}\,. \tag{2·25}$$

The operators $\tilde{\boldsymbol{N}}$ and $\hat{\Phi}$ satisfy

*) Strictly speaking, the operator $e^{i\hat{\Phi}}$ is not unitary, because $(e^{i\hat{\Phi}})(e^{i\hat{\Phi}})^{\dagger}=1-|0)(0|$ although $(e^{i\hat{\Phi}})^{\dagger}(e^{i\hat{\Phi}})=1$, where $|0)$ is the vacuum for the monopole boson, $\boldsymbol{b}|0)=0$. Nevertheless, we regard $e^{i\hat{\Phi}}$ as a unitary operator, since we are interested in a condensate of the monopole bosons. Also, we disregard the projection operator onto the physical space in the expressions (2·18) and (2·19); see Ref. 16).

$$[\hat{\boldsymbol{\phi}}, \tilde{\boldsymbol{N}}] = i\,, \tag{2·26}$$

$$[\boldsymbol{H}_0 + \boldsymbol{H}_{\mathrm{P}}, \tilde{\boldsymbol{N}}] = 0\,. \tag{2·27}$$

Thus, $\tilde{\boldsymbol{N}}$ and $\hat{\boldsymbol{\phi}}$ may be regarded*) as the exact canonical variables representing the pairing rotational mode, the leading-order terms of which correspond to $\tilde{\boldsymbol{N}}^{(0)}$ and $\hat{\boldsymbol{\phi}}^{(0)}$ introduced through the RPA. In place of (2·16), one can now determine the ground state $|\Psi_0)$ by the condition

$$\tilde{\boldsymbol{N}}|\Psi_0) = 0\,. \tag{2·28}$$

The solution of (2·28) is

$$\begin{aligned} |\Psi_0) &= e^{i\Pi\hat{\phi}}|0) \\ &= \mathcal{N}^{-1/2} \exp\left\{-\frac{1}{2}\tilde{\boldsymbol{b}}^{\dagger}\tilde{\boldsymbol{b}}^{\dagger} + \frac{1}{3\sqrt{\Pi}}\tilde{\boldsymbol{b}}^{\dagger}\tilde{\boldsymbol{b}}^{\dagger}\tilde{\boldsymbol{b}}^{\dagger} - + \cdots\right\}|\mathrm{coh}) \end{aligned} \tag{2·29}$$

with

$$\mathcal{N} = \frac{\Pi!}{\Pi^{\Pi}\, e^{-\Pi}}\,, \tag{2·29a}$$

which is correctly normalized, $(\Psi_0|\Psi_0) = 1$. By comparing (2·29) with (2·17), we see that the divergence in the norm of the RPA ground state $|\Psi_0^{(0)})$ stems from the fact that $\tilde{\boldsymbol{N}}$ is approximated in the RPA by $\tilde{\boldsymbol{N}}^{(0)}$.

2.4. *P+QQ Hamiltonian in the quasiparticle representation*

Next, we express the quadrupole interaction as well as the pairing interaction in terms of the boson-number fluctuation operator $\tilde{\boldsymbol{N}}$ and the angle operator $\hat{\boldsymbol{\phi}}$ introduced above. Then, the P+QQ Hamiltonian defined by (I·2·28),

$$H_0 + H_{\mathrm{P}} + H_{\mathrm{QQ}} = (\varepsilon - \lambda)\sqrt{2\Omega}B_{00}^{\dagger} - G\Omega A_{00}^{\dagger}A_{00} - \frac{1}{2}\chi q^2 \sum_{\mu} B_{2\mu}^{\dagger}B_{2\mu}\,,$$

may be written for the superconducting system under consideration as follows:

$$\boldsymbol{H} = \boldsymbol{H}_0 + \boldsymbol{H}_{\mathrm{P}} + \boldsymbol{H}_{\mathrm{QQ}}\,, \tag{2·30}$$

$$\boldsymbol{H}_0 + \boldsymbol{H}_{\mathrm{P}} = W + E\hat{\boldsymbol{n}} + \frac{1}{2\mathcal{J}}(\tilde{\boldsymbol{N}})^2 + \frac{1}{2\mathcal{J}}\hat{\boldsymbol{n}}\tilde{\boldsymbol{N}}\,, \tag{2·30a}$$

$$\boldsymbol{H}_{\mathrm{QQ}} = \boldsymbol{H}_{\mathrm{QQ}}^{X} + \boldsymbol{H}_{\mathrm{QQ}}^{Y} + \boldsymbol{H}_{\mathrm{QQ}}^{V}\,, \tag{2·30b}$$

*) We consider it appropriate to define the pairing rotational mode within the monopole-boson space, because it is a mode associated with the monopole-boson condensation. Corresponding to (2·13a)~(2·13c), we have now the set of equations, (2·26), (2·27) and $[\boldsymbol{H}_0 + \boldsymbol{H}_{\mathrm{P}}, i\hat{\boldsymbol{\phi}}] = (1/\mathcal{J})\tilde{\boldsymbol{N}} + (1/2\mathcal{J})\hat{\boldsymbol{n}}$. According to the above definition, the second term $(1/2\mathcal{J})\hat{\boldsymbol{n}}$ should be regarded as representing the coupling effects to the intrinsic quasiparticle modes.

$$\boldsymbol{H}^{X}_{\mathrm{QQ}}=-2\chi q^{2}\frac{(\Omega v^{2}+\tilde{\boldsymbol{N}})\,(\Omega u^{2}-\hat{\boldsymbol{n}}-\tilde{\boldsymbol{N}})}{(\Omega-\hat{\boldsymbol{n}})\,(\Omega-\hat{\boldsymbol{n}}-1)}\sum_{\mu}\boldsymbol{A}^{\dagger}_{2\mu}\boldsymbol{A}_{2\mu}\,,$$

$$\boldsymbol{H}^{Y}_{\mathrm{QQ}}=-\sqrt{2}\,\chi q^{2}\Big\{\frac{\Omega(u^{2}-v^{2})-2\tilde{\boldsymbol{N}}-\hat{\boldsymbol{n}}}{\Omega-\hat{\boldsymbol{n}}}\sqrt{\frac{(\Omega v^{2}+\tilde{\boldsymbol{N}}+1)\,(\Omega u^{2}-\hat{\boldsymbol{n}}-\tilde{\boldsymbol{N}}+1)}{(\Omega-\hat{\boldsymbol{n}}+1)\,(\Omega-\hat{\boldsymbol{n}}+2)}}$$

$$\times e^{-i\hat{\boldsymbol{\phi}}}\sum_{\mu}\boldsymbol{A}^{\dagger}_{2\mu}\boldsymbol{B}_{2\mu}+\mathrm{h.c.}\Big\}\,,\qquad(2\cdot30\mathrm{c})$$

$$\boldsymbol{H}^{V}_{\mathrm{QQ}}=-\chi q^{2}\Big\{\sqrt{\frac{(\Omega v^{2}+\tilde{\boldsymbol{N}}+1)(\Omega v^{2}+\tilde{\boldsymbol{N}}+2)(\Omega u^{2}-\hat{\boldsymbol{n}}-\tilde{\boldsymbol{N}}+1)(\Omega u^{2}-\hat{\boldsymbol{n}}-\tilde{\boldsymbol{N}}+2)}{(\Omega-\hat{\boldsymbol{n}}+1)\,(\Omega-\hat{\boldsymbol{n}}+2)\,(\Omega-\hat{\boldsymbol{n}}+3)\,(\Omega-\hat{\boldsymbol{n}}+4)}}$$

$$\times e^{-2i\hat{\boldsymbol{\phi}}}\sum_{\mu}\boldsymbol{A}^{\dagger}_{2\mu}\boldsymbol{A}^{\dagger}_{2\mu}+\mathrm{h.c.}\Big\}\,,\qquad(2\cdot30\mathrm{d})$$

where $\boldsymbol{A}^{\dagger}_{2\mu}$ and $\boldsymbol{B}_{2\mu}$ are the pair operators in terms of the ideal quasiparticles, defined by (I·2·17). If we neglect the third and fourth terms in (2·30a), and if we also neglect the terms involving powers of $1/\Omega$ after expanding (2·30b) $\sim$(2·30d) in terms of $1/\Omega$, then the Hamiltonian (2·30) reduces to the conventional P+QQ Hamiltonian in the BCS approximation. We note that the exact expression (2·30) always accompanies the angle operators, $e^{-i\hat{\boldsymbol{\phi}}}$ etc., whenever the Hamiltonian changes the seniority quantum numbers represented by the ideal quasiparticle numbers. In other words, the presence of the angle operator is here playing the role of assuring the nucleon-number conservation. This is readily understood by noting that

$$[\boldsymbol{H},\hat{\Pi}]=[\boldsymbol{H},\tilde{\boldsymbol{N}}]+[\boldsymbol{H},\tfrac{1}{2}\hat{\boldsymbol{n}}]=0\,,\qquad(2\cdot31)$$

whereas $[\boldsymbol{H},\tilde{\boldsymbol{N}}]\neq0$ and $[\boldsymbol{H},\hat{\boldsymbol{n}}]\neq0$.

§ 3. Use of canonical transformation method with auxiliary variables

3.1. *Introduction of auxiliary number- and angle-operators*

We are now in a stage to transform our state vectors and the Hamiltonian into a representation which is analogous to the one in the particle-rotor model. For this purpose, we use the canonical transformation method with auxiliary variables.[14),15)]

First, we introduce redundant number- and angle-variables (i.e., auxiliary variables), $\mathring{\Pi}$ and $\mathring{\boldsymbol{\phi}}$, which satisfy the canonical commutation relation

$$[\mathring{\boldsymbol{\phi}},\mathring{\Pi}]=i\,,\qquad(3\cdot1)$$

and are independent of the ideal quasiparticle operators $(\boldsymbol{a}_{\alpha}^{\dagger},\boldsymbol{a}_{\alpha})$ and the monopole boson operators $(\boldsymbol{b}^{\dagger},\boldsymbol{b})$:

$$[\mathring{\boldsymbol{\phi}},\boldsymbol{a}_{\alpha}^{\dagger}]=[\mathring{\boldsymbol{\phi}},\boldsymbol{a}_{\alpha}]=[\mathring{\boldsymbol{\phi}},\boldsymbol{b}^{\dagger}]=[\mathring{\boldsymbol{\phi}},\boldsymbol{b}]=0\,,$$
$$[\mathring{\Pi},\boldsymbol{a}_{\alpha}^{\dagger}]=[\mathring{\Pi},\boldsymbol{a}_{\alpha}]=[\mathring{\Pi},\boldsymbol{b}^{\dagger}]=[\mathring{\Pi},\boldsymbol{b}]=0\,.\qquad(3\cdot2)$$

In order to compensate for the overcompleteness in the degrees of freedom due to the introduction of the auxiliary variables, we impose on the state vectors a supplementary condition

$$\mathring{\boldsymbol{\phi}}|\Psi\rangle=0\,. \tag{3·3}$$

Since the original Hamiltonian $\boldsymbol{H}$ is independent of the auxiliary variables introduced, i.e.,

$$[\boldsymbol{H},\mathring{\Pi}]=[\boldsymbol{H},\mathring{\boldsymbol{\phi}}]=0\,, \tag{3·4}$$

the Schrödinger equation

$$\boldsymbol{H}|\Psi\rangle=E|\Psi\rangle \tag{3·5}$$

with the supplementary condition (3·3) is exactly equivalent to the starting Schrödinger equation without auxiliary variables.

3.2. *Canonical transformation*

Now, let us define the following canonical transformation:

$$\begin{aligned} &U=U_1U_2U_1\,,\\ &U_1=\exp i\mathring{\boldsymbol{\phi}}\hat{\Pi},\quad U_2=\exp -i\mathring{\Pi}\hat{\boldsymbol{\phi}}\,, \end{aligned} \tag{3·6}$$

where $\hat{\Pi}$ and $\hat{\boldsymbol{\phi}}$ are given by (2·24) and (2·23), respectively. The following relations are then easily derived:

$$\begin{aligned} &U\hat{\Pi}U^{-1}=\mathring{\Pi},\qquad U\hat{\boldsymbol{\phi}}U^{-1}=\mathring{\boldsymbol{\phi}}\,,\\ &U\mathring{\Pi}U^{-1}=-\hat{\Pi},\quad U\mathring{\boldsymbol{\phi}}U^{-1}=-\hat{\boldsymbol{\phi}}\,. \end{aligned} \tag{3·7}$$

This implies that, in the representation after the canonical transformation, the number- and angle-operators $\hat{\Pi}$ and $\hat{\boldsymbol{\phi}}$ are completely replaced by the redundant variables $\mathring{\Pi}$ and $\mathring{\boldsymbol{\phi}}$, respectively. After the canonical transformation, the Schrödinger equation (3·5) becomes

$$\mathcal{H}|\mathring{\Psi}\rangle=E|\mathring{\Psi}\rangle \tag{3·8}$$

with the supplementary condition

$$\hat{\boldsymbol{\phi}}|\mathring{\Psi}\rangle=0\,, \tag{3·9}$$

where

$$\mathcal{H}=U\boldsymbol{H}U^{-1},\quad |\mathring{\Psi}\rangle=U|\Psi\rangle\,. \tag{3·10}$$

Equation (3·4) is transformed into

$$[\mathcal{H},\hat{\Pi}]=[\mathcal{H},\hat{\boldsymbol{\phi}}]=0\,, \tag{3·11}$$

which implies that the number- and angle-degrees of freedom $(\hat{\Pi}, \hat{\phi})$ involved implicitly in the original Hamiltonian $\boldsymbol{H}$ are completely replaced by the auxiliary variables $(\mathring{\Pi}, \mathring{\phi})$. Explicitly, the boson operators are transformed as

$$U\tilde{\boldsymbol{b}}^{\dagger}U^{-1} = -\sqrt{\Pi} + \sqrt{\mathring{\Pi} - \tfrac{1}{2}\hat{\boldsymbol{n}}}\, e^{i\mathring{\phi}}, \tag{3·12}$$

$$U\tilde{\boldsymbol{N}}U^{-1} = (\mathring{\Pi} - \Pi) - \tfrac{1}{2}\hat{\boldsymbol{n}}, \tag{3·13}$$

while the following operators are invariant under the U-transformation:

$$U\hat{\boldsymbol{n}}U^{-1} = \hat{\boldsymbol{n}}, \tag{3·14}$$

$$U\boldsymbol{B}^{\dagger}_{J\mu}U^{-1} = \boldsymbol{B}^{\dagger}_{J\mu}, \tag{3·15}$$

$$U(e^{-i\hat{\phi}}\boldsymbol{A}^{\dagger}_{J\mu})\,U^{-1} = e^{-i\hat{\phi}}\boldsymbol{A}^{\dagger}_{J\mu}. \tag{3·16}$$

3.3. *Transformed state vectors*

The original state vectors expressed in the ideal boson-quasiparticle space, (I·2·19), are rewritten in terms of the angle-operator $e^{i\hat{\phi}}$ as

$$\begin{aligned}\frac{1}{\sqrt{n!}}\frac{1}{\sqrt{p!}}(\boldsymbol{A}_2^{\dagger})^{n}_{\alpha JM}(\boldsymbol{b}^{\dagger})^{p}|0\rangle|0) &= \frac{1}{\sqrt{n!}}(\boldsymbol{A}_2^{\dagger})^{n}_{\alpha JM}\, e^{ip\hat{\phi}}|0\rangle|0) \\ &= \frac{1}{\sqrt{n!}}(e^{-i\hat{\phi}}\boldsymbol{A}_2^{\dagger})^{n}_{\alpha JM}\, e^{i\Pi\hat{\phi}}|0\rangle|0) \\ &= \frac{1}{\sqrt{n!}}(e^{-i\hat{\phi}}\boldsymbol{A}_2^{\dagger})^{n}_{\alpha JM}|0\rangle|\Psi_0). \quad (n+p=\Pi)\end{aligned} \tag{3·17}$$

After the canonical transformation U, they are transformed into the form

$$\frac{1}{\sqrt{n!}}(\boldsymbol{A}_2^{\dagger})^{n}_{\alpha JM}|0\rangle\otimes e^{i\Pi\mathring{\phi}}|\mathring{0}), \tag{3·18}$$

which takes precisely the same form as in the particle-rotor model: The part $(n!)^{-1/2}(\boldsymbol{A}_2^{\dagger})^{n}_{\alpha JM}|0\rangle$ represents the intrinsic wave function while the part $e^{i\Pi\mathring{\phi}}|\mathring{0})$ stands for the rotating wave function, with $|\mathring{0})$ being the transformed boson vacuum, $|\mathring{0}) = U|0)$. In obtaining (3·18), we have used the supplementary condition (3·9). The physical meaning of this condition is now clear;[14] that is, it expresses the requirement that, after the canonical transformation, the ideal quasiparticle excitation should be confined in the body-fixed frame.

Combining the relations (3·13) and (3·14) with the representation (3·18) we see that the following analogy to the well-known particle-rotor model holds in the representation after the canonical transformation; the monopole-boson-number fluctuation operator, $\tilde{\boldsymbol{N}} = \hat{\boldsymbol{N}} - \Pi$, corresponds to the angular momentum $\boldsymbol{R}$ of the collective rotation, the auxiliary nucleon-pair number measured from Π, $\mathring{\Pi} - \Pi$, to the total angular momentum $\boldsymbol{I}$, and the number of ideal quasiparticle pairs, $\frac{1}{2}\hat{\boldsymbol{n}}$,

to the intrinsic angular momentum $\boldsymbol{j}$ of the particle-rotor model.

If we only consider a system with fixed nucleon-pair number $\mathit{\Pi}$, then the rotational wave function $e^{i\Pi\mathring{\phi}}|\mathring{0}\rangle$ is common to all intrinsic states and therefore does not play any role. At the same time, *the nucleon-number conservation is always assured* by the use of the effective Hamiltonian obtained after the canonical transformation, even when we only consider the intrinsic state vectors

$$\left\{\frac{1}{\sqrt{n!}}(\boldsymbol{A}_2^\dagger)^n_{\alpha J\mathcal{M}}|0\rangle\,,\quad n=0,1,2,\cdots,\mathit{\Pi}\right\}, \tag{3·19}$$

in which the number of ideal quasiparticle pairs is *not* conserved.

3.4. *Transformed Hamiltonian*

After the canonical transformation, the P+QQ Hamiltonian (2·30) takes the following form:

$$\mathcal{H}=U\boldsymbol{H}U^{-1}=\mathcal{H}_0+\mathcal{H}_{\mathrm{P}}+\mathcal{H}_{\mathrm{QQ}}\,, \tag{3·20}$$

$$\mathcal{H}_0+\mathcal{H}_{\mathrm{P}}=W+E\hat{\boldsymbol{n}}-\frac{1}{2\mathcal{J}}\left(\frac{\hat{\boldsymbol{n}}}{2}\right)^2, \tag{3·20a}$$

$$\mathcal{H}_{\mathrm{QQ}}=\mathcal{H}^X_{\mathrm{QQ}}+\mathcal{H}^Y_{\mathrm{QQ}}+\mathcal{H}^V_{\mathrm{QQ}}\,,$$

$$\mathcal{H}^X_{\mathrm{QQ}}=-2\chi q^2\frac{(\Omega v^2-\frac{1}{2}\hat{\boldsymbol{n}})(\Omega u^2-\frac{1}{2}\hat{\boldsymbol{n}})}{(\Omega-\hat{\boldsymbol{n}})\,(\Omega-\hat{\boldsymbol{n}}-1)}\sum_\mu \boldsymbol{A}^\dagger_{2\mu}\boldsymbol{A}_{2\mu}\,, \tag{3·20b}$$

$$\mathcal{H}^Y_{\mathrm{QQ}}=-\sqrt{2}\,\chi q^2\left\{\frac{\Omega(u^2-v^2)}{\Omega-\hat{\boldsymbol{n}}}\sqrt{\frac{(\Omega v^2-\frac{1}{2}\hat{\boldsymbol{n}}+1)\,(\Omega u^2-\frac{1}{2}\hat{\boldsymbol{n}}+1)}{(\Omega-\hat{\boldsymbol{n}}+1)\,(\Omega-\hat{\boldsymbol{n}}+2)}}\sum_\mu \boldsymbol{A}^\dagger_{2\mu}\boldsymbol{B}_{2\mu}+\mathrm{h.c.}\right\}, \tag{3·20c}$$

$$\mathcal{H}^V_{\mathrm{QQ}}=-\chi q^2\left\{\sqrt{\frac{(\Omega v^2-\frac{1}{2}\hat{\boldsymbol{n}}+1)(\Omega v^2-\frac{1}{2}\hat{\boldsymbol{n}}+2)(\Omega u^2-\frac{1}{2}\hat{\boldsymbol{n}}+1)(\Omega u^2-\frac{1}{2}\hat{\boldsymbol{n}}+2)}{(\Omega-\hat{\boldsymbol{n}}+1)\,(\Omega-\hat{\boldsymbol{n}}+2)\,(\Omega-\hat{\boldsymbol{n}}+3)\,(\Omega-\hat{\boldsymbol{n}}+4)}}\right.$$
$$\left.\times\sum_\mu \boldsymbol{A}^\dagger_{2\mu}\boldsymbol{A}^\dagger_{2\bar{\mu}}+\mathrm{h.c.}\right\}. \tag{3·20d}$$

In the course of obtaining the above equation, 1) we have dropped the operator $e^{-i\hat{\phi}}$ and 2) replaced the operator $\mathring{\mathit{\Pi}}$ and $(\Omega-\mathring{\mathit{\Pi}})$ by their eigenvalues $\mathit{\Pi}=\Omega v^2$ and $\Omega-\mathit{\Pi}=\Omega u^2$, respectively. This is because the state vectors on which $\mathcal{H}$ operates always take the form (3·18) satisfying the supplementary condition (3·9). The transformed Hamiltonian (3·20) may be regarded as an effective intrinsic Hamiltonian (for the system with nucleon number $\mathcal{N}=2\mathit{\Pi}$) acting on the intrinsic state vectors (3·19). If we neglect the third term of (3·20a), and if we also neglect the higher-order terms involving powers of $1/\Omega$ after expanding $\mathcal{H}_{\mathrm{QQ}}$ in terms of $1/\Omega$, then (3·20) reduces to the conventional quasiparticle Hamiltonian in the BCS approximation.

3.5. *Transformed nucleon-pair operators*

In the same way as above, the nucleon-pair operators defined by (I·2·1) are expressed after the U-transformation as

$$\begin{aligned} A^{\dagger}_{2\mu} \to & -\frac{\sqrt{2(\mathring{\Pi}-\frac{1}{2}\hat{\boldsymbol{n}})\,(\Omega-\mathring{\Pi}-\frac{1}{2}\hat{\boldsymbol{n}}+1)}}{\Omega-\hat{\boldsymbol{n}}}\, e^{i\mathring{\Phi}}\mathring{\boldsymbol{B}}^{\dagger}_{2\mu} \\ & +\sqrt{\frac{(\Omega-\mathring{\Pi}-\frac{1}{2}\hat{\boldsymbol{n}}+1)(\Omega-\mathring{\Pi}-\frac{1}{2}\hat{\boldsymbol{n}}+2)}{(\Omega-\hat{\boldsymbol{n}}+1)\,(\Omega-\hat{\boldsymbol{n}}+2)}}\, e^{i\mathring{\Phi}}\boldsymbol{A}^{\dagger}_{2\mu} \\ & -\sqrt{\frac{(\mathring{\Pi}-\frac{1}{2}\hat{\boldsymbol{n}})(\mathring{\Pi}-\frac{1}{2}\hat{\boldsymbol{n}}-1)}{(\Omega-\hat{\boldsymbol{n}})\,(\Omega-\hat{\boldsymbol{n}}-1)}}\, e^{i\mathring{\Phi}}\boldsymbol{A}_{2\mu}, \end{aligned} \tag{3·21}$$

$$\begin{aligned} B^{\dagger}_{2\mu} \to & \quad \frac{\Omega(u^2-v^2)}{\Omega-\hat{\boldsymbol{n}}}\boldsymbol{B}^{\dagger}_{2\mu} \\ & +\sqrt{\frac{2\,(\Omega v^2-\frac{1}{2}\hat{\boldsymbol{n}}+1)\,(\Omega u^2-\frac{1}{2}\hat{\boldsymbol{n}}+1)}{(\Omega-\hat{\boldsymbol{n}}+1)\,(\Omega-\hat{\boldsymbol{n}}+2)}}\boldsymbol{A}^{\dagger}_{2\mu} \\ & +\sqrt{\frac{2\,(\Omega v^2-\frac{1}{2}\hat{\boldsymbol{n}})\,(\Omega u^2-\frac{1}{2}\hat{\boldsymbol{n}})}{(\Omega-\hat{\boldsymbol{n}})\,(\Omega-\hat{\boldsymbol{n}}-1)}}\boldsymbol{A}_{2\mu}. \end{aligned} \tag{3·22}$$

In (3·21), we have retained the operator $\mathring{\Pi}$, instead of replacing it by its eigenvalue as in (3·22), in order to emphasize that it operates on the final state. The appearance of the angle operator $e^{i\mathring{\Phi}}$ in (3·21) expresses the fact that $A^{\dagger}_{2\mu}$ increases the nucleon-pair number Π by one unit. Needless to say, in the representation after the canonical transformation, the change in the number of ideal quasiparticles (in the intrinsic space) does not interfere at all with the requirement of nucleon-number conservation.

§ 4. Convergence of perturbative expansion

4.1. *Expansion in terms of $1/\Omega$*

The formulation presented above is exact. Therefore, the diagonalization of the effective Hamiltonian (3·20) within the intrinsic states (3·19) is equivalent to the diagonalization of the original Hamiltonian (I·2·29) in the number-conserving basis states (3·17). Thus, in the rather special case of single j-shell, the interplay between the pairing and intrinsic (quasiparticle) modes of excitation can be treated exactly in either representation. On the other hand, in the general many j-shell case, the pairing vibrational modes come into play in addition to the pairing rotations under consideration. In this case, it appears more appropriate to adopt the quasiparticle representation (rather than the original nucleon representation), and to develop the mode-mode coupling theory in a form of perturbative expansion in terms of the small parameter $1/\Omega$.

In the single j-shell model, one can estimate the convergence of this expansion

as follows. The pairing Hamiltonian, $\mathcal{H}_0+\mathcal{H}_P$, terminates at the order $1/\Omega$; thus giving the exact solution already at this order. As for the quadrupole force, the coupling effects are originally contained in the operators $\hat{u}\hat{v}$ and $(\hat{u}^\dagger\hat{u}-\hat{v}^\dagger\hat{v})$, see (I·2·29). After the canonical transformation, they take the following forms:

$$\hat{u}\hat{v}\to\frac{\sqrt{(\Omega v^2-\frac{1}{2}\hat{n}+1)(\Omega u^2-\frac{1}{2}\hat{n})}}{\Omega-\hat{n}}$$

$$=uv\left\{1-\frac{(u^2-v^2)^2}{2u^2v^2}\frac{\hat{n}}{2\Omega}+\frac{1}{2\Omega v^2}+\cdots\right\}, \tag{4·1}$$

$$\hat{u}^\dagger\hat{u}-\hat{v}^\dagger\hat{v}\to\frac{\Omega(u^2-v^2)}{\Omega-\hat{n}}$$

$$=(u^2-v^2)\left\{1+\frac{\hat{n}}{\Omega}+\left(\frac{\hat{n}}{\Omega}\right)^2+\cdots\right\}. \tag{4·2}$$

We immediately see that n/Ω is a crucial quantity which determines the convergence property of this expansion: (4·2) is strongly dependent upon n/Ω, whereas (4·1) only weakly depends especially in the middle of the j-shell. Namely, (4·2) greatly increases compared with its BCS value, (u^2-v^2), and approaches unity as the seniority $v=n$ increases towards the maximum value $v_{\max}=\mathcal{N}$.*) Consequently, the coupling effect is expected[1] to manifest mainly through the enhancement of $\mathcal{H}^Y_{QQ}$ as well as the $1/\Omega$ effect of the pairing force; see the explicit expression of $\mathcal{H}^Y_{QQ}$ in (3·20c).

4.2. *Numerical examples*

With the same approximation scheme as described in I, the effective Hamiltonian (3·20) may be transcribed into the boson representation (A·1) given in the Appendix. In obtaining the boson Hamiltonian (A·1), approximations have been introduced only for the intrinsic matrix elements, and thus the dynamical couplings to the pairing rotation are taken into account to the infinite order. Consequently, the diagonalization of (A·1) within the d-boson space gives the same results as Figs. 1(a), 2 and 3(a) presented in I. Now, we compare these results with those of the perturbative treatment of the mode-mode couplings. The perturbation implies the expansion of (A·1) in terms of $1/\Omega$, with the order unity corresponding to the conventional BCS approximation. Figures 1∼3 show the results of calculation in which the coupling effects are taken into account to the order $1/\Omega$ or $1/\Omega^2$. The adopted parameters are the same as in I, i.e., $j=29/2$, $\mathcal{N}=12$ and $G\Omega=2$[MeV]. The excitation spectra, Figs. 1 and 2, should be compared with Figs. 1 and 3 in I, respectively. Figure 3 shows a closer comparison among the results of the perturbative calculation (to the order $1/\Omega$ and $1/\Omega^2$), of the

*) We here assume that $\mathcal{N}$ is smaller than Ω. If $\mathcal{N}$ is larger than Ω, then $\mathcal{N}$ should be replaced by $(\Omega-\mathcal{N})$.

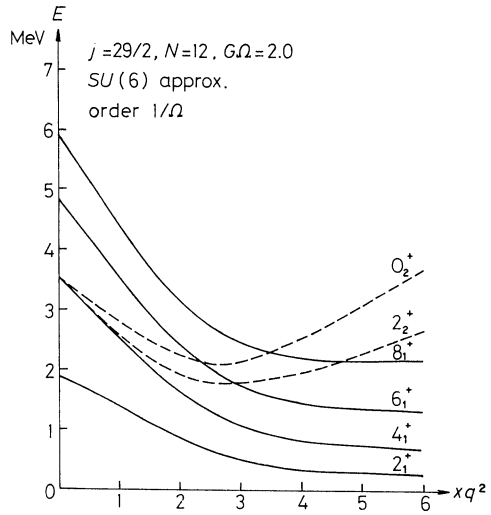

Fig. 1. Energy eigenvalues of the yrast and the second 0^+, 2^+ states in the $j=29/2$, $\mathcal{N}=12$ system, calculated as functions of the quadrupole-force strength χq^2. The effects of pairing rotation are taken into account to the order $1/\Omega$. The pairing-force strength G is fixed at $2/\Omega=0.133$(MeV) which corresponds to the quasiparticle energy of 1 MeV in the BCS approximation. The many-phonon norm matrices are evaluated under the $SU(6)$ approximation.[1)]

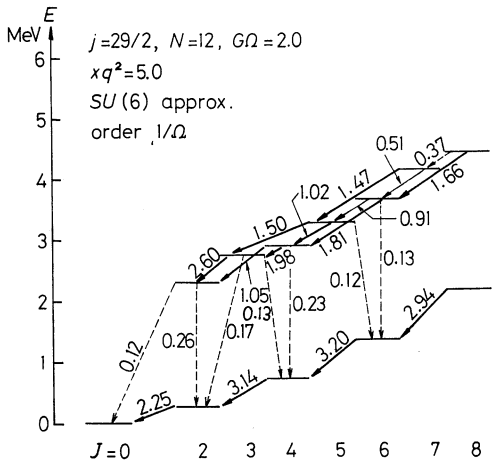

Fig. 2. Excitation energy versus angular momentum for the yrast and yrare states, calculated by taking into account the effects of pairing rotation to the order $1/\Omega$. The quadrupole-force strength χq^2 is fixed at 5.0 (MeV). Other parameters are the same as in Fig. 1 Numbers on the arrows denote the B(E2) values in unit of the B(E2; $2^+\to0^+$) value in the Tamm-Dancoff approximation.

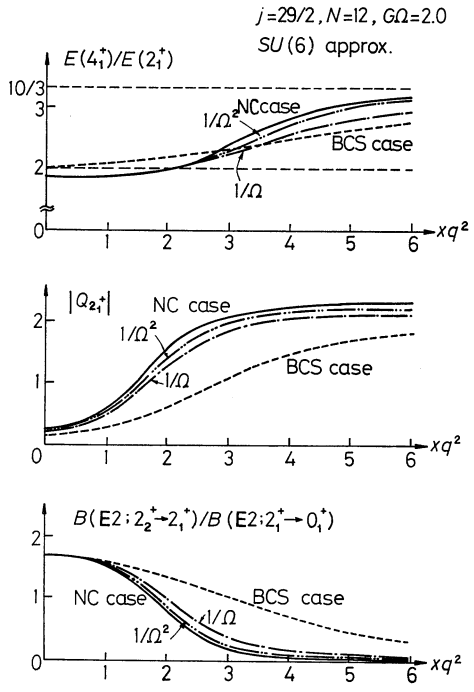

Fig. 3. Various quantities which characterize the band structure, calculated as functions of the quadrupole-force strength χq^2: Excitation energy ratio $E(4_1^+)/E(2_1^+)$: Absolute value of the spectroscopic quadrupole moment for the first 2^+ state (arbitrary unit): Ratio of the reduced transition probabilities B(E2; $2_2^+\to2_1^+$)/B(E2; $2_1^+\to0_1^+$). Adopted parameters are the same as in Fig. 1. Dotted line shows the results in the BCS approximation; dash-dotted line those including the effects of the pairing rotation to the order $1/\Omega$; dash-doubly-dotted line to the order $1/\Omega^2$, solid line to the infinite order (i.e., in the number-conserving case).

BCS approximation (to the order unity), and of the nucleon-number conserving case (to the infinite order). As emphasized in I, the transition from vibrational to rotational excitation patterns is greatly enhanced by the coupling effects. Figure 3 shows that this enhancement is clearly seen already when the leading-order coupling effect, the order $1/\Omega$, is taken into account. If the coupling effects are considered further to the order $1/\Omega^2$, then the perturbative treatment almost reproduces the results of number-conserving treatment also quantitatively.

§ 5. Concluding remarks

We have developed a microscopic method to treat the mode-mode couplings between many-quasiparticle excitations and pairing rotations. The canonical transformation method with auxiliary number- and angle-variables has been employed to extract, without violating the Pauli principle, the pairing rotational degree of freedom. In the special case of single j-shell, the mode-mode couplings can be treated exactly, the analytical expressions of which have been used to test the convergence of the perturbative expansion of the couplings in terms of $1/\Omega$. The numerical examples presented in § 4 indicate that the major effect of the pairing rotations may be included by only taking the low-order coupling effects into account. Thus, in a succeeding paper, we shall extend the formulation presented here into the general many j-shell case in a form suitable for such a perturbative expansion.

Acknowledgements

We are grateful to Professor M. Yamamura for discussions. One of us (T.S.) thanks the Yukawa Foundation for the fellowship. Numerical calculations were carried out by using FACOM M-190 at the Data Processing Center of Kyoto University.

Appendix

If the effective Hamiltonian (3·20) is mapped onto the boson space such that there is a one-to-one correspondence between the many-phonon states and the d-boson states, i.e.,

$$\mathcal{N}_{n\alpha J}^{-1/2}\frac{1}{\sqrt{n!}}(A_2^\dagger)^n_{\alpha JM}|0\rangle \leftrightarrow \frac{1}{\sqrt{n!}}(d^\dagger)^n_{\alpha JM}|0),$$

and if the $SU(6)$ approximation[1] to the norm $\mathcal{N}_{n\alpha J}$ of the many-phonon states is adopted, then we obtain the boson Hamiltonian given below:

$$\mathcal{H}\to\mathring{\mathcal{H}}=W-\frac{1}{2\mathcal{J}}(\hat{n}_d)^2+\hat{\omega}_d'\cdot\hat{n}_d$$

$$+\frac{1}{2}\sum_{\lambda\mu}\hat{f}_X'(\lambda)\,(d^\dagger d^\dagger)_{\lambda\mu}(dd)_{\lambda\mu}$$
$$+\{\hat{f}_Y'\sum_{\mu}(d^\dagger d^\dagger)_{2\mu}d_\mu+\text{h.c.}\}$$
$$+\{\hat{f}_V'(d^\dagger d^\dagger)_{00}+\text{h.c.}\}, \tag{A·1}$$

where

$$\hat{\omega}_d'=2E-2\chi q^2\frac{(\Omega u^2-\hat{n}_d)\,(\Omega v^2-\hat{n}_d)}{(\Omega-2\hat{n}_d)\,(\Omega-2\hat{n}_d-1)}, \tag{A·1a}$$

$$\hat{f}_X'(\lambda)=C_X(\lambda)\cdot\frac{(\Omega u^2-\hat{n}_d)\,(\Omega v^2-\hat{n}_d)}{(\Omega-2\hat{n}_d)\,(\Omega-2\hat{n}_d-1)}, \tag{A·1b}$$

$$\hat{f}_Y'=C_Y\cdot\frac{\Omega(u^2-v^2)}{\Omega-2\hat{n}_d}\sqrt{\frac{(\Omega u^2-\hat{n}_d+1)\,(\Omega v^2-\hat{n}_d+1)}{\Omega(\Omega-2\hat{n}_d+1)}}, \tag{A·1c}$$

$$\hat{f}_V'=C_V\sqrt{\frac{(\Omega u^2-\hat{n}_d+1)(\Omega u^2-\hat{n}_d+2)(\Omega v^2-\hat{n}_d+1)(\Omega v^2-\hat{n}_d+2)}{\Omega^2(\Omega-2\hat{n}_d+1)\,(\Omega-2\hat{n}_d+3)}}. \tag{A·1d}$$

Evidently, this is equivalent to the boson Hamiltonian (I·3·11) which operates on the *sd*-boson space $\{(n_s!n_d!)^{-1/2}(s^\dagger)^{n_s}(d^\dagger)^{n_d}_{\alpha JM}|0)\}$.

In the same way, we obtain boson representations of the nucleon-pair operators, $A^\dagger_{2\mu}$ and $B^\dagger_{2\mu}$, as

$$A^\dagger_{2\mu}\to\mathring{A}^\dagger_{2\mu}=\sqrt{\frac{(\Omega u^2-\hat{n}_d+1)\,(\Omega u^2-\hat{n}_d+2)}{\Omega(\Omega-2\hat{n}_d+1)}}\,e^{i\mathring{\phi}}d_\mu^\dagger$$
$$-\sqrt{\frac{(\Omega v^2-\hat{n}_d)\,(\Omega v^2-\hat{n}_d+1)}{\Omega(\Omega-2\hat{n}_d-1)}}\,e^{i\mathring{\phi}}d_{\tilde{\mu}}$$
$$+10\sqrt{2}\begin{Bmatrix}2&2&2\\j&j&j\end{Bmatrix}\frac{\sqrt{(\Omega v^2-\hat{n}_d)\,(\Omega u^2-\hat{n}_d+1)}}{\Omega-2\hat{n}_d}\,e^{i\mathring{\phi}}(d^\dagger d)_{2\mu}, \tag{A·2}$$

$$B^\dagger_{2\mu}\to\mathring{B}^\dagger_{2\mu}=\sqrt{\frac{2(\Omega v^2-\hat{n}_d+1)(\Omega u^2-\hat{n}_d+1)}{\Omega(\Omega-2\hat{n}_d+1)}}d_\mu^\dagger$$
$$+\sqrt{\frac{2(\Omega v^2-\hat{n}_d)\,(\Omega u^2-\hat{n}_d)}{\Omega(\Omega-2\hat{n}_d-1)}}d_{\tilde{\mu}}$$
$$-10\begin{Bmatrix}2&2&2\\j&j&j\end{Bmatrix}\frac{\Omega(u^2-v^2)}{\Omega-2\hat{n}_d}(d^\dagger d)_{2\mu}, \tag{A·3}$$

which are equivalent to (I·3·8) and (I·3·9), respectively. In the expression of the two-nucleon transfer operator, (A·2), the u, v factors are those pertinent to the final states.

References

1) T. Suzuki, M. Fuyuki and K. Matsuyanagi, Prog. Theor. Phys. **61** (1979), 1682.
2) A. Bohr, *Nuclear Structure: Dubna Symposium 1968* (International Atomic Energy Agency, Vienna, 1969), p. 179.
3) A. Bohr and B. R. Mottelson, *Nuclear Structure,* vol. II (Benjamin, 1975).
4) D. R. Bès and R. A. Broglia, *Proceedings of the International School of Physics, "Enrico Fermi",* course LXIX (1977), p. 55.
5) K. Hara and S. Kusuno, Nucl. Phys. **A245** (1975), 147.
6) E. R. Marshalek and J. Weneser, Phys. Rev. **C2** (1970), 1682.
7) D. J. Thouless, Nucl. Phys. **21** (1960), 225; **22** (1961), 78.
8) T. Kammuri, Prog. Theor. Phys. **37** (1967), 1131.
9) E. R. Marshalek and J. Weneser, Ann. of Phys. **53** (1969), 569.
10) R. Beck, M. Kleber and H. Schmidt, Z. Phys. **250** (1972), 155.
11) S. T. Belyaev and V. G. Zelevinsky, Yadern Fiz. **16** (1972), 1195; Soviet J. Nucl. Phys. **16** (1973), 657.
12) R. V. Jolos, V. G. Kartavenko and V. Rybarska, Teor, Mat. Fiz. **20** (1974), 353; Theor. Math. Phys. **20** (1975), 873.
13) V. Alessandrini, D. R. Bès and B. Machet, Phys. Letters **80B** (1978), 9; Nucl. Phys. **B142** (1978), 489.
14) S. Hayakawa and T. Marumori, Prog. Theor. Phys. **18** (1957), 396.
15) A. Kuriyama, T. Marumori, K. Matsuyanagi, F. Sakata and T. Suzuki, Prog. Theor. Phys. Suppl. No. 58 (1975), 9.
16) T. Suzuki and K. Matsuyanagi, Prog. Theor. Phys. **56** (1976), 1156.

1.C

Nuclear Physics **A348** (1980) 237–260;

NUCLEAR FIELD THEORY TREATMENT OF COMPLEX NUCLEAR SPECTRA

R. A. BROGLIA

The Niels Bohr Institute, University of Copenhagen, DK-2100 Copenhagen Ø, Denmark

K. MATSUYANAGI

Kyoto University, Department of Physics, Kyoto, Japan

and

H. SOFIA and A. VITTURI

The Niels Bohr Institute, University of Copenhagen, DK-2100 Copenhagen Ø, Denmark

Received 24 March 1980

Abstract: Closed forms for the many-body matrix elements of the pairing-plus-quadrupole hamiltonian can be obtained within the framework of the nuclear field theory, making the ansatz that pairs of fermions can only couple to $\lambda = 0$ and $\lambda = 2$. This ansatz, which otherwise is hardly justified, leads to strong simplifications in the calculations. The resulting model seems to be very similar to a microscopic version of the interacting boson model.

1. Introduction

The treatment of the interplay between collective and fermion degrees of freedom provided by the nuclear field theory [1, 2]) (NFT) is perturbative and graphical. Thus, no diagonalizations are to be performed but the different transitions as well as energies are to be calculated by summing up the corresponding graphical contributions to the order † in $1/\Omega$ desired. The basis states are product states of the collective vibrational modes observed in nature, i.e. surface modes, pairing vibrations, spin and isospin modes and of single particles ††.

The central feature of the NFT is that fermions and bosons are treated on par. Thus, the Pauli principle is properly taken care of at every order of perturbation.

In the present paper we attempt to extend the scope of the NFT to deal with some non-perturbative situations, in particular with moderately anharmonic nuclear

† The small parameter of the NFT is the ratio n/Ω of the number of active pairs of particles n, and the degeneracy of the single-particle subspace in which they move.

†† Note that the elementary modes of excitation which can be viewed as building blocks of the nuclear spectrum are: (a) single particles [3]), (b) shape vibrations and rotations [4]), (c) spin and isospin modes [2]), and (d) pairing vibrations and rotations [2, 5]).

spectra. This is done by utilizing the result that particles moving in single-particle orbitals and interacting through a pairing and a quadrupole force display the main properties of rotational, vibrational and transitional spectra [7]). We also use the simplifying ansatz of the quadrupole phonon model [QPM; cf. refs. [12,13])] and of the interacting boson model [IBM: cf. ref. [6]) and references therein].

2. The rules of the game

The basic mechanism determining the properties of the nuclear spectrum is the competition between the shell structure and the pairing and quadrupole correlations. Many model studies of these correlations have been carried out in single j shells. Recently, special attention has been paid [8-10]) to solutions in which the residual interaction is allowed to act only among pairs of fermions coupled to $\lambda = 0$ or $\lambda = 2$ [cf. also sect. 3 of ref. [6])]. The results compare well with full shell-model diagonalizations [cf. pages 93 and 121 of ref. [6]), and refs. [10,11])], for a choice of the parameters leading to vibrational and to moderately anharmonic spectra. In this case, many of the low-lying levels lie within the $\lambda = 0, 2$ fermion subspace, (SD subspace), and the overlap between the approximate and "exact" wave functions is ~ 0.95. For parameters leading to more rotational spectra the wave function overlaps become smaller, and a larger number of levels lie outside the SD subspace [11]).

In the rest of the present paper we thus assume that the SD subspace model provides an adequate description of some of the basic properties of vibrational and moderately anharmonic complex nuclear spectra. Our first task is then that of identifying the NFT graphs which give rise to the pairing-plus-quadrupole matrix elements obtained in the SD space.

In refs. [9,10]) it has been shown that there exists a mapping † between the SD subspace and the sd subspace spanned by the states of the type $|n_s, n_d\rangle \equiv N(s^+)^{n_s}(d^+)^{n_d}|0\rangle$, the pair of operators s^+, s and d^+, d fulfilling exact boson conmutation relations. The corresponding matrix elements of the different physical operators can be obtained within the framework of the NFT utilizing the following rules †† [cf. also ref. [14])]:

(a) The basis states are monopole and quadrupole pairing modes or single-particle states (odd case) which are determined by the energy and particle-vibration coupling strength.

† The operators $A^+_{JM} \equiv \sqrt{\frac{1}{2}}[c^+_j c^+_j]_{JM}$ ($J = 0, 2$) and $B^+_{J'M'}$ ($J' = 0, 1, 2, 3, 4$) of the SD fermion subspace, which do not form a closed algebra, can be mapped into the 35 generators (d^+s), (s^+d) and $(d^+d)_{J'M'}$ of the group SU(6). The mapping allows one to write the pairing-plus-quadrupole hamiltonian in terms of these generators. The calculation of matrix elements in the sd subspace is much simpler than in the SD space. Note that the approximation $c_0 = c_2 = c_4$ is introduced [9]) in working out the SD → sd mapping. The relation of this approach to the SU(6) approximation [12]), to the interacting boson model [6]) and to related approaches [13]) has been touched upon in ref. [9]) and will thus not be discussed here.

†† In the calculation of each diagram all the standard NFT rules [1]) of course apply.

(b) All graphs of order $1/\Omega$ leading to interactions between the phonons as well as of the phonons with the eventual odd particle have to be considered. In the case that the d-phonons do not interact in lowest order with the s-bosons, the next order graphical contributions have to be included.

(c) The contribution of each graph associated with processes in which particle number is not changed has to be symmetrized by replacing (n_s+a) by $(n_s+a) \times (1-(n_s-a)/\Omega')$, $\Omega' = \Omega - 2n_d$ being the effective degeneracy left for the correlation of the monopole Cooper pairs.

(d) Graphical contributions to a transition amplitude which also can be obtained by the combined effect of an already included transition amplitude graph, plus the energy diagonalization, are to be excluded.

The above rules have been empirically obtained and are still lacking a "first principle" derivation.

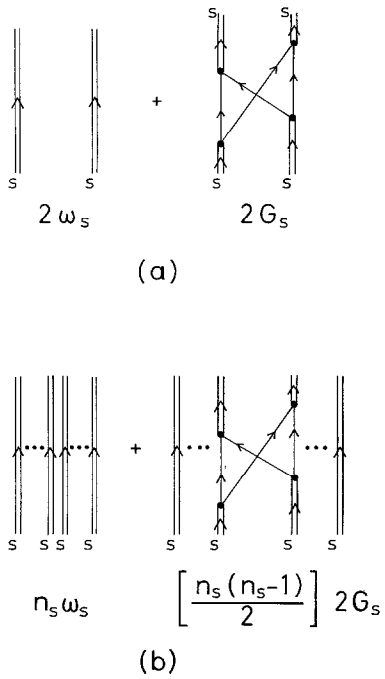

Fig. 1. Lowest-order contributions to the energy of a set of monopole pairing phonons. The single-arrowed lines represent fermions, while the doubled-arrowed lines represent pairing phonons. In (a) the graphs associated with the two-phonon system are shown, and the contributions are written below each graph. The first graph corresponds to the unperturbed propagation of the phonon. The second, to the Pauli principle correction contribution where the phonons exchange particles. The higher-order contributions can be shown [15]) to be zero for the case of a single j-shell. The extension to the case of many phonons shown in (b) is straightforward. The problem is similar to the previous one, but now there are $\frac{1}{2}n_s(n_s-1)$ pairs of phonons interacting.

2.1. PARTICLES MOVING IN A SINGLE j-SHELL AND INTERACTING THROUGH THE MONOPOLE PAIRING FORCE

Defining the pairing hamiltonian as

$$H = -G_0 \Omega A_{00}^{+} A_{00}, \tag{1}$$

where

$$A_{00}^{+} = \sqrt{\tfrac{1}{2}}[c_j^{+} c_j^{+}]_0, \tag{2}$$

the TD correlation energy associated with a two-particle system is

$$\omega_s = -G_0 \Omega. \tag{3}$$

The quantity

$$\Omega = j + \tfrac{1}{2}, \tag{4}$$

is the number of pairs that the j-shell admits.

For a system of four particles, the exact correlation energy is obtained in the NFT already to order $1/\Omega$ (cf. fig. 1a), the higher-order contributions being identically zero [15]). For a system with n_s pairs of particles we obtain (cf. fig. 1b)

$$\begin{aligned} \Delta E &= n_s \omega_s + [\tfrac{1}{2} n_s (n_s - 1)] 2 G_0 \\ &= -\tfrac{1}{4} G_0 N (2\Omega - N + 2), \end{aligned} \tag{5}$$

where $N = 2n_s$ is the total number of particles. This again is the exact answer of the problem [cf. e.g. ref. [16])].

2.2. PERTURBATIVE AND EXACT TRANSITION AMPLITUDES, SYMMETRIZATION

The diagonal matrix element of the quadrupole operator is, in zeroth order, equal to (cf. fig. 2a)

$$\begin{aligned} (Q_2(\mathrm{d} \to \mathrm{d}))_{\text{zeroth}} &= \langle n_s n_d v' \alpha'; I' || Q_2 || n_s n_d v \alpha; I \rangle \\ &= n_d S_1, \end{aligned} \tag{6}$$

where S_1 contains statistical factors and fractional parentage coefficients [cf. appendix A, eq. (A.30)].

Through the diagonalization, the d-bosons feel the presence of the condensator of s-bosons, before and after the electromagnetic field has acted, but not during the time it acts (cf. fig. 2d). According to the rules (b) and (c) one has to calculate all contributions until the lowest-order coupling to the s-phonon condensate is also included. This is achieved in the next order of perturbation [$(1/\Omega$, cf. fig. 2b]. The analytic expression of this contribution is

$$(Q_2(\mathrm{d} \to \mathrm{d}))_{1/\Omega} = 2 \frac{n_d n_s}{\Omega} S_1. \tag{7}$$

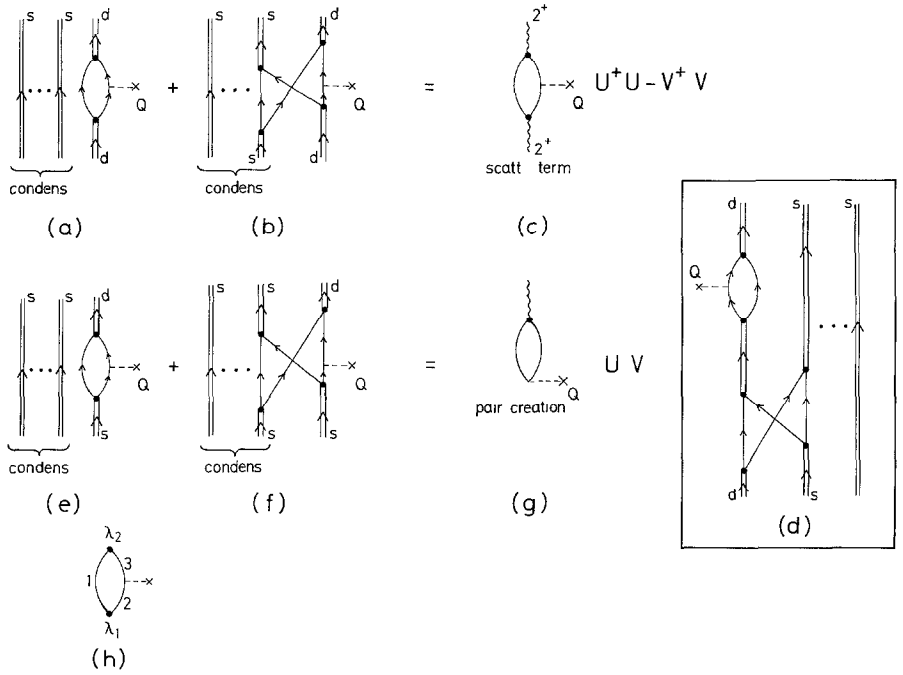

Fig. 2. Graphical contributions to the static quadrupole moment and to the quadrupole electromagnetic transition amplitude. The single-arrowed lines represent particles while the double-arrowed lines represent multipole pairing phonons. The dotted horizontal lines stand for the single-particle electromagnetic field.

In (a) the quadrupole field induces a transition between two quadrupole pairing phonons which during this process, propagate without realizing the presence of the pairing condensate. This coupling is taken care of by graph (b), where exchange of particles takes place between the condensate and the quadrupole phonon which is affected by the external quadrupole field. Coupling between the d-phonons and the condensate before and after the action of the external field are included in a straightforward way through the diagonalization process (cf. fig. 2d).

Graphs 2e and 2f are associated with the quadrupole transition amplitude. Coupling to the condensate takes place already in zeroth order.

Graphs (c) and (g) represent the processes under discussion in the standard quasiparticle representation.

Substituting $\Omega' = \Omega - 2n_d$ for Ω, the sum of the contributions is equal to

$$\begin{aligned} Q_2(\mathrm{d} \to \mathrm{d}) &= -n_d(1-2n_s/\Omega')S_1 \\ &= -n_d(U^2-V^2)S_1, \end{aligned} \tag{8}$$

which coincides † with the sd subspace result [9]). The quantities

$$U = (1-n_s/\Omega')^{\frac{1}{2}}, \tag{9}$$

$$V = (n_s/\Omega')^{\frac{1}{2}} \tag{10}$$

† Note that in writing (8), we have made the substitution $\Omega \to \Omega' = \Omega - 2n_d$, n_d being the number of quadrupole phonons. The blocking produced by the presence of the d-phonons arises, in the NFT, from diagrams where d- and s-bosons interact to higher order in $1/\Omega$.

are the BCS occupation parameters, when pairs of particles coupled to zero and to two are simultaneously present †.

In the standard quasiparticle language the sum of graphs (a) and (b) gives the static quadrupole moment of the two-quasiparticle (particle-hole) phonon (cf. fig. 2c). In this process the external field acts on a particle with a weight V^2. In the representation used in the present paper, graph 2a contributes a factor of 1 while graph 2b contributes a factor †† $-2V^2$. Thus $1-2V^2 = U^2-V^2$.

In the case of the matrix element associated with the quadrupole transition amplitude displayed in fig. 2e, one obtains,

$$\begin{aligned}(Q_2(\mathrm{d}\rightarrow \mathrm{s}))_{\mathrm{zeroth}} &= \langle n_s n_d v\alpha; I||Q_2||n_s+1, n_d-1, v'\alpha'; I'\rangle \\ &= (n_s+1)^{\frac{1}{2}}(n_d)^{\frac{1}{2}}S_1.\end{aligned} \tag{11}$$

In this case the d-phonon couples, already in zeroth order, with the s-phonon condensate. Using rule (c) we make the replacement

$$(n_s+1)^{\frac{1}{2}} \rightarrow (n_s+1)^{\frac{1}{2}}\left(1-\frac{n_s}{\Omega'}+\frac{1}{\Omega'}\right)^{\frac{1}{2}} = \left(\frac{(n_s+1)((\Omega'-n_s)+1)}{\Omega'}\right)^{\frac{1}{2}}, \tag{12}$$

and obtain the result of the algebraic treatment of ref. [9]) (sd subspace) [cf. eq. (A.34)].

In quasiparticle language the graph of fig. 2e contributes a factor V while the graph of fig. 2f is proportional to $-1/2V^3$. These are the first two terms in the expansion $VU = V\sqrt{1-V^+V} = V(1-\frac{1}{2}(V^+V)+\ldots)$. All the matrix elements and quadrupole transition amplitudes are discussed in appendix A and collected in table 1.

3. The parameters of the model

Because we carry out a microscopic pairing-plus-quadrupole diagonalization, admittedly in a non-standard way, there are no free parameters in the model. In fact, $Z_s = G\Omega$ is the correlation energy of a pair of particles interacting through a monopole pairing force. It is also equal to twice the pairing gap Δ determined by the even-odd mass difference. The quantity Z_d is the correlation energy of a pair of particles coupled to angular momentum two [17]), and interacting through a quadrupole pairing force. Finally $\kappa = 120/A^{5/3}$ $(M\omega_0/\hbar)$ is the self-consistent value of the particle-hole quadrupole force [2]). This force acts between like as well as between unlike particles. Although in the present calculations we have made no distinction between the strengths associated with the (π, π), (ν, ν) and (π, ν) channels (where π: proton and ν: neutron), a detailed analysis of experimental data [18]) leads to $\kappa_{\nu\pi} \sim 2\kappa_{\nu\nu} \sim 2\kappa_{\pi\pi}$. We note that the difference between $\kappa_{\pi\pi}$, $\kappa_{\nu\nu}$ and $\kappa_{\pi\nu}$ plays a central role in the IBM [6]).

† Note that the NFT calculations do conserve the number of particles. The reference to BCS occupation number parameters is made only for illustration, and to connect with the standard quasiparticle picture.

†† Note that to each s-phonon can be associated a factor $(n_s/\Omega')^{1/2}$ which properly written in operator form is equal to [9]) $(s^+s/(\Omega-2\hat{n}_d))^{1/2}$.

4. Applications

The model discussed in the previous sections has been utilized to calculate the spectrum and electromagnetic transition probabilities † of ^{78}Kr. This nucleus displays a rather complex spectrum typical of transitional nuclei [19]).

The value of the parameters used in the calculations are

$$\kappa = \frac{120}{A^{5/3}} \left(\frac{M\omega}{\hbar} \right)^2 \text{MeV},$$
$$Z_s = 2 \text{ MeV}, \qquad Z_d = 0.3 \text{ MeV}. \tag{13}$$

No isospin dependence was given to these coupling strengths. The resulting spectrum and transition probabilities are shown in figs. 3 and 4 in comparison with the experimental data. The quality of the fittings is typical.

In what follows we discuss these results in term of the extreme rotational and vibrational limits.

5. Comparison with the rotational and with the vibrational limits

In fig. 5 we show schematically how the multiphonon states associated with the vibrational limit are related in terms of bands. This classification has been shown [20]) to be useful to order the states of the nuclear spectrum, in particular for soft and transitional nuclei. The predictions for the extreme rotational and vibrational models are shown in fig. 6, in comparison with the model predictions.

In what follows we focus our attention on the ground-state band and on the quasi-γ-band. The ability of a model to reproduce the structure of the side bands is a sensitive criterion of its validity. In this sense the study of the quasi-β-band is of similar relevance. However, because of the central role played in this case by the many j-shell structure, and by the pairing vibrations [8,21–23]) the eventual success or failure of the single j-shell model for the quasi-β-band is not very relevant ††.

The predicted excitation pattern of the γ-band (cf. fig. 6) is typical of a transitional situation in which both the vibrational and the rotational features coexist. In particular, the intensity pattern of the quadrupole transition probabilities with $\Delta I = -1$ and $\Delta I = -2$ within the quasi-γ-band (odd-even staggering), shows properties typical of both rotational and vibrational nuclei.

The predicted B(E2) values within the ground-state band show an attenuation in the high-spin region ††† ($I \leqq 10$). Although this trend resembles that of the data, one should be wary of overinterpreting it. In fact, it is possible that there exists a

† Calculations for the Kr isotopes utilizing a phenomenological version of the IBM have been reported in refs. [19,29]).

†† The extension to the many j-shell situation and the inclusion of other monopole pairing phonons (pairing vibrations) should lead to a more realistic model.

††† It is noted that we only consider relative transition probabilities.

TABLE 1

Matrix elements of the pairing-plus-quadrupole hamiltonian and quadrupole transition amplitudes calculated in the NFT utilizing the rules of sect. 2; the corresponding diagrams are displayed in figs. 2 and 8

Matrix elements of $H = H_{s.p.} + H(\alpha = |2|, \lambda = 0) + H(\alpha = |2|, \lambda = 2) + H(\alpha = 0, \lambda = 2)$

Graph 8b and term proportional to Z_s of graph 8c

$$\langle n_s n_d v\alpha; I|H|n_s n_d v\alpha; I\rangle = -Gn_s - Gn_s[(\Omega - 2n_d) - n_s]$$

Graphs 8d and 8h

$$\langle n_s n_d v\alpha; I|H|n_s + 2n_d - 2v'\alpha'; I\rangle = \left(\frac{Z_s Z_d}{Z_s + Z_d} - \kappa q^2\right)\left\{2\sqrt{5}\sqrt{\frac{(\Omega - n - n_d + 1)(\Omega - n - n_d + 2)}{(\Omega - 2n_d)^2}}\right.$$
$$\left. \times \sqrt{\frac{(n - n_d + 2)(n - n_d + 1)}{\Omega^2}}\sqrt{n_d(n_d - 1)}(n_d - 2v'\alpha'; I'; n_d = 2(0)|\}n_d v\alpha I)\right\}.$$

Graph 8e

$$\langle n_s n_d v\alpha; I|H|n_s + 1\ n_d - 1\ v'\alpha'; I\rangle = -\left(\frac{16Z_d^4 Z_s}{(9Z_d^2 - Z_s^2)(Z_s + Z_d)^2} - \kappa q^2\right)20\sqrt{2}\begin{Bmatrix} 2 & 2 & 2 \\ j & j & j \end{Bmatrix}$$
$$\times \sqrt{\frac{(\Omega - n - n_d + 1)(n - n_d + 1)}{(\Omega - 2n_d)\Omega}}(n_d - 1)\sqrt{n_d}\sum_{\alpha'' I'' v''}(n_d - 2v''\alpha'' I''; n_d = 2(2)|\}n_d v\alpha I)(n_d - 2v''\alpha'' I''|\}n_d - 1v'\alpha' I').$$

Term proportional to Z_d in graphs 8c and 8h

$$\langle n_s n_d v\alpha; I|H|n_s n_d v\alpha; I\rangle = -Z_d n_d + (Z_d - 2\kappa q^2)\frac{\Omega - n - n_d}{\Omega - 2n_d}\frac{2}{\Omega}n_s n_d$$

Contribution of graph 8f

$$\langle n_s n_d v\alpha; I|H|n_s n_d v'\alpha'; I\rangle = Z_d n_d(n_d - 1)\sum_{v''\alpha'' I'' I'''} 50\begin{Bmatrix} j & j & 2 \\ j & j & 2 \\ 2 & 2 & I''' \end{Bmatrix}(n_d - 2v''\alpha'' I''; n_d = 2(I''')|\}n_d v'\alpha'; I)$$
$$\times (n_d - 2\,v''\alpha'' I''; n_d = 2(I''')|\ \}n_d v\alpha; I)\left\{\frac{(\Omega' - n_s)^2}{\Omega'^2} + \frac{n_s^2}{\Omega'^2}\right\}$$

Contribution of graph 8j

$$\langle n_s n_d v'\alpha'; I|H|n_s n_d v\alpha; I\rangle = 4\kappa q^2\frac{n_s(\Omega' - n_s)}{\Omega'(\Omega' + 1)}n_d(n_d - 1)\sum_{\alpha'' v'' I'' \lambda} c_\lambda(n_d - 2\,v''\alpha'', I''; n_d = 2(\lambda)|\ \}n_d v\alpha; I)$$
$$\times (n_d - 2\,v''\alpha'', I''; n_d = 2(\lambda)|\ \}n_d v'\alpha'; I)$$

$$c_\lambda = 50\begin{Bmatrix} j & j & 2 \\ j & j & 2 \\ 2 & 2 & \lambda \end{Bmatrix} + (1 - \delta(\lambda, 0))\frac{100}{\Omega - 2}\begin{Bmatrix} \lambda & 2 & 2 \\ j & j & j \end{Bmatrix}^2 + \delta(\lambda, 0)\frac{5}{\Omega(\Omega - 1)}$$

TABLE 1 (continued)

Matrix elements of the quadrupole operator

Contributions of graphs 2a and 2b

$$\langle n_s n_d v'\alpha'; I'||Q_2||n_s n_d v\alpha; I\rangle = -\left(1-\frac{2n_s}{\Omega}\right) n_d 10\sqrt{5}q(2I'+1)^{\frac{1}{2}}(2I+1)^{\frac{1}{2}} \begin{Bmatrix} 2 & 2 & 2 \\ j & j & j \end{Bmatrix}$$
$$\times \sum_{v''\alpha''I''} (-1)^{I+I''} \begin{Bmatrix} 2 & 2 & 2 \\ I'' & I' & I \end{Bmatrix} (n_d-1\, v''\alpha''; I''|\ \}n_d v'\alpha'; I')(n_d-1\, v''\alpha''; I''|\ \}n_d v\alpha; I)$$

Contribution of graph 2e

$$\langle n_s n_d v\alpha, I||Q_2||n_s+1\, n_d-1\, v'\alpha', I'\rangle$$
$$= \sqrt{\frac{2(2I+1)}{\Omega}}\, q \sqrt{\frac{(n-n_d+1)(\Omega-n-n_d+1)}{\Omega-2n_d}}\sqrt{n_d}(-1)^{I-I'}(n_d-1 v'\alpha'; I'|\ \}n_d v\alpha; I).$$

Note that the factor in curly brackets in the contribution from graph 8f as well as the full contribution of graph 8k were taken from the results of ref. [9]).

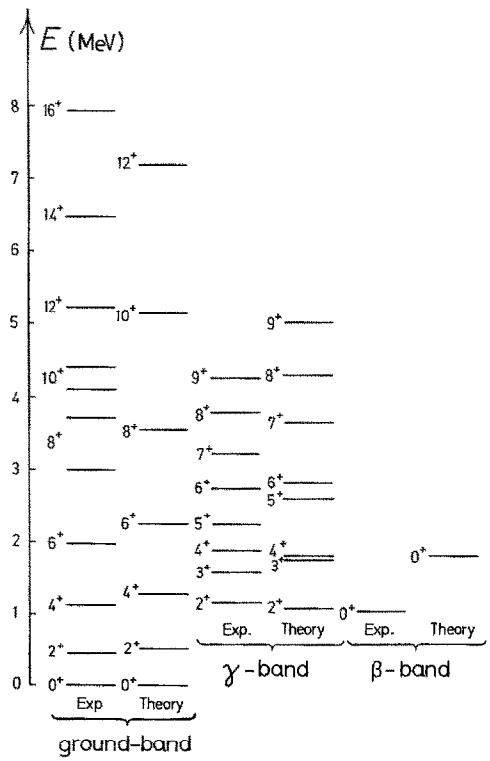

Fig. 3. Predicted energy spectrum of $^{76}_{36}Kr_{42}$. Two groups of levels connected by strong quadrupole transition probabilities can be identified. They correspond to the ground state and quasi-γ-band. The identification of the third group of states (quasi-β-band) is much more tentative. The experimental levels are also displayed.

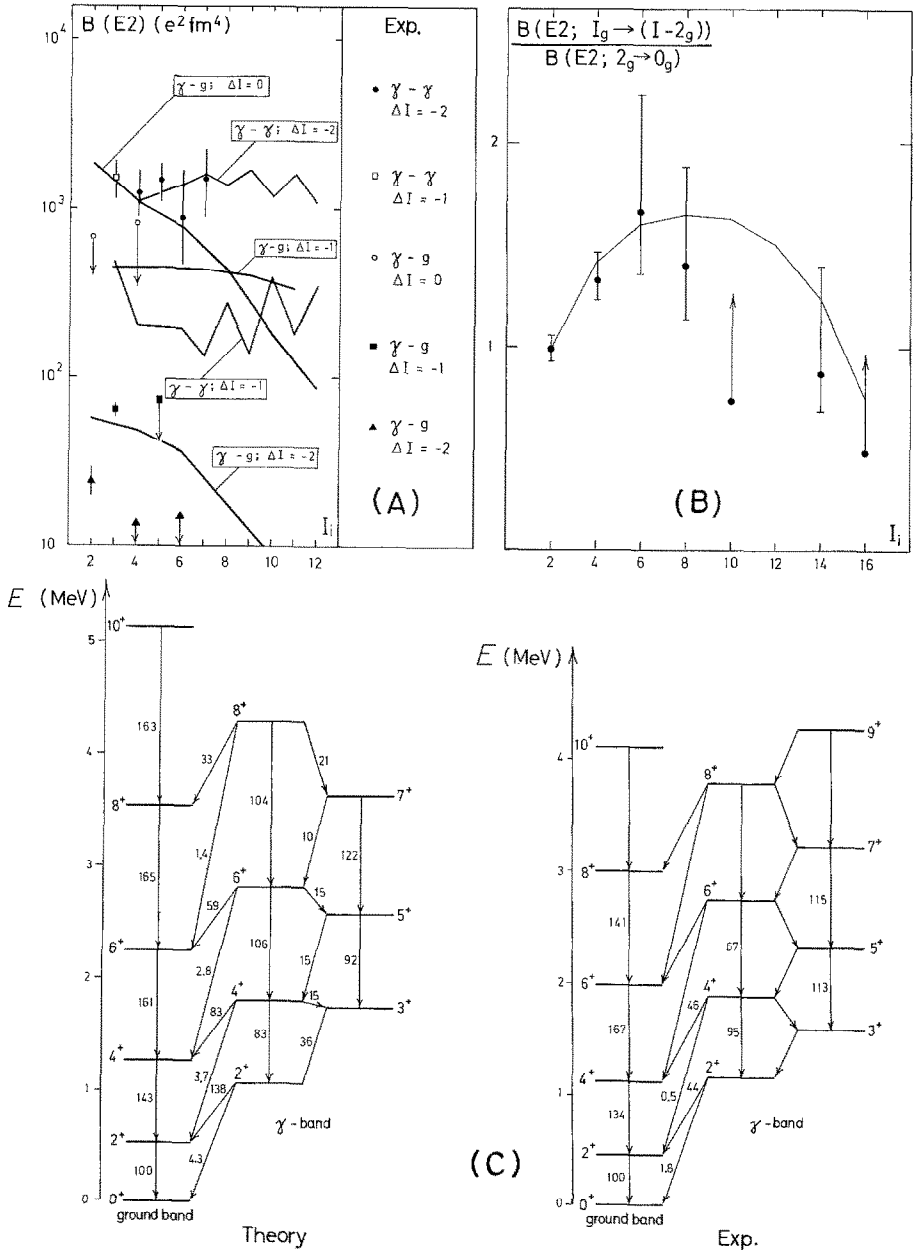

Fig. 4. In-band and inter-band transition probabilities associated with the ground state and with the quasi-γ-band. The corresponding experimental data are also displayed (cf. also fig. 3).

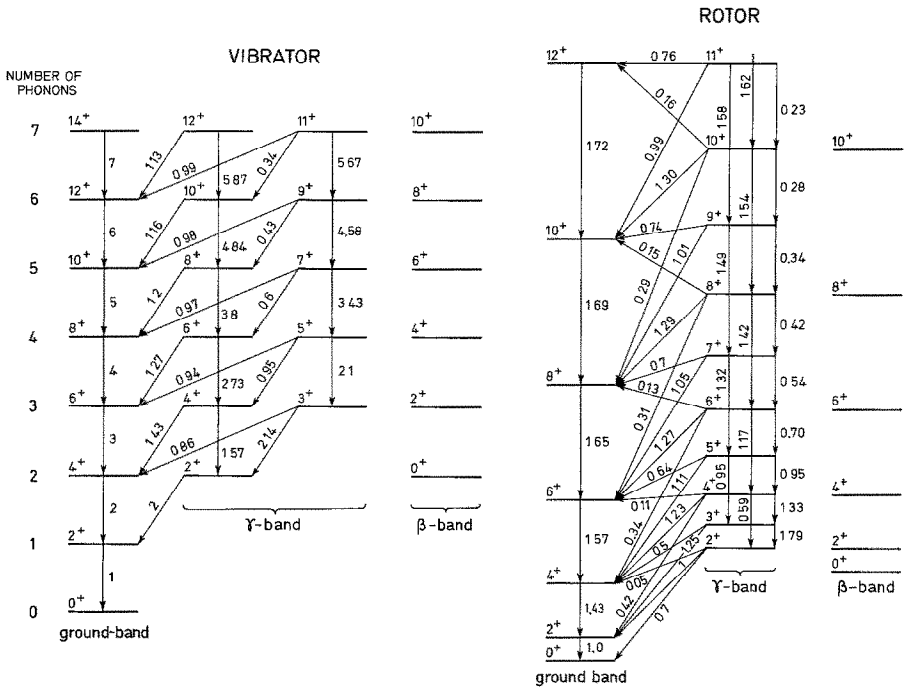

Fig. 5. Schematic representation of the group of levels leading to the ground, quasi-γ- and quasi-β-bands, in the vibrational and rotational limit. The transitions within the ground-state rotational band and the γ-band are normalized to the electromagnetic transition probability $B(E2; 2_g^+ \rightarrow \text{g.s.})$. The transitions between the γ-band and the ground-state band are normalized to $B(E2; 2_\gamma^+ \rightarrow 2_{g.s.}^+)$. Note that all these transitions involve an off-diagonal matrix element of the quadrupole operator whose relation to the intrinsic quadrupole moment associated with the ground-state rotational band depends on the detailed motion of the nucleons and thus is arbitrary in the macroscopic model.

band crossing in the region of angular momenta $I = 10$–12 [cf. ref. [24])]. Note also that the accuracy of the model is expected to become poorer closer to the band termination point ($I_{max} = 16$ in the present case).

6. Conclusions

The pairing-plus-quadrupole particle-hole model in a single j-shell in a basis of pairs of fermions coupled to $\lambda = 0$ and $\lambda = 2$, has a mapping onto a space of monopole and quadrupole pairing phonons. It is possible to find a set of rules such that the mapped matrix elements can be calculated in the framework of the NFT. The model contains some of the features of transitional nuclei as well as the vibrational and, in some very approximate way, the rotational patterns. The model being fully microscopic, contains no free parameters, but the known strengths of the monopole and the quadrupole pairing forces as well as the strength of the quadrupole

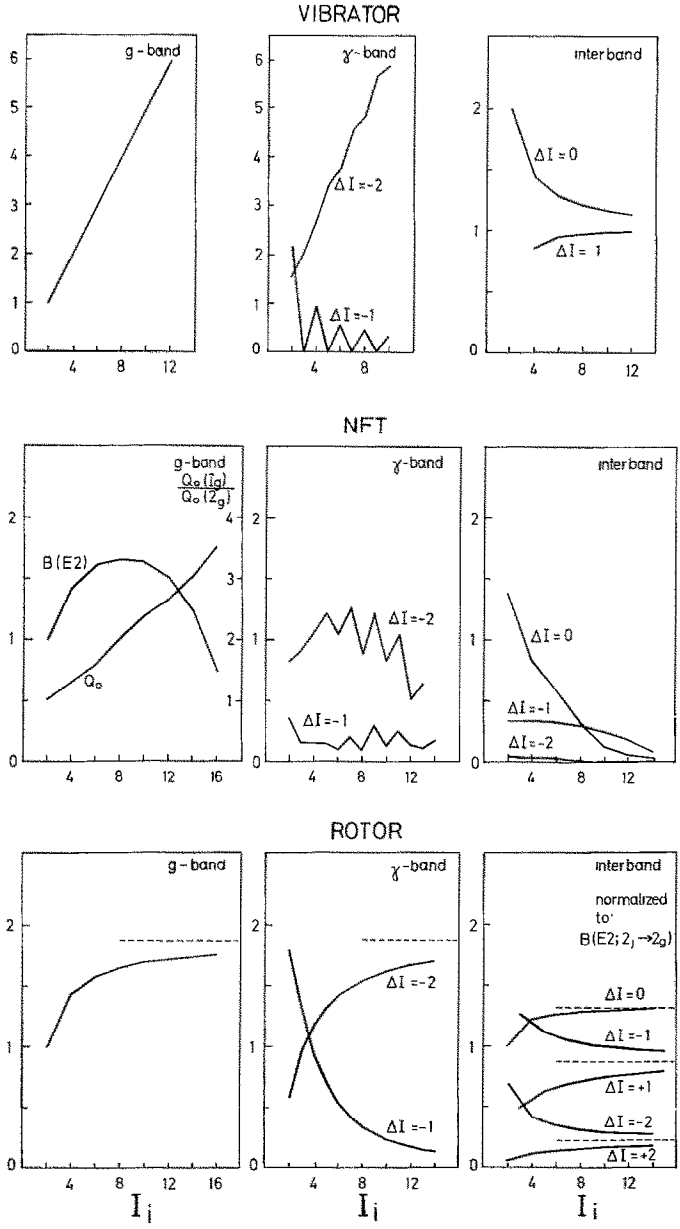

Fig. 6. Transition probabilities associated with the ground band and quasi-γ-band in both the vibrational and rotational limits. The asymptotic limits are indicated by dotted lines. The NFT predictions are also given.

particle-hole interaction. The resulting fits cannot reproduce essential features of the nuclear system like, for example, the energy splitting between the pair of states 3^+–4^+, 5^+–6^+, etc., belonging to the quasi-γ-band. Because of the single j-shell approximation and thus the absence of pairing vibrational modes, the observed features of the quasi-β-band are poorly reproduced.

7. Prospects

The two obvious extensions of the model lie in the inclusion of many j-shells and in the treatment of odd nuclei [cf. refs. [14, 25, 26])]. The first step would allow, among other things, the introduction of a second monopole pairing boson (s′-boson) associated with the fluctuations of the pairing gap (pairing vibrations), and thus for a more realistic description of the β-vibrational modes.

Discussions with A. Bohr, C. H. Dasso, F. Iachello, E. Maglione, B. R. Mottelson, O. Scholten and T. Suzuki are gratefully acknowledged. We are indebted to E. Maglione for his help in different steps of the calculations, and to F. Sakata for the comparisons between the exact and the SD space calculations.

Appendix A

In this appendix we collect the different expressions of the matrix elements and transition amplitudes associated with a system of pairs of particles coupled to $\lambda = 0$ and $\lambda = 2$ which move in a single j-shell and interact via a monopole and quadrupole pairing force and a quadrupole particle-hole force. A résumé is given in table 1.

The monopole and quadrupole pairing modes are defined, in the NFT, as solutions of the random phase approximation equations. Thus, the dispersion relation through which the energies are determined is [cf. e.g. ref. [1])]

$$\frac{1}{4\pi G_\lambda} = \sum_{k_1 \geqq k_2} \left(\frac{|\langle k_1 \| T_\lambda \| k_2 \rangle|^2}{E_{k_1 k_2} - W_\kappa(2, \lambda)} \frac{1}{1+\delta(1,2)} \right) + \sum_{i_1 \geqq i_2} \left(\frac{|\langle i_1 \| T_\lambda \| i_2 \rangle|^2}{E_{i_1 i_2} - W_\kappa(-2\lambda)} \frac{1}{1+\delta(1,2)} \right), \quad \text{(A.1)}$$

where the multipole operator is given by

$$T_{\lambda\mu} = Y_{\lambda\mu}(\hat{\boldsymbol{r}}), \quad \text{(A.2)}$$

that is, we have chosen a constant for the form factor. It has been empirically shown that such a choice leads to a strength value [18])

$$G_\lambda \sim 27/A \text{ MeV}, \quad \text{(A.3)}$$

which is almost independent of λ for $\lambda = 0$, 2, 4 and 6. This result has been given firmer theoretical grounds, in terms of the surface δ-force [27]).

The index k stands for the quantum numbers of a particle moving above the Fermi surface, while i is associated with the quantum numbers of a particle moving

below the Fermi surface. In a single j-shell, only the sum over k's is possible, and it reduces to a single term, that is,

$$Z_\lambda = \varepsilon - W_\lambda = 2\pi G_\lambda |\langle j||T_\lambda||j\rangle|^2, \tag{A.4}$$

where $\varepsilon = E_{j_1 j_2}$ is the energy of the two-particle configuration, and $W_\lambda = W(2, \lambda)$ the phonon energy.

The RPA amplitude associated with forwards scattering is

$$d_n(k_1 k_2 i\lambda) = \frac{\Lambda_n(2\lambda)\ \langle k_1||T_\lambda||k_2\rangle}{(1+\delta(1,2))^{\frac{1}{2}}\ E_{k_1 k_2} - W_n(2\lambda)}, \tag{A.5}$$

which for a j-shell leads to

$$Z_\lambda = \varepsilon - W_\lambda = \sqrt{\tfrac{1}{2}}\,\Lambda_\lambda \langle j||T_\lambda||j\rangle. \tag{A.6}$$

Thus the quantity Z_λ determines both the particle-vibration coupling strength Λ_λ and the energy denominator $\varepsilon - W_\lambda$ of all graphs involving pairing vertices (cf. fig. 7).

The order of magnitude of the different quantities in terms of the small parameter $1/\Omega$ can be estimated for the case of $\lambda = 0$. Using the results:

$$\langle j||T_0||j\rangle = \mathrm{O}(\Omega^{\frac{1}{2}}), \tag{A.7}$$

$$\varepsilon - W_\lambda = \mathrm{O}(1), \tag{A.8}$$

we obtain:

$$\Lambda_\lambda = \mathrm{O}(1/\Omega^{\frac{1}{2}}), \tag{A.9}$$

$$G_\lambda = \mathrm{O}(1/\Omega). \tag{A.10}$$

To calculate matrix elements of a two-body interaction we make use of the boson fractional parentage coefficients, and write the basis states in the following alternative ways

$$\begin{aligned}
|n_s n_d v\alpha; I\rangle &= |n_s\rangle |n_d v\alpha; I\rangle \\
&= \sqrt{n_s}\,|n_s - 1\rangle |n_s = 1\rangle |n_d v\alpha; I\rangle \\
&= \sqrt{n_d}\,|n_s\rangle \sum_{v'\alpha' I'} (n_d - 1 v'\alpha'; I'|\}n_d v\alpha; I)\{|n_d - 1 v'\alpha'; I'\rangle |n_d = 1\rangle\}_I \\
&= \sqrt{\tfrac{1}{2}n_s(n_s-1)}\,|n_s - 2\rangle |n_s = 2\rangle |n_d v\alpha; I\rangle \\
&= \sqrt{n_s n_d}\,|n_s - 1\rangle |n_s = 1\rangle \sum_{v'\alpha' I'} (n_d - 1 v'\alpha'; I'|\}n_d v\alpha; I) \\
&\quad \times \{|n_d = 1 v'\alpha'; I'\rangle |n_d = 1\rangle\}_I \\
&= \sqrt{\tfrac{1}{2}n_d(n_d-1)}\,|n_s\rangle \sum_{v'\alpha' I' I''} (n_d - 2 v'\alpha'; I', n_d = 2(I'')|\}n_d v\alpha; I) \\
&\quad \times \{|n_d - 2 v'\alpha'; I'\rangle |n_d = 2, I''\rangle\}_I .
\end{aligned} \tag{A.11}$$

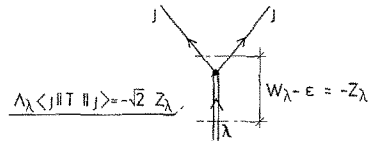

Fig. 7. Schematic representation of the multipole pairing particle vibration coupling. The strength of this coupling is $\Lambda_\lambda\langle j||T_\lambda||j\rangle$ [cf. ref. [1])] while the correlation energy of the collective mode is $\varepsilon - W_\lambda$.

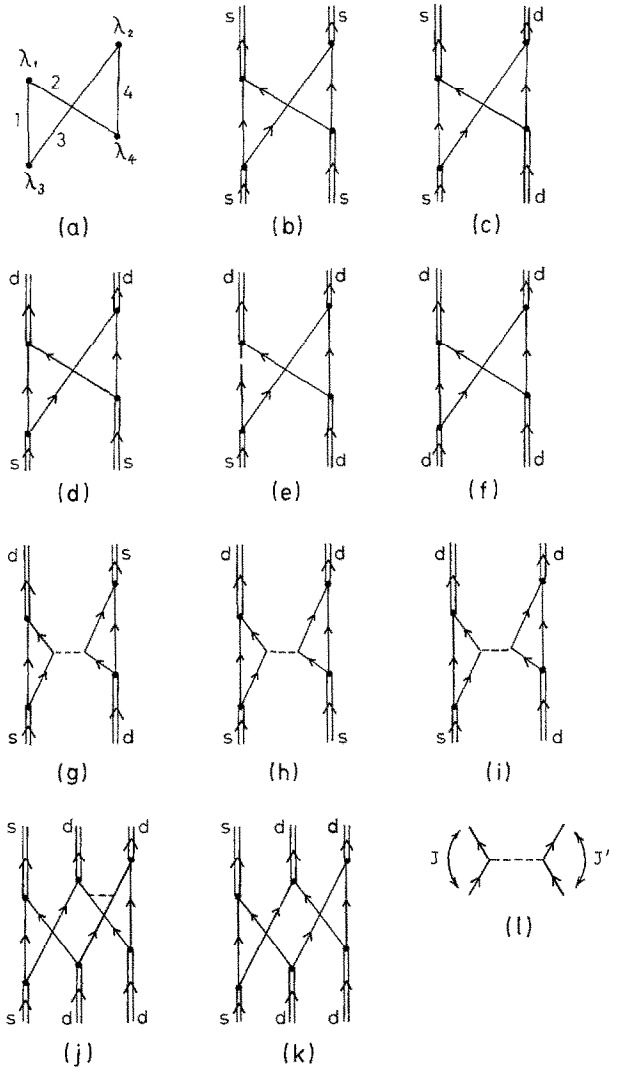

Fig. 8. Graphical representation of the pairing-plus-quadrupole matrix elements. Graphs (b)–(i) correspond to the $1/\Omega$ contributions. The horizontal dotted line represents the particle-hole quadrupole interaction. Both graphs (j) and (k) are of higher order. In (l) we display the coupling associated with action of quadrupole particle-hole force in graphs (g)–(i).

The quantities $(n_d-1\,v'\alpha'; I'|\}n_d v\alpha; I)$ and $(n_d-2v'\alpha'; I', n_d=2(I'')|\}\ n_d v\alpha; I)$ are the single and double fractional parentage coefficients associated with the d-boson.

The graphs leading to the same matrix elements of the pairing-plus-quadrupole hamiltonian as obtained with the algebraic method of ref. [9]) (sd subspace) are collected in fig. 8. The basic structure common to all the butterfly-like diagrams (Pauli principle diagrams) is shown in fig. 8a. It is equal to

$$\begin{aligned}
&\langle\{[c^+_{j_1}c^+_{j_2}]_{\lambda_1}[c^+_{j_3}c^+_{j_4}]_{\lambda_2}\}_J|\{[c^+_{j_1}c^+_{j_3}]_{\lambda_3}[c^+_{j_2}c^+_{j_4}]_{\lambda_4}\}_J\rangle \\
&= -\langle(j_1j_2)\lambda_1(j_3j_4)\lambda_2; J|(j_1j_3)\lambda_3(j_2j_4)\lambda_4; J\rangle \\
&= -((2\lambda_1+1)(2\lambda_2+1)(2\lambda_3+1)(2\lambda_4+1))^{\frac{1}{2}}\begin{Bmatrix} j_1 & j_2 & \lambda_1 \\ j_3 & j_4 & \lambda_2 \\ \lambda_3 & \lambda_4 & J \end{Bmatrix}. \qquad \text{(A.12)}
\end{aligned}$$

In table 2 we collect the values associated with a single j-shell and the different possible combinations of the phonon angular momenta.

In what follows we give the contribution associated with each graph calculated according to the standard rules of the NFT supplement by rules (a)–(d) presented in sect. 2 [cf. also ref. [14])].

SYMMETRIZED EXPRESSIONS FOR ENERGY MATRIX ELEMENTS AND TRANSITION AMPLITUDES; PAULI PRINCIPLE CORRECTION MATRIX ELEMENTS

Contribution of graph 8b and contribution proportional to Z_s of graph 8c. The contribution of graph 8b is

$$\tfrac{1}{2}n_s(n_s-1)\frac{2Z_s}{\Omega}, \qquad \text{(A.13)}$$

while that of 8c proportional to Z_s is

$$n_s n_d \frac{2Z_s}{\Omega}. \qquad \text{(A.14)}$$

To these contributions we should add the energy of the unperturbed s-phonons

$$n_s\omega_s. \qquad \text{(A.15)}$$

The sum of these terms is equal to ($\varepsilon^{(0)}=0$)

$$\langle n_s n_d v\alpha; I|H|n_s n_d v\alpha; I\rangle = -G_s n_s - G_s n_s[(\Omega-2n_d)-n_s], \qquad \text{(A.16)}$$

and coincides with the result obtained using the algebraic method of ref. [9]) (sd subspace).

TABLE 2

Value of the recoupling coefficient $-\langle (j_1 j_2)\lambda_1 (j_3 j_4)\lambda_2; J|(j_1 j_3)\lambda_3 (j_2 j_4)\lambda_4; J\rangle$ associated with the Pauli diagrams (cf. fig. 8)

λ_1	λ_2	λ_3	λ_4	
d	d	d	d	$-25 \begin{Bmatrix} j & j & 2 \\ j & j & 2 \\ 2 & 2 & J \end{Bmatrix}$
d	s	d	d	$\frac{5}{\sqrt{2j+1}} \begin{Bmatrix} 2 & 2 & 2 \\ j & j & j \end{Bmatrix} \delta(J,2)$
s	d	d	d	
s	s	d	d	$-\frac{\sqrt{5}}{(2j+1)}\delta(J,0)$
d	s	s	d	
d	s	d	s	$-\frac{\delta(J,2)}{2j+1}$
s	d	d	s	
s	d	s	d	
s	s	s	s	$-\frac{\delta(J,0)}{2j+1}$

Contribution of graph 8d. The symmetrized contribution associated with graph 8d is

$$\langle n_s n_d v\alpha; I|H|n_s+2, n_d-2, v'\alpha'; I\rangle = \left(\frac{Z_s Z_d}{Z_s+Z_d}\right)\left\{2\sqrt{5}\sqrt{\frac{(\Omega-n-n_d+1)(\Omega-n-n_d+2)}{(\Omega-2n_d)^2}}\right.$$

$$\left.\times\sqrt{(n-n_d+2)(n-n_d+1)/\Omega^2}\sqrt{n_d(n_d-1)}(n_d-2v'\alpha', I'; n_d=2(0)|\,\}n_d v\alpha I)\right\}. \quad \text{(A.17)}$$

This expression coincides with the corresponding sd-subspace matrix elements [9]), aside from differences like $(\Omega-n-n_d+2)$ instead of $(\Omega-n-n_d+1)$, which in any case are of order $1/\Omega$ smaller than the main contribution. The identification to be made is

$$\frac{Z_s Z_d}{Z_s+Z_d} = \kappa(2,2), \quad \text{(A.18)}$$

where $\kappa(2,2)$ is the strength of the pairing quadrupole force as defined in ref. [1]).

A subtle difference between the sd subspace matrix elements and those calculated in the NFT, are that the latter depend on both the monopole and quadrupole pairing strengths, while the former only on the quadrupole pairing strength. The reason for this is to be traced back to the energy denominators of the NFT expressions. They

display the typical asymmetry associated with the Rayleigh-Schrödinger perturbation theory due to the difference between initial and final states. A way to average this asymmetry out is by setting $Z_s = Z_d$ in which case

$$Z_d = 2\kappa(2, 2). \tag{A.19}$$

Contribution of the graph 8e. The symmetrized contribution of graph 8e is

$$\langle n_s n_d v\alpha; I|H|n_s+1\ n_d-1\ v'\alpha'; I\rangle = -\frac{16Z_d^4 Z_s}{(9Z_d^2-Z_s^2)(Z_s+Z_d)^2}\left\{\sqrt{2}\cdot 20\begin{Bmatrix}2 & 2 & 2\\ j & j & j\end{Bmatrix}\right.$$
$$\times\sqrt{\frac{(\Omega-n-n_d+1)(n-n_d+1)}{(\Omega-2n_d)\Omega}}\,(n_d-1)\sqrt{n_d}\sum_{\alpha''I''}(n_d-2\,v''\alpha''I''; n_d=2|\,\}n_d v\alpha I)$$
$$\left.\times(n_d-2\,v''\alpha''I''|\,\}n_d-1\,v'\alpha'I')\right\}, \tag{A.20}$$

which differs from the exact expression by a factor $(1-2n_s/\Omega') = U^2-V^2$. Identifying the factor outside curly brackets in (A.20) with $\kappa(2, 2)$ we obtain, for $Z_s = Z_d$, $Z_d = 2\kappa(2, 2)$.

Contribution of the graph 8f and contribution proportional to Z_d of graph 8c. The contribution of the component proportional to Z_d of graphs 8c and 8f are equal to

$$\langle n_s n_d v\alpha; I|H|n_s n_d v\alpha; I\rangle = -Z_d\left\{1-\frac{\Omega-n-n_d}{\Omega-2n_d}\,\frac{2}{\Omega}\,n_s\right\}n_d, \tag{A.21}$$

$$\langle n_s n_d v\alpha; I|H|n_s n_d v'\alpha'; I\rangle$$
$$= \tfrac{1}{2}Z_d n_d(n_d-1)100\sum_{I''',v'',\alpha'',\ I''}(n_d-2v''\alpha'', I''; n_d=2(I''')|\}n_d v'\alpha'; I)$$
$$(n_d-2v''\alpha''I''; n_d=2(I''')|\}n_d v\alpha; I)\begin{Bmatrix}j & j & 2\\ j & j & 2\\ 2 & 2 & I'''\end{Bmatrix}, \tag{A.22}$$

respectively. The factor in the curly brackets in (A.21) can be written as

$$\left\{1-\frac{\Omega-n-n_d}{\Omega-2n_d}\,\frac{2}{\Omega}\,n_s\right\} = 1-2U^2V^2\left(\frac{\Omega'}{\Omega}\right), \tag{A.23}$$

and should be compared with the exact expression $U^4+V^4 = 1-2U^2V^2$. The difference is thus higher order in $1/\Omega$.

Turning now to the matrix element (A.22) we note that it does not contain the factor n_s. The d-bosons propagate without interacting with the s-boson condensate, as is obvious from graph 8f. The expression obtained with the algebraic method [9]) (sd

subspace) differs from (A.22) by the factor

$$1-2U^2V^2. \tag{A.24}$$

The correction $-2U^2V^2$ should arise from the graph (k). We have however not calculated it in detail but empirically incorporated the factor (A.24) in (A.22).

Contributions to quadrupole transition amplitudes of graphs 2a and 2b. The basic structure of the zeroth-order diagrams is given in fig. 2h and is equal to

$$\langle [c^+_{j_1}c^+_{j_3}]_{\lambda_2}|\{Q_2[c^+_{j_1}c^+_{j_2}]_{\lambda_1}\}_{\lambda_2}\rangle = (-1)^{j_1+j_2+\lambda_1}\sqrt{5(2\lambda_1+1)}\begin{Bmatrix}2 & j_3 & j_2\\ j_1 & \lambda_1 & \lambda_2\end{Bmatrix}, \tag{A.25}$$

where

$$Q_{2\mu} = \sqrt{\tfrac{1}{5}}\sum_{jj'}\langle j||Q_2||j'\rangle[c^+_{j'}c_j]_{2\mu}. \tag{A.26}$$

For a single j-shell we obtain

$$\langle [c^+_j c^+_j]_0|\{Q_2[c^+_j c^+_j]_2\}_0\rangle = \frac{1}{\sqrt{2j+1}}\langle j||Q_2||j\rangle, \tag{A.27}$$

$$\langle [c^+_j c^+_j]_2|\{Q_2[c^+_j c^+_j]_2\}_2\rangle = -\sqrt{5}\begin{Bmatrix}2 & 2 & 2\\ j & j & j\end{Bmatrix}\langle j||Q_2||j\rangle. \tag{A.28}$$

The contribution of graph 2a is equal to

$$\langle n_s n_d v'\alpha'; I'||Q_2||n_s n_d v\alpha; I\rangle = -n_d S_1, \tag{A.29}$$

where

$$S_1 = 10(2I'+1)^{\frac{1}{2}}(2I+1)^{\frac{1}{2}}\begin{Bmatrix}2 & 2 & 2\\ j & j & j\end{Bmatrix}\sum_{v''\alpha''I''}(-1)^{I+I''}\begin{Bmatrix}2 & 2 & 2\\ I'' & I' & I\end{Bmatrix}$$
$$\times(n_d-1\ v''\alpha''; I''|\ }n_d v'\alpha'; I')(n_d-1\ v''\alpha''; I''|\ }n_d v\alpha; I)\langle j||Q_2||j\rangle, \tag{A.30}$$

$$\langle j||Q_2||j\rangle = \langle j||v^2Y_2||j\rangle. \tag{A.31}$$

The contribution of graph 2b for all those time orderings in which the external field acts within the four vertices is equal to

$$\langle n_s n_d v'\alpha'; I'||Q_2||n_s n_d v\alpha; I\rangle = n_d n_s\frac{2}{\Omega}S_1. \tag{A.32}$$

The sum of the two contributions is then

$$\langle n_s n_d v'\alpha'; I'||Q_2||n_s n_d v\alpha; I\rangle = (1-2n_s/\Omega)S_1, \tag{A.33}$$

to be compared with the exact expression $(1-2n_s/\Omega')S_1$. The difference is again of higher order in $1/\Omega$.

Contribution of the quadrupole transition amplitude of graph 2e. The symmetrized expression of the contribution of graph 2e to the quadrupole transition amplitude is

$$\langle n_s n_d v\alpha, I||Q_2||n_s+1\ n_d-1\ v'\alpha', I'\rangle = 2\sqrt{\tfrac{1}{5}(2I+1)}\frac{\langle j||Q_2||j\rangle}{\sqrt{2j+1}}$$

$$\times\sqrt{\frac{(n-n_d+1)(\Omega-n-n_d+1)}{\Omega-2n_d}}\sqrt{n_d}(-1)^{I-I'}(n_d-1\ v'\alpha'; I'|\ \}n_d v\alpha; I), \quad \text{(A.34)}$$

and coincides with the result of the algebraic method of ref. [9]) (sd subspace).

Quadrupole particle-hole matrix elements. The quadrupole particle-hole matrix elements are displayed in figs. 8g–8j. The first three are separable (cf. figs. 8l and 9) and can be calculated in terms of the quadrupole transition amplitudes displayed in figs. 2a and 2e.

Defining the quadrupole particle-hole hamiltonian

$$H_Q = -\kappa\sum_\mu(-1)^\mu Q_{2\mu}Q_{2-\mu}, \quad \text{(A.35)}$$

and setting $Z_s = Z_d$ we obtain the following result

$$\frac{\text{graph (g)}}{\text{graph (c)}} = \frac{\text{graph (h)}}{\text{graph (d)}} = \frac{\text{graph (i)}}{\text{graph (e)}} = -\frac{kq^2}{Z_d}, \quad \text{(A.36)}$$

The quantity q is defined as

$$q = \sqrt{\tfrac{1}{5}}\langle j||Q_2||j\rangle. \quad \text{(A.37)}$$

The result (A.36) coincides with the result obtained utilizing the algebraic method of ref. [9]) (sd subspace).

To incorporate the contribution of graphs 8g–8i in the general matrix elements we can make the replacements

$$Z_d \to (Z_d - 2\kappa q^2) \qquad \text{in eq. (A.21)},$$

$$\frac{Z_s Z_d}{Z_s+Z_d} \to \left(\frac{Z_s Z_d}{Z_s+Z_d} - \kappa q^2\right) \qquad \text{in eq. (A.17)},$$

$$\frac{16Z_d^4 Z_s}{(9Z_d^2-Z_s^2)(Z_s+Z_d)^2} - \left(\frac{16Z_d^4 Z_s}{(9Z_d^2-Z_s^2)(Z_s+Z_d)^2} - \kappa q^2\right). \qquad \text{in eq. (A.20)}$$

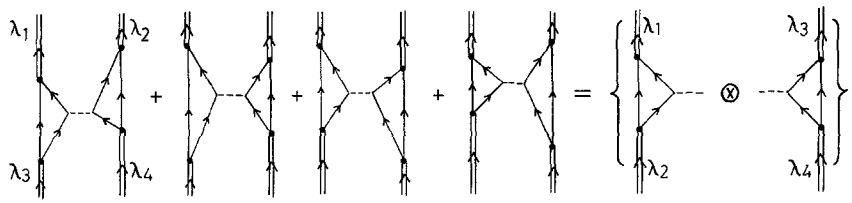

Fig. 9. Separability of some of the quadrupole particle-hole graphs. To the extent that the energy of the initial state $\omega_{\lambda 3}+\omega_{\lambda 4}$ is approximately equal to that of the final state $\omega_{\lambda 1}+\omega_{\lambda 2}$, the four-point vertex graph can be weritten as a product of two transition diagrams [cf. ref. [28])].

In the results of the algebraic method [9]) (sd subspace) there exists one quadrupole matrix element more which is equal to

$$\langle n_s n_d v'\alpha'; I|H_Q|n_s n_d v\alpha; I\rangle = 4\kappa q^2 \frac{n_s(\Omega'-n_s)}{\Omega'(\Omega'+1)} n_d(n_d-1)$$
$$\times \sum_{\lambda\alpha'' I''} c_\lambda(n_d-2\alpha'', I''; n_d = 2(\lambda)|\}n_d v\alpha; I)$$
$$\times(n_d-2\alpha'', I''; n_d = 2(\lambda)|\}n_d v'\alpha'; I), \tag{A.38}$$

where

$$c_\lambda = 50 \begin{Bmatrix} j & j & 2 \\ j & j & 2 \\ 2 & 2 & \lambda \end{Bmatrix} + (1-\delta(\lambda,0))\frac{100}{\Omega-2}\begin{Bmatrix} \lambda & 2 & 2 \\ j & j & j \end{Bmatrix}^2 + \delta(\lambda,0)\frac{5}{\Omega(\Omega-1)}. \tag{A.39}$$

Because it is an exchange type of graph, and because it has a term linear in n_s, it means that the two d-bosons interact with the s-bosons already in lowest order. The graph corresponding to this process is displayed in fig. 8j. Although this graph can be calculated we have in the present paper directly used the expression (A.38).

Appendix B

THE HAMILTONIAN

The particles moving in a single j-shell interact through the multipole ($\lambda = 0, 2$) pairing force and through the quadrupole particle-hole interaction. The multipole pairing hamiltonian is defined as in ref. [1]) and reads

$$H_p(\lambda) = -G_\lambda(2\lambda+1)\sum_\mu P^+_{\lambda\mu}P_{\lambda\mu}, \tag{B.1}$$

where, for a single j-shell

$$P^+_{\lambda\mu} = \left(\frac{2\pi}{2\lambda+1}\right)^{\frac{1}{2}} \langle j\|T_\lambda\|j\rangle [c^+_j c^+_j]^\lambda_\mu/\sqrt{2}. \tag{B.2}$$

As mentioned in appendix A, assuming $T_\lambda = Y_{\lambda\mu}$, one obtains $G_\lambda \sim 27/A$ MeV ($\lambda = 0, 2$ and 4).

The particle-hole quadrupole hamiltonian is equal to

$$H_Q = -\kappa \sum_\mu (-1)^\mu Q_{2\mu} Q_{2-\mu}, \tag{B.3}$$

where

$$Q_{2\mu} = \sqrt{\tfrac{1}{5}} \langle j||Q_2||j\rangle [c_j^+ c_j]_\mu^2, \tag{B.4}$$

$$\kappa = \frac{120}{A^{5/3}} \left(\frac{M\omega}{\hbar}\right)^2 \text{MeV}. \tag{B.5}$$

The hamiltonian (B.1) is used to define the monopole and quadrupole pairing phonons, i.e. to determine the collective energies W_λ and the particle vibration coupling vertices Λ_λ.

No phonon is ascribed to H_Q. This residual interaction couples the pairing phonons pairwise, by scattering fermions in the intermediate states.

Appendix C

According to the rule (c), the contribution of each graph associated with processes in which the particle number is not changed, has to be symmetrized by making the replacement

$$(n_s+a) \to \frac{1}{\Omega'}(n_s+a)(\Omega'-n_s+a) = \frac{1}{\Omega'}[(n_s)+a][(\Omega'-n_s)+a]$$

$$= (n_s+a)\left(1-\frac{n_s}{\Omega'}+\frac{a}{\Omega'}\right). \tag{C.1}$$

In the second form for the substitution, the symmetry between pairs of particles n_s and pairs of holes $(\Omega'-n_s)$ is apparent.

Let us see how the prescription works in a concrete situation like, for example, the contribution of graph (d) of fig. 8. The non-symmetrized contribution of this graph is

$$\langle n_s n_d v\alpha; I|H|n_s+2n_d-2v'\alpha'; I\rangle$$

$$= \frac{Z_s Z_d}{Z_s+Z_d}\{2\sqrt{5}\sqrt{(n_s+2)(n_s+1)n_d(n_d-1)}$$

$$\times (n_d-2v'\alpha', I'; n_d = 2, (0)|\}n_d v\alpha I)\}. \tag{C.2}$$

Using (C.1) we obtain

$$\sqrt{n_s+1} \to \sqrt{(n-n_d+1)\frac{\Omega-n-n_d+1}{\Omega-2n_d}}, \tag{C.3}$$

$$\sqrt{n_s+2} \to \sqrt{(n-n_d+2)\frac{\Omega-n-n_d+2}{\Omega-2n_d}}. \tag{C.4}$$

Making these replacements in (C.2) we obtain the final expression (A.17).

References

1) P. F. Bortignon, R. A. Broglia, D. R. Bès and R. Liotta, Phys. Reports **30C** (1977) 305 and references therein
2) A. Bohr and B. R. Mottelson, Nuclear structure, Vol. II, (Benjamin, New York, 1975)
3) M. G. Mayer and J. H. D. Jensen, Elementary theory of nuclear shell structure (Wiley, New York, 1955)
4) A. Bohr and B. R. Mottelson, Mat. Fys. Medd. Dan. Vid. Selsk. **27** (1953) no. 16
5) A. Bohr, Compt. Rend. Congrès Int. de physique nucleaire, Paris, 1964, ed. Centre National de la Recherche Scientifique, vol. I, p. 487;
D. R. Bès and R. A. Broglia, Nucl. Phys. **80** (1965) 289;
R. A. Broglia, Proc. XII Summer Meeting of Nuclear Physicists, Herceg Novi, ed. L. Šips Vol. I, (Nuclear Energy Commission Yugoslavia, 1966) p. 201
6) Interacting bosons in nuclear physics, Ettore Majorana International Science Series, ed. F. Iachello, (Plenum, New York, 1979)
7) D. R. Bès and R. A. Sorensen, The pairing-plus-quadrupole model, Advances in Nuclear Physics Vol. 2 (Plenum, New York, 1969) p. 129;
K. Kumar and M. Baranger, Nucl. Phys. **A92** (1967) 608; **A110** (1968) 490; 529;
S. T. Belyaev, Mat. Fys. Medd. Dan. Vid. Selsk. **31** (1959) No. 11; Nucl. Phys. **64** (1965) 17
8) S. Iwasaki, T. Marumori, F. Sakata and K. Takada, Prog. Theor. Phys. **56** (1976) 1846;
F. Sakata and G. Holzworth, Prog. Theor. Phys. **61** (1979) 1649
9) S. Suzuki, M. Fuyuki and K. Matsuyanagi, Prog. Theor. Phys. **61** (1979) 1682
10) T. Otsuka, A. Arima, F. Iachello and I. Talmi, Phys. Lett. **76B** (1978) 139; **66B** (1977) 205;
11) F. Sakata, private communication;
T. Otsuka, A. Arima and F. Iachello, Nucl. Phys. **A309** (1978) 1
12) D. Janssen, R. V. Jolos and F. Dönau, Yad, Fiz. **22** (1975) 965; Sov. J. Part. Nucl. **8** (1977) 138
13) G. Holzwarth, D. Janssen and R. V. Jolos, Nucl. Phys. **A261** (1976) 1
14) D. R. Bès and R. A. Broglia, Interacting bosons in nuclear physics, Ettore Majorana International Science Series, ed. F. Iachello (Pergamon, New York, 1979) p. 143
15) P. Bortignon, R. A. Broglia and D. R. Bès, Phys. Lett. **76B** (1978) 153
16) B. R. Mottelson, The many body problem, Les Houches, Session 1958, Dunod Paris (1959) p. 283
17) R. A. Broglia, D. R. Bès and B. S. Nilsson, Phys. Lett. **50B** (1974) 213
18) D. R. Bès, R. A. Broglia and B. Nilsson, Phys. Reports **16C** (1975) 1
19) H. P. Hellmeister, U. Kaup, J. Keinomen, K. P. Lieb, R. Rascher, R. Ballini, H. Delanuey and H. Dumont, Phys. Lett. **85B** (1979) 34; Nucl. Phys. **A332** (1979) 241
20) M. Sakai and A. C. Rester, Nucl. Data Tables **20** (1977) 441;
M. Sakai and Y. Gono, Quasi-ground, quasi-beta, and quasi-gamma bands, preprint INS-J-160 (1979)
21) D. R. Bès, Nucl. Phys. **49** (1963) 544
22) N. Kansaki, T. Marumori, F. Sakata and K. Takada, Prog. Theor. Phys. **49** (1973) 181; **50** (1973) 867
23) A. Kuriyama, T. Marumori, T. Matsuyanagi, F. Sakata and T. Suzuki, Prog. Theor. Phys. Suppl. No. **58** (1975) 9, 184

24) J. H. Hamilton, Nucleonika **24** (1979) 561
25) O. Civitarese, R. A. Broglia and D. R. Bès, Phys. Lett. **72B** (1977) 45
26) F. Iachello and O. Scholten, Phys. Rev. Lett. **43** (1979) 679
27) S. Mozkowski, private communication
28) R. A. Broglia, V. Paar and D. R. Bès, Phys. Lett. **37B** (1971) 159
29) A. Gelberg and U. Kaup, Interacting bosons in nuclear physics, Ettore Majorana International Science Series, ed. F. Iachello (Pergamon, New York, 1979) p. 60;
U. Kaup and A. Gelberg, Z. Phys. **A293** (1979) 311